



**Small is the next  
big thing**

# Micro Process Engineering – An Interdisciplinary Approach

Micro Process Engineering, the science of enhanced transport process in microstructured devices

## Basic Understandings

Scaling down to micrometer dimensions changes not only the length or volume of a device, but also influences the performance of unit operations.

## **Relevant Books**

Microflows and Nanoflows - Fundamentals and Simulation by George Karniadakis, Ali Beskok, Narayan Aluru; Springer, 2005.

MICRODROPS AND DIGITAL MICROFLUIDICS by Jean Berthier, William Andrew Inc. 2008.

Transport Phenomena in Micro Process Engineering, by Norbert Kockmann, Springer, 2006.

# **Topics to be covered**

Overview – length and time scales

Manufacturing practices – top down and bottom up

Transport in microchannels – heat pipes

Continuum, scaling

Balance and transport equations, convective flow and heat transfer in microchannels

Microfluidic networks

Electrowetting and digital microfluidics  
Lecture 1

# Differences between fluid mechanics at microscales and in the macromdomain :

- *Non-continuum effects*: Both viscosity and the no-slip condition are concepts developed under the framework of continuum. Slip / Contact line motion?
- *Surface-dominated effects*: Friction, electrostatic forces, viscous effects
- *Low Reynolds number effects*:
- *Multiscale and multiphysics effects*.

Microdevices tend to behave differently from the objects we are used to handling in our daily life.

The **inertial forces** tend to be quite small, and **surface effects** tend to dominate the behavior of these small systems.

Friction, electrostatic forces, and viscous effects due to the surrounding air or liquid become increasingly important as the devices become smaller.

Example: Forces present in a thin film of liquid

# Navier Stokes Equation

$$\rho \left( \frac{\partial v_z}{\partial t} + v_x \frac{\partial v_z}{\partial x} + v_y \frac{\partial v_z}{\partial y} + v_z \frac{\partial v_z}{\partial z} \right) = - \frac{\partial P}{\partial z} + \mu \left[ \frac{\partial^2 v_z}{\partial x^2} + \frac{\partial^2 v_z}{\partial y^2} + \frac{\partial^2 v_z}{\partial z^2} \right] + \rho g_z$$

$$\rho \left( \frac{\partial v_z}{\partial t} + v_x \frac{\partial v_z}{\partial x} + v_y \frac{\partial v_z}{\partial y} + v_z \frac{\partial v_z}{\partial z} \right) =$$

$$- \frac{\partial P}{\partial z} + \mu \left[ \frac{\partial^2 v_z}{\partial x^2} + \frac{\partial^2 v_z}{\partial y^2} + \frac{\partial^2 v_z}{\partial z^2} \right] + \rho g_z$$

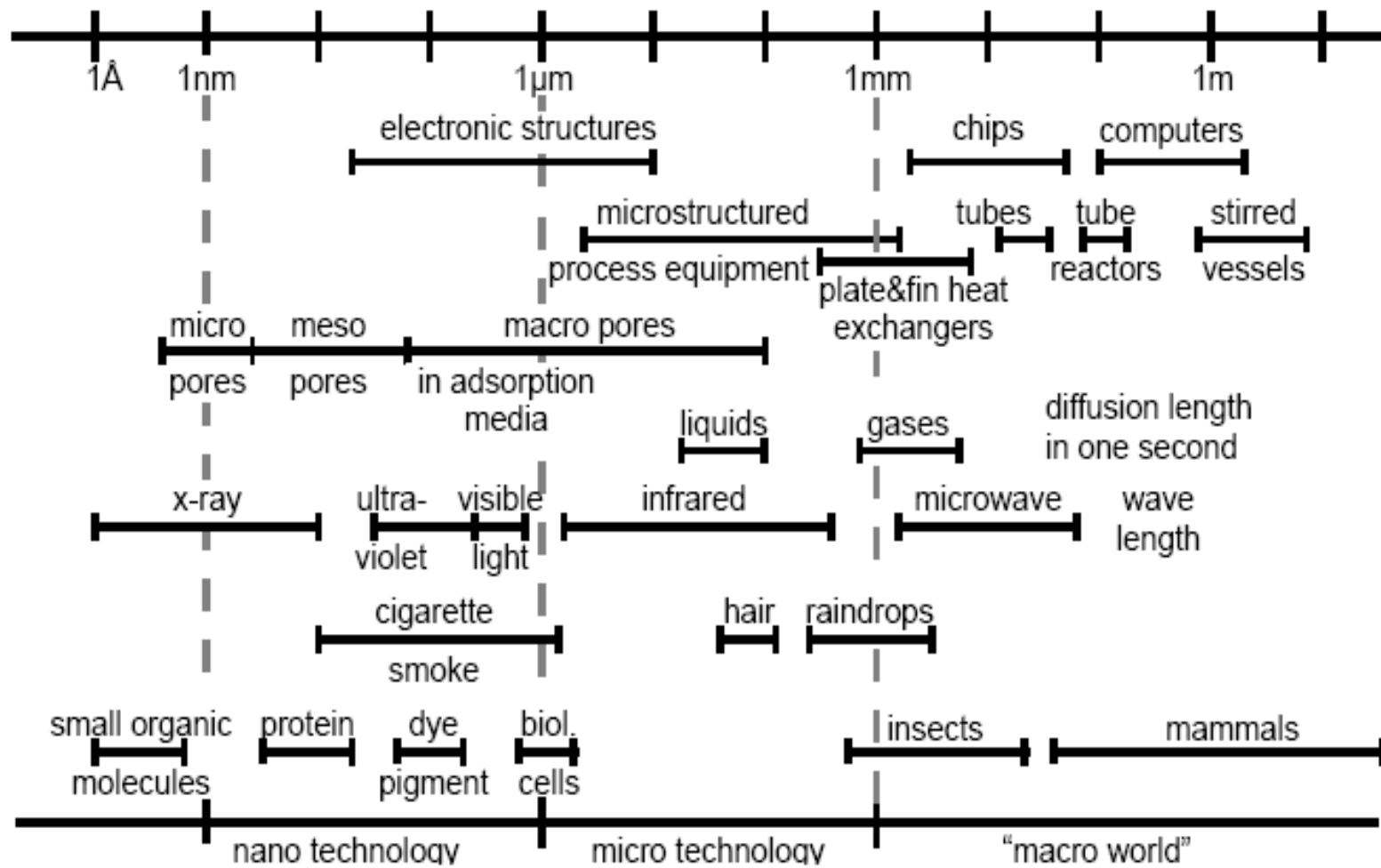
the z - momentum equation

$$v^* \frac{\partial w^*}{\partial y^*} + w^* \frac{\partial w^*}{\partial z^*} = - \frac{\partial p}{\partial z^*} + \frac{\partial}{\partial y^*} \left[ \eta^* \frac{\partial w^*}{\partial y^*} \right] + \frac{1}{Re^2} \frac{\partial}{\partial z^*} \left[ \eta^* \frac{\partial w^*}{\partial z^*} \right],$$

Micromechanical systems started to enter technical systems in the 80s and 90s, enabling fluidic systems to be developed.

Starting from data processing, microsystems have now integrated mechanical, optical, fluid mechanical, and chemical functions for tasks like sensing and analyzing, controlling larger systems, or producing suitable goods and growing application fields for therapeutics and diagnostics.

Due to the reduced length scale of microstructured process equipment, the transfer lengths are short and precisely defined, and the areas are small, but high surface-to-volume ratios and tiny volumes dominate everything.



Characteristics lengths of important processes and equipment in chemical engineering and microsystems technology

Overview of miniaturization effects and beneficial phenomena e.g. in microchannels with characteristic dimensions from 10 to 1000  $\mu\text{m}$ .

Process intensification in chemical engineering benefits from the miniaturization of channels and ducts within devices, where the characteristic lengths reach into the scale of boundary layers.

The higher transport rates can be used for many different purposes such as rapid mixing, temperature-sensitive reactions, temperature homogenization, nanoparticle precipitation.

## Square-Cube Law

When an object undergoes a proportional increase in size, its new volume is proportional to the cube of the multiplier and its new surface area is proportional to the square of the multiplier.

### Example from Biology

If an animal were scaled up by a considerable amount, its relative muscular strength would be severely reduced, since the **cross section of its muscles would increase by the *square* of the scaling factor** while its **mass would increase by the *cube* of the scaling factor**.

Cardiovascular and respiratory functions would be severely burdened.

In general, properties ( $p$ ) that are a function of the area of interaction ( $A$ ) decrease more slowly than properties that depend on the volume ( $V$ ), as expressed by the “***square-cube law***:

$$\frac{p_1(A)}{p_2(V)} \propto \frac{L^2}{L^3} \propto \frac{1}{L}$$

$L$  is the characteristic dimension of the microdevice. This has interesting application in microdevices.

A typical order of magnitude of the ratio is  $10^6 \text{ m}^2/\text{m}^3$ .

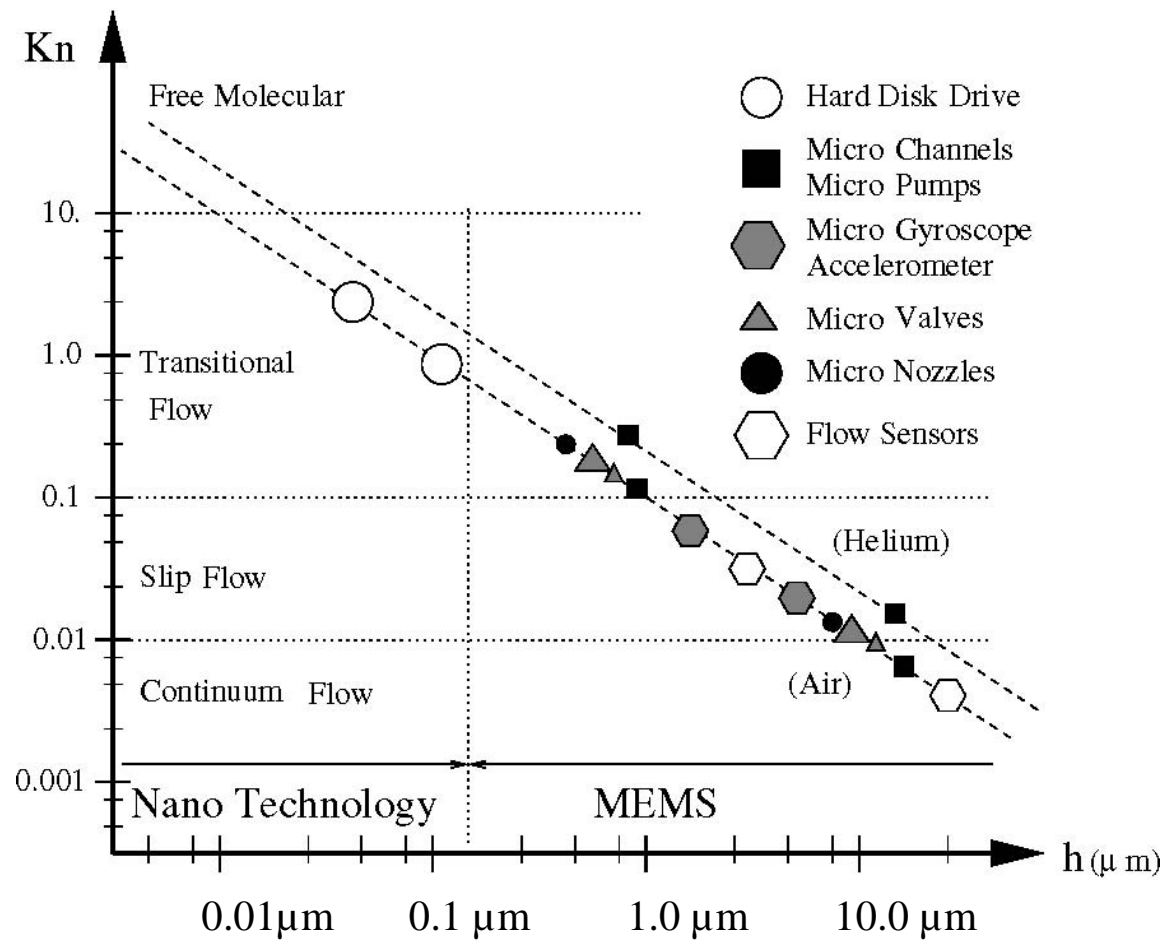
Surface tension effects are dominant at these scales, and micropumps and microvalves have been fabricated taking advantage of this principle

Early applications in computer components – the Winchester-type hard disk drive mechanism, where the read/write head floats 50 nm above the surface of the spinning platter. Smaller the gap - greater the recording capacity.

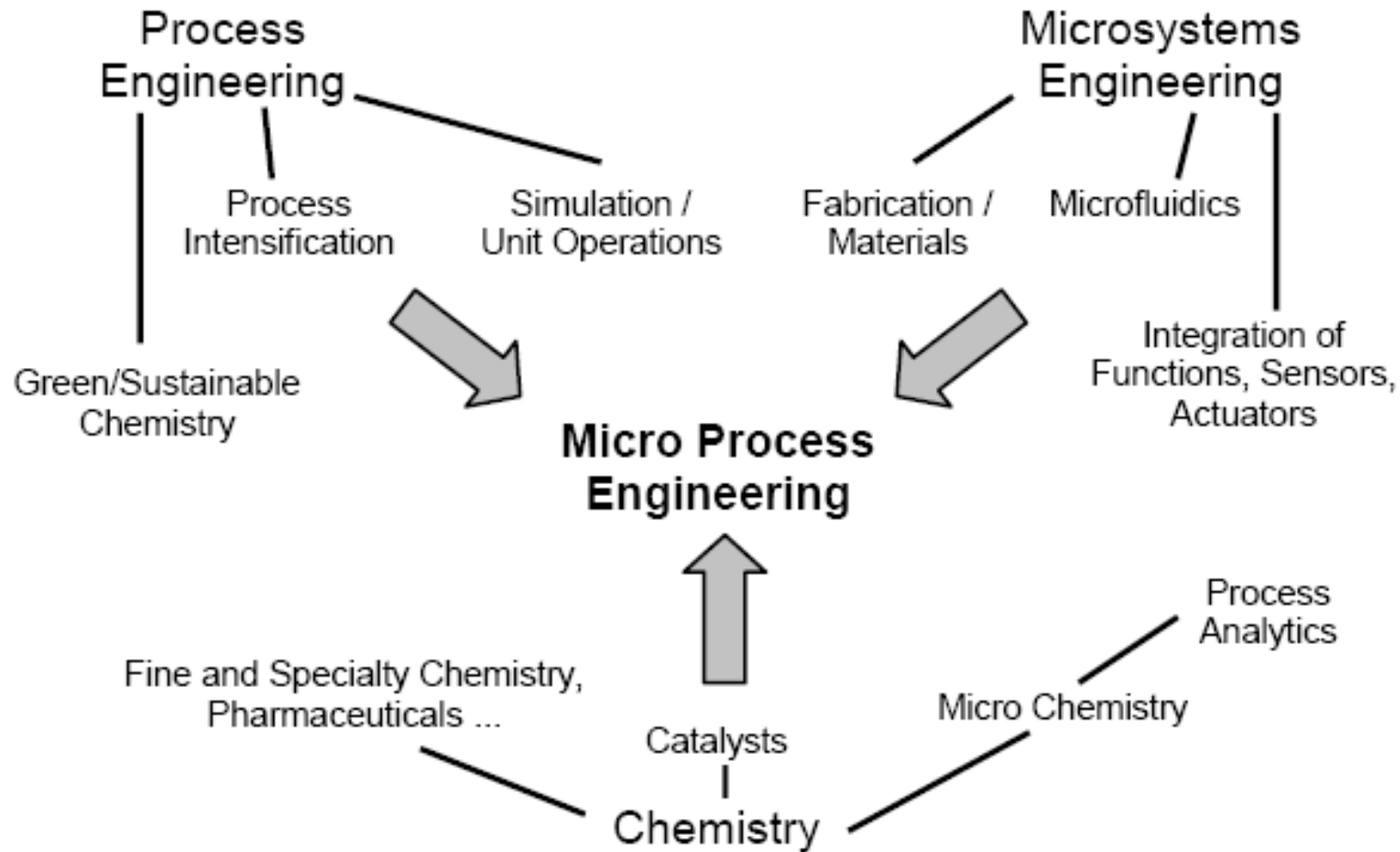
Correspond to low Reynolds and Mach number, e.g., less than 0.6 and 0.3, respectively.

*The corresponding Knudsen number, ( $\lambda / L$ ), is relatively large. –*

**Continuum Limit?**



Typical MEMS and nanotechnology applications in standard atmospheric conditions span the entire Knudsen regime (Continuum, slip, transition, and free-molecular flow). Here  $h$  denotes a characteristic length scale for the microflow.



Microprocess Engineering – an interdisciplinary field  
with inputs from various disciplines  
Lecture 1

# Issues to be looked into

Characteristic length and time scales

Transport phenomena in microstructures

Continuum range

Micro process engineering

Momentum and heat transfer in microchannels

- Micromixers, Micro heat pipes

Coupled transport processes

Micro fabrication technology – process intensification

~~Transfer lengths are short, areas are small but high surface-to-volume ratios and tiny volumes dominate everything~~

~~Small channels allow short transport lengths for heat and mass transfer.~~

This results in high transfer rates, as described for diffusive mass transfer with the mean transport length from the

Einstein-Smoluchovski equation

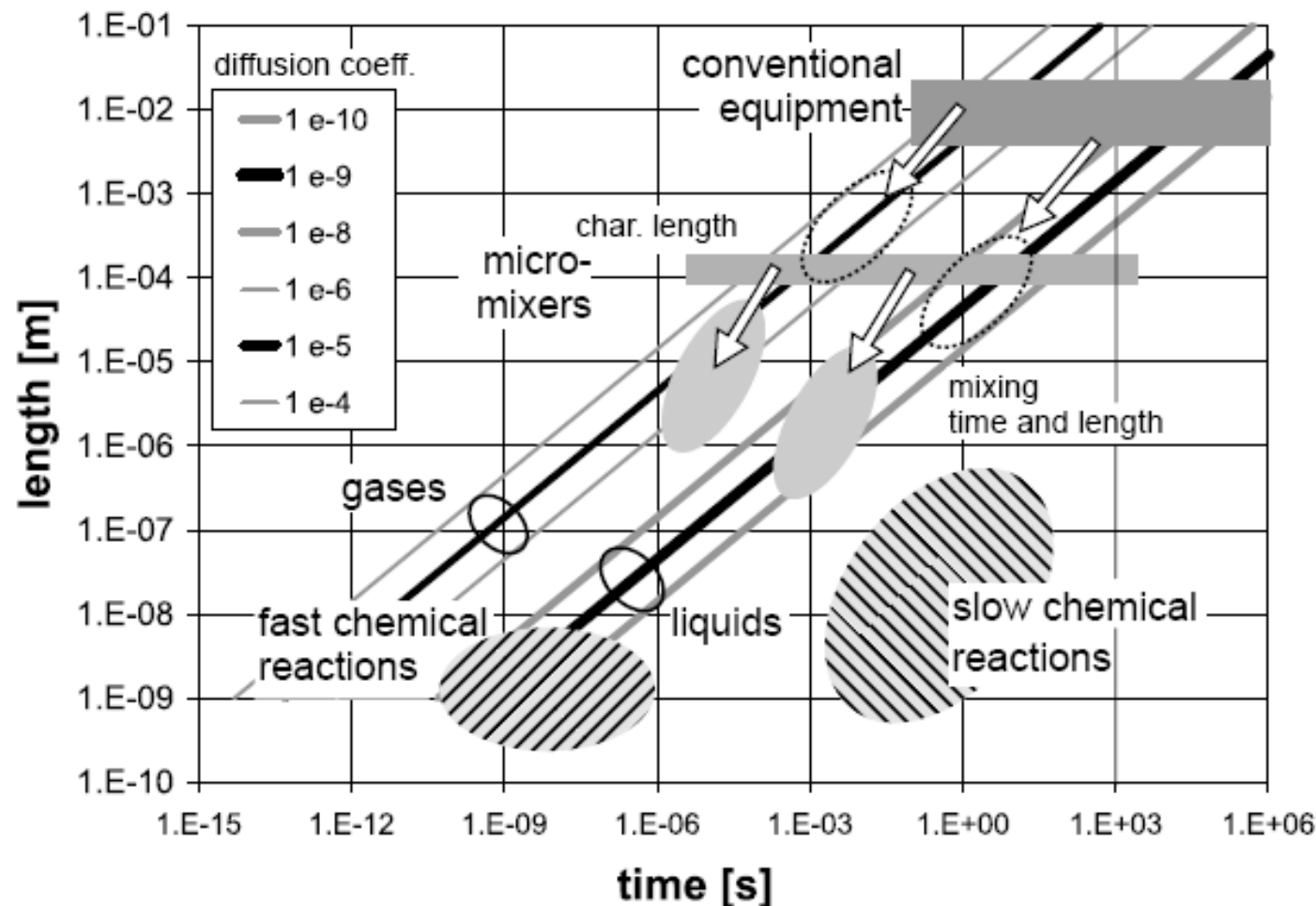
$$x^2 = 2 D t$$

The transport lengths by diffusive mixing in gases ( $D = 10^{-6} \text{ m}^2/\text{s}$ ) and in liquids with low viscosity ( $D = 10^{-10} \text{ m}^2/\text{s}$ ) are shown in the next figure.

In general, the shorter the length, the shorter the characteristic time for transport processes will be, and the higher the transformation frequencies.

$$x^2 = 2 D t$$

For diffusion of a species in a surrounding fluid, the typical diffusion length within one second is approx. 7 mm in gases (air) and approx. 70  $\mu\text{m}$  in liquids such as water.



Characteristics length and time scales for mixing in  
microstructured devices with chemical reaction

Conventional equipment has typical geometries in the range of centimeters and produces fluid structures in the range from 100  $\mu\text{m}$  to 1 mm. The corresponding diffusion time in gases is approx. 1 ms and in liquids in the range of 1 s.

Microstructured devices with typical length scales from 100  $\mu\text{m}$  to 1 mm provide fluid structures with length scales of approx. 1  $\mu\text{m}$ . These small fluid structures lead to mixing times shorter than 100  $\mu\text{s}$  in gases and approx. 1 ms in liquids.

This is the main reason for the enhanced selectivity and high yield of chemical reactions in microreactors.

The conduction length - from the basic balance equation

$$\text{momentum } x_p = \sqrt{2\nu t} \quad \text{heat transfer } x_q = \sqrt{2\alpha t}$$

Thermal diffusivity  $\alpha = \frac{k}{\rho c_p}$  m<sup>2</sup>/s

k = Thermal conductivity

$\nu$  = Kinematic viscosity =  $\mu/\rho$  , m<sup>2</sup>/s

Einstein-Smoluchovski equation

$$x^2 = 2 D t$$

The characteristic time is proportional to the square of the length variation and to the transport coefficient

Information about typical length and time scales for fast chemical reactions like neutralizations or slow chemical reactions such as polymerization are required to compare the processes.

The mass transfer in micromixers acts on a length scale of a few microns within milliseconds or less.

Different time scales are typical for partial reactions in complex reaction systems.

With properly designed micromixers and an adjustment of the component concentration, the selectivity of a complex reaction can be increased.

Important - the scale of fluid residence time within the device.

Within small devices, the fluids rest only briefly (seconds or less), which can be detrimental to slow reactions. A slow reaction may be incomplete at the channel outlet.

Fast reactions require short and small channels and a sufficiently high number of channels. They benefit from the rapid mixing and heat exchange.

Reactions with slower side-reactions or unstable intermediates show higher selectivity and higher yield in microstructured devices.

Reactions with high energy demand or release are suitable for micro devices.

The heat transfer in a straight channel with laminar flow is described by a constant Nusselt number Nu,

$$Nu = \frac{h d_h}{k} = 3.65$$

for constant wall temperature.

With smaller channel diameter  $d_h$ , the heat transfer coefficient  $h$  increases.

Additionally, convective effects in bent channels can increase the Nusselt number for better performance but also increase the pressure loss

The fluid temperature  $T$  in the channel quickly approximates the wall temperature according to the following equation

$$T(x) \propto e^{-x/l_h}$$

with the characteristic length of

$$l_h = \frac{m c_p}{3.65 \pi k}$$

Combining the channel distance and the mean residence time

with the mean velocity  $x = \bar{w}t$

Solve the wall temperature relation for the time-dependent temperature change to obtain the fluid temperature

$$T(t) \propto e^{-t/t_h}$$

The characteristic time,  $t_h$  is defined as

$$t_h = \frac{\rho c_p d_h^2}{3.65 \pi k}$$

With decreasing channel diameter, the fluid temperature exponentially approaches the wall temperature.

Efficient heat transfer is also important for **high exothermic chemical reactions** to transport the heat away from the reaction zone and to avoid hot spots.

The **high surface-to-volume ratio** is also responsible for the fast heat transfer in microchannels.

Additionally, a high surface-to-volume ratio is beneficial for **surface reactions** such as heterogeneous catalysis, emulsification or transport-limited processes

With unsteady heat transfer, the characteristic time  $t$  for heating or cooling of a body is proportional to the temperature difference and the ratio of the heat capacity  $mc_p$  to the heat transfer  $h A$  within the environment.

$$t = \frac{mc_p}{hA} = \frac{\rho c_p V}{hA} = \frac{\rho c_p}{ha_V} \propto \frac{\rho c_p}{h} \cdot d_h$$

$h$  is the heat transfer coefficient,  $A$  the surface area

With a smaller length scale  $d_h$ , the surface-to-volume ratio  $a_V$  increases and this characteristic relaxation time  $t$  becomes shorter.

# Lecture 2

## Microscale Manufacturing Practices

# Review

Mass transfer in micromixers acts on a length scale of a few microns within milliseconds or less.

Fast reactions require short and small channels and a sufficiently high number of channels, problems for slow reactions.

Combined reactions with slower side-reactions or unstable intermediates will show a higher selectivity and higher yield in micro-structured devices.

Reactions with high energy demand or release are suitable for micro-devices.

In the case of chemical reactions in microchannels, the **mixing patterns** can be controlled very effectively.

Hence **mass transfer limited reactions** are well-suited.

The characteristic dimensions of microreactors are in the range from **50 to 500 µm**, which produces a high specific surface and allows effective heat and mass transfer.

For continuously operating microstructured reactors, heat transfer, temperature control, mixing and residence time characteristics, are optimal for **a channel diameter of approx. 200 µm.**

## Two Approaches in Micro/Nano Manufacturing

Top-down processes: one starts on the macro scale and proceeds to create fine features by processing the bulk on a fine scale - Microelectronics

More expensive as the feature dimensions become smaller

Bottom-up processes: starts at the smallest possible scale, at the atoms and molecules themselves, and builds complexity up from there. Processes controlled by self-assembly

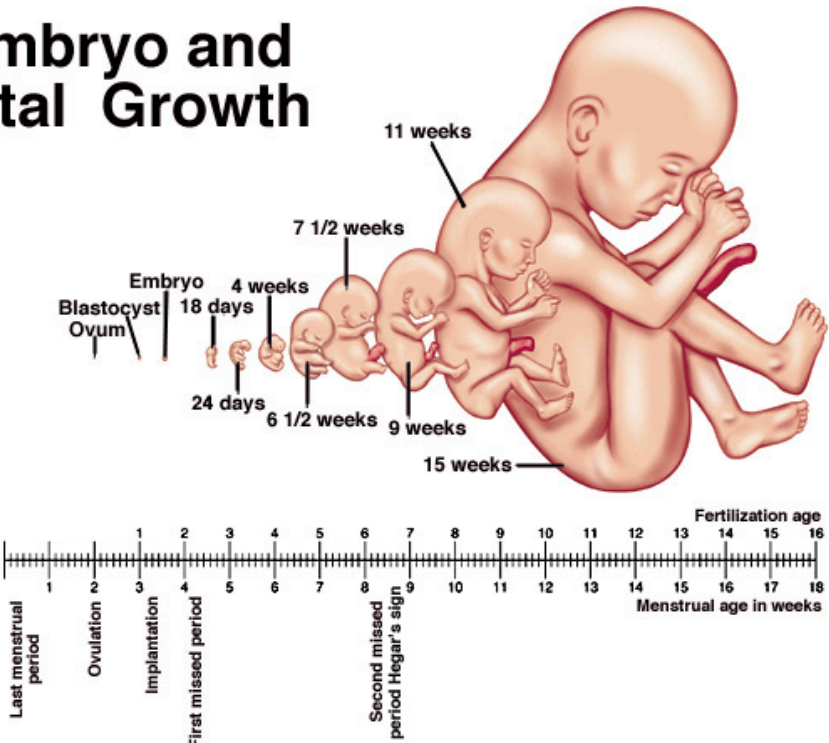
Embryology is the ultimate bottom-up process of producing a macro-scale complex entity by manipulation at the smallest scale possible.

# Micro-Nano Manufacturing



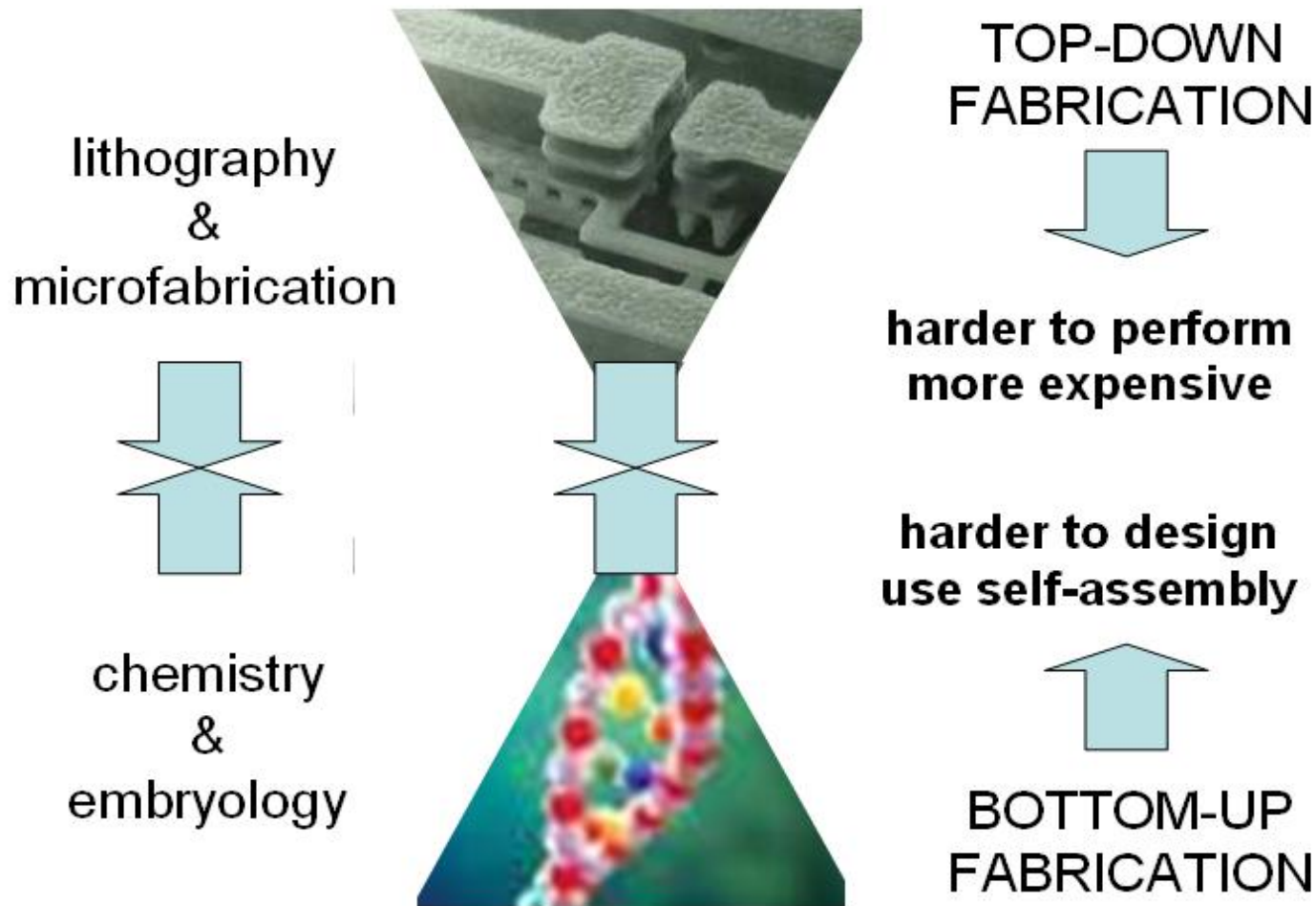
Byer/Shainberg/Galliano *Dimensions Of Human Sexuality*, 5e. Copyright © 1999. The McGraw-Hill Companies, Inc. All Rights Reserved.

## Embryo and Fetal Growth



Kailash Temple, Ellora

# Top-down and Bottom-up Processes



# Lithography – Basics

## Photolithography – Printing with Light

- Lithography is a process that uses focused radiant energy on chemical films that are affected by this energy to create precise temporary patterns in silicon wafers or other materials.
- These temporary patterns can be used to add or remove material from a given area

# Lithography - Basics

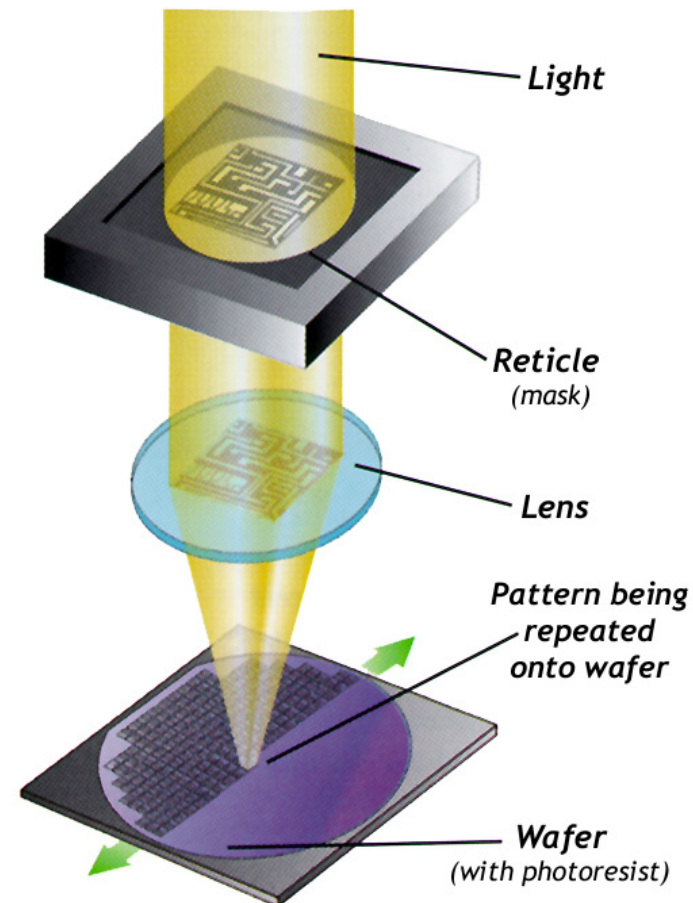
- Lithography in the top-down approach
  - Lithography
  - Etching
  - Deposition
  - Doping
- In order to perform the other 3 processes, we must precisely define where to perform these operations
  - Lithography Does This

# Role of Lithography in the Process

- With multiple etch, deposition, and doping processes taking place in the fabrication of a device, the lithography process is repeated many times.
- The precision and accuracy of lithography in the manufacturing process controls the success in building a device.

# Overview of the Photolithography Process

- Photolithography uses light energy passing through a patterned mask
- The light is focused onto the photosensitive surface
- Chemical changes in the surface coating occur
- Subsequent chemical development creates a temporary pattern on the surface.



# Photolithography –Printing with Light

## STEPS

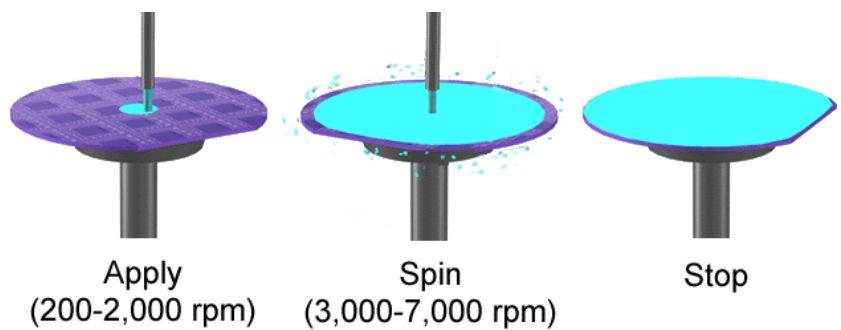
1. Cleaning - RCA cleaning/Peroxide cleaning
2. Preparation – Heat + adhesion promoter
3. Photoresist application – Spin coating + baking -  $\mu\text{m}$
4. Exposure and developing – UV + Metal ion free developers + post exposure bake
5. Etching – wet (liquid, isotropic) and dry (plasma, anisotropic)
6. Photoresist removal – resist stripper or plasma with  $\text{O}_2$

Limited by the wavelength of the light and the lens system  
minimum feature sizes 50 nm.

# Steps in Lithography

- Silicon wafers are commonly used substrates in the top-down process.
- The first step is to coat the clean surface of the wafer with a light sensitive chemical emulsion known as photoresist

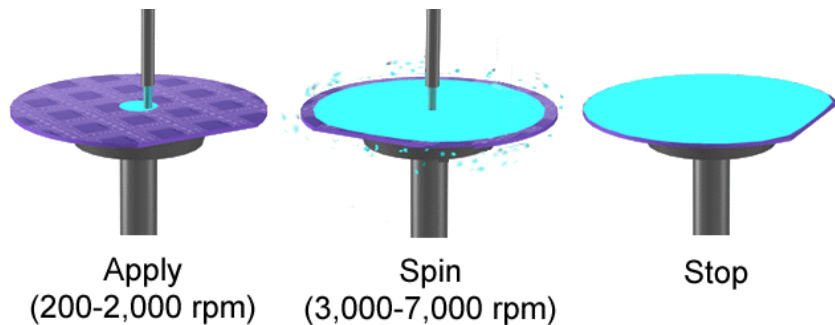
Photoresist Dispensing (Spinners)



# Steps in Lithography

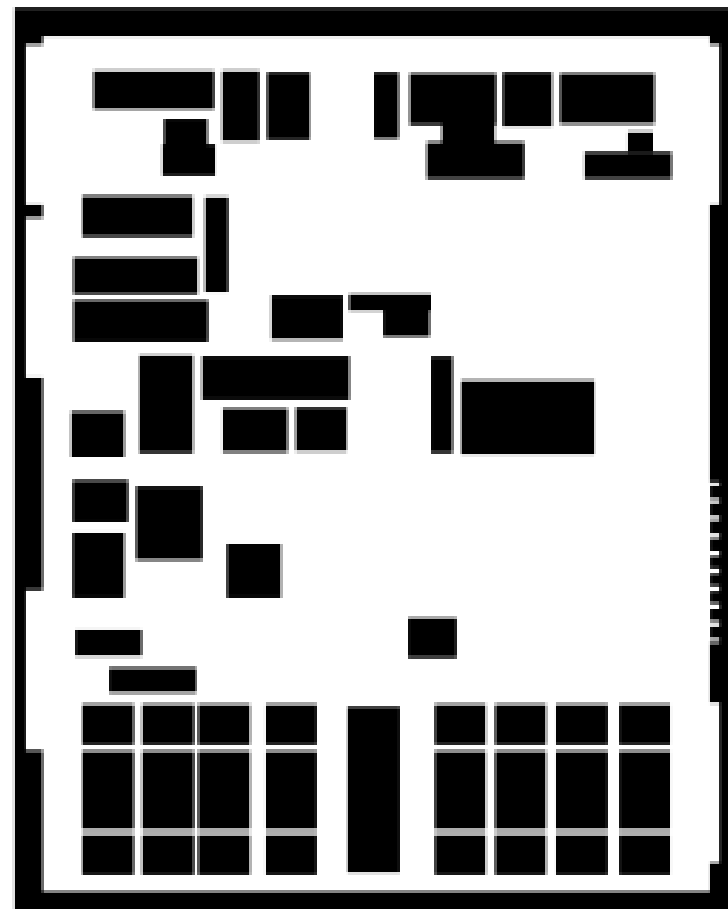
- Baking the resist causes it to form a solid layer.
- The chemical properties of the photoresist define what wavelengths of light will affect it.

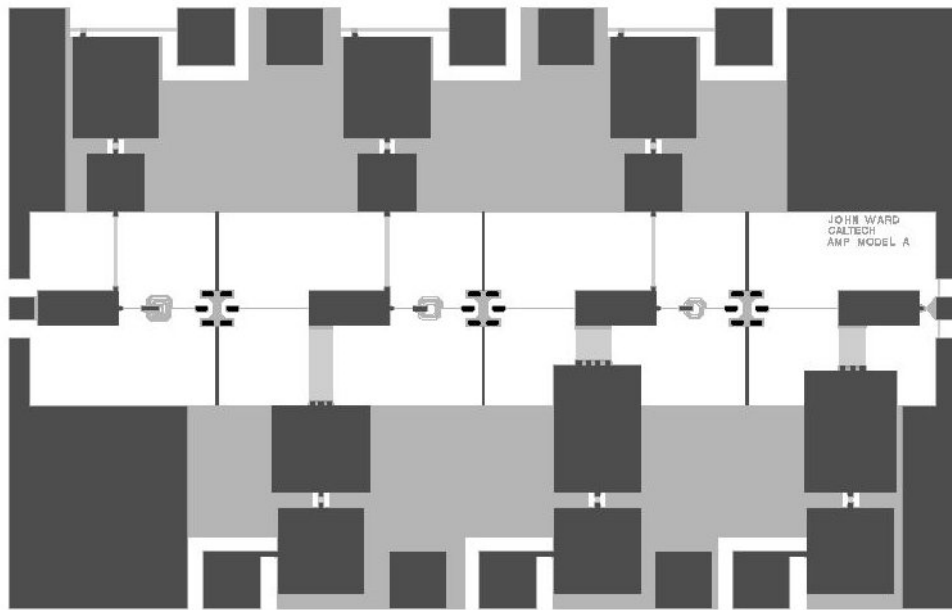
Photoresist Dispensing (Spinners)



# Steps in Lithography

- A photomask, typically made of quartz with a chrome plating, controls where the radiant energy will strike the photoresist.
- Photomasks are often made with electron beam patterning tools



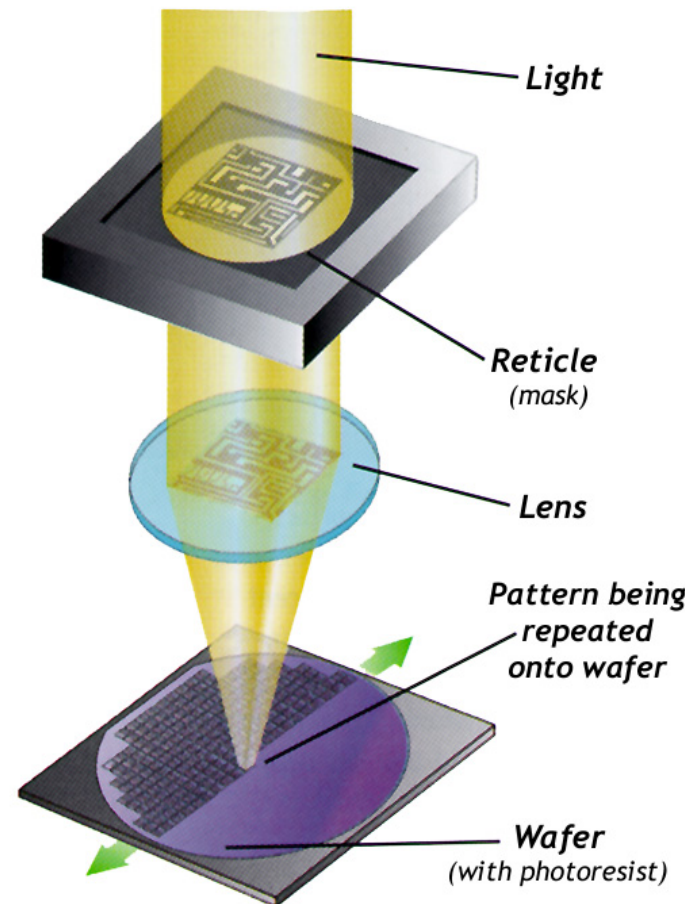


CAD layout of an entire circuit, eventually going to be reduced to fit on a chip 2.5 x 3.8 mm

On a single chip, the width of those connecting lines in there is going to 0.014 microns or so. That's the limiting factor in device density today — the width on the chip of the smallest line we can transfer from a CAD layout pattern into actual metal on silicon.

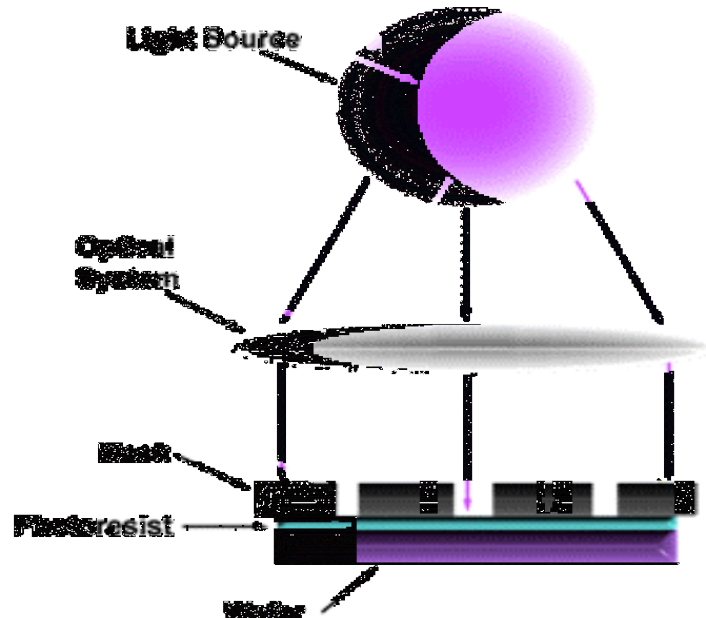
# Steps in the Lithography Process(3) - Exposure

- Exposure of the photoresist to the radiant energy pattern occurs next
- There are several ways to do this
  - Contact/proximity printing
  - Projection printing (shown here)
  - Projection scanning



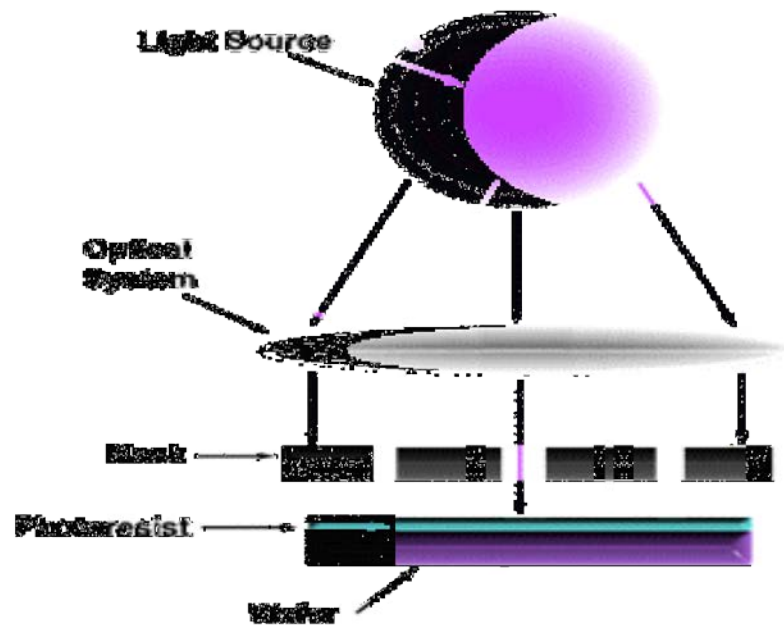
# Contact Printing

- The mask is directly in contact with the wafer
- Advantages
  - Simple
  - Low Cost
- Disadvantages
  - Poor for small features
  - Mask damage may occur from contact
  - Defects from contaminants on mask or wafer due to contacting surfaces



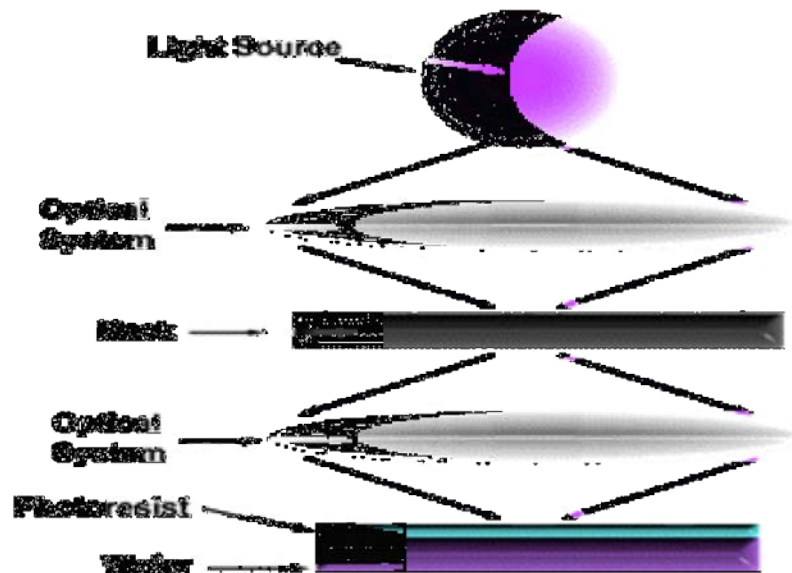
# Proximity Printing

- The mask is above the wafer surface
- Advantages
  - Mask damage is minimal
  - Good registration possible
- Disadvantages
  - Poorer resolution due to distance from the surface
  - Defects from contaminants on mask or wafer due to contacting surfaces
  - Diffraction errors



# Projection Printing (1)

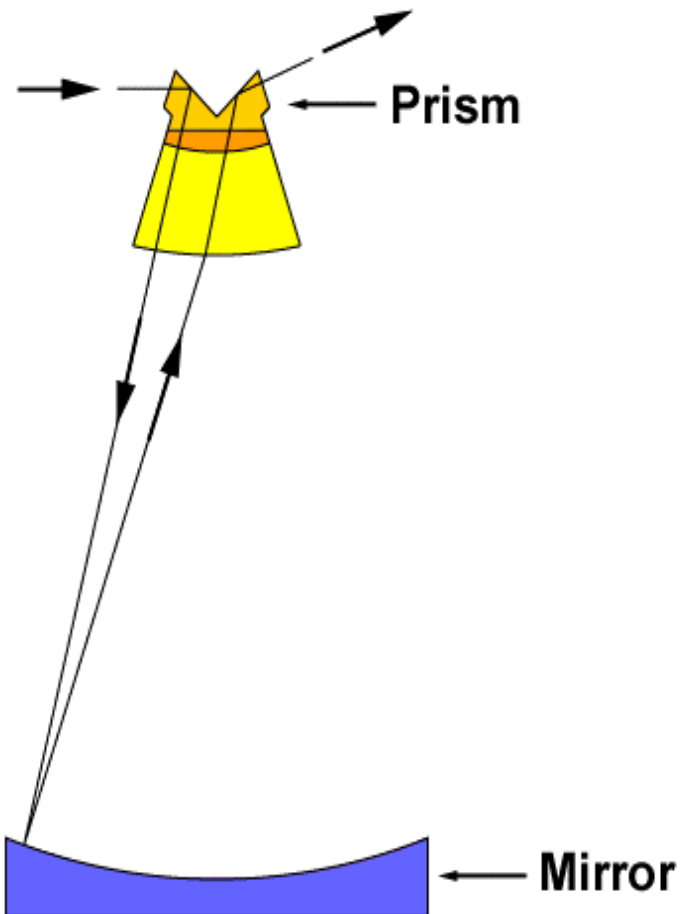
- An optical system focuses the light source and reduces the mask image for exposure on the surface
- Advantages
  - Higher resolution
  - Lens system reduces diffraction error
- Disadvantages
  - Errors due to focus of lens system may occur
  - Limiting factor in resolution can be due to optical system



The minimum feature size  $F = K$  (wavelength/NA) where  $K$  = process constant typically about 0.5. Numeric aperture is typically less than 1.

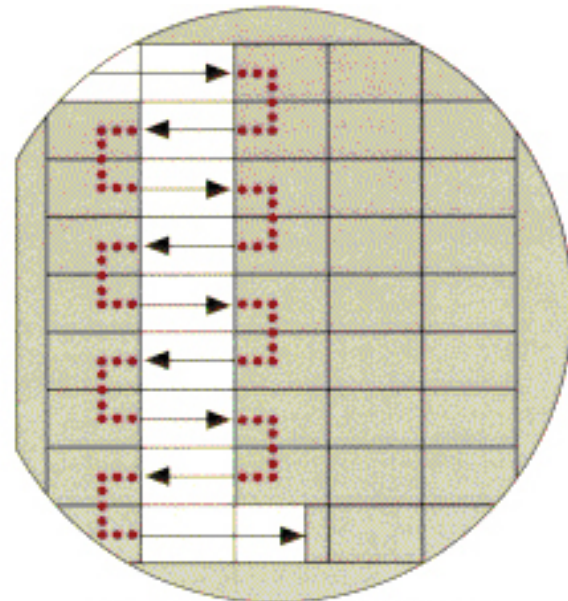
# Projection Printing (2)

- Step and repeat aligner
  - Lens reduction
  - Good throughput but resolution limited to about 0.35  $\mu\text{M}$
- Cadiotropic System
- Mirror, folding prisms and lenses 1:1 ratio
- Less common than steppers



# Step and Scan Aligner

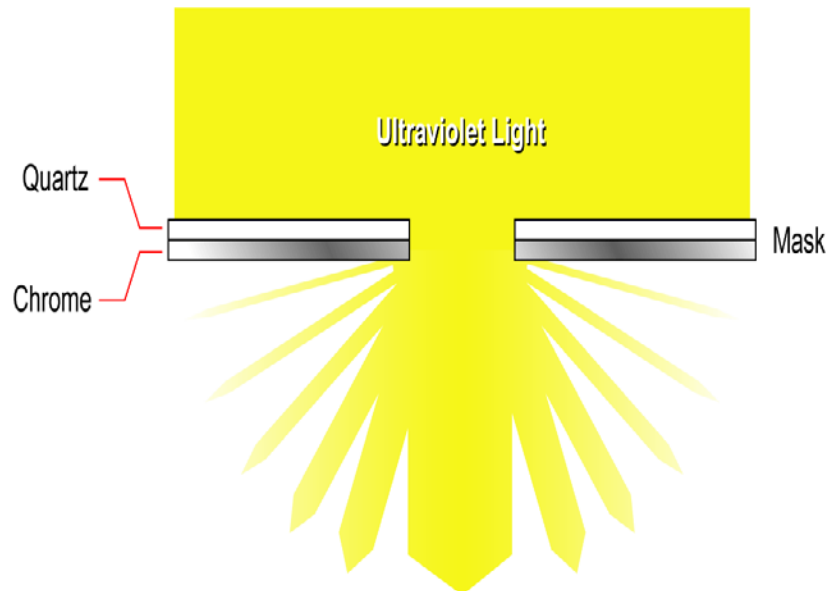
- Uses a spherical mirror and a scanning pattern
- Advantages
  - Improved throughput
  - Lens system aberration minimized
- Disadvantages
  - Complex motion system is required for alignment and precise tracing
  - Light source wavelength is still a factor limiting feature size



Courtesy of Silicon Valley Group

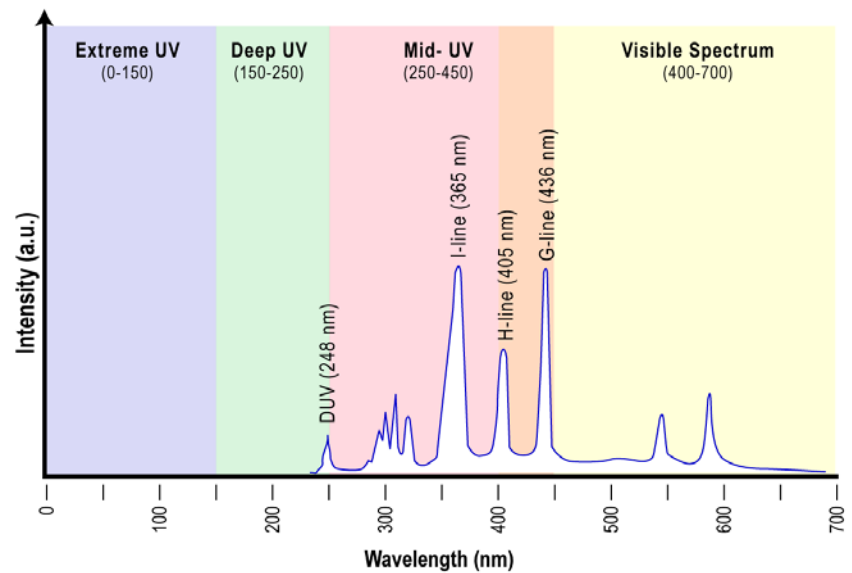
# Diffraction

- As feature sizes shrink in the mask, the wavelength of the light used as a source becomes a factor.
- Shrinking feature sizes require shorter wavelengths of light
- The photoresist must be optimized to match the light source used.



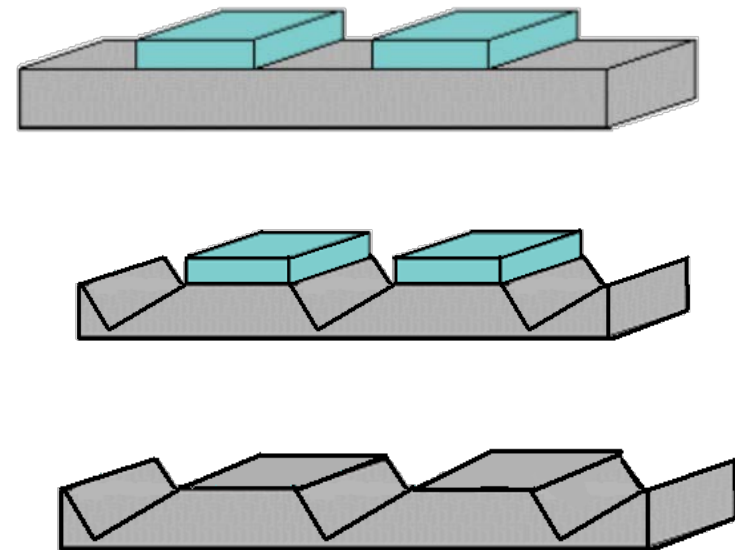
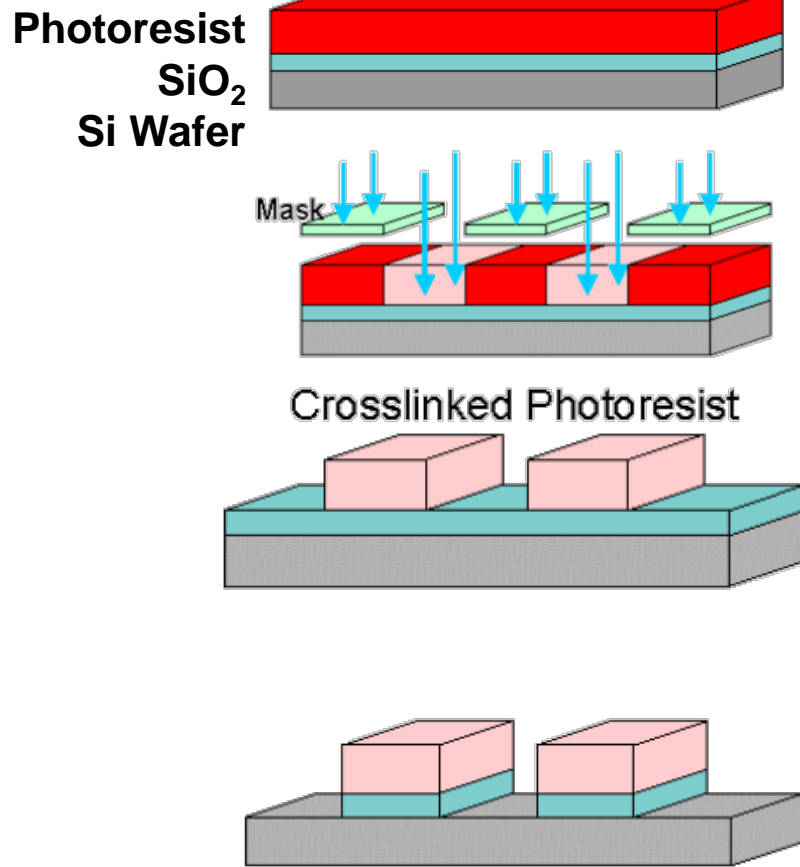
# Diffraction (2)

- The traditional mercury vapor lamp has peaks in certain ranges.
- The intensity of some UV peaks is low
- The photoresist must be optimized to match the light source used.



# Top-Down Approach

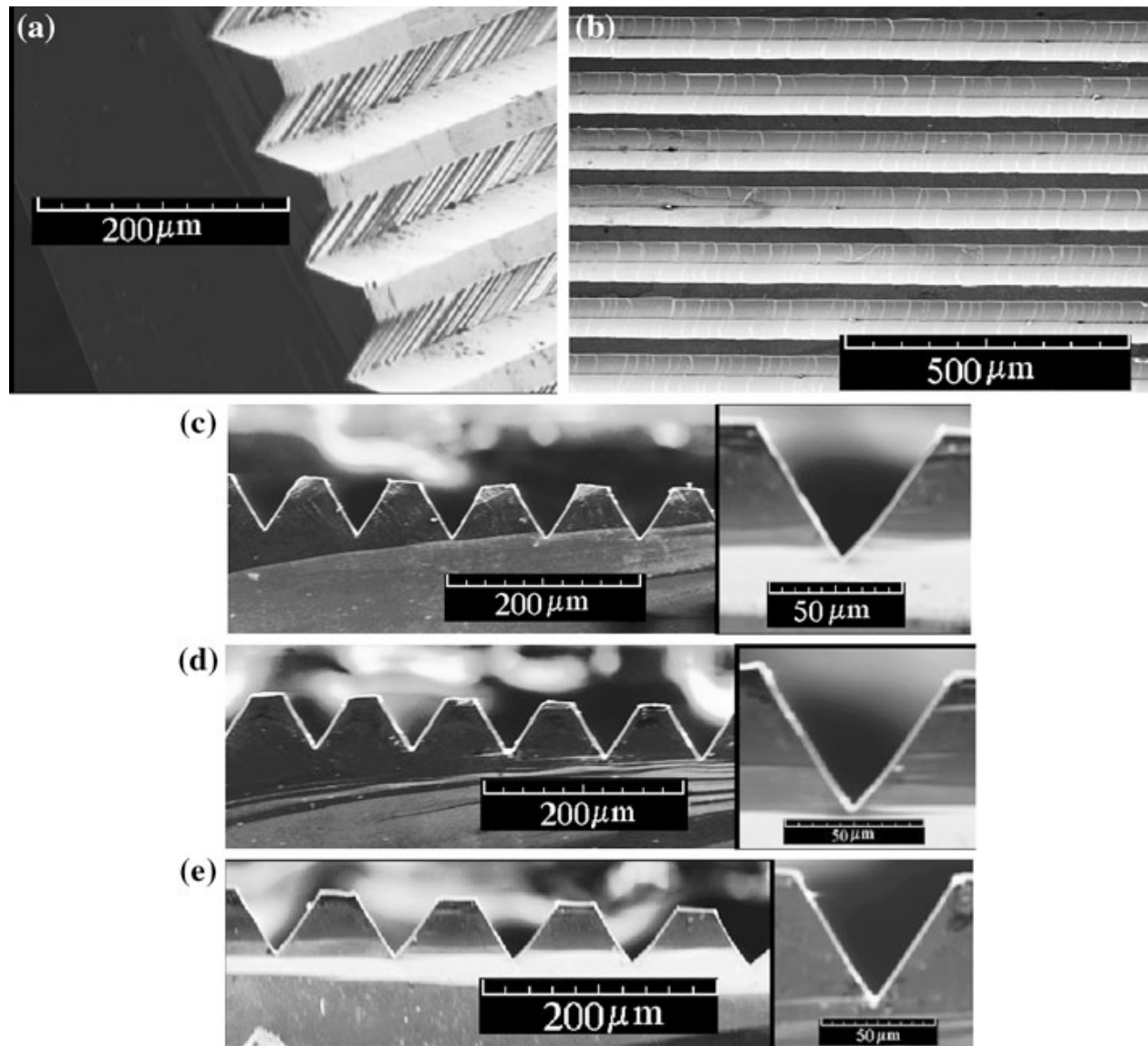
## Fabrication of V-grooves on Si wafer



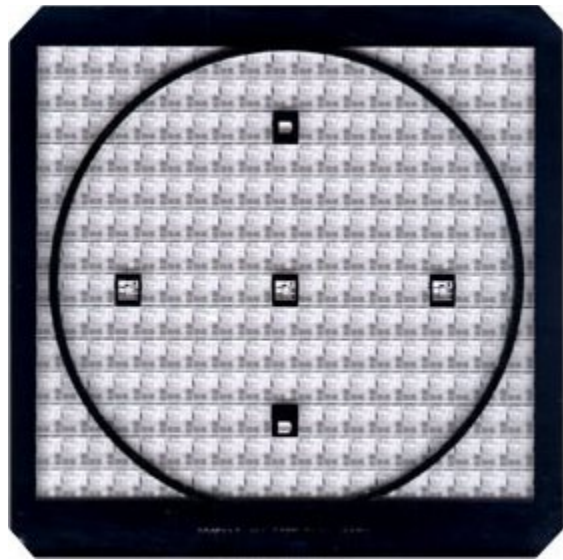
### Photoresist

- +ve - whatever shows, goes
- ve – opposite
- +ve - better process controllability for small geometry features. Popular in VLSI fabrication processes.

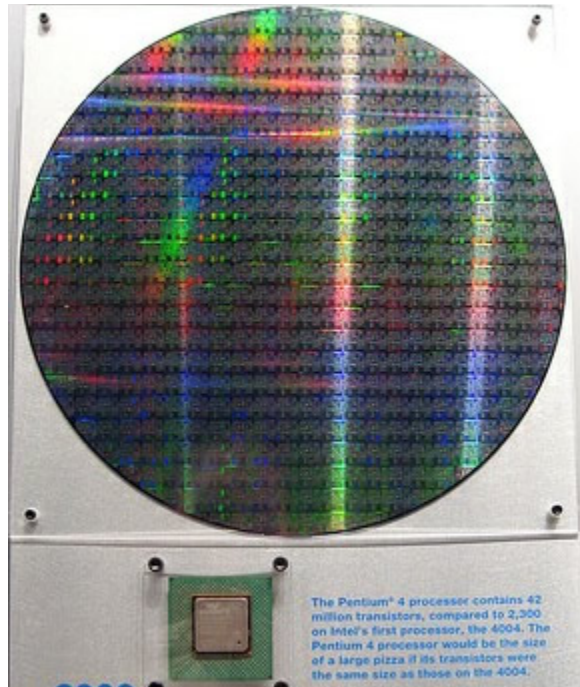
Photolithography, limited by the resolution of lithography



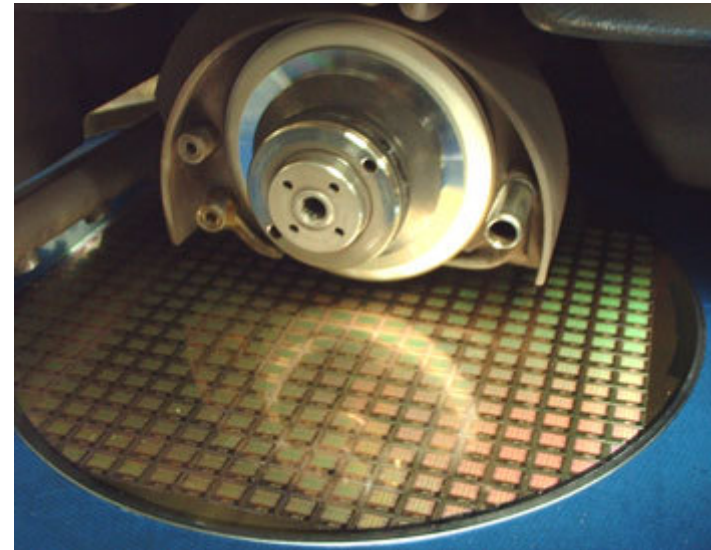
SEM of microgrooves on silicon substrate a - angular view of the microgrooves; b top view of the microgrooves; c-e Cross sectional views at three different locations along the length of microgrooves



Wafer mask for optical projection (one layer)



Wafer at the end of fabrication (many layers)

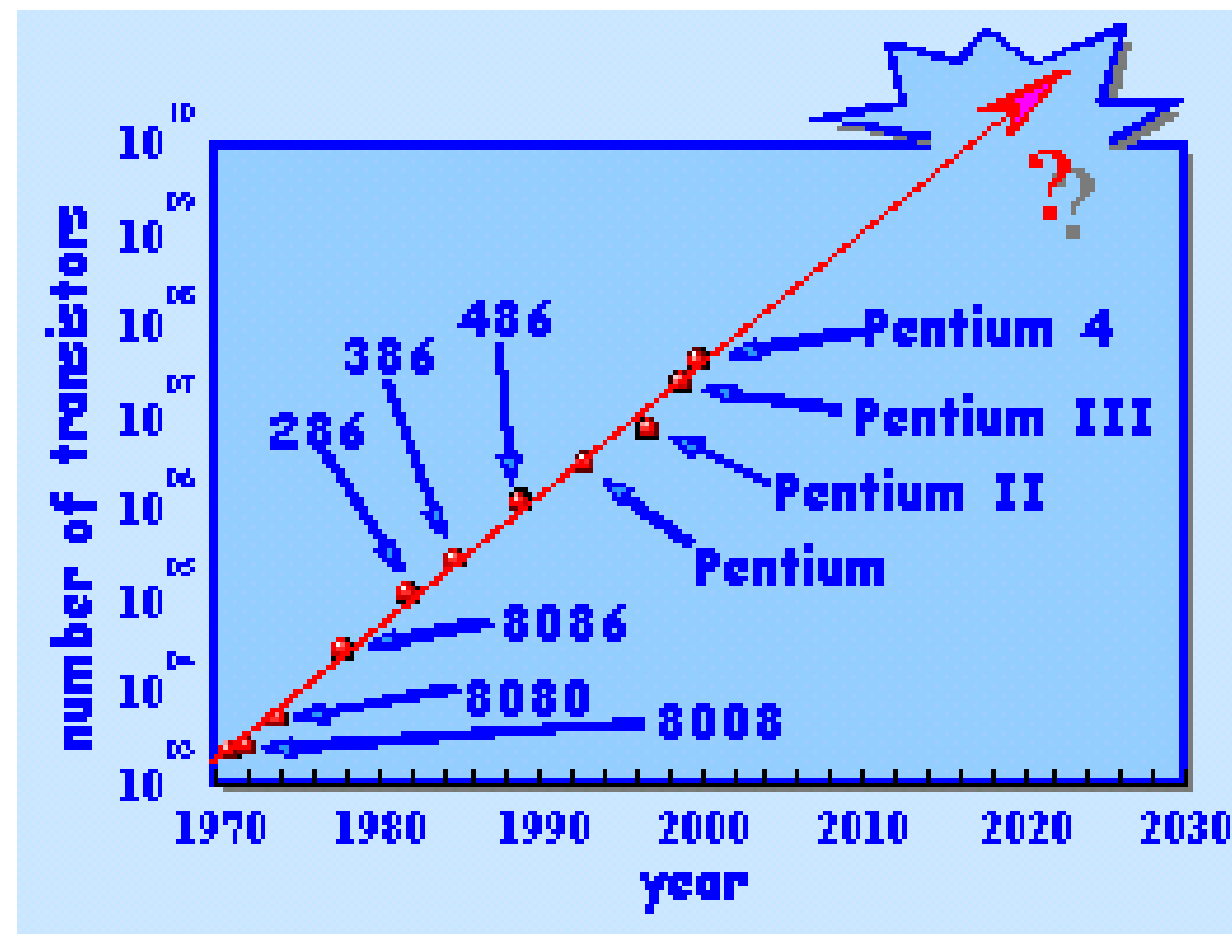


Wafer being cut up into chips after fabrication

**Picture of a wafer after all the photolithography steps (depositing, masking, etching) are done**

# Problems of Top-down Process

- Cost of newer technologies.
- Physical limits of photolithography
- heat dissipation

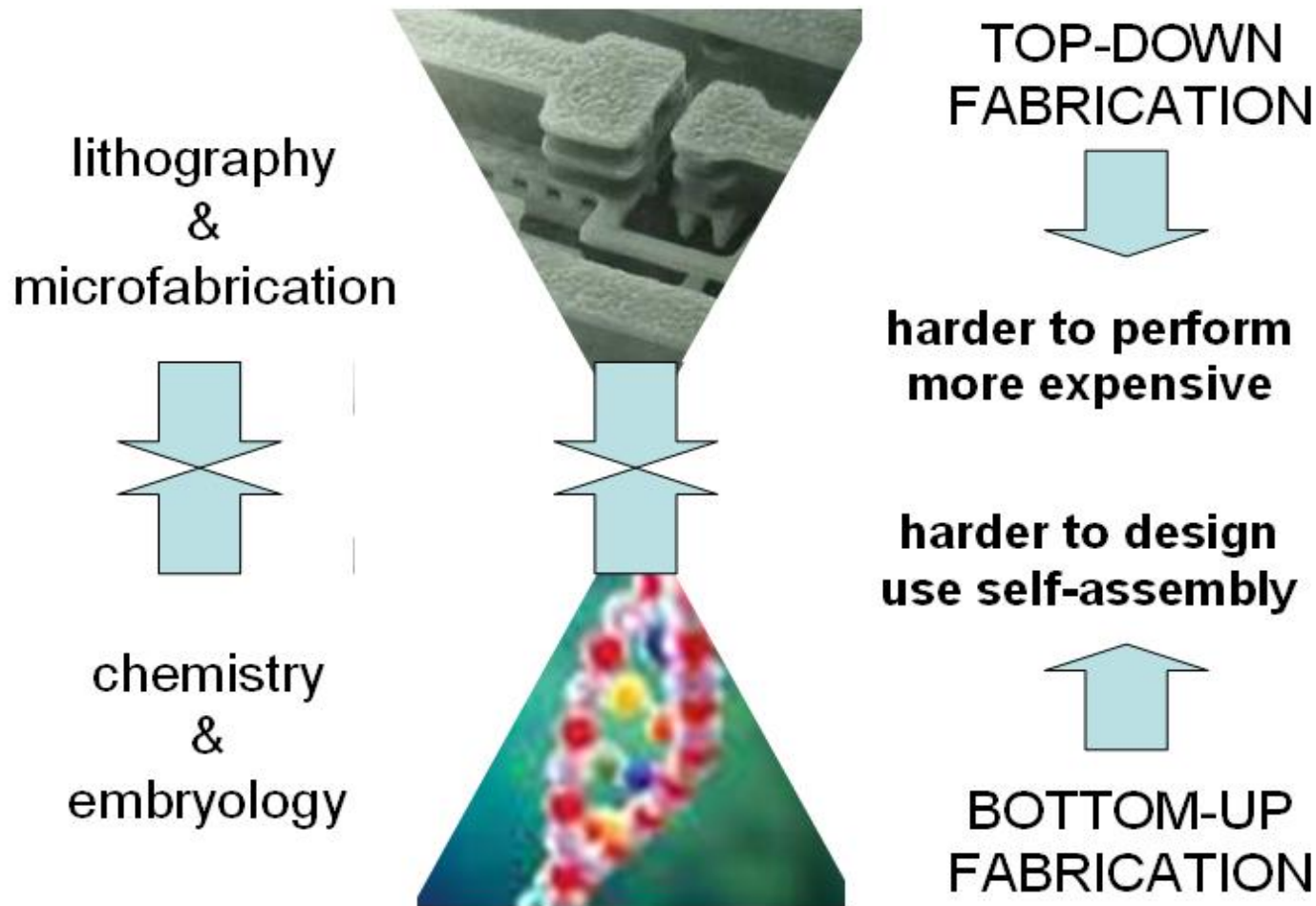


# Lecture 3

Microscale Manufacturing Practices

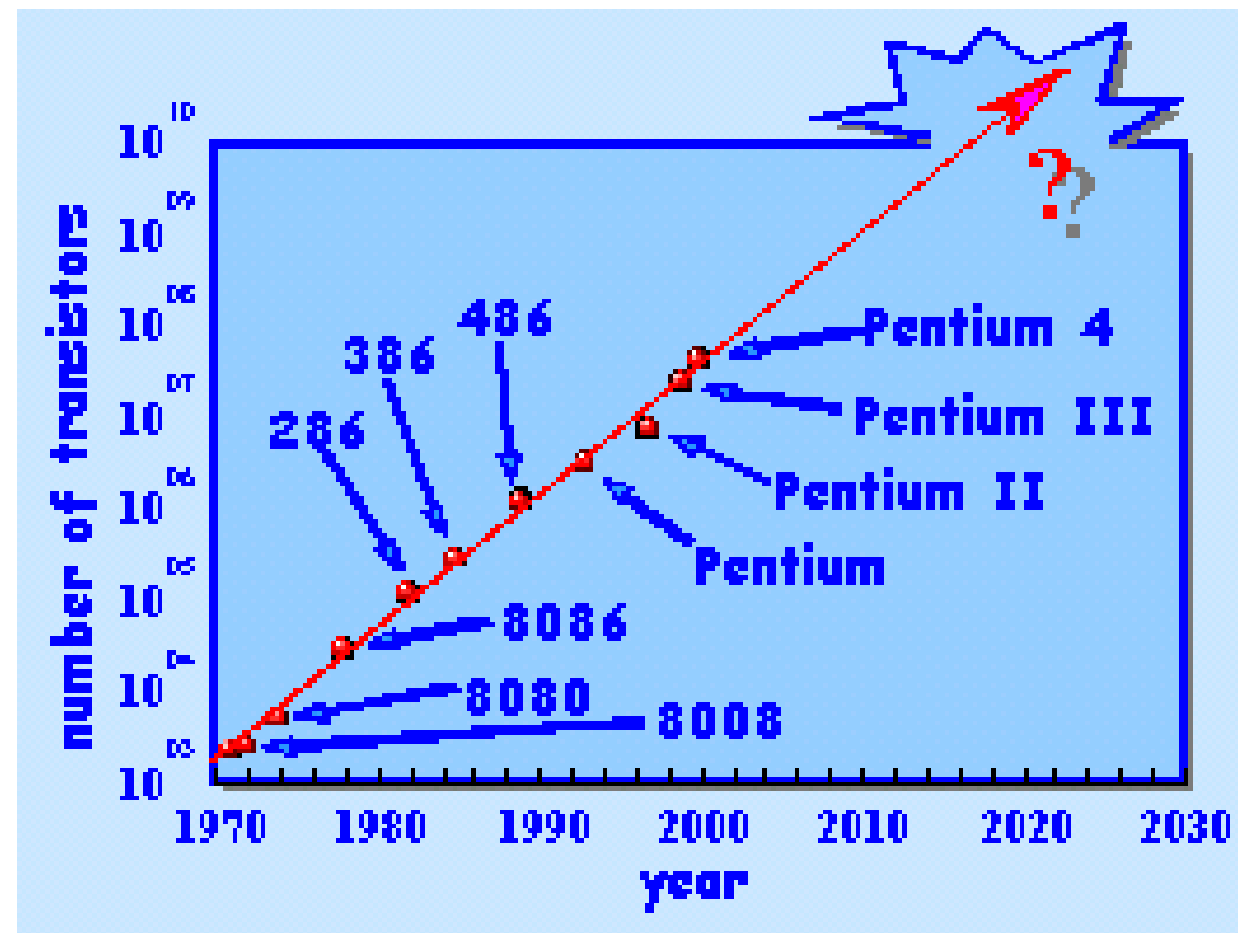
Bottom up Approach

# Top-down and Bottom-up Processes

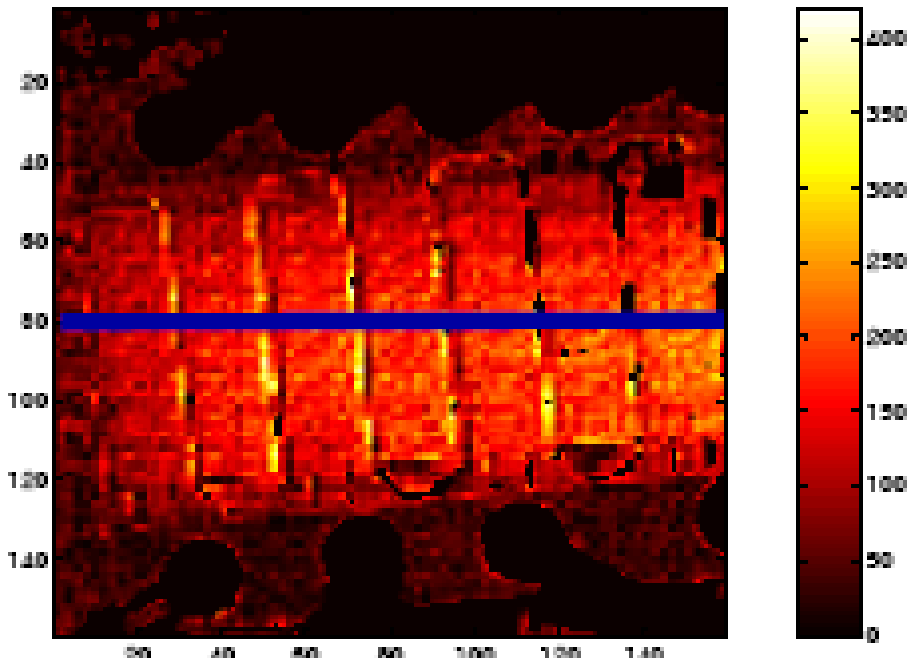


# Problems of Top-down Process

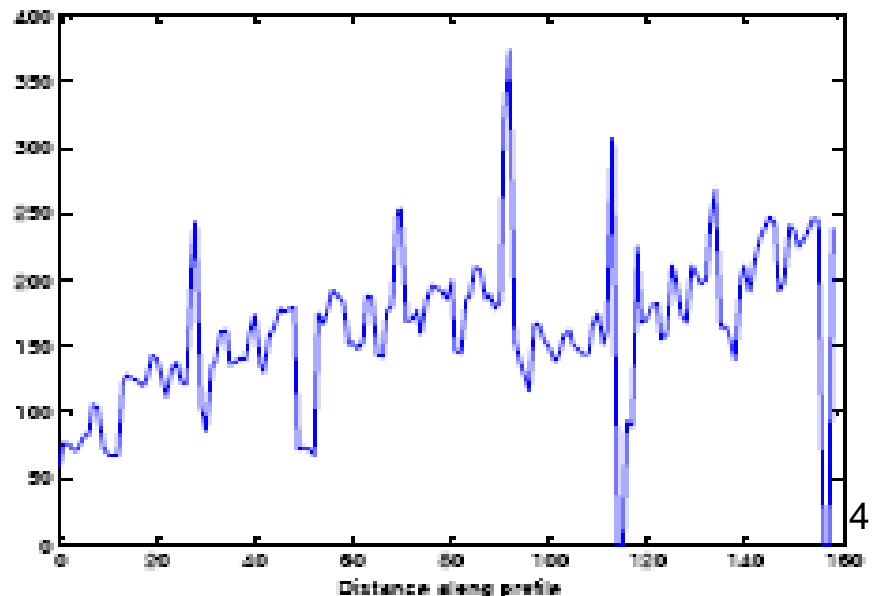
- Cost of newer technologies.
- Physical limits of photolithography
- heat dissipation



*Heat buildup is becoming one of the major limitations to creating tomorrow's more compact, complex micro devices".*



At 450 mA and 100  $\mu$ s on time and 1 KHz frequency



David Benson of Sandia National Laboratory's Advanced Packaging Department.

# Top-down Versus Bottom-up

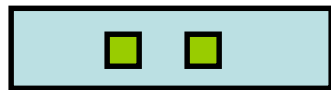
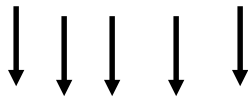
## Top Down Process



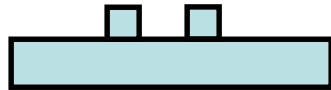
Start with bulk wafer



Apply layer of photoresist



Expose wafer with UV light through mask and etch wafer

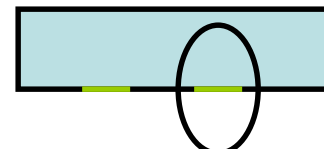


Etched wafer with desired pattern

## Bottom Up Process



Start with bulk wafer



Alter area of wafer where structure is to be created by adding polymer or seed crystals or other techniques.

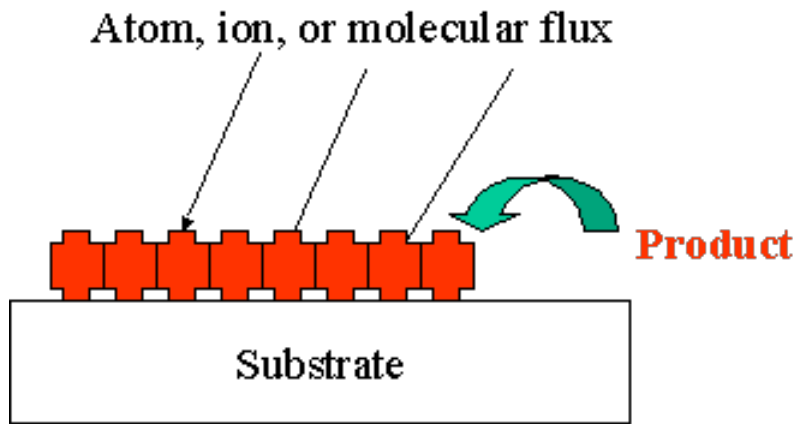


Grow or assemble the structure on the area determined by the seed crystals or polymer. (self assembly)

# Why is Bottom-Up Processing Needed?

- Allows smaller geometries than photolithography.
- Certain structures such as Carbon Nanotubes and Si nanowires are grown through a bottom-up process.
- New technologies such as organic semiconductors employ bottom-up processes to pattern them.
- Can make formation of films and structures much easier.
- Is more economical than top-down in that it does not waste material to etching.

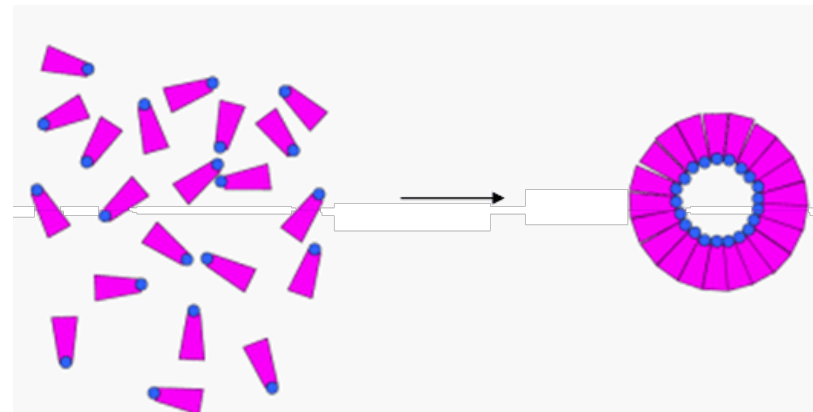
# Bottom-Up Approach



- The opposite of the top-down approach.
- The bottom-up approach selectively adds atoms to create structures.

# The Ideas Behind the Bottom-up Approach

- Nature uses the bottom up approach.
  - Cells
  - Crystals
  - Humans
- Chemistry and biology can help to assemble and control growth.



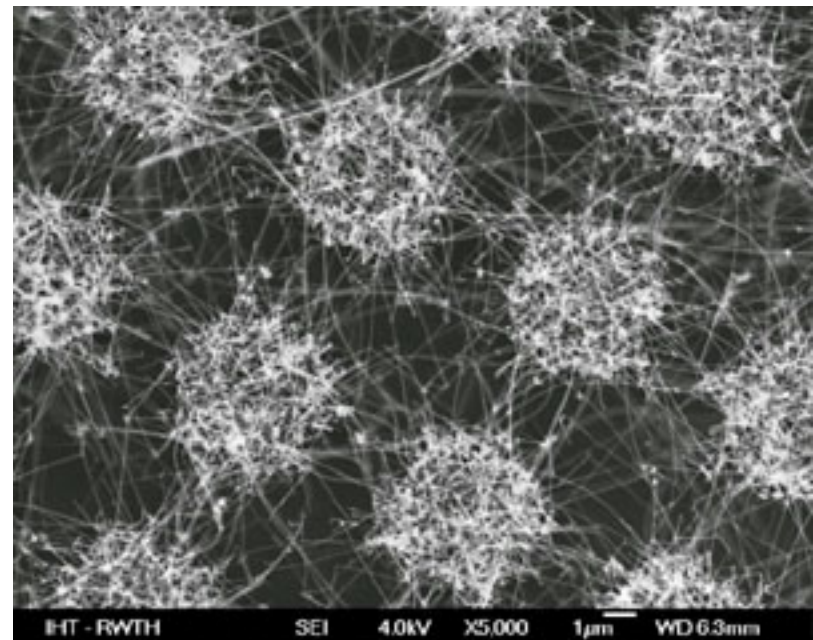
<http://www.csacs.mcgill.ca/selfassembly.htm>

# Self Assembly

- The principle behind bottom-up processing.
- Self assembly is the coordinated action of independent entities to produce larger, ordered structures or achieve a desired shape.
- Found in nature.
- Start on the atomic scale.

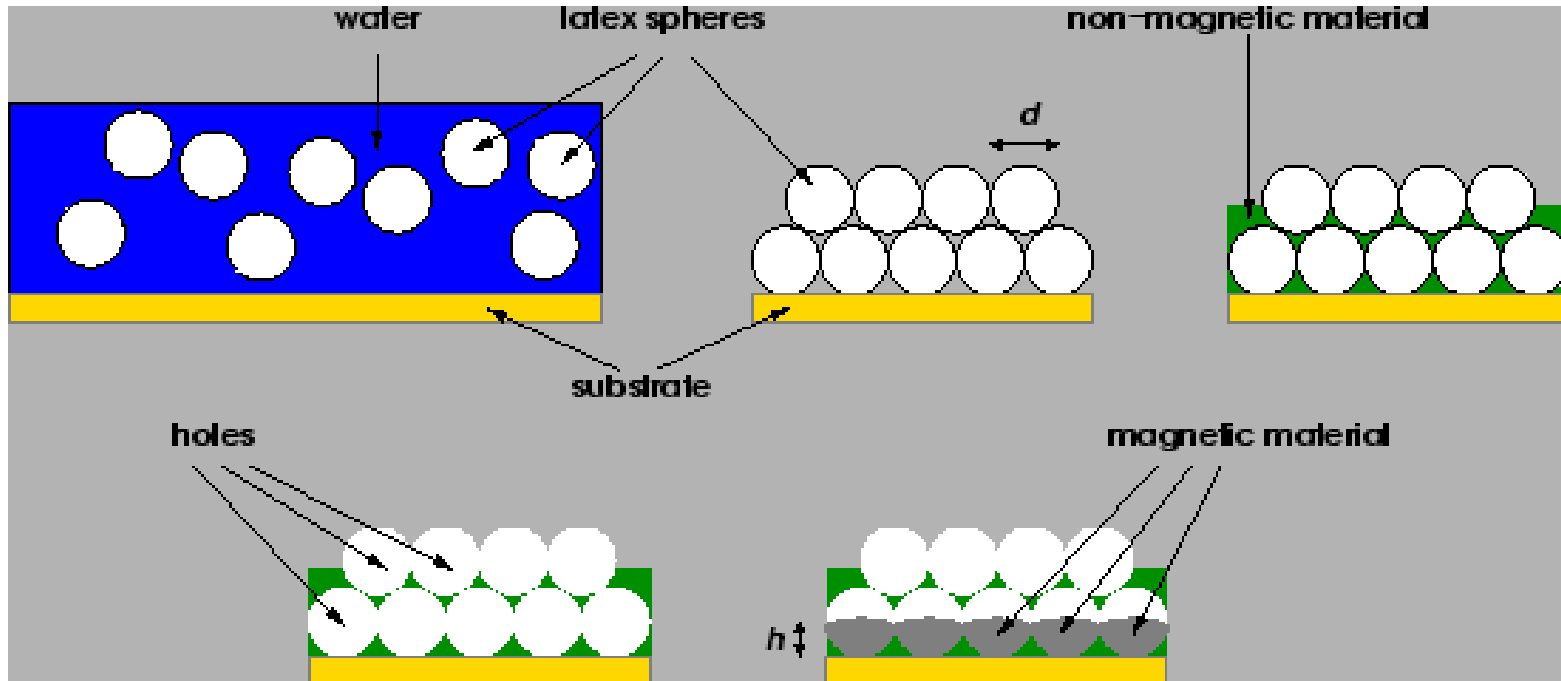
# Applications of Bottom-Up Processing

- Self-organizing deposition of silicon nanodots.
- Formation of Nanowires.
- Nanotube transistor.
- Self-assembled monolayers.
- Carbon nanotube interconnects.



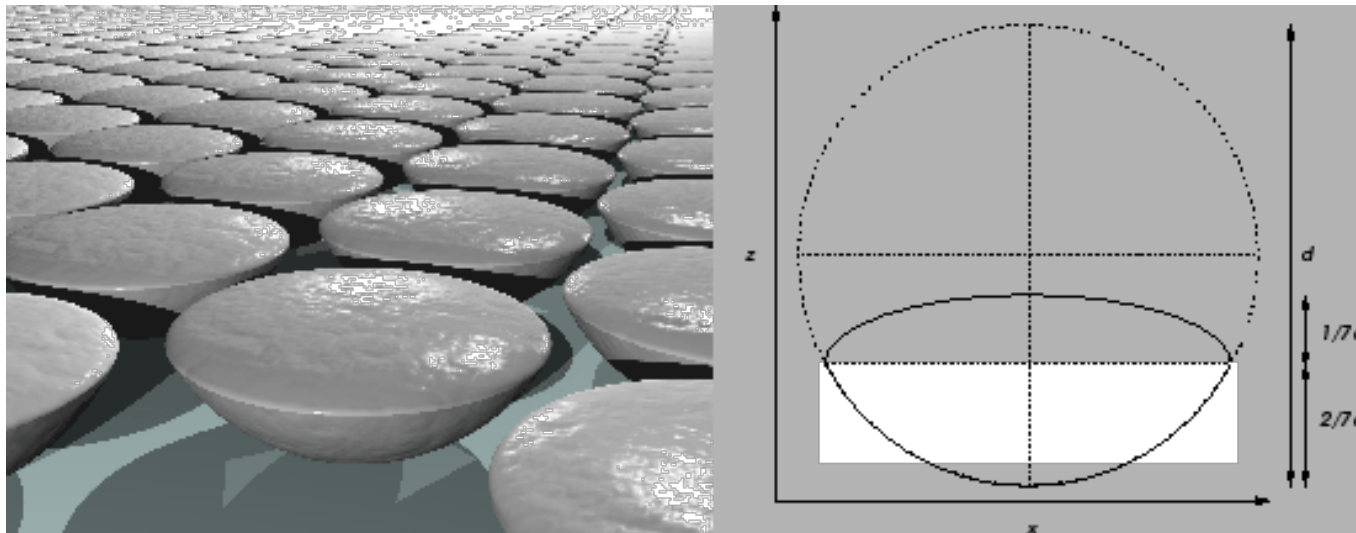
[http://web.ics.purdue.edu/~mmaschma/bias\\_image\\_gallery1.htm](http://web.ics.purdue.edu/~mmaschma/bias_image_gallery1.htm)

# Making of Nanodots



The **double-template self-assembly technique**. First, an aqueous suspension of latex spheres (top left) of diameter **d** is poured onto a substrate. As the water evaporates, the latex spheres are attracted to each other (top centre), forming a regular close-packed structure. This template can be filled with a non-magnetic material (top right) and the latex spheres etched away (bottom left). The resulting gaps can be filled with a magnetic material to a varying height **h** (bottom right) to form arrays of connected or disconnected part-spherical nanodots.

# Double-template self-assembly technique

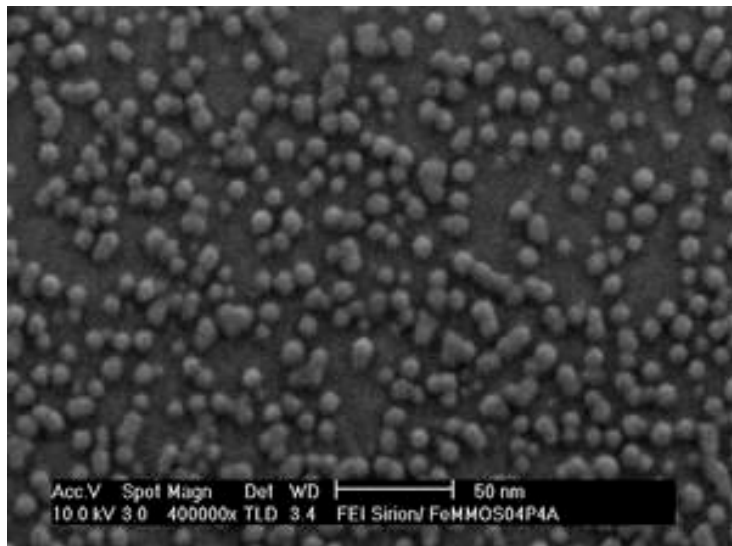


Using these templates, it is possible to create magnetic structures from sizes of 50nm to 1000nm by filling the spaces between the close-packed spheres with some material through electrochemical deposition.

By etching away the polystyrene spheres, another template is formed. This can then be filled with magnetic material, and by varying the fill amount of the resulting spherical holes, connected or disconnected arrays of dots can be formed. This is known as the **double-template self-assembly method**.

# Self-organizing Deposition of Silicon Nanodots.

High-density information storage



- Silicon nanodots are deposited onto silicon dioxide with no need for lithographic patterning.
- The nanodots can be thought of tiny magnets which can switch polarity to represent a binary digit.

[http://www.iht.rwth-aachen.de/en/Forschung/nano/  
bottomup/deposition.php](http://www.iht.rwth-aachen.de/en/Forschung/nano/bottomup/deposition.php)

Hard drives typically magnetize areas 200-250 nm long to store individual bits, while nanodots can be 50 nm in diameter or smaller

## Recent Developments

Silicon quantum dots (SiQDs) are semiconductor Si nanoparticles ranging from **1 to 10 nm**

Potential as optoelectronic devices and fluorescent bio-marking agents due to their ability to fluoresce blue and red light.

The methods for producing nanosized silicon particles include

1. Laser ablation and non-thermal plasma synthesis
2. Electrochemical etching, reduction of silicon halides, thermal destruction of silicon-rich oxides, hydrothermal decomposition of different Si-contained organic precursors, oxidation of sodium silicide, processing porous silicon etc

# Bottom-Up Approach

Developing a simple, efficient method to organize molecules and molecular clusters into precise, pre-determined structure

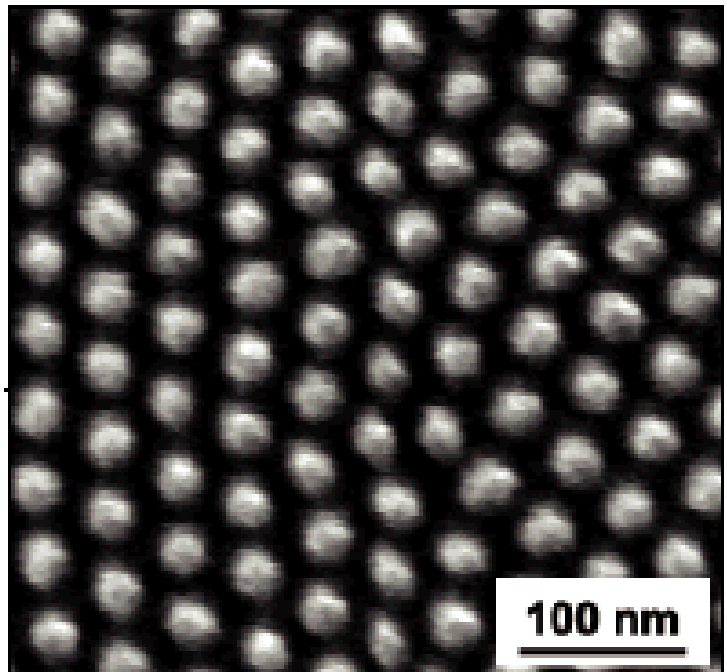
- Selectively adds atoms to create structures
- Nature - Cells, Crystals
- Chemistry and biology can help to assemble and control growth.

## Making Nanodots

Polymer template for nanodot

Self-assembled polymer film

Grow layer of desired material

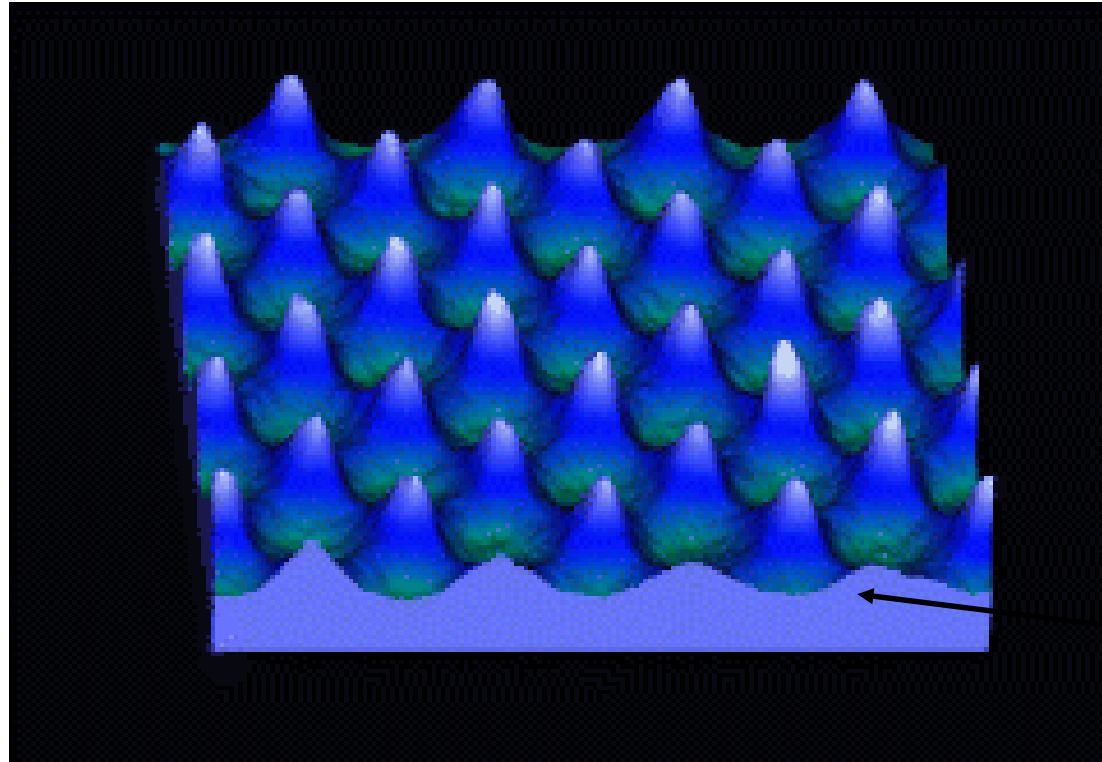


65 billion nanodots per square cm

## Self Assembled Nanodots

Each nanodot can hold one bit of information.

10 Trillion dots per square inch.



## Future: Nanodot-based Smartphone Batteries

**Energy storage** - extremely fast recharge, *nanodots*, chemically synthesized bio-organic peptide molecules that, due to their small size, improve electrode capacitance and electrolyte performance. The end result is batteries that can be fully charged in seconds.

It acts like a **supercapacitor** (with very fast charging), and on the other is like a **lithium electrode** (with slow discharge).

The electrolyte is modified with nanodots in order to make the multifunction electrode more effective.

## Summary

- Top-down processing – the prevalent choice - NOW
- Newer technologies for future products will require a bottom-up approach
- Combination of top-down and bottom-up processes to simplify fabrication?
- Self-assembly

## Process and Plant Design

The process and plant design procedure begins with a product idea or product formula, tested in the laboratory with stirred beakers or standard calorimeters.

The chemical recipes and protocols are developed, which must be transferred into a technical process.

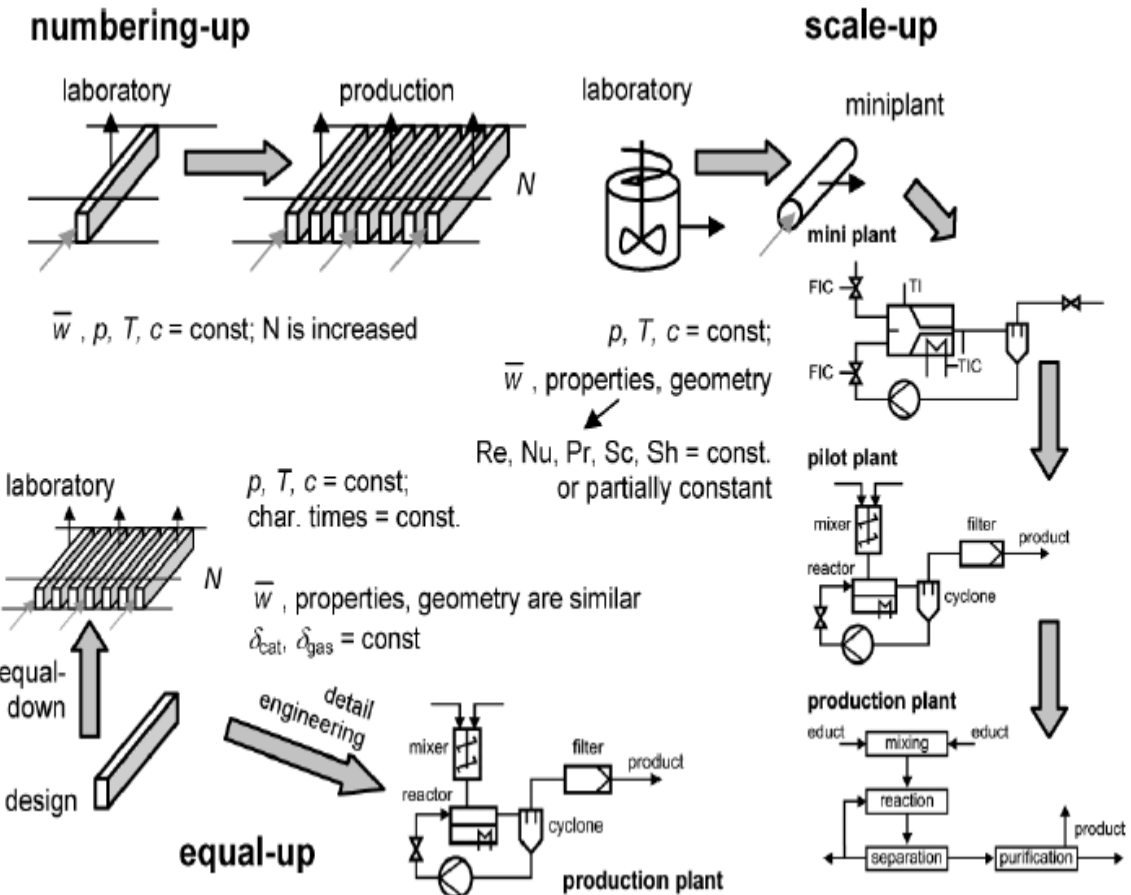
Conventional way,

Miniplant —→ Pilot Plant —→ Production facility

Right side of Figure

# Scale-up, Numbering-up

In conventional process engineering, the scale-up process is quite elaborate. Starting with laboratory experiments, the gained data are transferred to mini plants with almost the same length scale, but a more accurate representation of continuous flow processing.



The pilot plant provides feedback on a semi-industrial scale for the correct design of the final production plant. Wherever possible the process conditions of temperature, pressure and concentrations are kept constant.

Channels are the basic element of microstructured equipment, often with rectangular cross section.

Depending on the process conditions, such as temperature, pressure, and fluid properties, the channel cross section, catalyst layer (if necessary), and minimum numbers are determined on the basis of available fabrication technology and device material.

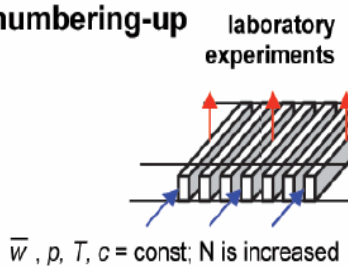
This process is called **equal-down**, because the small channel dimensions are determined according to the necessary heat and mass transfer and relevant chemical kinetics.

## equal-up or scale-out

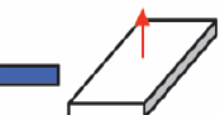
## microstructured devices

## scale-up

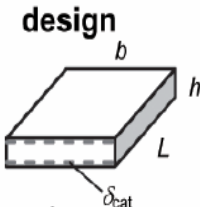
numbering-up



fabrication



equal-down



a)



flow

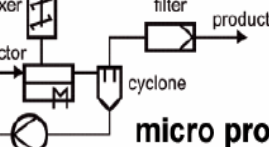
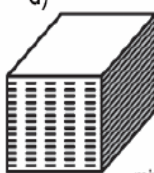
distribution



c)

engineering detail

equal-up



modified plant

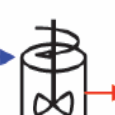
micro production plant

$p, T, c = \text{const}$ ; char. times = const.

$\bar{w}$ , properties, geometry are similar

$\delta_{\text{cat}}, \delta_l = \text{const}$

laboratory



$p, T, c = \text{const}$ ;

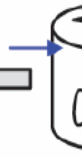
$\bar{w}$ , properties, geometry

$\text{Re}, \text{Nu}, \text{Pr}, \text{Sc}, \text{Sh} = \text{const}$  or partially constant

$D_{\text{al}}, D_{\text{all}} = \text{const}$  mass transfer

$D_{\text{all}}, D_{\text{alV}} = \text{const}$  heat transfer

batch mode



continuous mode

product

purification

separation

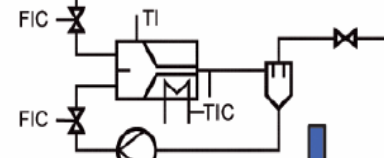
reaction

mixing

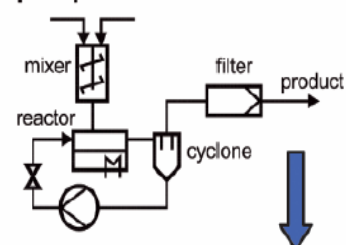
educt

product

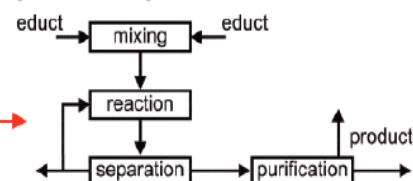
miniplant



pilot plant

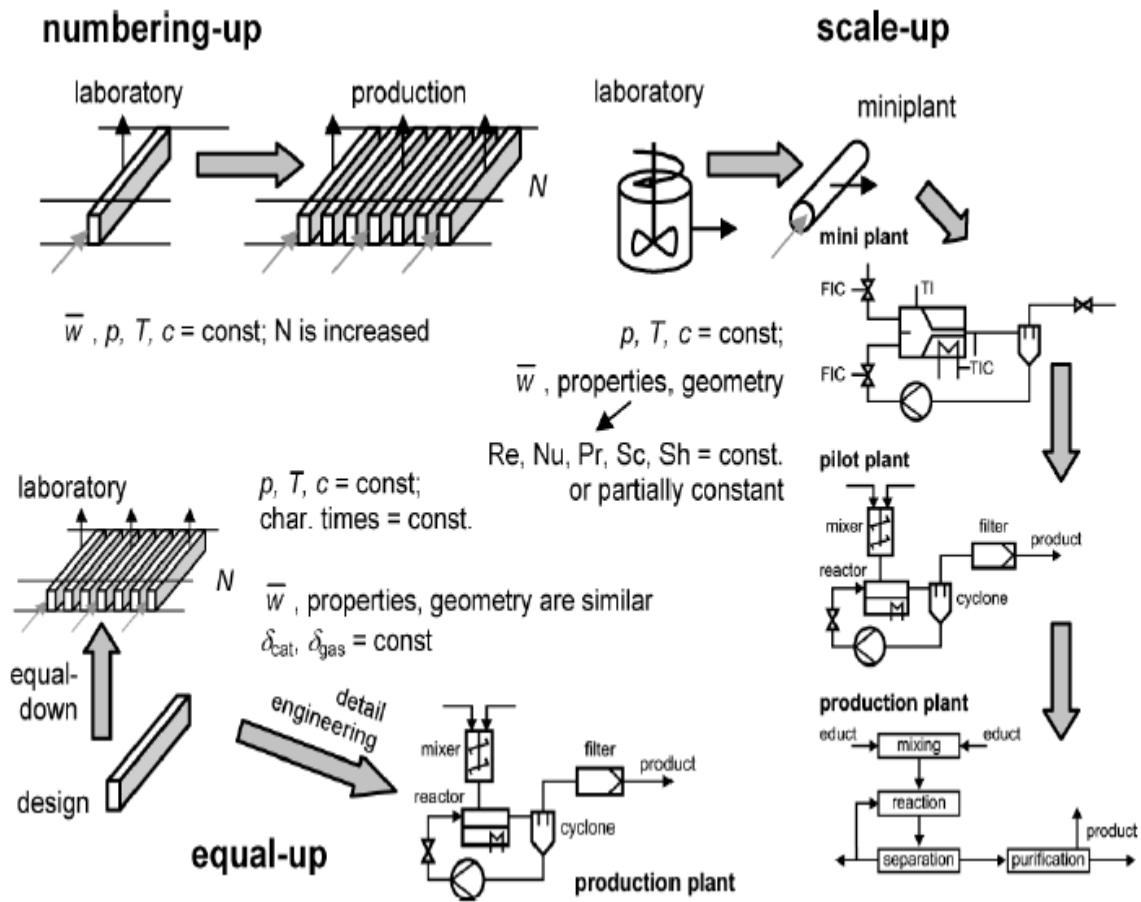


production plant



Equal-up and scale-up procedures with microstructured devices<sup>22</sup>

The geometry is represented along with suitable process parameters in dimensionless numbers like the Reynolds number Re or Sherwood number Sh, which are kept constant or at least partially constant for the process transfer.



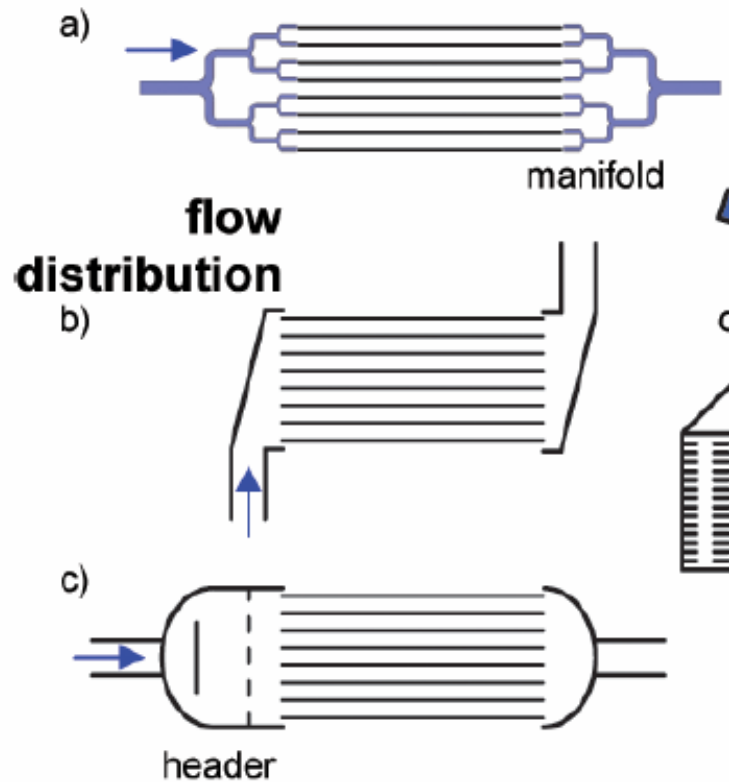
The **numbering-up** procedure increases, in the simplest approach, just the number of channels, to enlarge the capacity. The flow distribution and correct integration must be considered and are the major critical points for a successful implementation. With more channels in a microstructured device, well designed manifolds are extremely important for performance.

A laboratory device is fabricated and tested with the chemical system to yield experimental data. This data is compared with design assumptions and preliminary simulation results.

In case of successful experimental tests, the next design step is to layout a device or a number of devices handling the desired product capacity - **internal numbering-up** of these elements increases the entire flow rate.

The **flow distribution** and correct integration is the most critical point for successful implementation.

Depending on the size of the entire device, various **fluidic manifolds** or flow headers can be applied.



The velocity of the inlet flow is directed to the side walls by a central plate. With this arrangement, all channels are facing the same fluid velocity and are supplied with uniform flow rate.

The appropriate flow manifold depends on the number of channels as well as the shape of the entire device.

Microstructured devices for high flow rates often consist of a stack of microstructured plates.

Experimental experience and proper integration of microstructured elements in a conventional apparatus are essential in order to design and fabricate this plate stack.

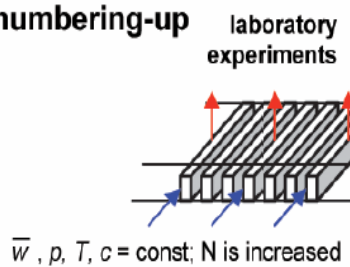
The **equal-up process** starts from the process or product to be realized, and the main effects and parameters are identified for miniaturization.

## equal-up or scale-out

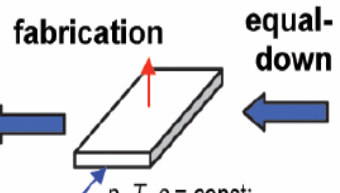
## microstructured devices

## scale-up

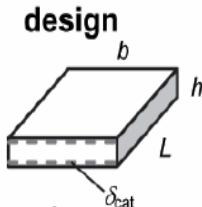
numbering-up



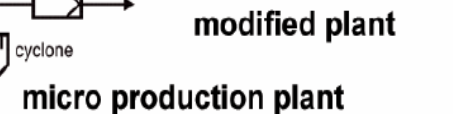
fabrication



equal-down



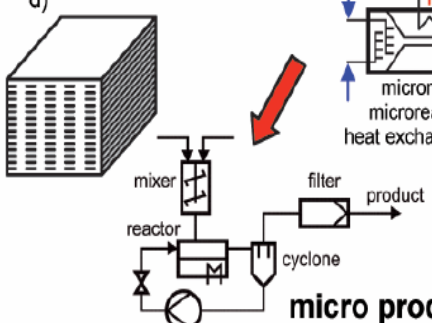
modified plant



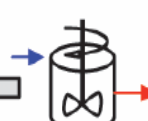
equal-up



micro production plant



laboratory



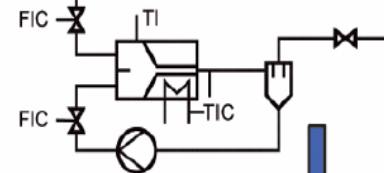
$p, T, c = \text{const.}$   
 $\bar{w}, \text{properties, geometry}$

$\text{Re, Nu, Pr, Sc, Sh} = \text{const.}$   
or partially constant

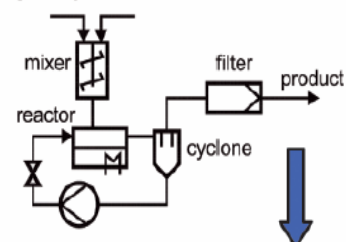
$D_{\text{al}}, D_{\text{all}} = \text{const.}$   
mass transfer

$D_{\text{all}}, D_{\text{alV}} = \text{const.}$   
heat transfer

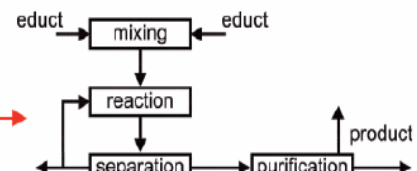
miniplant



pilot plant



production plant



continuous mode

Equal-up and scale-up procedures with microstructured devices<sup>27</sup>

These key parameters to the production design are with respect to key geometries, fluid dynamics, mixing, reaction kinetics, and heat management.

The experimental results indicate, which dimensions cause the benefits of the small length scale (e.g. the boundary layer  $\delta_{fl}$ ).

Other design parameters from fabrication have to be transferred to the production device, such as shape and structure of the active surface , e.g. the catalyst layer thickness  $\delta_{cat}$ .

# Main Issues of Successful Microstructures

## Example: Heat Exchangers

Microstructure devices are excellent tools for laboratory research in many application fields with specific advantages.

### **MANUFACTURING**

For lab-scale-type devices, single microchannel systems, either manufactured from silicon by semiconductor technologies or made from metals by mechanical micromachining, or wet chemical etching are mainly used for flow characterization, heat transfer, and experimental investigation of chemical reactions.

This led to a variety of microstructure devices suitable for several applications, namely heat exchange, evaporation, mixing, generation of emulsions, and running chemical reactions in the lab-scale range.

To achieve higher mass fluxes, parallelization of single microchannel devices, scaling up of the microchannel dimensions, or generation of internally parallelized multichannel systems, (equaling-up) are commonly used.

## PROCESS PARAMETER RESTRICTION

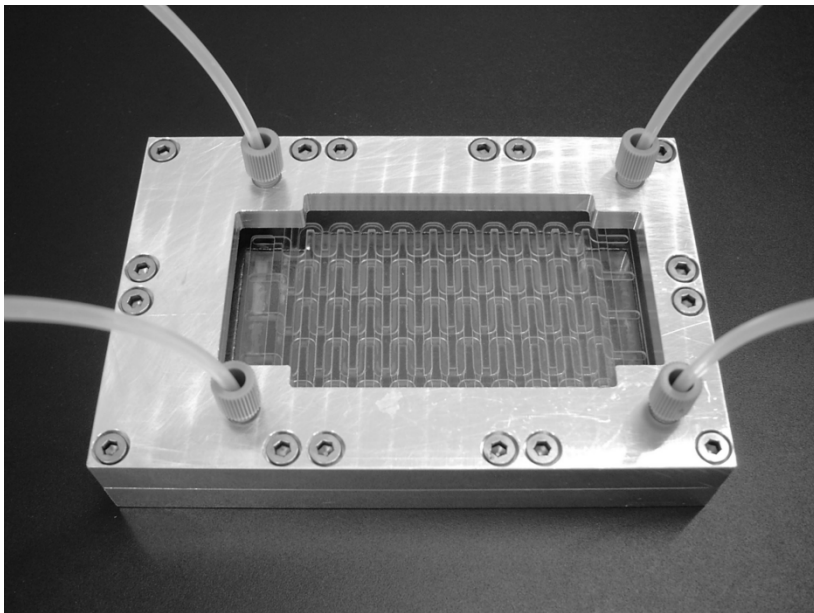
### Material Choice –

Temperature resistance, corrosion resistance, and thermal properties. **Thermal Stress / Corrosion?**

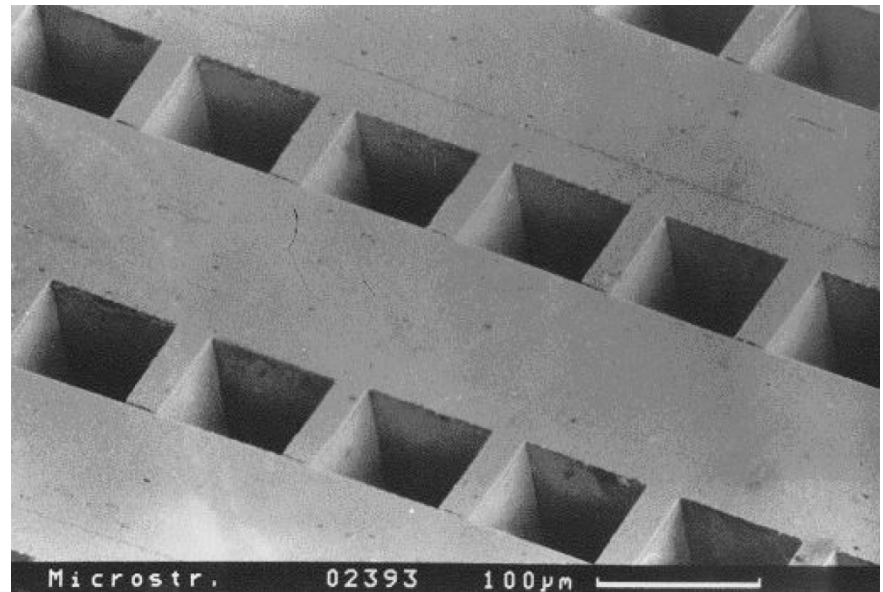
### Fluid Dynamics Restrictions

Laminar/turbulent, fouling, cleaning - use surface coatings, ultrasound?

# Microstructured Devices



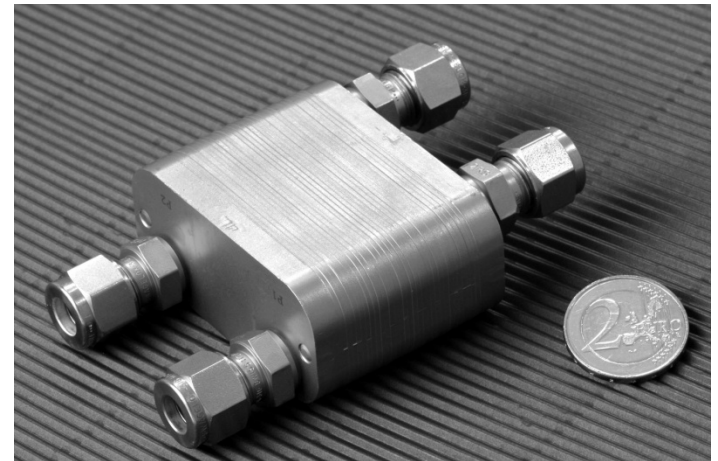
Temperature-controlled residence time module. This glass microstructure device is used to adjust the residence time of a chemical reaction mixture to obtain good performance



Crossflow-arrangement of mechanically machined microchannel foils. The foils are made of stainless steel and connected by diffusion bonding to form a stable stack.

# Microstructured Heat Exchangers

Microstructured heat exchangers deliver high transfer rates, but they also have drawbacks, application limits, during design and operation.



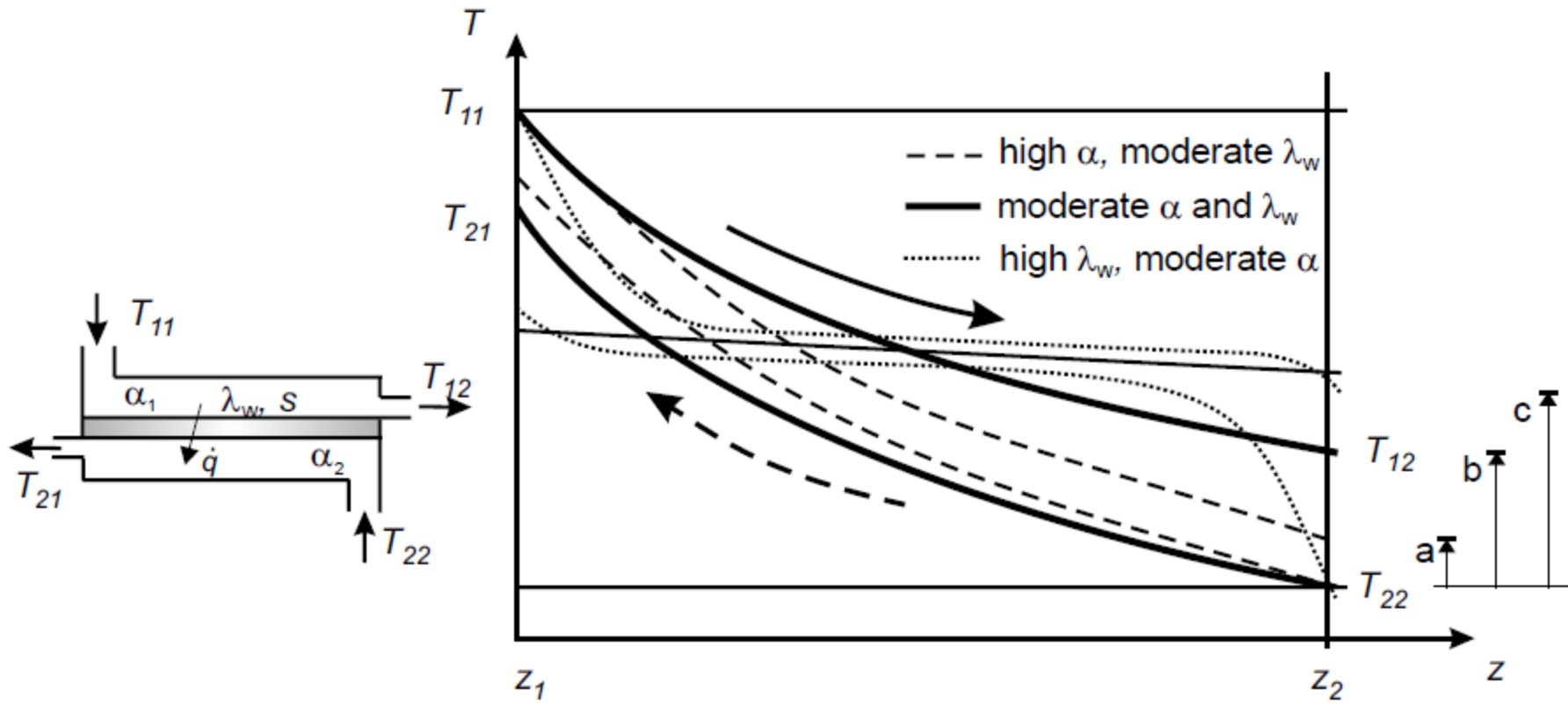
Stainless steel counterflow  
microstructured heat exchanger

1. Wall heat conductivity
2. Pressure loss, manifold design
3. Corrosion, fouling, and catalyst deactivation

## 1. Wall heat conductivity

The ratio of wall thickness to channel diameter is relatively high in microchannel devices, hence, a considerable amount of heat is transferred through the wall parallel to the flow direction, which lowers the driving temperature difference and decreases the amount of the transferred heat.

The amount of **parasitic heat flux** has to be considered for highly conductive wall materials like copper, alumina or silicon, and for a low heat capacity flow of the transfer media, such as gases or low flow velocities.



Heat transfer coefficient -  $\alpha$ , wall heat conductivity -  $\lambda_w$ .

Temperature profile along a counter-flow heat exchanger with different heat transfer coefficients  $\alpha$  and wall heat conductivity  $\lambda_w$ . The fine-dotted line displays the temperature profile in a microstructured heat exchanger with high heat conductivity in the wall and low overall heat transfer coefficient. The temperature difference at the end of the heat exchanger corresponds to the heat exchanger efficiency

## Three cases

- moderate axial wall heat conductivity with high convective heat transfer (case a),
- moderate axial wall heat conductivity with moderate convective heat transfer (case b), and
- high axial wall heat conductivity with moderate or even high convective heat transfer (case c).

The first case a) exhibits the best heat exchanger efficiency displayed as the temperature difference at the entrance or outlet of the heat exchanger.

The last case, with high axial heat transfer, also exhibits high heat transfer rates at both ends of the heat exchanger, however, in the middle of the device, only a marginal amount of heat is transferred. The temperatures of both fluids are almost identical in the middle of the device with little temperature change.

The area in the middle of the heat exchanger provides inefficient heat transfer and diminishes the device performance.

### 3. Corrosion, fouling, and catalyst deactivation

Surface roughness may play a dominant role in microchannels.

If the surface elements reach far into the channel, the hydraulic diameter is constricted, which increases the pressure loss and leads to an earlier transition to turbulent flow.

To include the surface roughness  $\varepsilon$ , a constricted hydraulic diameter  $d_{cf}$  is defined with the narrowest gap width instead of the mean inner distance  $d_t$  of the channel walls.

$$d_{cf} = d_t - 2\varepsilon$$

The corrected hydraulic diameter explains quite well the observed phenomena in rough microstructured channels

Corrosion becomes relevant in microchannels where the surface roughness influences the flow behavior and the transport characteristics. A corrosion layer of 100  $\mu\text{m}$  is tolerable in conventional systems, but may be fatal for microchannels.

Particle generation and processing are major steps in many applications. Particles may attach to the wall, decrease the cross section, and influence the pressure loss and flow velocity. The particles sticking to the wall may attract more particles and lead to fouling and blocking of the channels.

Heterogeneous catalysis with high exothermic or endothermic character are suitable, but catalyst deactivation or poisoning can be critical for long-term operation

## 2. Pressure loss

For high flow rates, small channels induce a **high pressure loss due to the high surface-to-volume ratio.**

Hence, low viscosity fluids are preferred for application in microchannels due to a tolerable pressure loss.

The pressure loss in a channel – from Bernoulli equation:

$$\Delta p_{12} = p_1 - p_2 + \frac{\rho}{2} (w_1^2 - w_2^2) + g (y_1 - y_2)$$

In microchannels, the gravitation force is negligible compared to friction forces

$$\Delta p_{12} = p_{tot,1} - p_{tot,2} \quad \text{with} \quad p_{tot} = p + \frac{\rho}{2} w^2$$

The pressure loss is calculated for a complex channel arrangement as:

$$\Delta p = \left( \lambda \frac{l}{d_h} + \zeta \right) \frac{\rho}{2} \bar{w}_{ref}^2$$

$\bar{w}_{ref}$  is the constant reference velocity,  $\lambda$  is the channel friction factor.

The pressure loss consists of portions from straight channels described by  $\lambda$  ( $l/d_h$ ) and portions from bends, curves, connections, and other internals described by  $\zeta$ .

The pressure loss coefficient  $\zeta$  is primarily defined for turbulent flow in devices and can be found in textbooks

In general, the flow below  $Re = 10$  can be regarded as straight laminar flow where no vortices appear and the pressure loss coefficient  $\zeta$  can be neglected.

For high Re numbers, especially for  $Re > Re_{crit}$ , the laminar contribution can be neglected.

In the transition regimes,  $10 < Re < Re_{crit}$ , a square fit of laminar and turbulent values can serve as a first estimation for the pressure loss.

hydraulic diameter  $d_h = 4A/lp$

For laminar flow in long straight channels the channel friction factor  $\lambda$  is inversely proportional to the Re number in the channel

$$\lambda = \frac{C_f}{Re} = \frac{C_f \eta}{\rho d_h w}$$

The channel friction factor  $\lambda$  is inversely proportional to the channel diameter  $d_h$ ; smaller channel increases the friction factor.

The pressure loss in a channel can be calculated from

$$\Delta p = \left( C_f \nu \frac{l}{d_h} + \zeta d_h \bar{w} \right) \frac{\rho \bar{w}}{2} = C_f \frac{\eta l}{2d_h^2} \bar{w} + \zeta \frac{\rho}{2} \bar{w}^2$$

In long straight channels, the pressure loss  $\Delta p$  depends mainly on the first term, hence

the pressure loss varies

- almost linearly with the velocity, channel length, and viscosity,
- inversely proportional to the square of the hydraulic diameter  $d_h$ .

In curved channels with internals, the hydraulic diameter influences the pressure loss only marginally, but convective effects determine the pressure loss coefficient  $\zeta$ .

The pressure loss can also be described as

$$\Delta p = \left( C_f \frac{l}{d_h} + \zeta \text{Re} \right) \frac{\rho v^2}{2} \frac{\text{Re}}{d_h^2}$$

The pressure loss depends on Re number with a linear and a quadratic part.

With decreasing device length dimensions, the pressure loss is nearly proportional to the square of the Re number.

The volume flow rate  $V$  through  $N$  nearly rectangular, parallel channels -

$$V \propto N \left( d_h^2 \bar{w} \right)$$

The final form of pressure drop for a system of  $N$  channels:

$$\Delta p = \left( C_f \eta l + \zeta \frac{V}{N} \right) \frac{\rho}{2} \frac{V}{N d_h^4}$$

This equation only accounts for **parallel channels with a single flow manifold.**

$$\Delta p = \left( C_f \eta l + \zeta \frac{V}{N} \right) \frac{\rho}{2} \frac{V}{N d_h^4}$$

The pressure loss consists of two parts,

1. the laminar part ( $C_f$ ) varies linearly on the volume flow rate.
2. The convective part of internals ( $\zeta$ ) depends on the square of the volume flow rate.

The hydraulic diameter plays a crucial role with the inverse dependency of the fourth power.

Decreasing the channel diameter and the resulting higher pressure loss can be balanced by either increasing the channel number or decreasing the channel length or volume flow rate.

$$\Delta p = \left( C_f \eta l + \zeta \frac{V}{N} \right) \frac{\rho V}{2 N d_h^4}$$

The pressure drop increases linearly with velocity and viscosity is less important in short, curved channels with many internals.

Within short microchannels, not only is the pressure loss low, but also precipitation or polymerization of various chemicals are possible due to proper mixing of the immiscible reactants.

However,

For gas-flow microreactors with long, straight channels, the pressure loss is approx. 2.5 times lower than in fixed bed reactors for the same mass transfer conditions

The key parameters of the production device, including channel height  $h$  or wall thickness  $s$ , are equal to the laboratory equipment,

however,

the geometry of the active surface or the fabrication techniques may differ, for example, the microchannels have the same cross section or only the same height, but differ in length.

## Application Examples - Recent Experiments on heat Sinks

Requirement of extremely high heat removal rates

- phase change heat transfer
- minimum temperature difference

This is particularly true in flow boiling applications, where only modest increases in device temperature will allow the removal of very large heat fluxes.

In the design of applications, such as microchannel two-phase flow heat sinks and micro thermal pumps, **the liquid/vapor two-phase flow pattern is critical**.

<http://www.rpi.edu/tphtl/research/lvfp/lvfp.html>

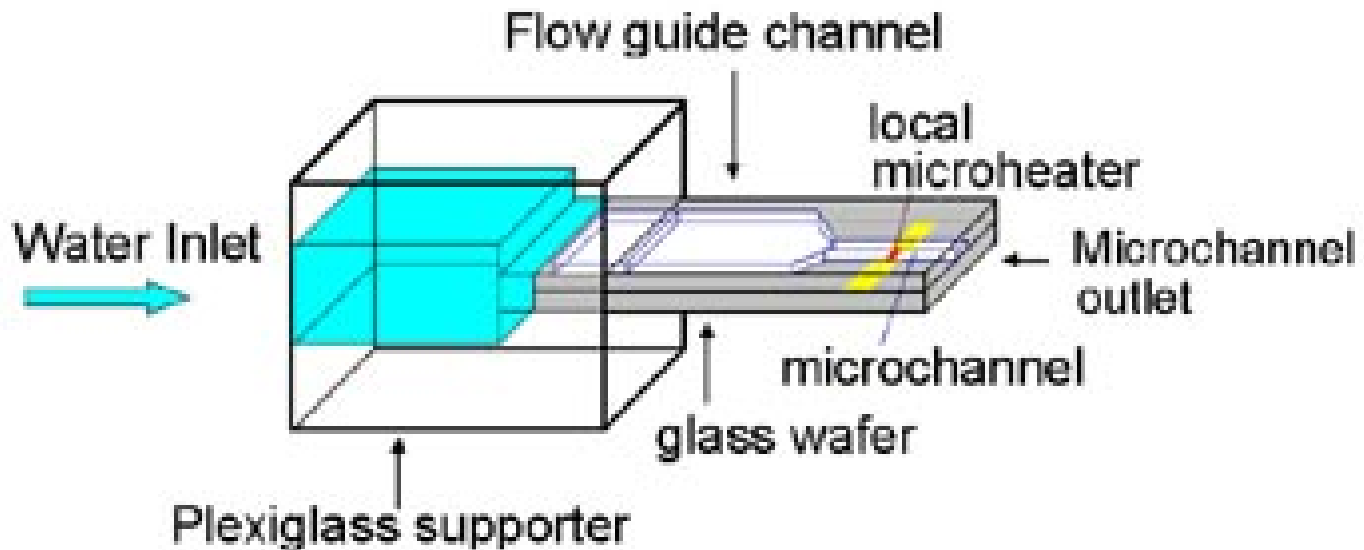
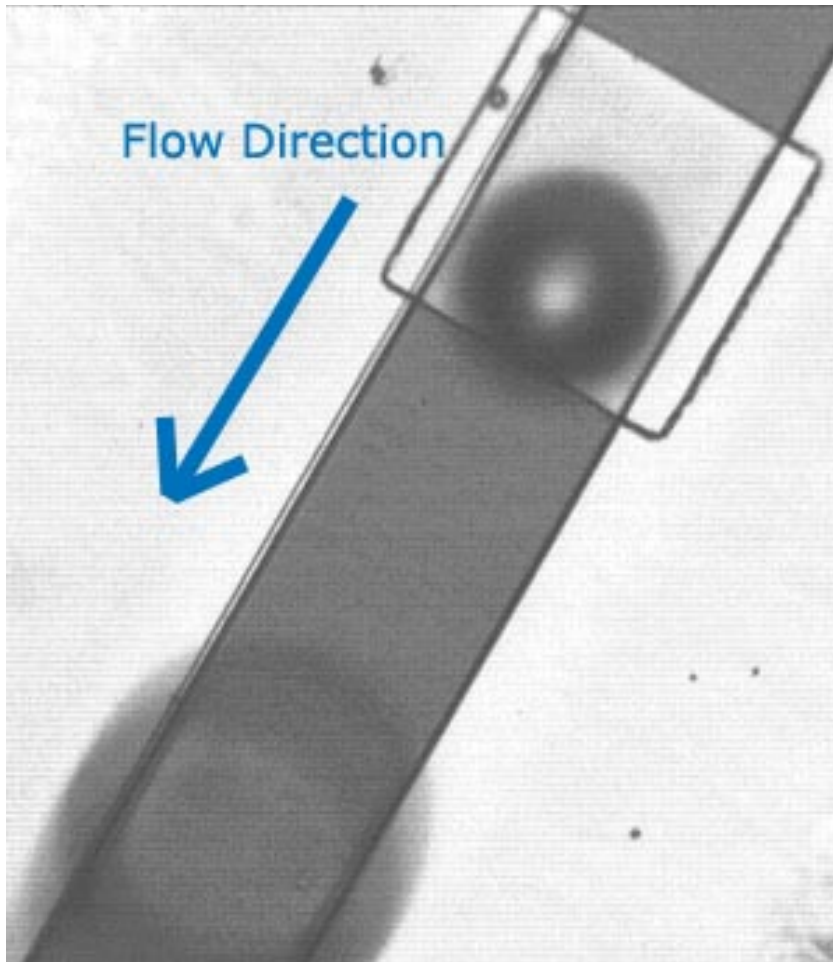


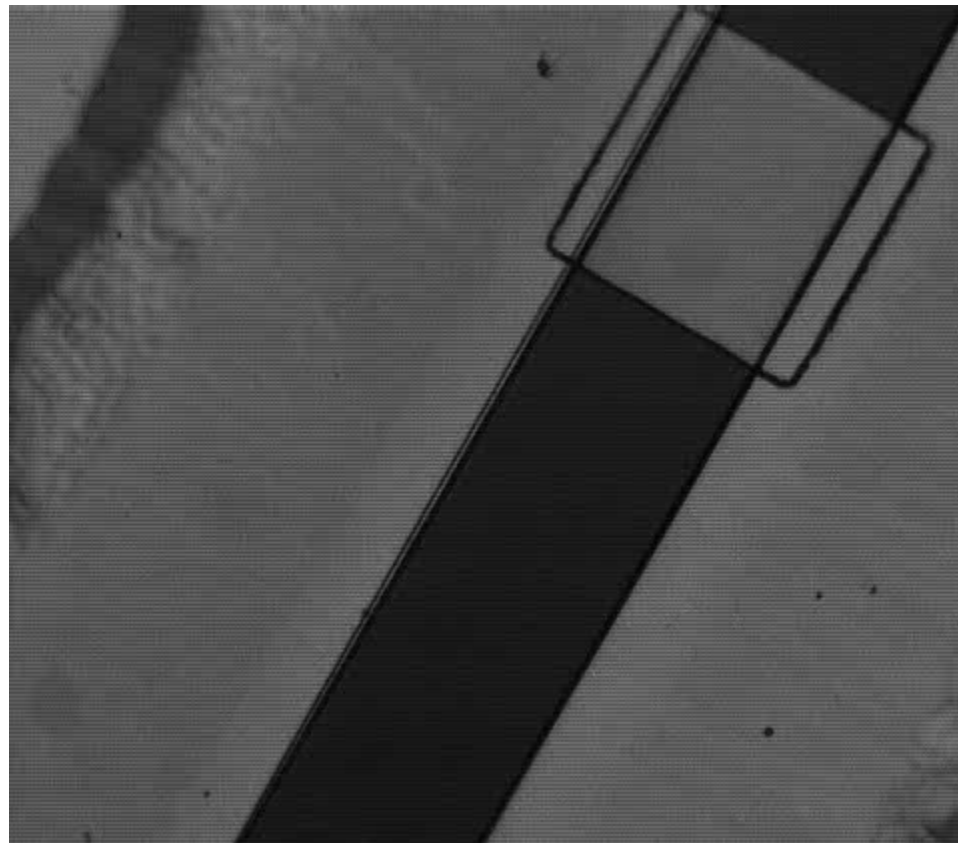
Fig.1 - Configuration of the experimental specimen and test section

- Microscale platinum heater fabricated on a Pyrex glass wafer
- Shallow trapezoidal microchannel with hydraulic diameter  $D_h = 56\mu\text{m}$
- Use high-speed digital CCD video camera and microscope,
- Study the two-phase flow patterns,

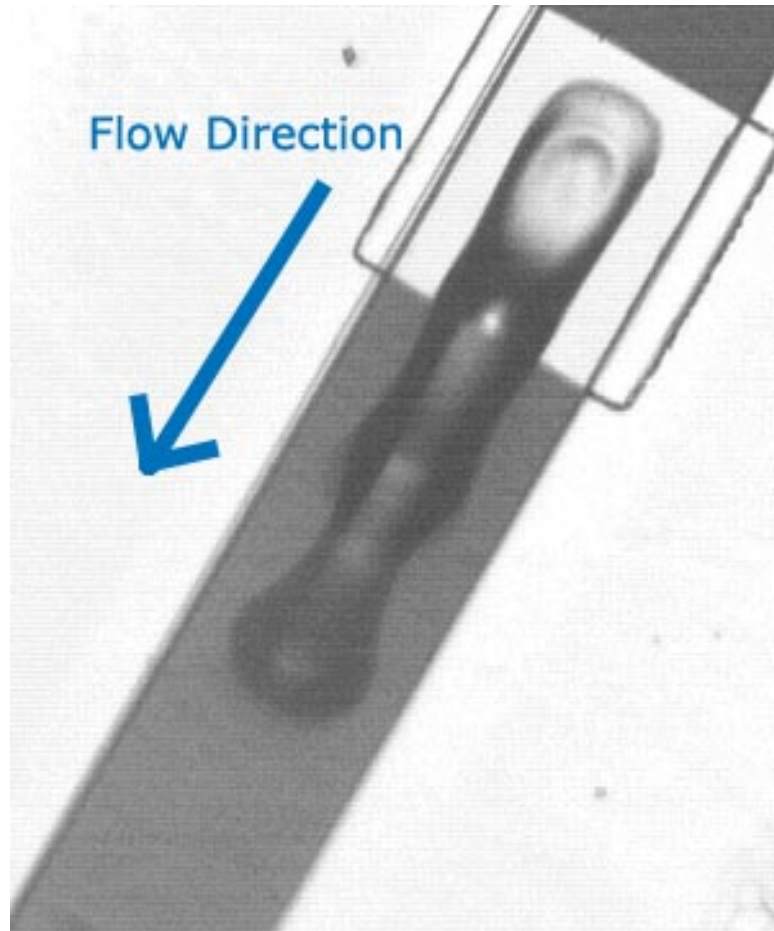
Impact of the size of the microchannel and the mass flow rate on the boiling incipience and two-phase flow patterns are analyzed.



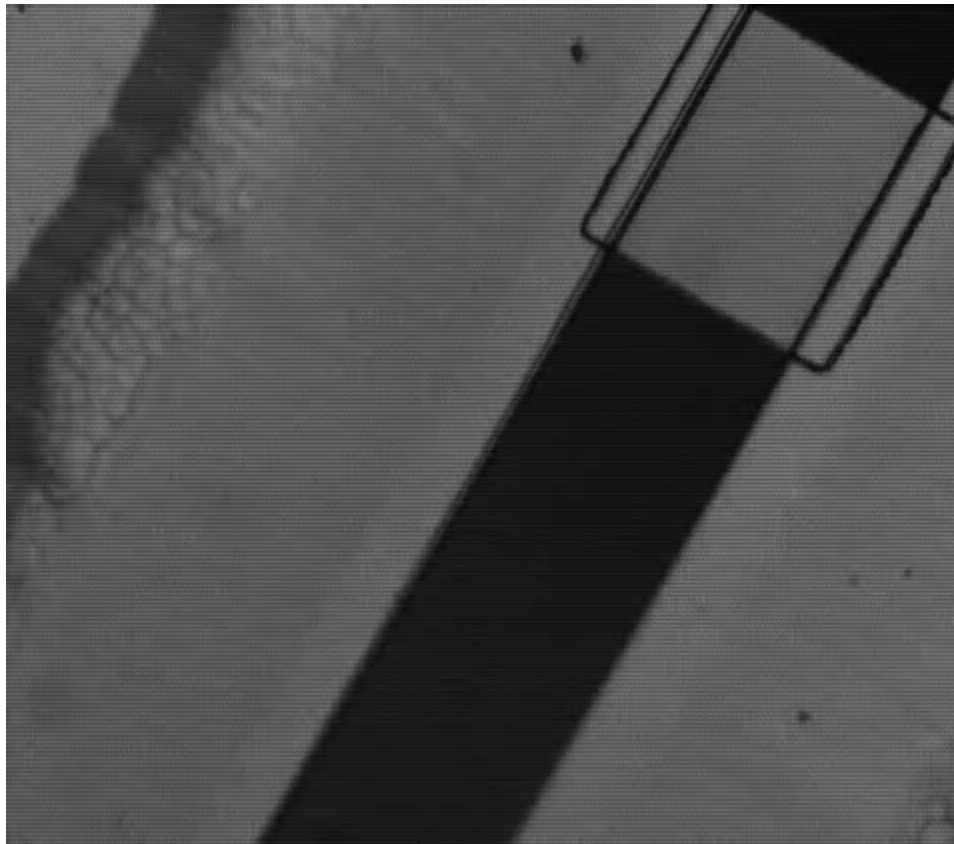
Bubbly flow in the microchannel under small flow rates and low power



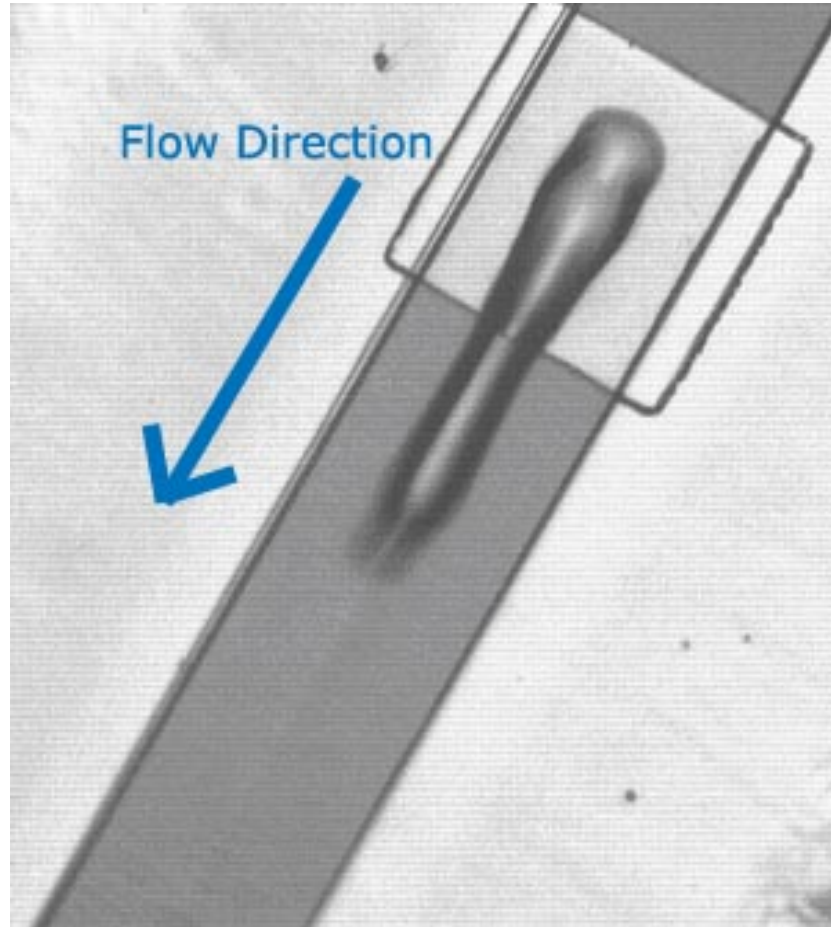
**Bubbly Flow**



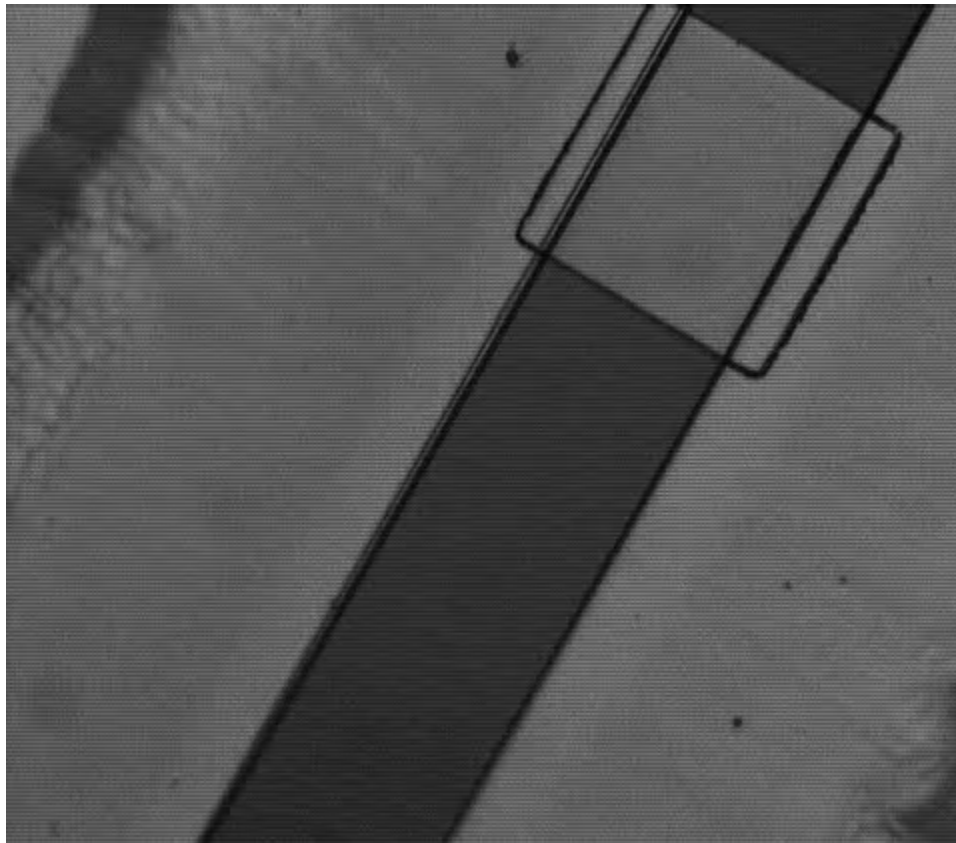
Wavy flow in the microchannel under moderate mass flow rate and moderate power



**Wavy Flow**



Annular Flow in the microchannel under large flow rates and high power



**Annular Flow**

**A better understanding of the fundamental phenomena occurring in these types of flows**

**Effects of surface geometry/modifications/properties/heat flux**

Microchannel devices present many *opportunities*

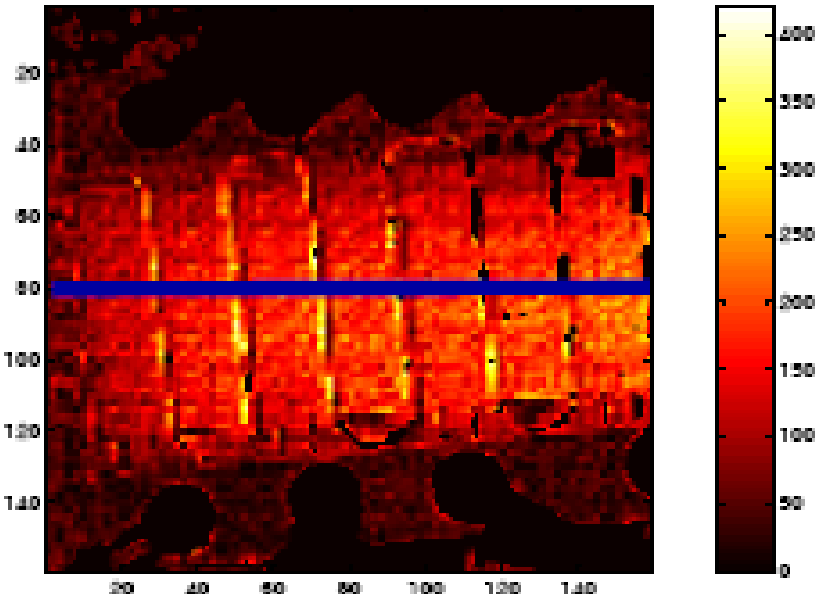
however,

their *disadvantages and special requirements* must be taken into consideration for successful application.

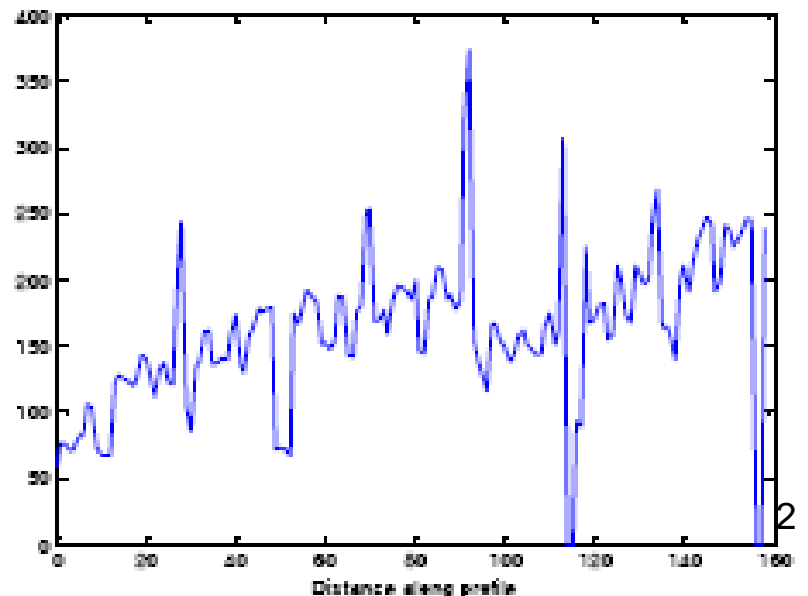
# Lectures 5 - 7

**Microscale Phase Change Heat Transfer  
for  
Electronics cooling**

*Heat buildup is  
becoming one of the  
major limitations to  
creating tomorrow's  
more compact,  
complex micro  
devices".*



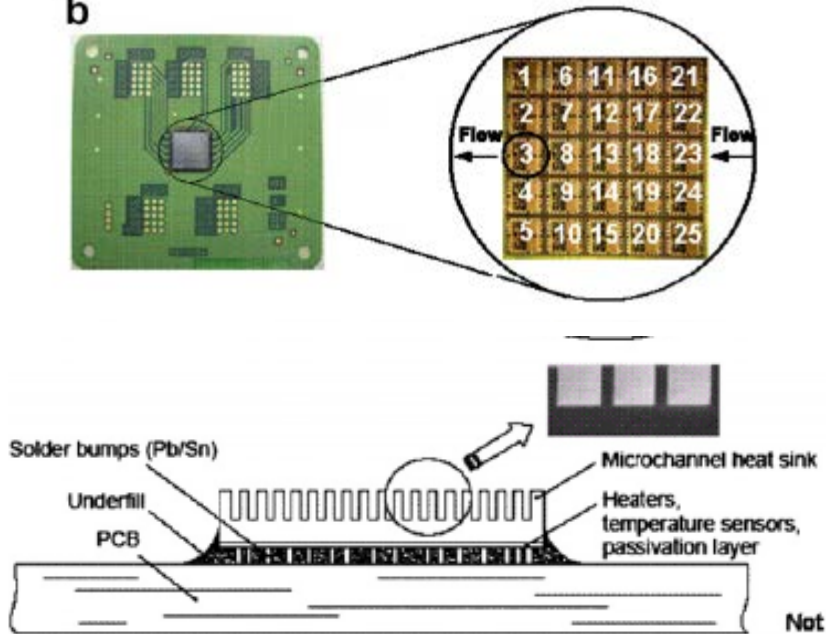
At 450 mA and 100  $\mu$ s on time and 1 KHz frequency



David Benson - Advanced  
Packaging Department,  
Sandia National  
Laboratory's.

# Electronics Cooling

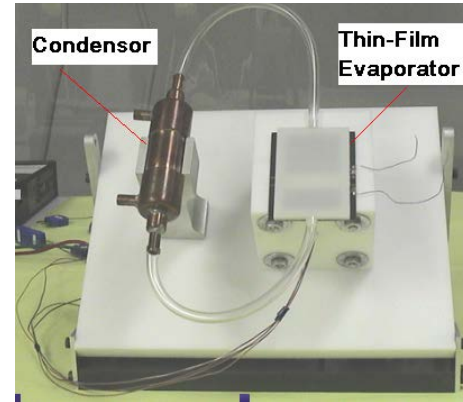
b



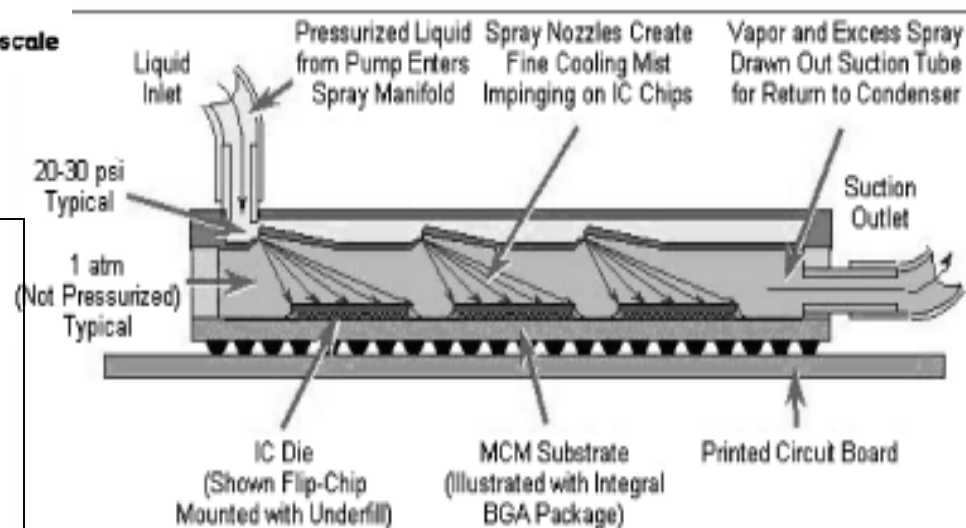
## 1. Micro Heat sink

- Growing demand for cooling systems  
- *high heat flux removal* .
- Convection - *single phase flows* not sufficient
- *Phase change* for high heat removal

$$h_{LV} \gg C_P$$

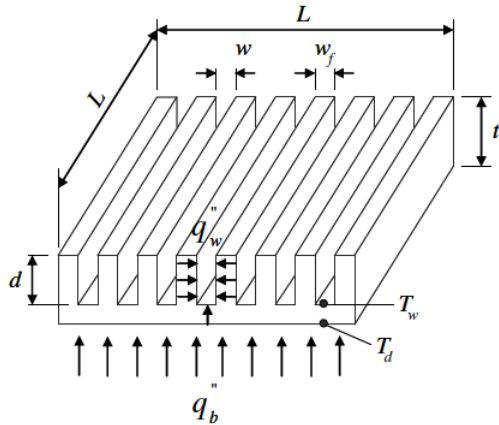


## 2. Thin Film evaporator

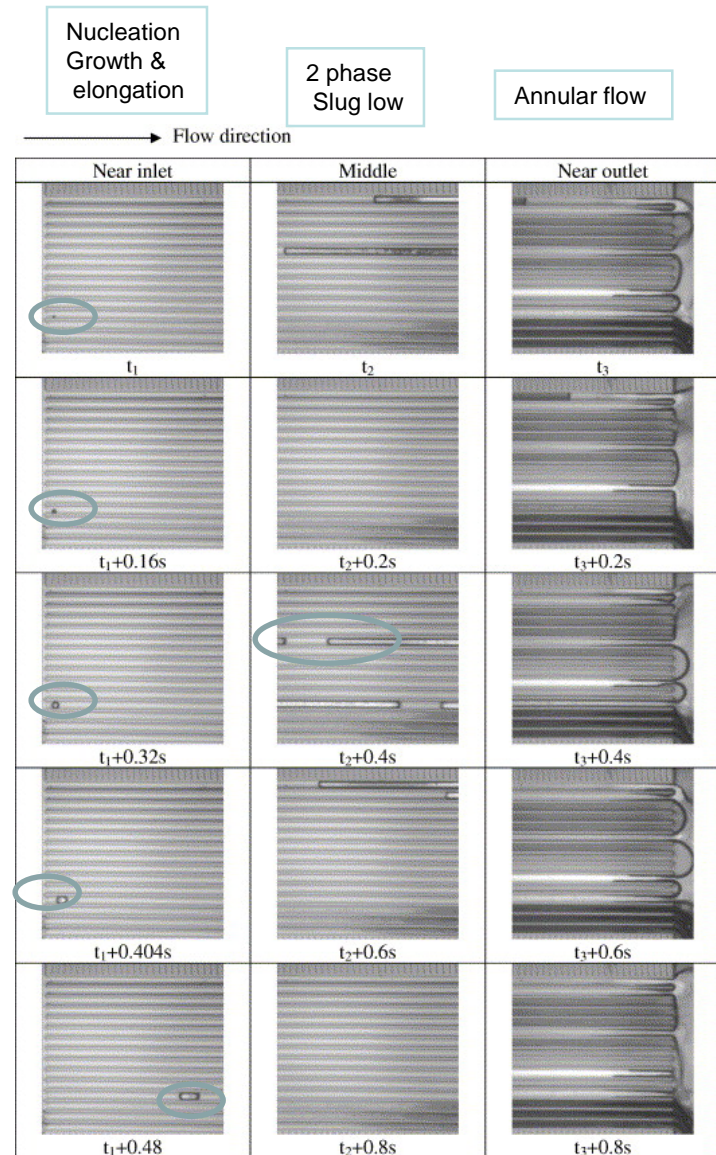


## 3. Spray Cooling

# 1. Micro Heat sink

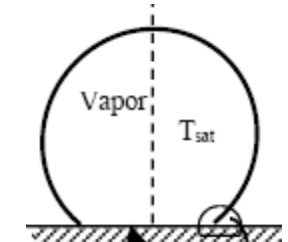
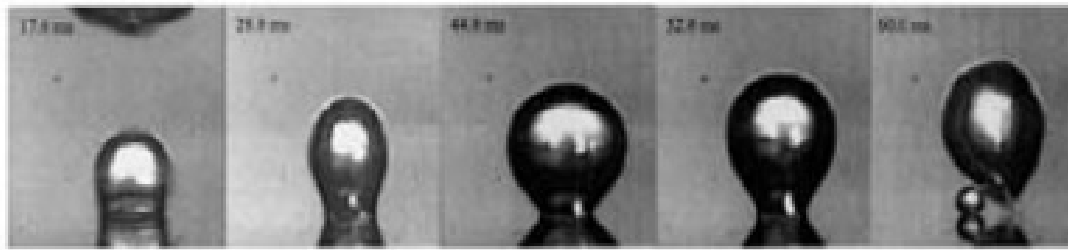


- Absorbs heat generated by electronic components ( $300 \text{ W/cm}^2$ )
- Microchannels of various shapes trapezoidal, triangular rectangular
- Mechanism: Boiling in the microgrooves  
*Nucleation*: formation of vapor bubbles  
*Two Phase Flow* : Growth and Elongation of bubbles to form slug flow and finally annular flow



Source : Chang (2007) Two-phase flow instability for boiling in a microchannel heat sink [International Journal of Heat and Mass Transfer, Volume 50, Issues 11-12, June 2007, Pages 2078-2088](#)

# Nucleation in microchannels



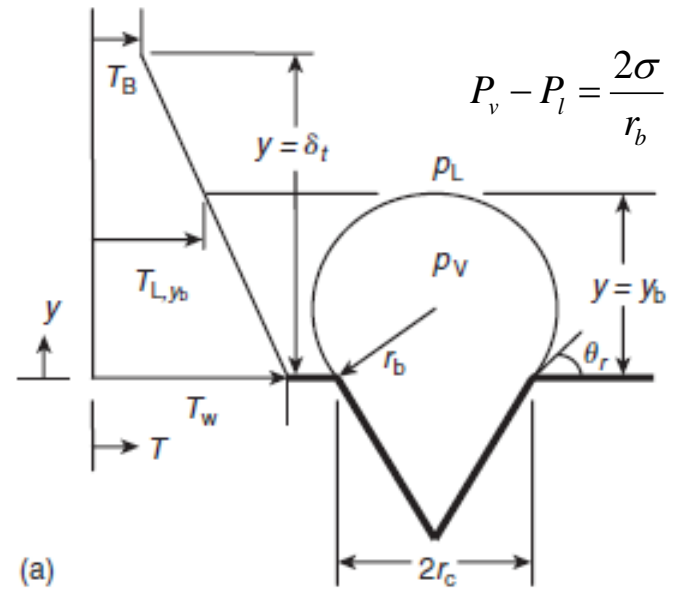
Source: Mukherjee, A. and Kandlikar, S. G., Numerical study of growth of a vapor bubble during flow boiling of water in a microchannel, ASME Paper No. ICMM 2004-2382, in *Proceedings of the Second International Conference on Microchannels and Minichannels 2004, Rochester, New York*, pp. 565–572, 2004

- Crevices serve as *nucleation sites*
- Wall superheat required for nucleation to occur on crevice of radius  $r_c$

$$\Delta T_{Sat|ONB \text{ at } r_c} = \frac{1.1r_c q''}{k_L \sin \theta_r} + \frac{2\sigma \sin \theta_r}{r_c} \frac{T_{Sat}}{\rho_V h_{LV}}$$

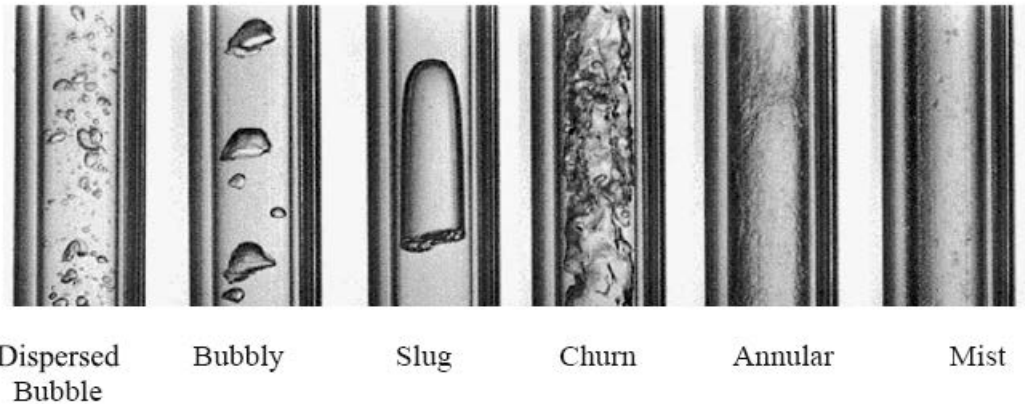
where

$$\Delta T_{Sat} = T_w - T_{Sat}$$



Source: Kandlikar, S. G. and Spiesman, P. H., Effect of surface characteristics on flow boiling heat transfer, Paper presented at the Engineering Foundation Conference on Convective and Pool Boiling, May 18–25, Irsee, Germany, 1997.

# Microchannel Two Phase flows

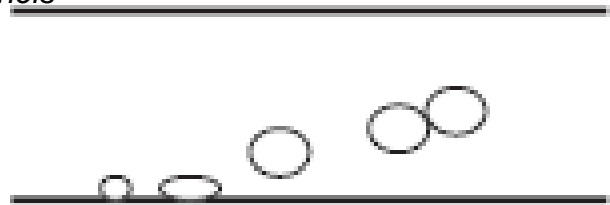


Source: Huo, X., Chen, L., Tian, W. and Karayannidis, T., (2003) Flow boiling and flow regimes in small diameter tubes, 8th UK National Heat Transfer Conference, Oxford, September 2003, Paper No.

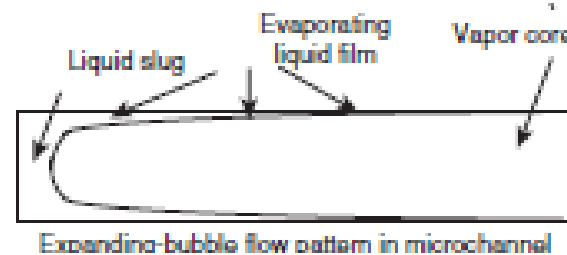
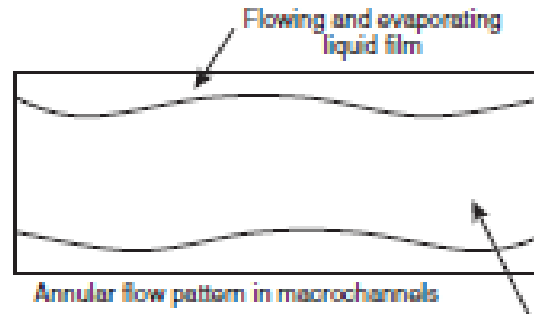
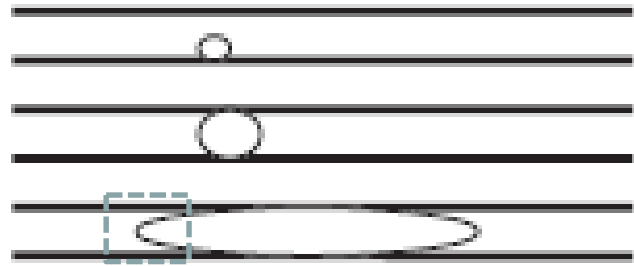
Dimensionless no	Expression	Relevance
<b>Bond or Eötvös no</b>	$Bo = \frac{g(\rho_l - \rho_v)L^2}{\sigma}$	Ratio of gravity force to <b>surface tension</b>
<b>Capillary no</b>	$Ca = \frac{\mu V}{\sigma}$	Ratio of Viscous to <b>surface tension</b> forces
<b>Weber no</b>	$We = \frac{LG^2}{\rho\sigma}$	Ratio of inertia to <b>surface tension</b> forces   G = mass flux = $\rho V$
<b>Jacob no</b>	$Ja = \frac{\rho_L}{\rho_V} \frac{c_{p,L}\Delta T}{h_{LV}}$	Ratio of Sensible heat for reaching $T_{sat}$ to the <b>latent heat</b>

# Comparison of flow boiling in Macro and Microchannel

Macrochannels



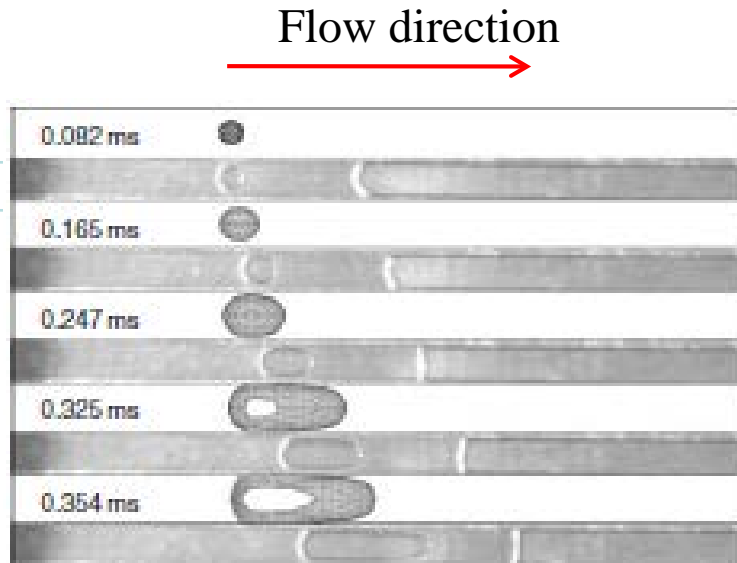
Microchannels



- *Macrochannels* : Bubbles grow in size and depart due to inertia of flow contributing to bubbly flow. When the bubble coalesce they form *bubbly* and *annular flows*.
- *Microchannels* : Bubbles grow and hit the walls and spread over the channel wall. Flow pattern similar to film under a growing vapor bubble. *Strong dependence of heat transfer coefficient* during flow boiling in microchannels indicating dominance of *nucleate boiling* .

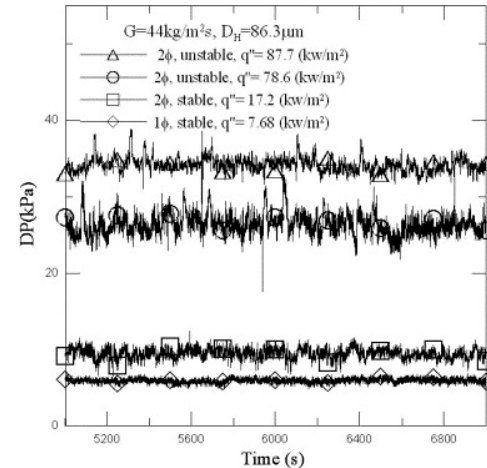
# Flow Instability due to growing Bubbles

Simulation  
Experimental

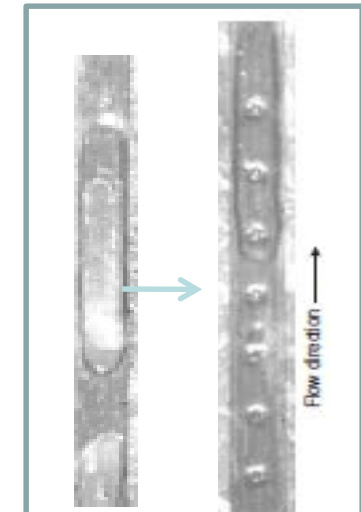


\*Source :Mukherjee, A. and Kandlikar, S. G., Numerical study of growth of a vapor bubble during flow boiling of water in a microchannel, ASME Paper No. ICMM 2004-2382, in *Proceedings of the Second International Confer. on Microchannels and Minichannels 2004, Rochester, New York, pp. 565–572, 2004*

- Growth of bubble and their expansion causes *flow reversal* leading to instability - a major concern for flow boiling .
- Two methods for reducing instability
  - Pressure drop element* at the inlet
  - Flow stabilization with artificial *nucleation sites*



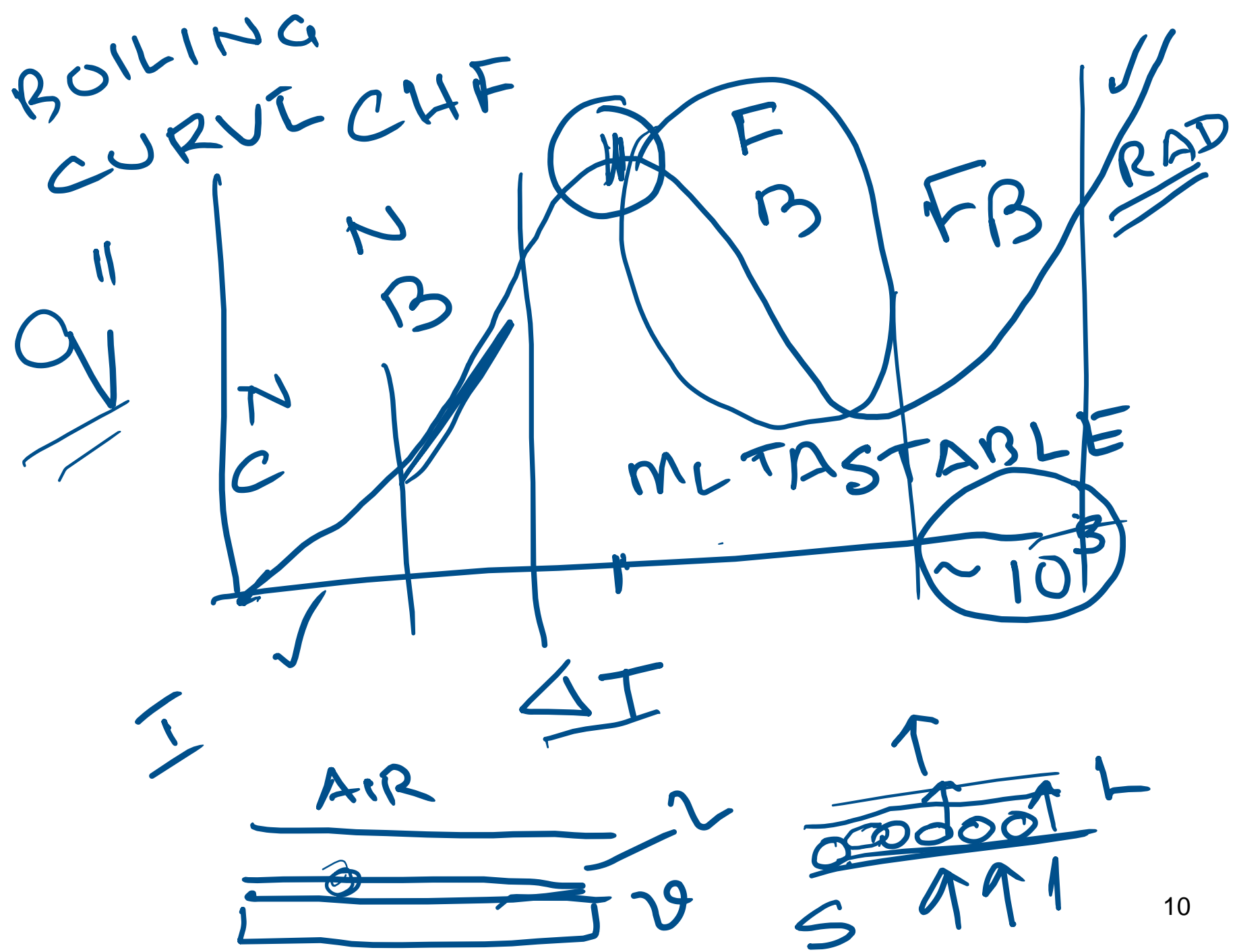
Pressure fluctuation



Stabilized flow with fabricated nucleation sites

## 2. Ultra Thin Film evaporation cooling

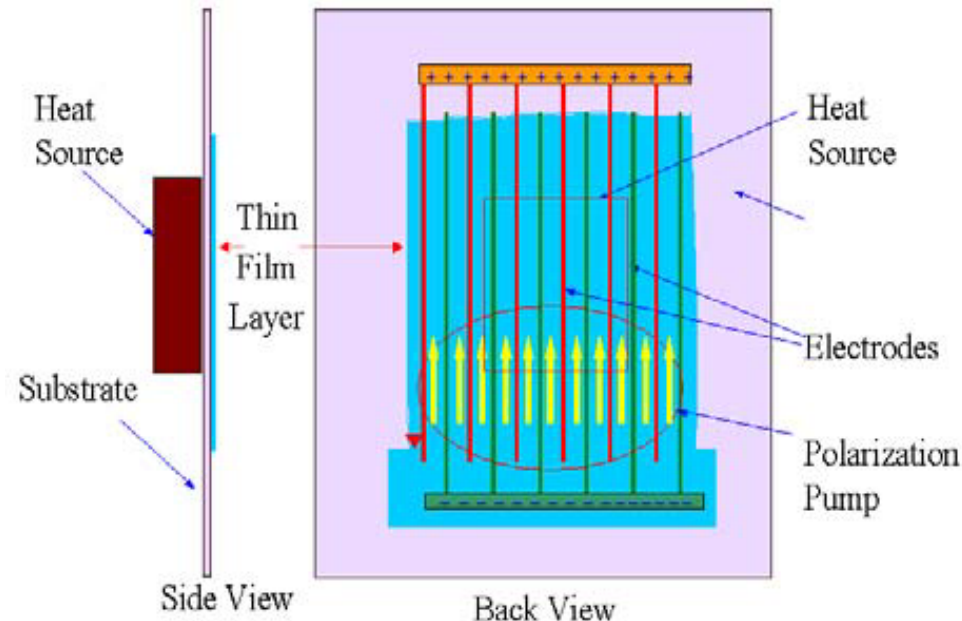
- During Phase change heat transfer, heat is absorbed by the working fluid as *heat of vaporization* or latent heat.
- Two main regimes of phase change for cooling are:  
→ *boiling* and *thin film evaporation*.
- Concerns of boiling:
  1. *minimum superheat* required for boiling inception.
  2. *relatively thick boundary layer*.
  3. *inherently low critical heat flux*.
- These limitations can be overcome if a *thin film* (several microns) of the working liquid continuously covers (*wets*) the heated surface.
- Advantages of UTF evaporation over boiling:
  1. A very *small temp rise* above saturation temperature .
  2. Unlike nucleate boiling , it is *stable* because there is only conduction across a thin film.



# EHD enhanced polarization pump

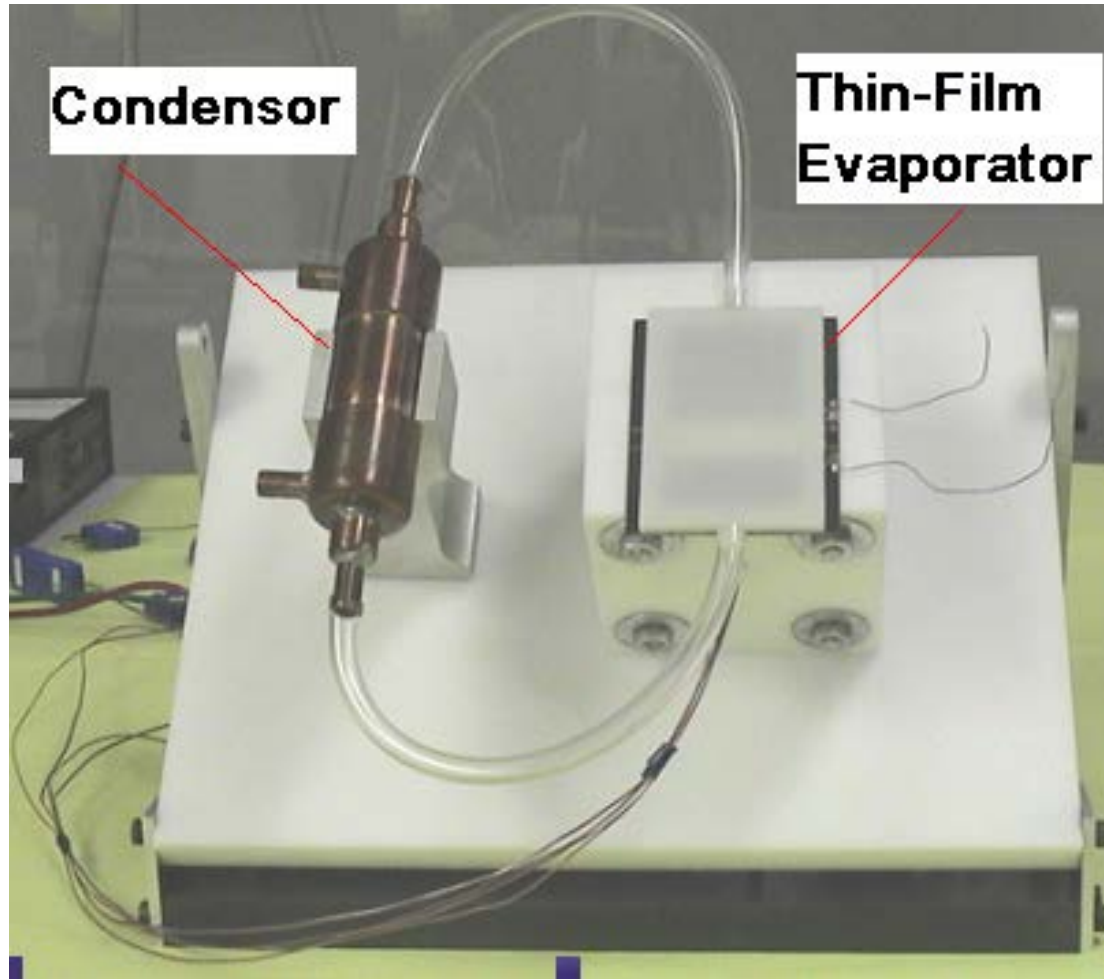
The Electrohydrodynamic (EHD) pump is a non-mechanical pump which induces flow in a dielectric liquid under a high voltage electric field by injection or generation of ions in the vicinity of the electrodes.

The free charges begin to move towards the electrode with opposite polarity. The movement of charged particles exerts a drag force on the liquid molecules resulting in a net flow along the channel.



S. Kakaç et al. (eds.), *Microscale Heat Transfer*, 321 338.  
© 2005 Springer. Printed in the Netherlands.

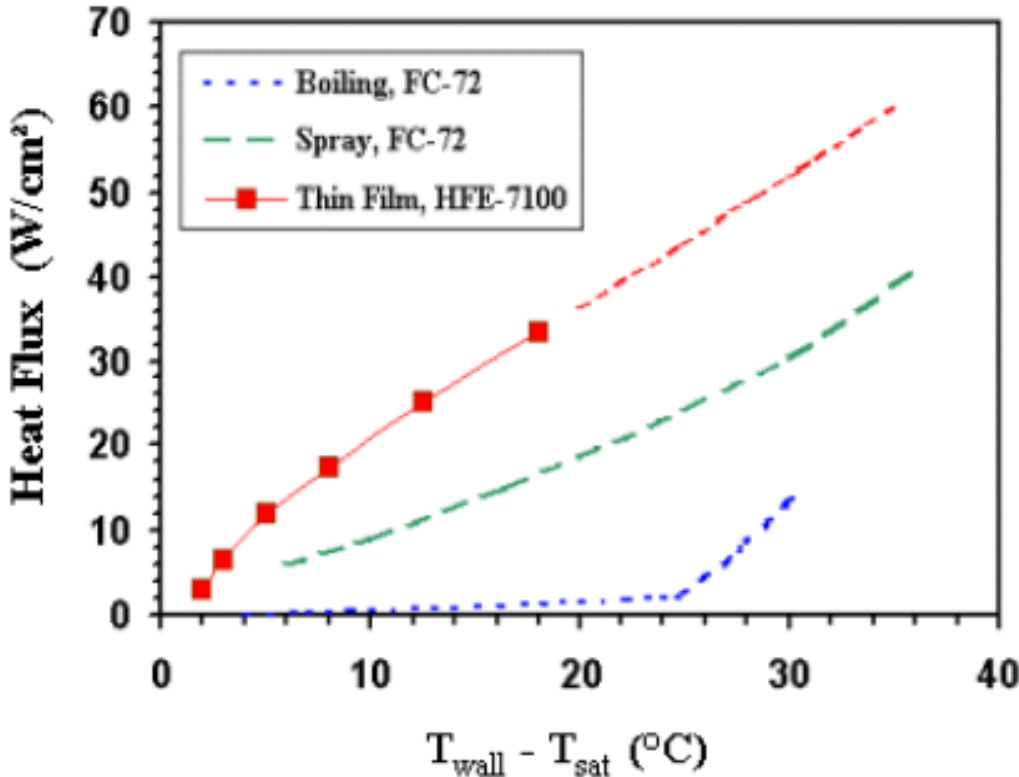
- Array of EHD electrodes draws an *ultra thin liquid film* over the hot surface.
- The power required is very low, leading to higher pumping efficiencies.



### The thermosyphon test system

The ultra thin film evaporator can be packaged into a wide variety of configurations depending on the electronic components to be cooled.

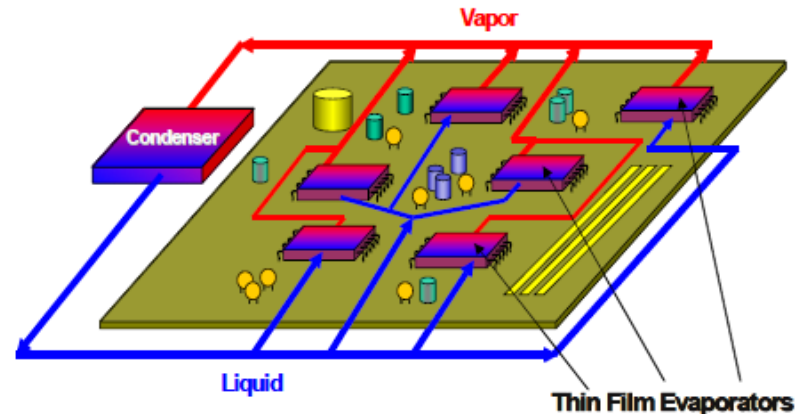
# Comparison of boiling, spray and thin film



*S. Kakaç et al. (eds.),  
Microscale Heat Transfer,  
321 338. © 2005 Springer..*

- The thin film evaporator can remove heat fluxes of  $20-40 \text{ W/cm}^2$  with a temperature difference that is about  $10-15^{\circ}\text{C}$  less than spray cooling and about  $30^{\circ}\text{C}$  less than pool boiling.
- Optimizing the electrode pattern on the thin-film evaporator will generate *ultra thin (micron-size) films* on evaporator surfaces, higher cooling rates, and a more robust operation.

- Cooling systems based on the ultra thin film evaporator will be *quiet, compact, light-weight*, and energy efficient.
- The high rate of cooling will minimize the *operating temperature* of the electronic components being cooled.

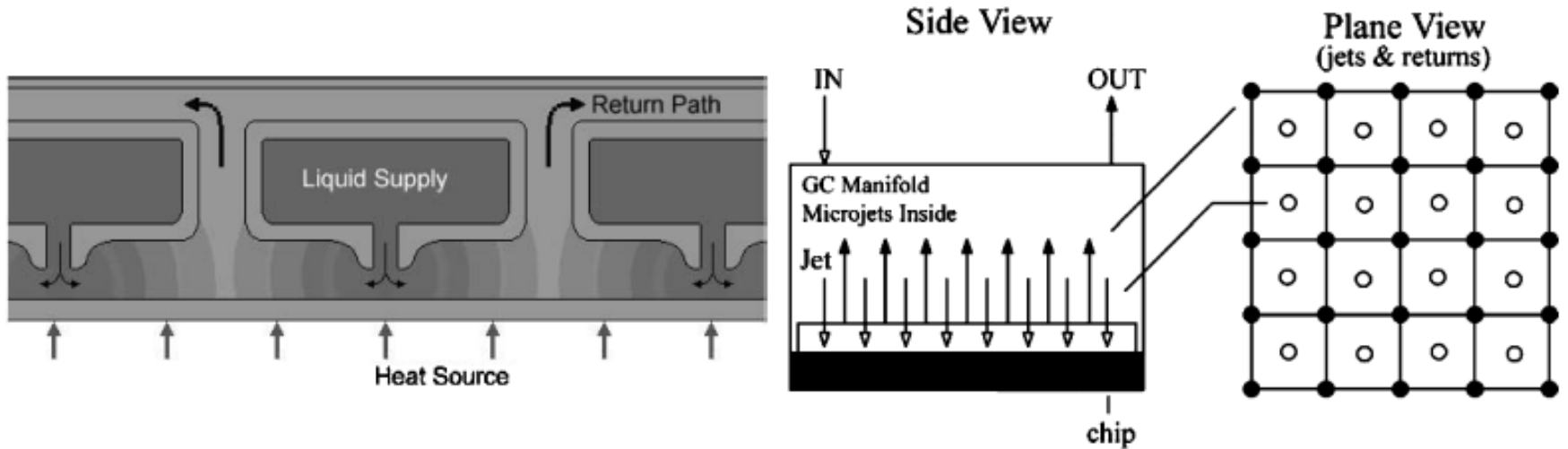


Example of thin film cooling architecture

## Conclusions

- This technology can substantially increase cooling capacity and lead to major *weight/volume reductions* in the next generation thermal management systems.
- *Only a fraction of the amount of fluid* used in spray or jet cooling systems is necessary for UTF and with few ancillary components.
- Its *power consumptions* are extremely low and thus highly energy efficient for cooling of high heat-flux devices.

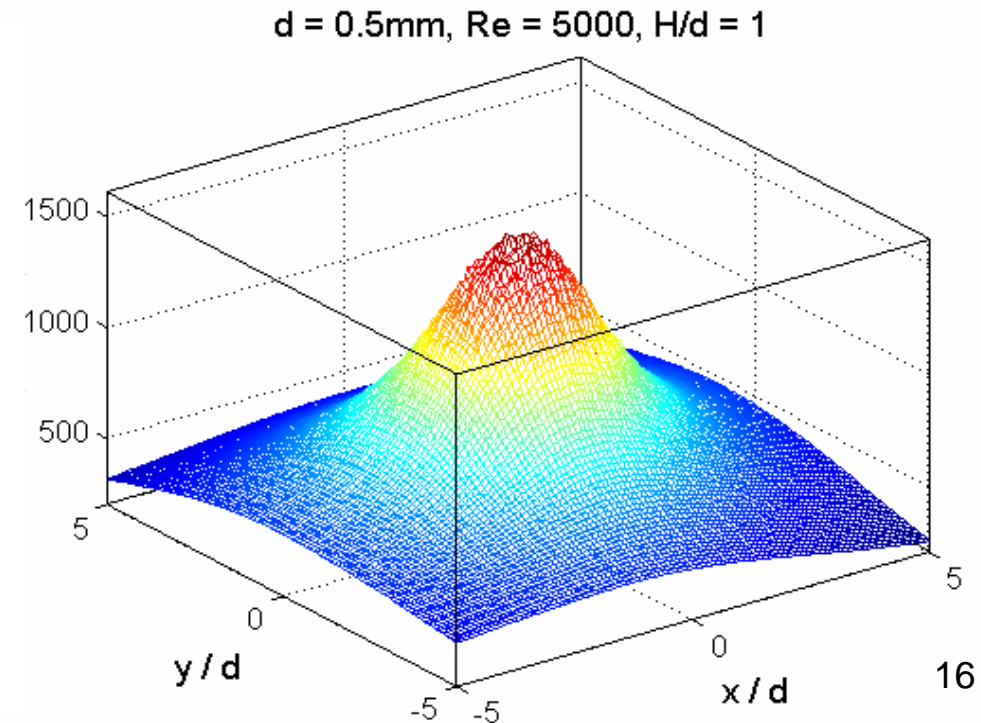
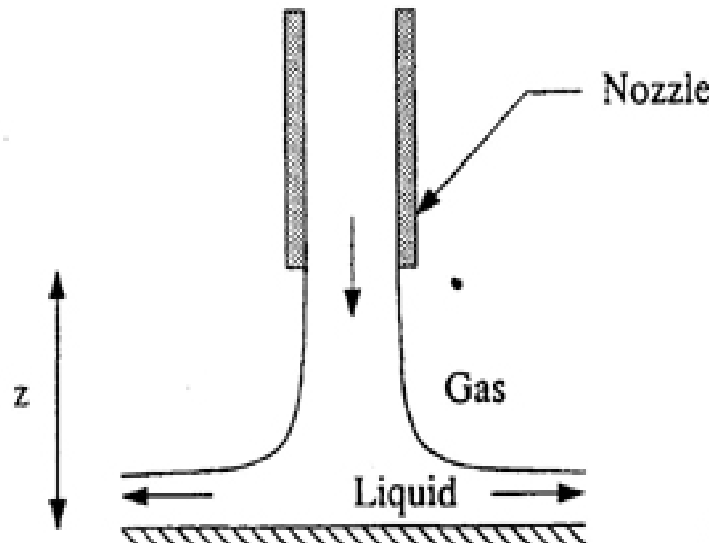
### 3. Microjet Impingement Cooling



- Applications: Plasma, optical beams, Semiconductor Laser Arrays
- *High Speed jets* from nozzles hit target , flow radially and return.
- *Very Thin Boundary Layer* is formed under the jet and high heat transfer coefficient
- Multiple nozzles to maintain temperature uniformity.

# Basics

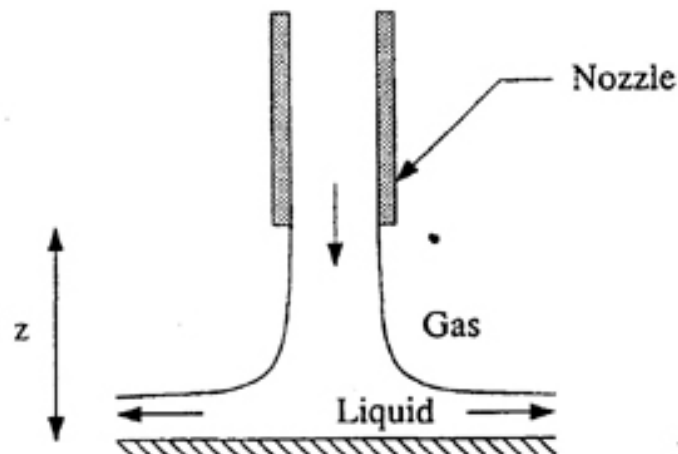
- A *high speed jet* issue from nozzles and impinge on the target plate.
- The main reason for *high heat transfer coefficient* of around  $250\text{W/cm}^2$  is that a very *thin boundary layer* is formed under the jet.
- As fluid start flowing radially outward the boundary layer thickens, and heat transfer is adversely affected.



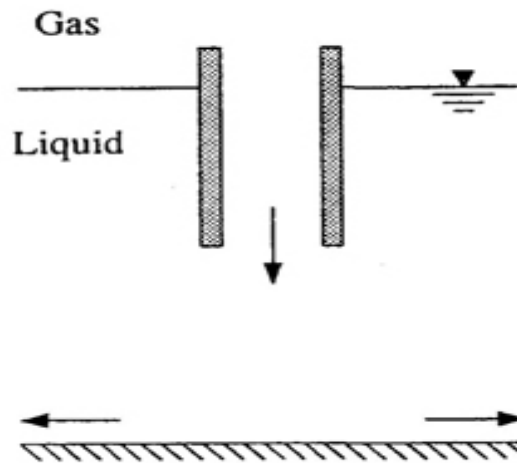
# Types of Jet Impingement

1. *Free Jet Impingement.*
2. *Submerged Jet Impingement.*

- Heat transfer coefficient for the system is a complex function of many parameters like Prandtl No, Reynolds No, nozzle to plate spacing, displacement from the stagnation point etc.



Free Jet Impingement.



Submerged Jet Impingement.

# Characteristics: Advantages and disadvantages

## Advantages

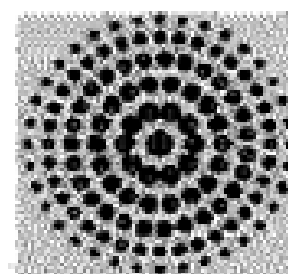
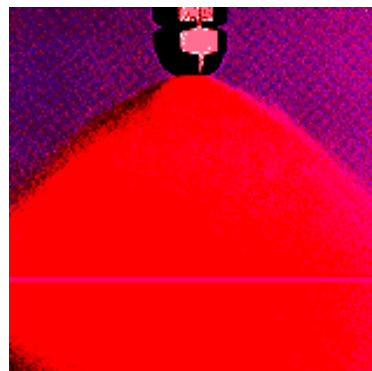
- Under Nucleate Boiling Mode: increased bubble departure frequency and *higher heat transfer coefficient*
- Offers good solution for localized cooling.

## Disadvantages

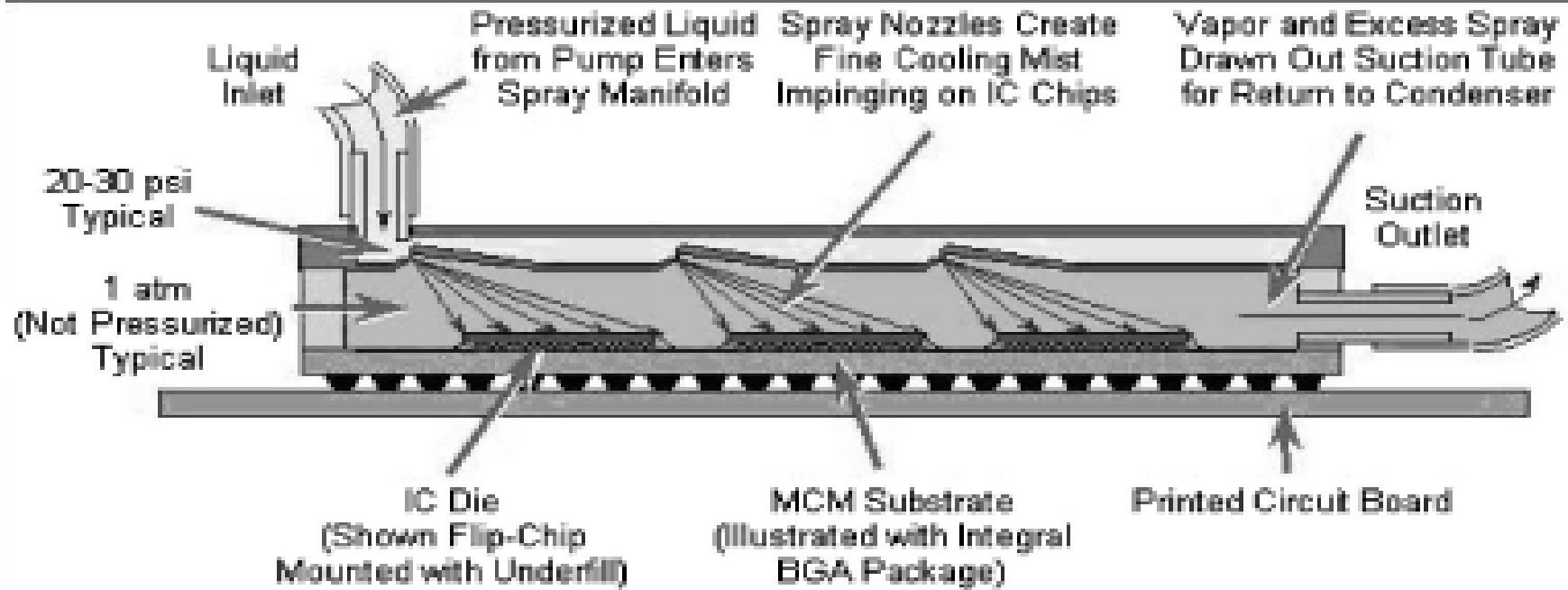
- *Multiple jets necessary.*
- Nozzle arrangement, return paths extremely important for uniform temperature distribution
- At micro-processor level cooling, management of inlet outlets, jet geometry and configuration, jet velocity parameters to be optimized

## 4. Spray cooling

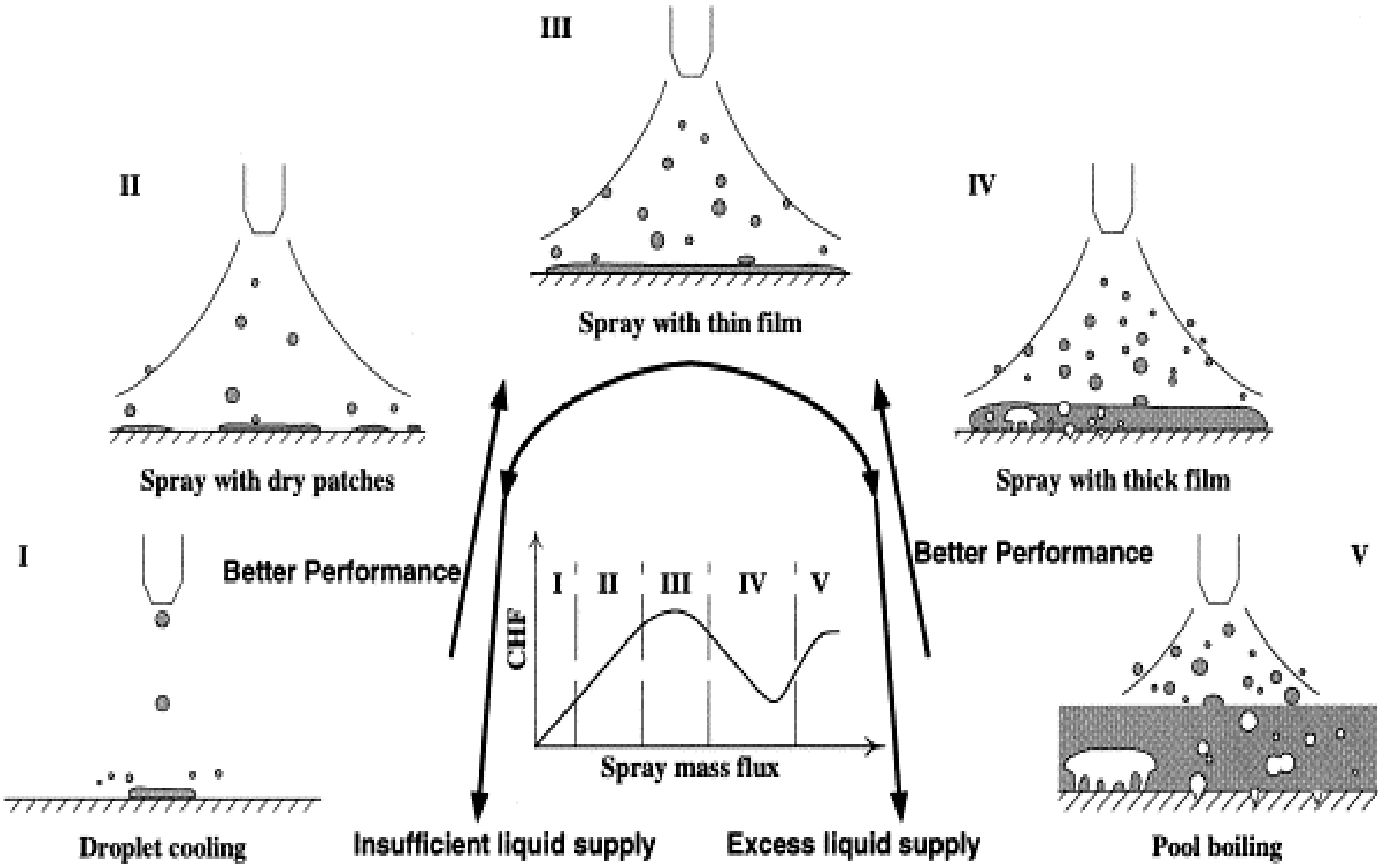
- Spray cooling occurs when liquid is forced through a small orifice, shatters into a dispersion of fine droplets, which then impact on a heated surface.
- Droplets spread on the surface and evaporate by forming **thin liquid films**.
- Dissipate large amounts of heat due to latent heat of evaporation.
- Supply of cold liquid decides the performance of cooling.
- Spray inclination angle will also affect the performance of cooling



# Spray Cooling



- Liquid droplets impinge on the surface.
- Thin films are formed on the surface .
- Large heat removed by evaporation (phase change) .
- $500\text{W/cm}^2$



# **Characteristics: Advantages and disadvantages**

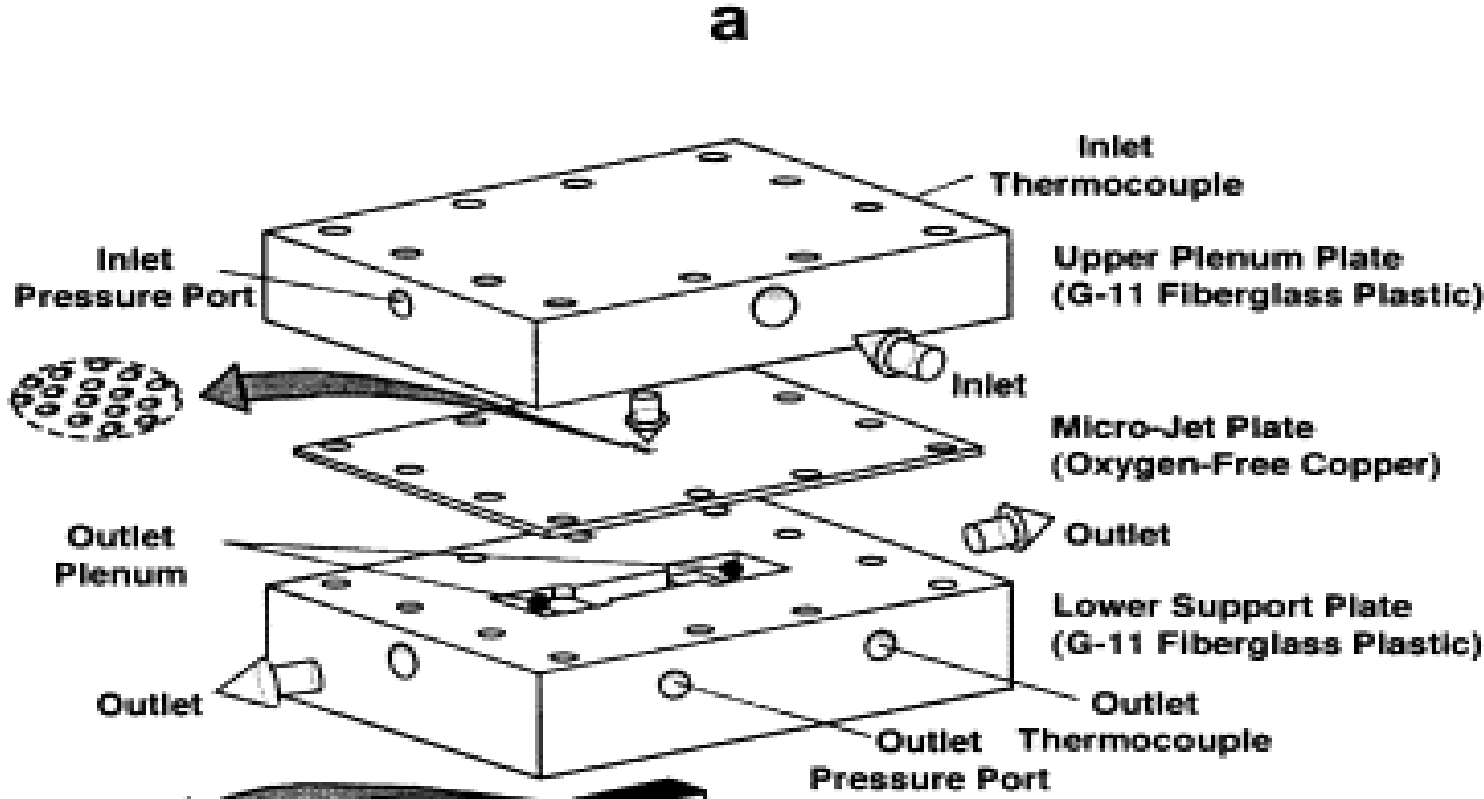
## Advantages

- Possibility of uniformly cooling *larger surfaces*.
- *Less resistance* to the removal of vapor from the heated surface.

## Disadvantages

- Multiple sprays necessary.
- Heat transfer is a complex function of droplet size distribution, droplet number density, velocity of liquid flow rate.
- *High Pressure drop*.

# Hybrid Scheme for cooling

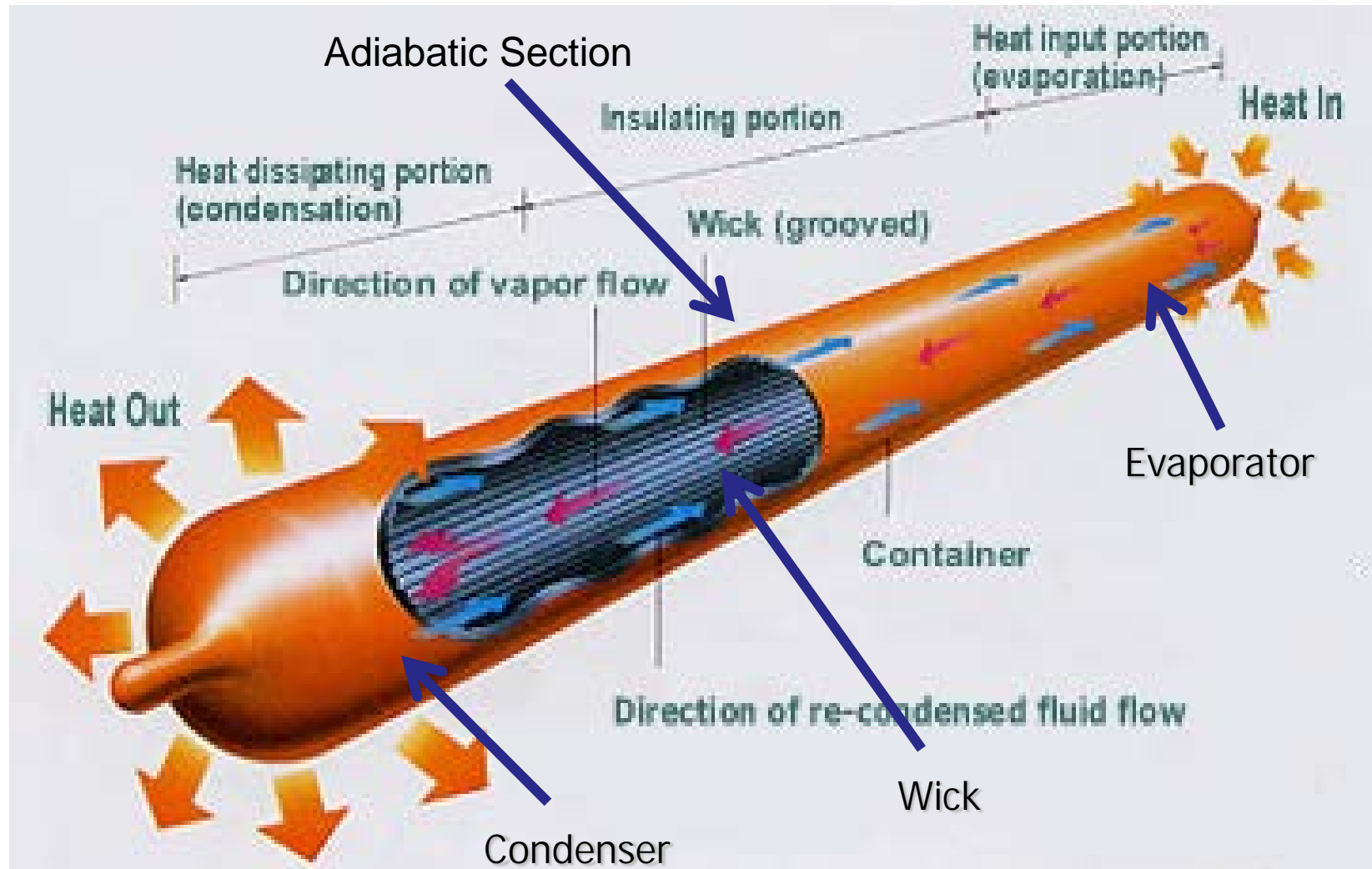


Hybrid scheme test module (high performance) 6. Schmidt, R., 2000, "Low Temperature Electronic Cooling", Electronics Cooling, Vol.6 (3), pp.18-24.

In jet impingement, problems arise due to flow blockage between closely spaced jets. It is a combination of impingement cooling and channel cooling for maintaining fairly uniform temperatures.

# Heat Pipes

Evaporator - Adiabatic Section - Condenser - Liquid flow towards the evaporative section, due to capillary pumping,



# Typical values of heat transfer coefficients

Description	Heat Transfer Coefficient (W/m <sup>2</sup> K)
Natural convection, air	3-25
Natural convection, water	15-1000
Forced convection, air	10-200
Forced convection, water	50-10,000
Condensing steam	5000-50,000
Boiling water	3000-100,000
Ultra thin film evaporation	10,000-500,000
<b>Microchannel Cooling</b>	<b>10,000-1,000,000</b>

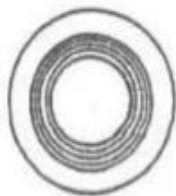
(Ref: Ohadi et al. 2005)

# Advantages of Heat Pipes

- Very high thermal conductivity. Less temperature difference needed to transport heat than traditional materials (thermal conductivity up to 90 times greater than copper for the same size) (Faghiri, 1995) resulting, in low thermal resistance.
- Efficient transport of concentrated heat. (Faghiri, 1995)
- Temperature Control. The evaporator and condenser temperature may remain nearly constant (at  $T_{sat}$ ) (Faghiri, 1995) .

# Types of Wicks

## Screen Mesh



Wrapped Screen

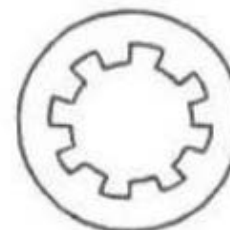


Utilizes multiple wire layers to create a porous wick.

Sintering can be used.

## Axial Grooves

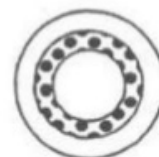
### **Axial Groove Wick**



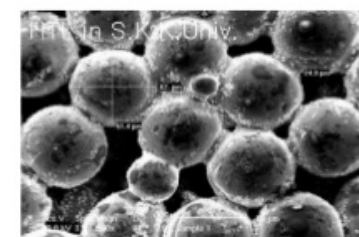
Axial Groove



## Sintered Powdered Wick



Sintered Metal

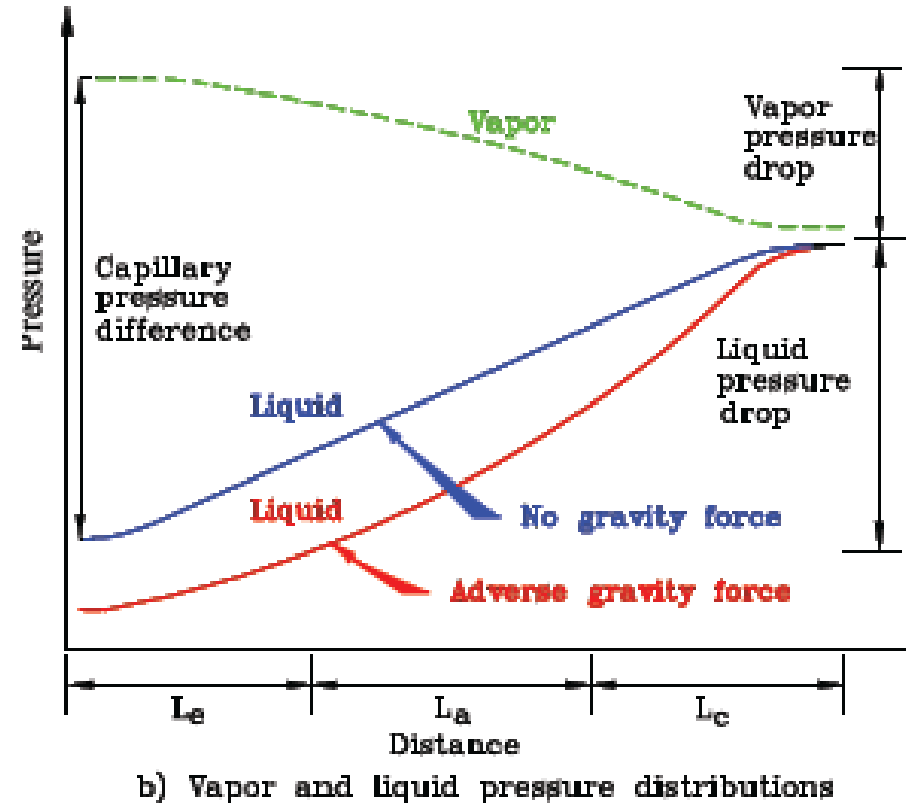
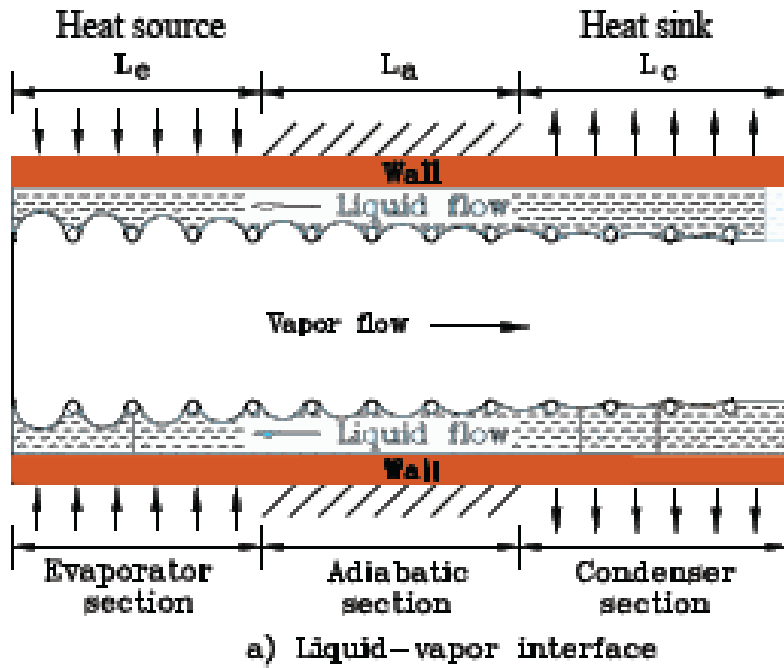


Utilizes densely packed metal spheres.

Sintering must be used to solidify the spheres<sup>27</sup>

# Desired Characteristics of a Heat Pipe & Coolant

- Compatibility of the coolant with the wick and the heat pipe material
- Wettability
- Low liquid and vapor viscosities
- Thermal stability
- High latent heat
- High thermal conductivity
- Surface tension – high or low?



Axial variation of the liquid vapor interface and the vapor and liquid pressures along the heat pipe

## Characteristics of pressure drops in Heat Pipes

Vapor pressure changes along the heat pipe - due to friction, inertia, evaporation (blowing) and condensation (suction)

Liquid pressure changes mainly due to friction

Liquid vapor interface is flat near the condenser end-cap (zero local pressure gradient) at very low vapor flow rates

Maximum pressure difference occurs near the evaporator end-cap. This maximum local capillary pressure is equal to the sum of the pressure drops in the vapor and the liquid across the heat pipe in the absence of body forces.

If body forces are present, the liquid pressure drop is greater.

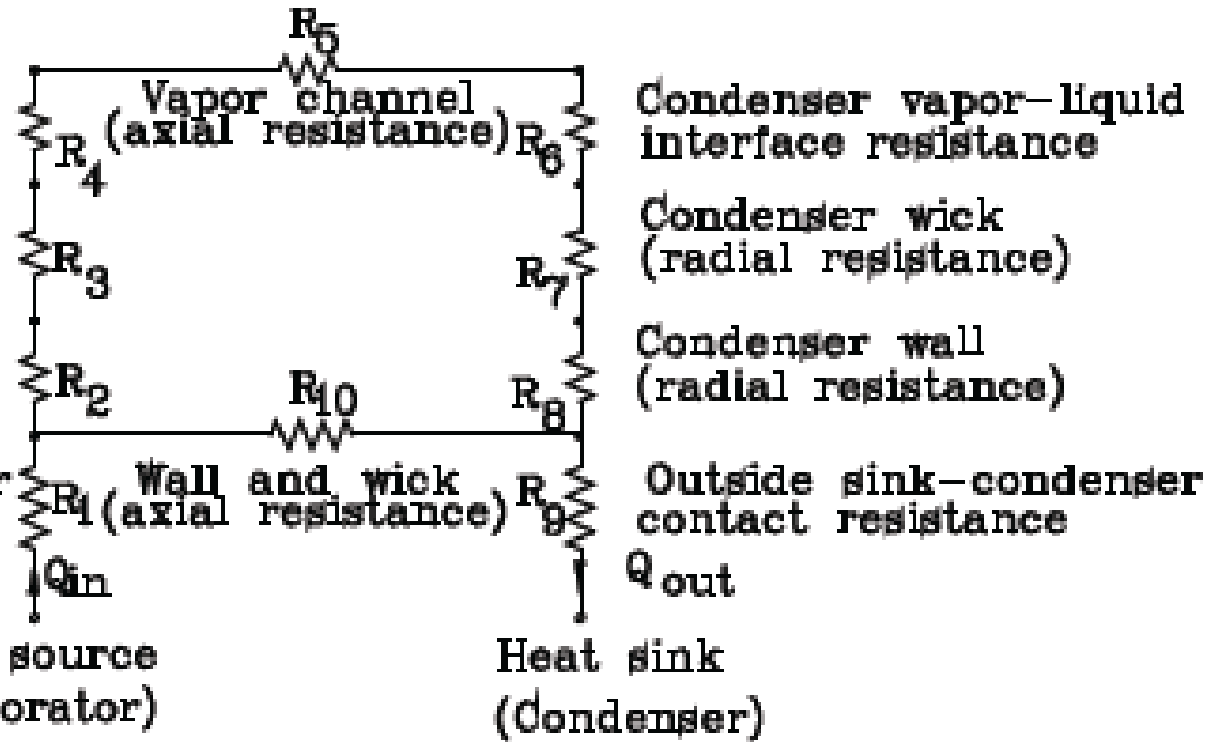
At moderate vapor flow rates, dynamic effects cause the vapor pressure drop and recovery along the condenser section.

Evaporator liquid-vapor interface resistance

Evaporator wick (radial resistance)

Evaporator wall (radial resistance)

Outside source-evaporator contact resistance



Thermal resistance model of a typical heat pipe

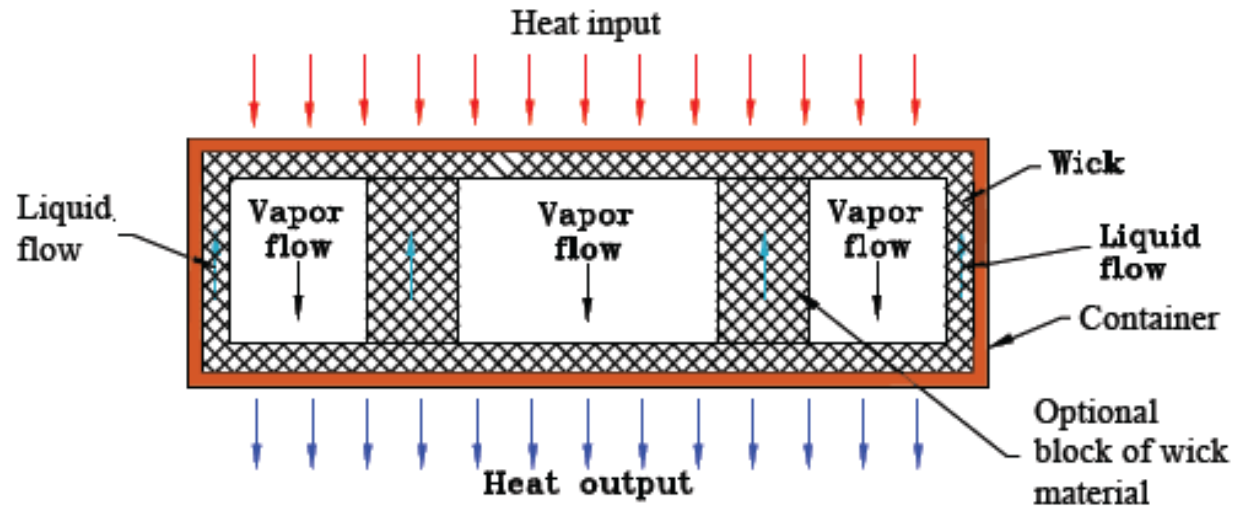
## Heat Pipe Applications

- Electronics cooling - small high performance components cause high heat fluxes and high heat dissipation demands. Used to cool transistors and high density semiconductors.
- Aerospace - cool satellite solar array during reentry (ISRO uses ammonia heat pipes).
- Heat exchangers- power industries use heat pipe heat exchangers as air heaters on boilers.
- Other applications - production tools, medicine and human body temperature control, engines and automotive industry.

## Types of Heat Pipes

### Flat Plate

Rectangular. Used to cool semiconductor or transistor packages assembled in arrays on the top of the heat pipe.

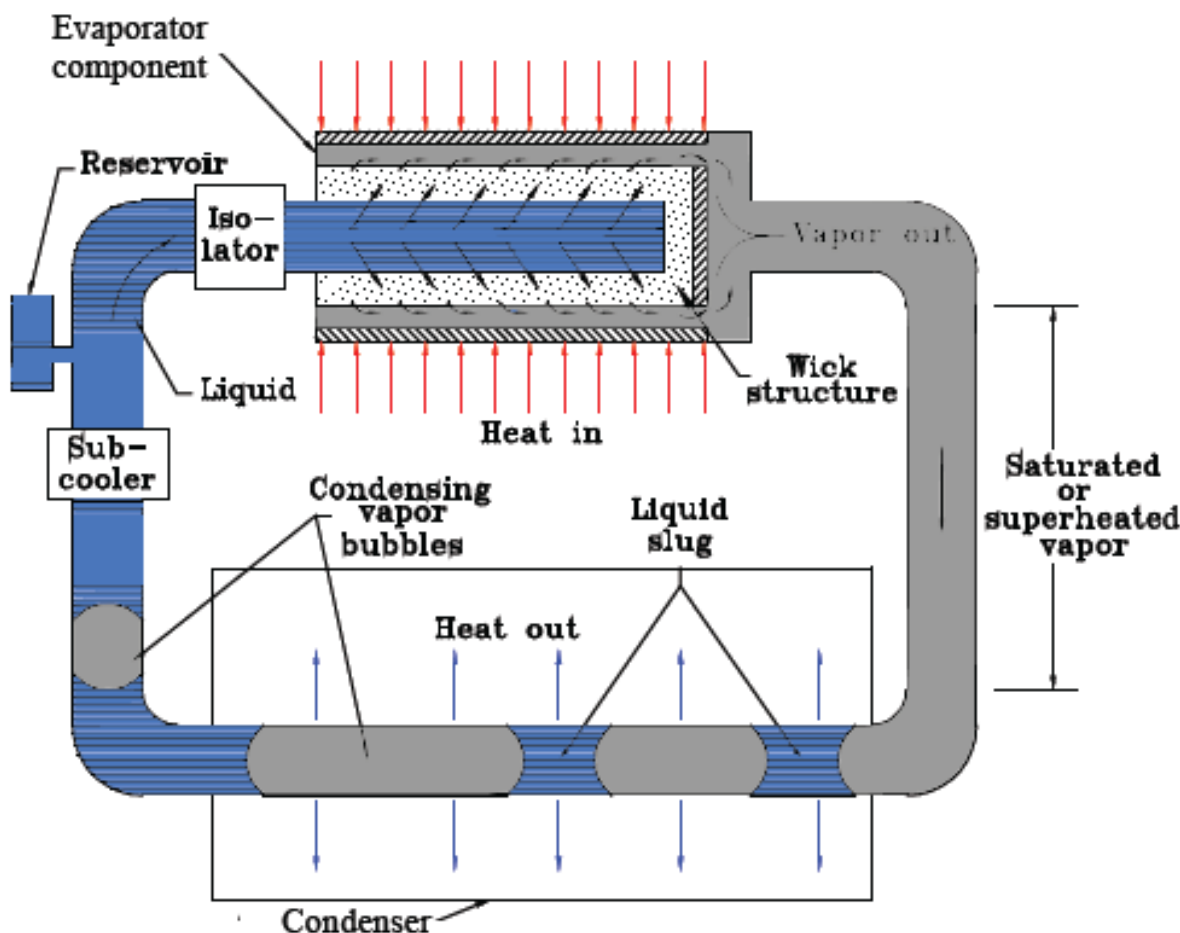


## Types of Heat Pipes

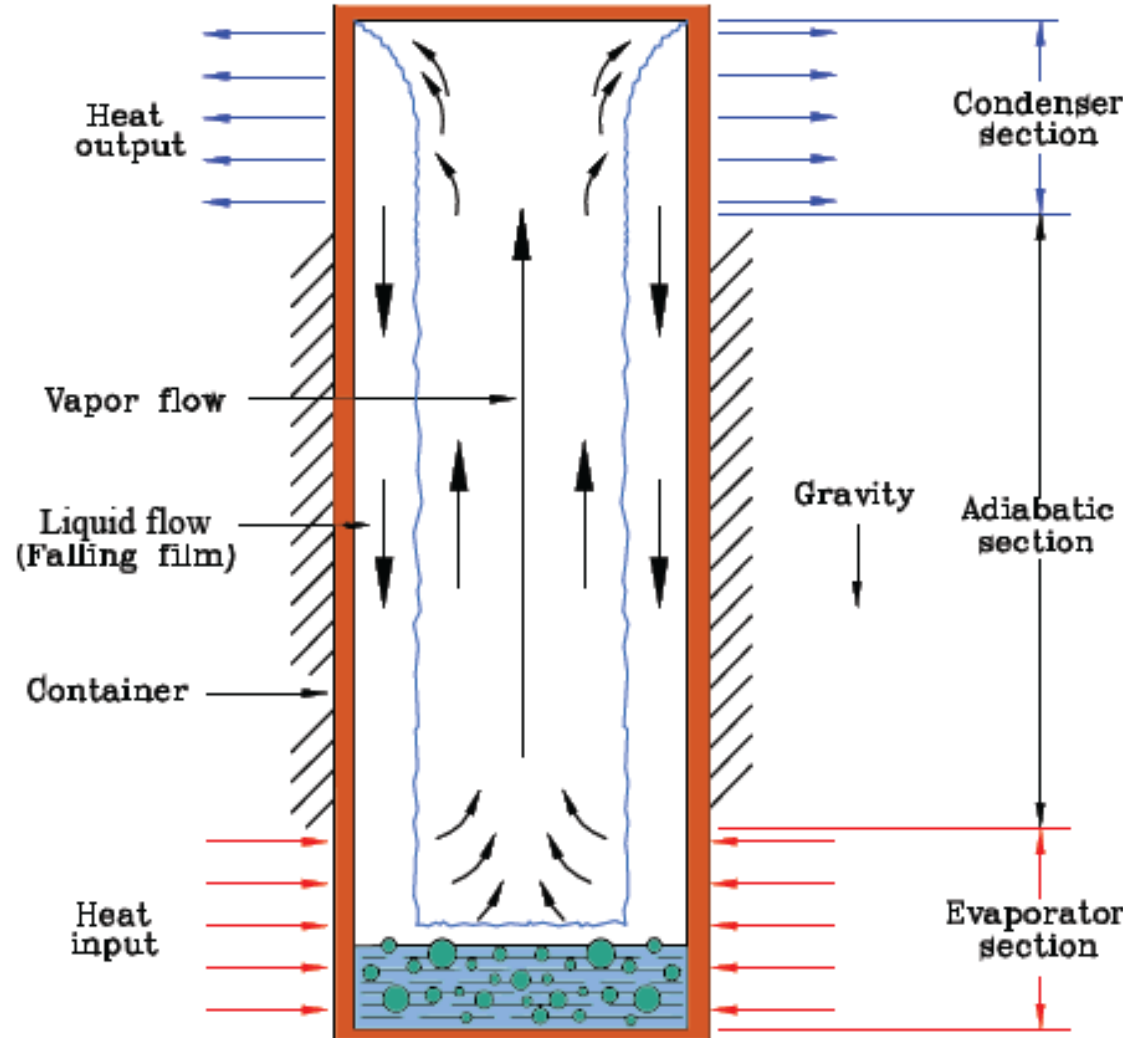
### Capillary pumped loop heat pipe

For systems where the heat fluxes are very high or where the heat needs to be moved far away. The vapor travels in a loop where it condenses and returns to the evaporator.

Used in electronics cooling.



# Types of Heat Pipes

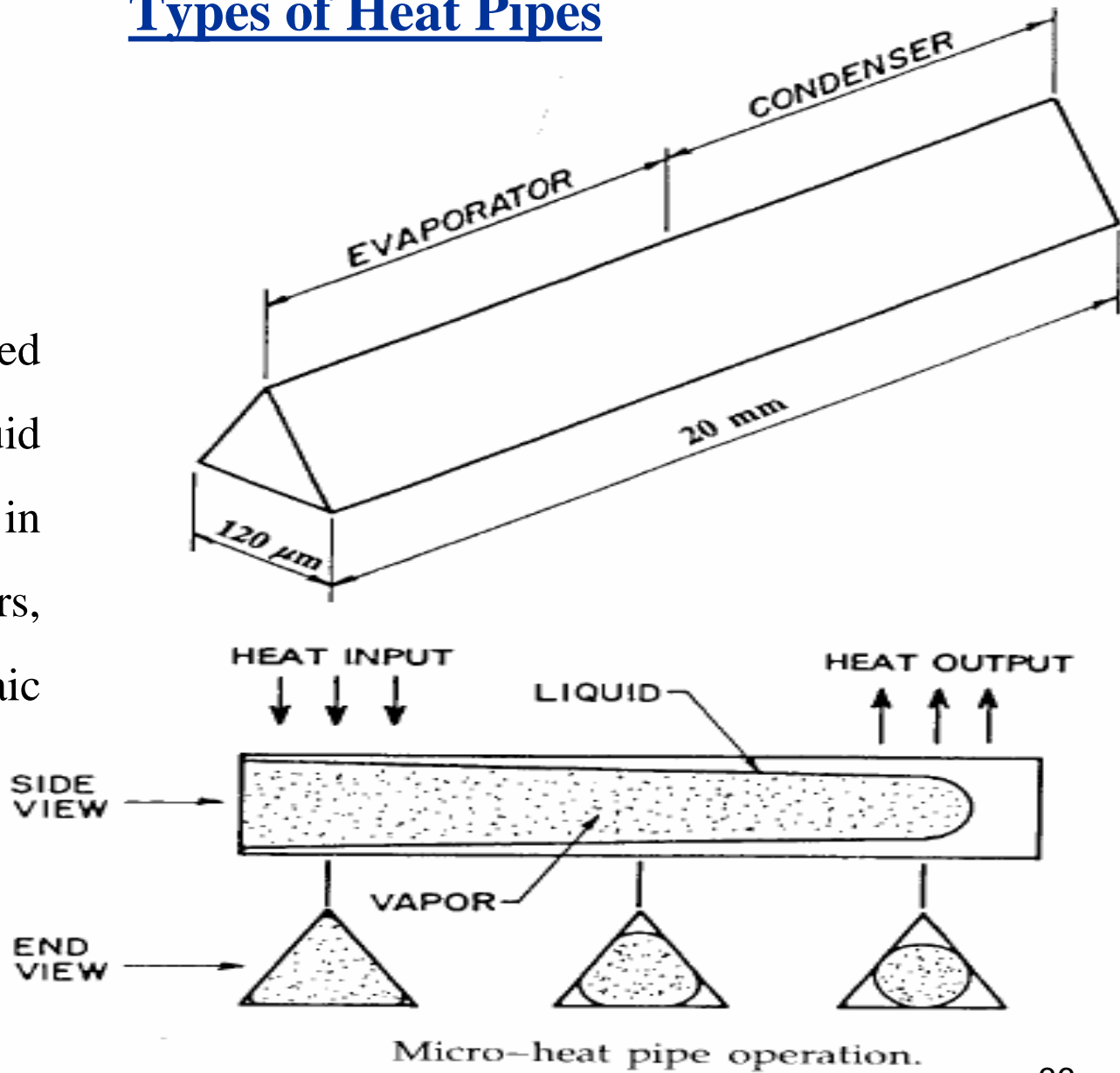


Gravity assisted wickless heat pipe (two phase closed thermosyphon)

## Types of Heat Pipes

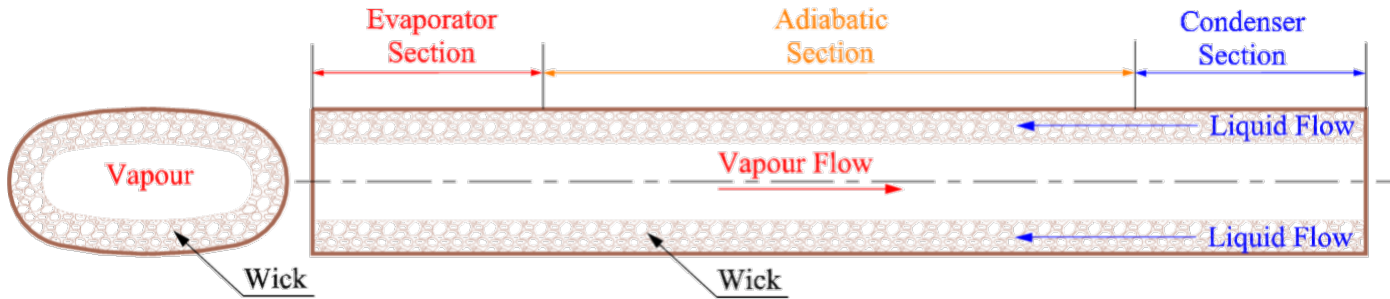
### Micro heat pipes

Noncircular, angled corners act as liquid arteries. Employed in cooling semiconductors, laser diodes, photovoltaic cells, medical devices.

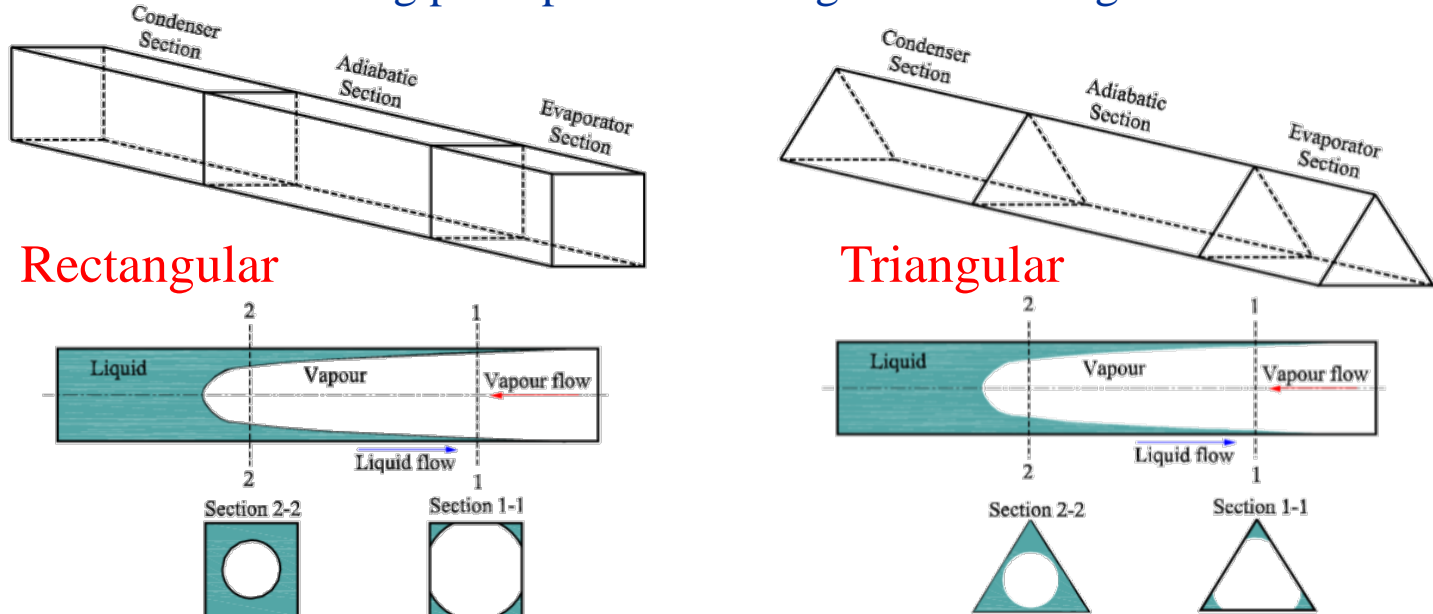


# Conventional vs. Micro Heat Pipe

Schematic representation of working principle of a conventional (wicked) heat pipe



Schematic representation of working principle of a rectangular and triangular micro heat pipes

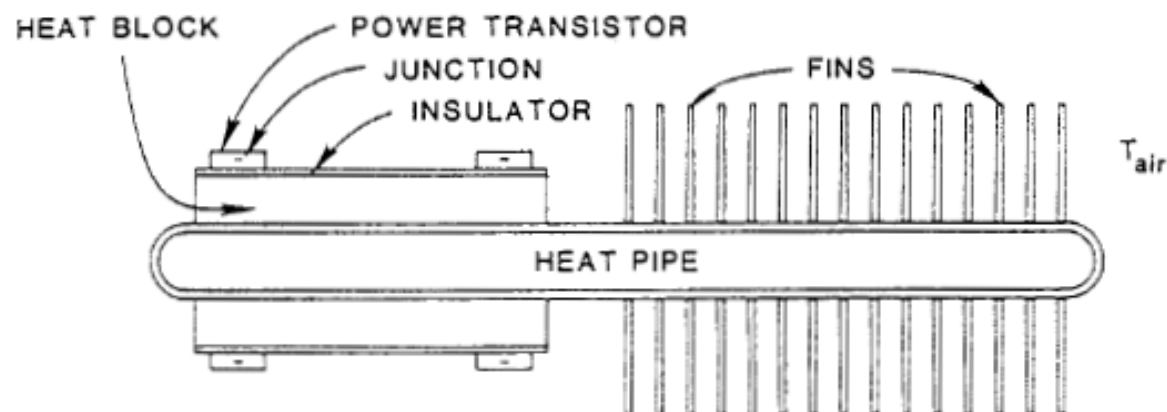


# Heat Pipes in Electronics Cooling

- Common heat pipes used in electronics cooling:
  - Micro heat pipes
  - Capillary looped heat pipes
  - Flat plate heat pipes
  - Variable conductance heat pipes

# Heat Pipes in Electronics Cooling

- The heat pipe's evaporator may be attached to a heat source (chip or power transistor).
- The condenser is attached to a heat sink to dissipate the heat through free or forced convection.

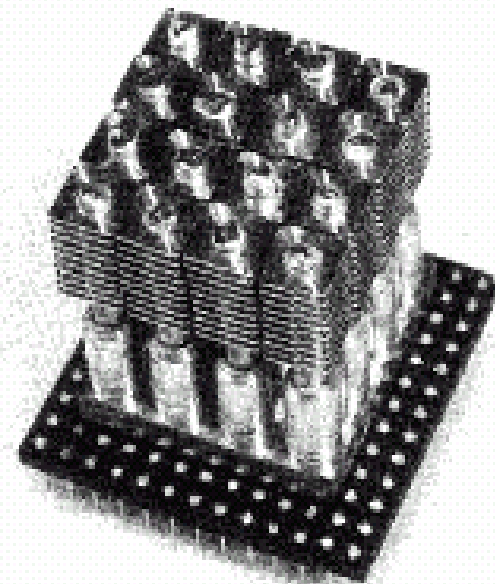


Heat pipe heat sink for power transistors (Murase et al., 1982).

## Heat Pipes in Electronics Cooling

Micro heat pipes may be used for cooling individual semiconductors or an array.

Good for applications where space is limited like laptops.



Micro heat pipe array (courtesy of Itoh Research

# Heat Pipes in Electronics Cooling

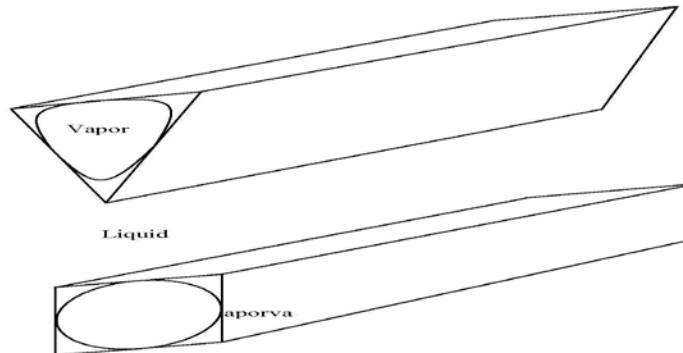
- Summary:
  - Heat pipes enable devices with higher density meet heat dissipation requirements with greater reliability.
  - Proven alternative to conventional methods

## Micro Heat Pipes

A micro heat pipe is a **wickless, non-circular channel** with a diameter of 10–500  $\mu\text{m}$  and a length of 10–20mm

A micro heat pipe is "so small that the mean curvature of the liquid-vapor interface is comparable in magnitude to the reciprocal of the hydraulic radius of the total flow channel" - Cotter, 1984.

The fluid flow inside the pipe is caused by **change in pressure** (due to changes in capillary and intermolecular force field) along the length of the heat pipe.



High efficiency,  
reliability and cost  
effective

Schematic of triangular and rectangular heat pipes

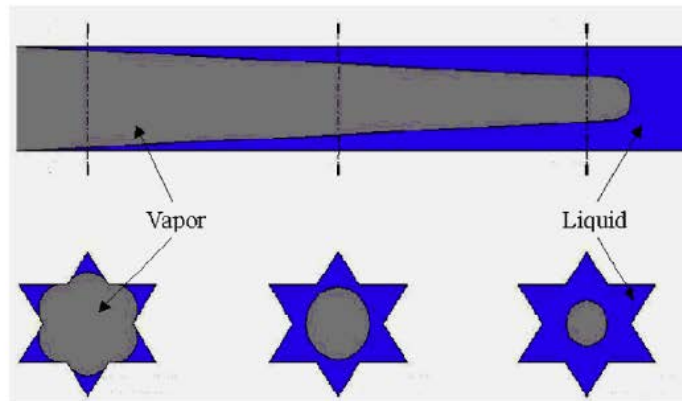
## Basic Mechanisms of Transport in MHP

The net capillary force is generated by the integral effect of the evaporating and condensing menisci.

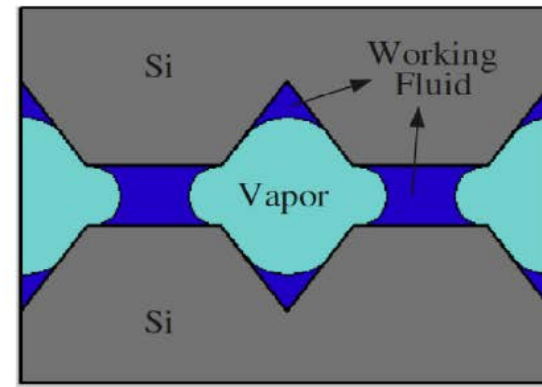
The surface tension forces, wettability and the solid–liquid interactions primarily govern the behavior of the various interfaces, particularly the liquid–vapor interface.

The fluid flow in the evaporating meniscus results from a change in the meniscus profile

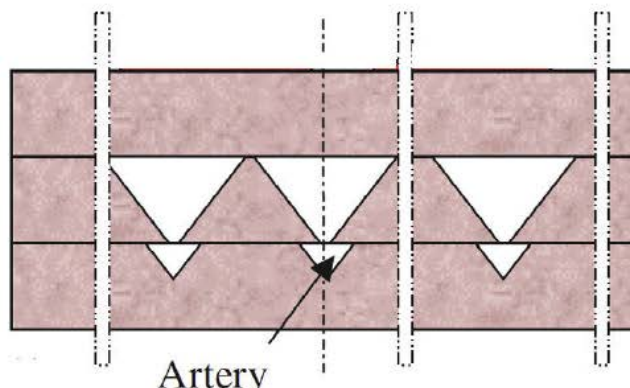
- Flow due to a difference in curvature
- Evaporation from ultrathin films where intermolecular forces predominate



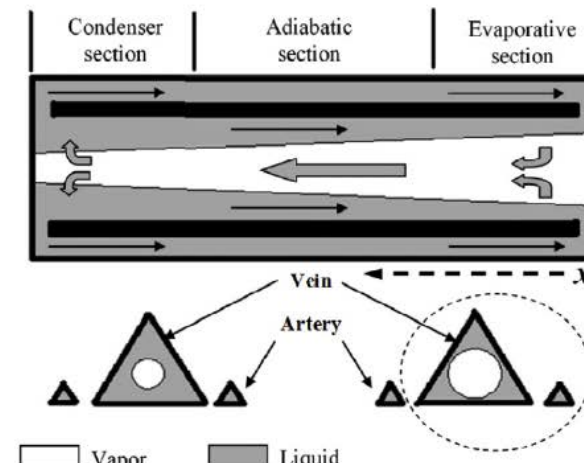
(a)



(b)



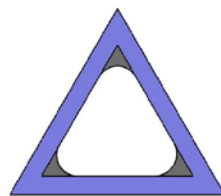
(c)



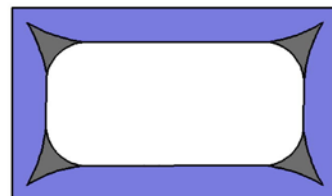
(d)

Schematic diagram of micro-GHPs with diverse novel channel structures to enhance capillarity: (a) star grooves micro-GHP (b) rhombus grooves micro-GHP; (c) triangular channels coupled with arteries (d) micro-GHP with vein and two neighboring arteries

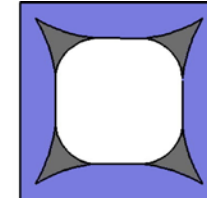
## Cross sections of individual MHPs



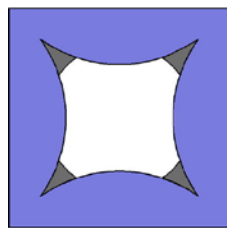
(a)



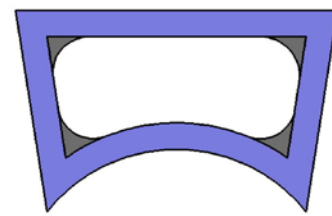
(b)



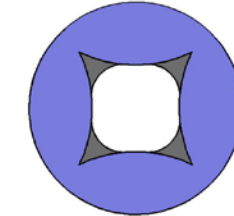
(c)



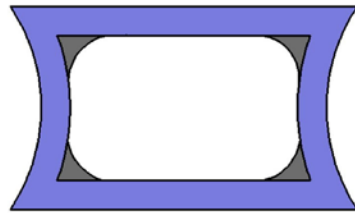
(d)



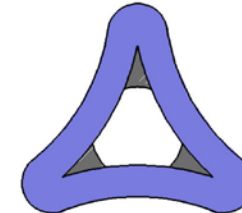
(e)



(f)

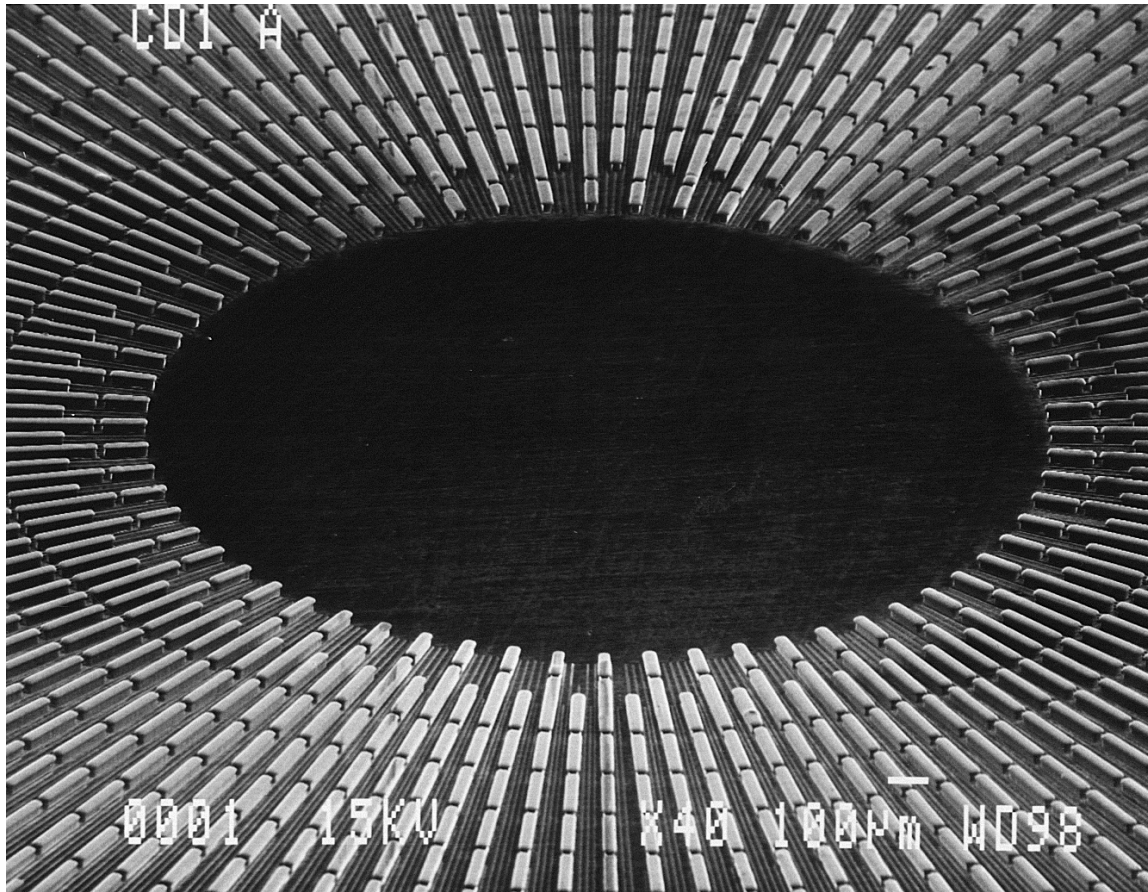


(g)



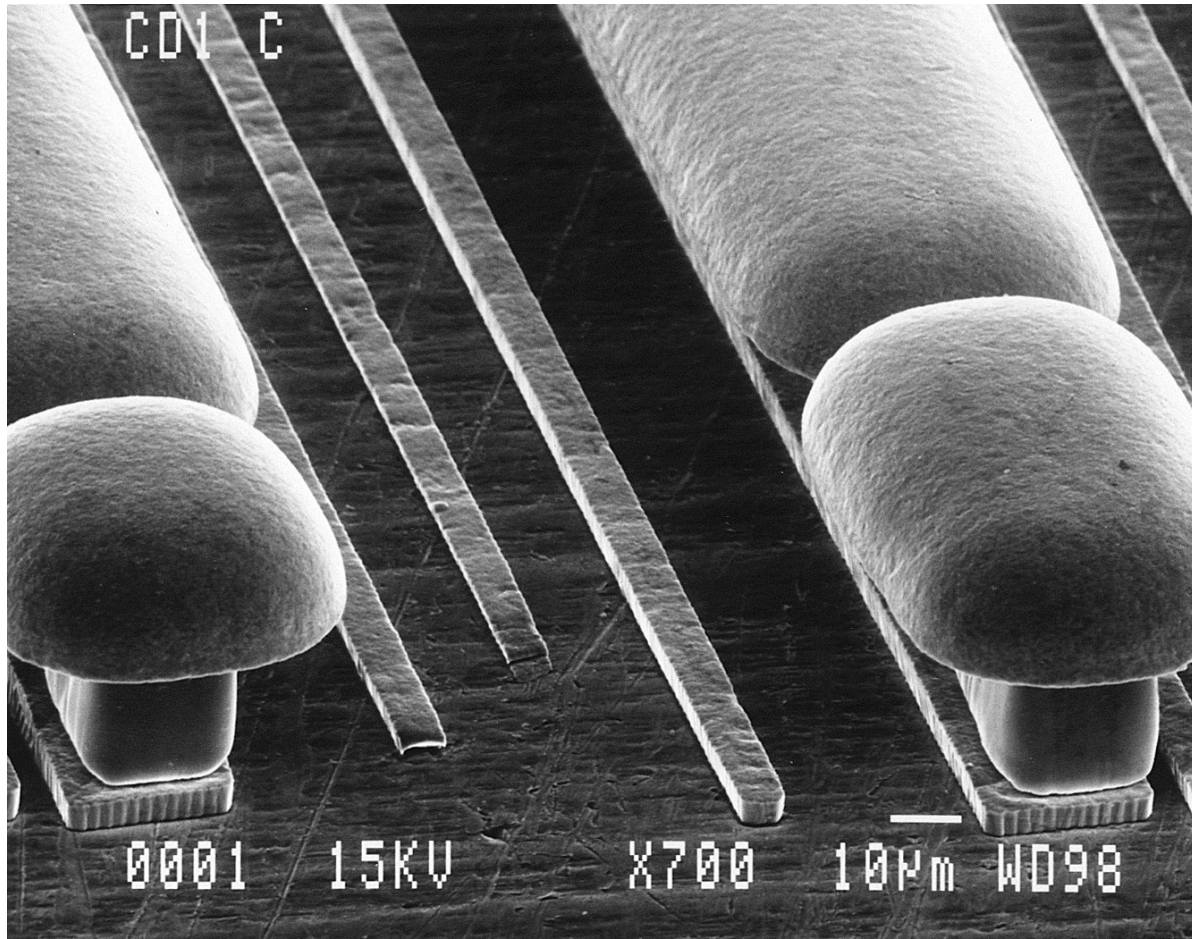
(h)

(a) and (h) triangular section; (b) and (g) rectangular section; (c), (d) and (f) square section; (e) trapezoidal section



Sandia  
National  
Lab, 2006

Configuration of micron-scale ridges and valleys forms a radial network of passages within the substrate that, when injected with a coolant, efficiently moves heat away from an operating microchip, which would be adhered to the substrate near the center of the array.

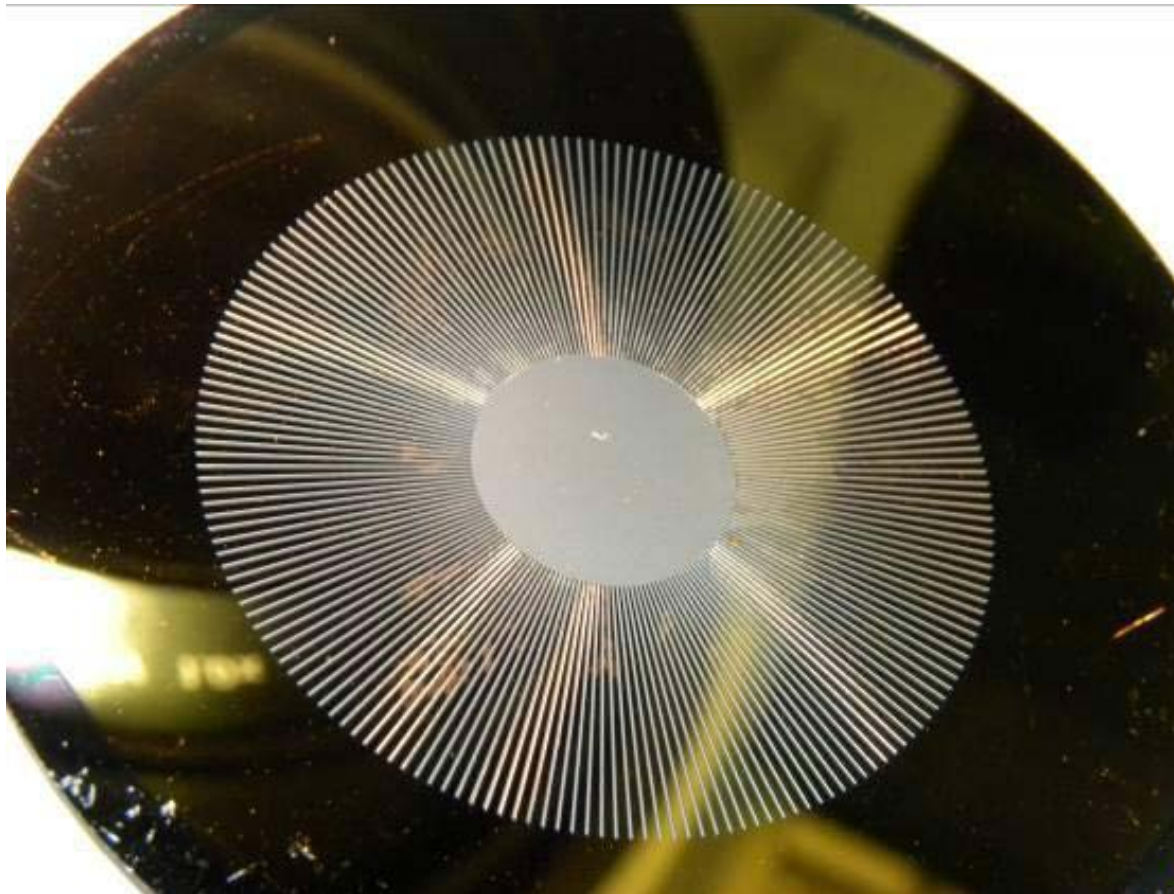


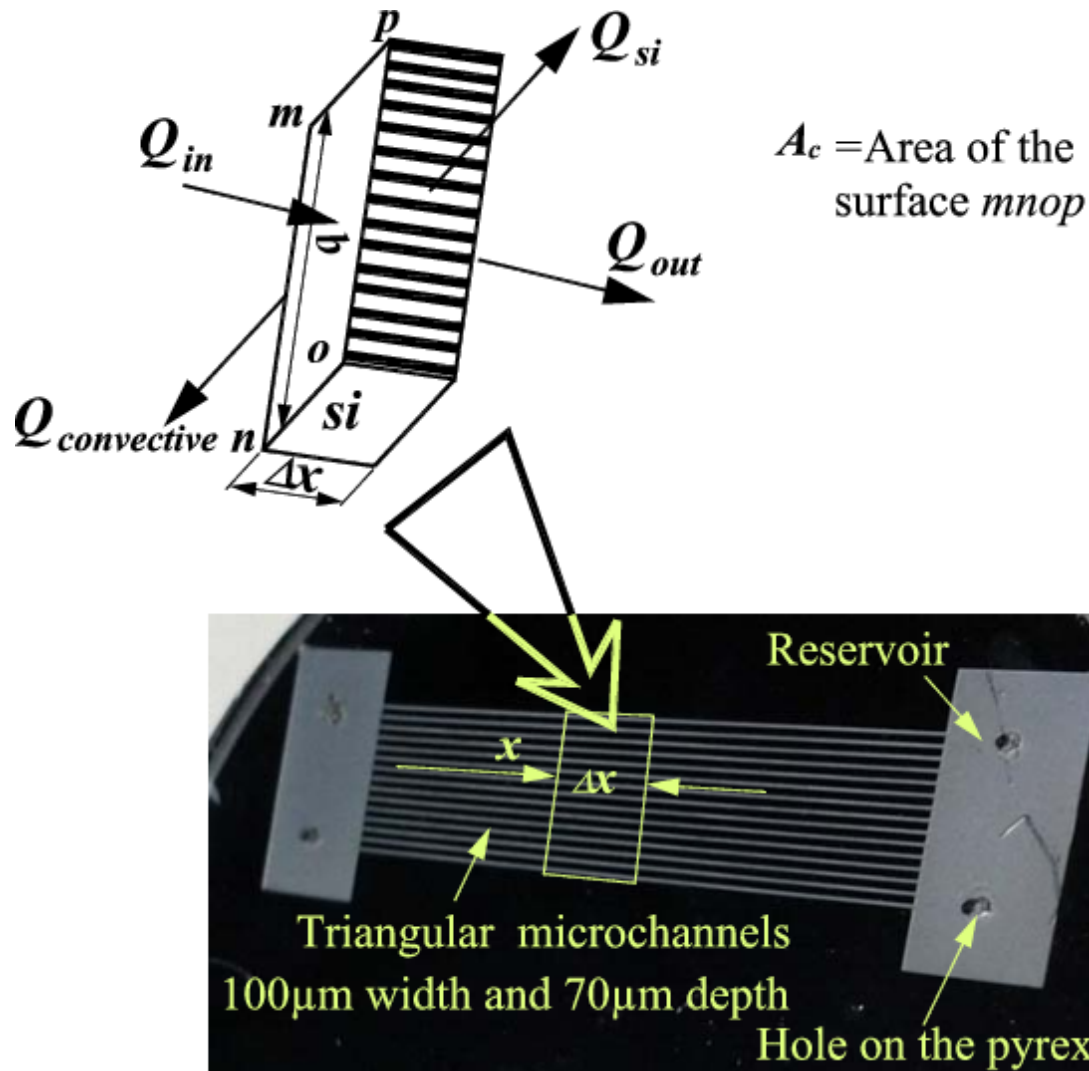
The large ridges are 10-20 microns wide; the smaller are about 5 microns wide

Summary of some typical charging and packaging methods for MEMS-based MHPs.

Working fluids	Charging methods	Volume control	Packaging methods
Methanol	Fully fill working fluid vapor characterized by high pressure and then condense into desired amount of liquid	Accurate	Ionic or ultraviolet bonding
DI water	Fully fill working fluid and then partially remove through evaporation	Less accurate	Sealed with silicone sealant
Ethanol and methanol	Fully fill condensate from working fluid as a vapor and then partially remove through pumping out	Accurate	Sealed with close valve
Water and methanol	Backfill the working fluid after evacuation, and then fill with a micro-metering valve controllably	Accurate	Sealed with close valve
DI water	Fully fill working fluid and then partially remove through pumping out	Less accurate	Fuse the filling glass tube connected to the filling hole

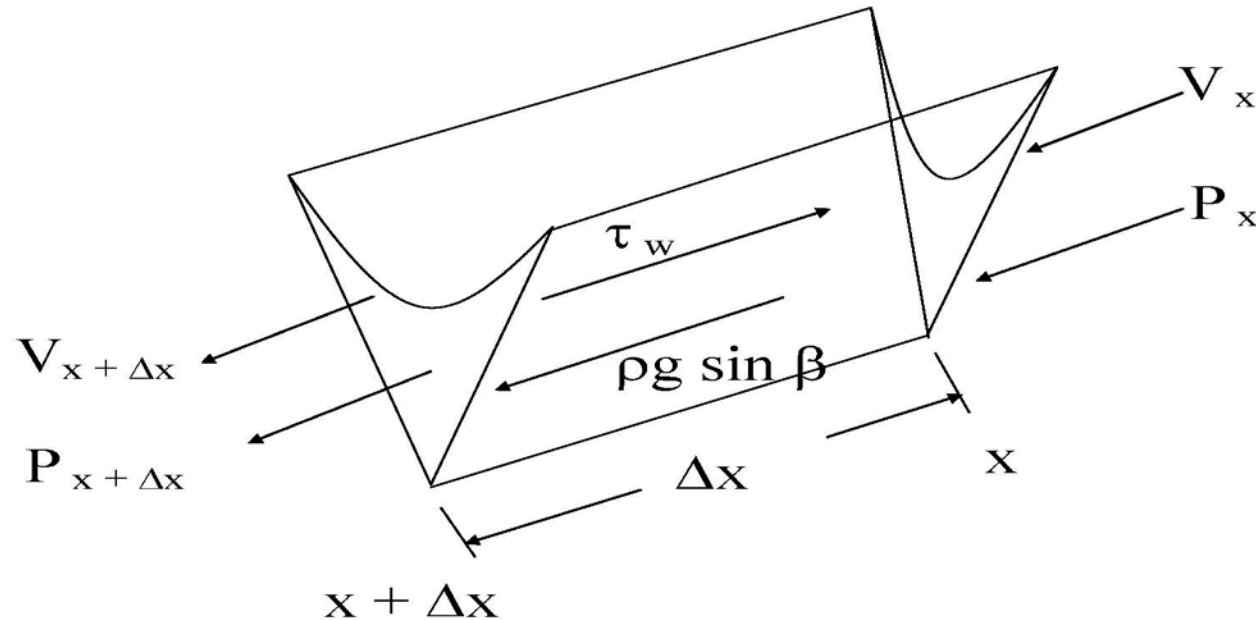
**Radial Grooved U shaped (100 µm x 40 µm)  
Microchannel Arrays - RIE  
IIT Kharagpur**





Closed microchannel arrays on silicon with reservoirs

# Modeling of Flow and Heat Transfer in Microchannels



The liquid pressure as a function of the radius of curvature – from Young-Laplace equation, 
$$\frac{dP}{dx} = \frac{\sigma}{R^2} \frac{dR}{dx}$$

$\frac{dP}{dx}$  and  $\frac{dR}{dx}$  - pressure and radius of curvature gradient respectively

The steady state momentum balance in differential form

$$\rho A_l V \frac{dV}{dx} + A_l \frac{dP}{dx} + 2 L_h \tau_w - \rho g \sin(\beta) A_l = 0$$

convective momentum      pressure force      wall shear      gravity

A macroscopic approach to develop a general model for a heat pipe with grooves of any shape.

Axial flow due to the change in the radius of curvature.

The effect of body forces incorporated.

## Differential form of the mass balance

$$\frac{d}{dx}(\rho V A_l) + \frac{Q_v R_l}{\lambda} = 0$$

Net mass entering the volume element is equal to the mass evaporated from the volume element

## Energy balance in the volume element

$$\rho C_p V A_l \frac{dT}{dx} = Q W_b - Q_v R_l$$

Heat supplied to the element is equal to the evaporative heat leaving the element

## Boundary Conditions

$$x = 0$$

$$V = 0$$

$$x = L \quad R = R_o$$



$$P = P_{v_o} - \frac{\sigma}{R_o}$$

from geometry for filled groove

$$p_v - p_l = \frac{\sigma}{r}$$

$$\rho \left[ \frac{\partial V}{\partial t} + (\bar{V} \cdot \nabla) \bar{V} \right] = -\nabla P + F_B + \mu \nabla^2 \bar{V}$$

Because the flow rate is very small, the convective term in the equation can be neglected

$$\frac{dp_l}{dx} + \rho_l g \sin \beta + F_v = 0,$$

$$\frac{dP_l}{dx} = -\frac{d}{dx}(P_v - P_l) = -\frac{d}{dx}\left(\frac{\sigma}{r(x)}\right)$$

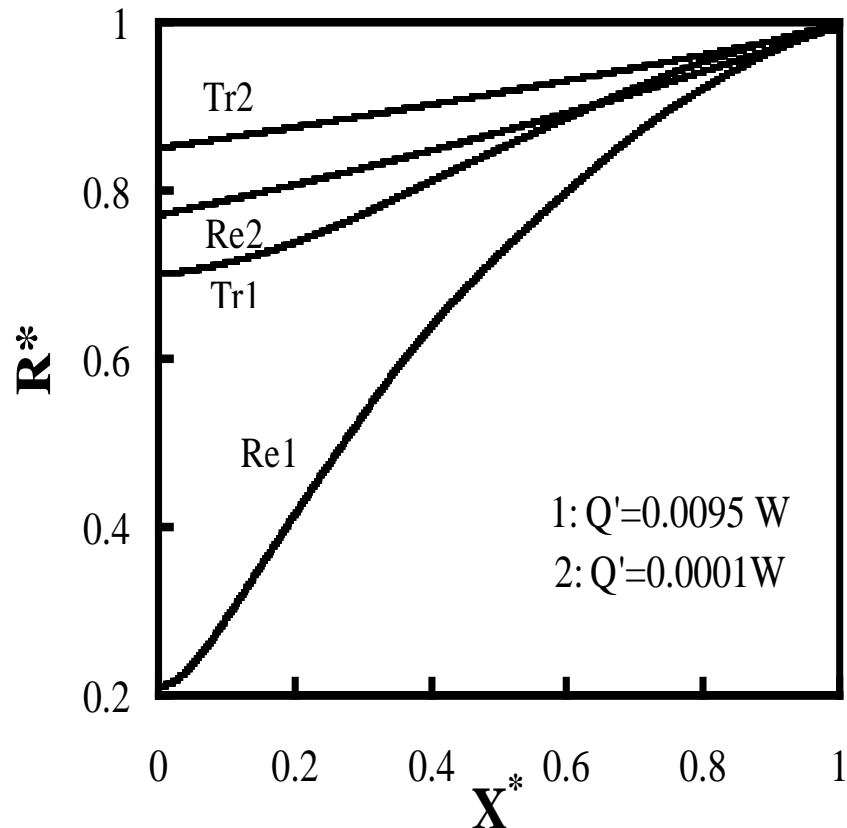
$$\frac{d}{dx} \left( \frac{\sigma}{r(x)} \right) = \left( \frac{2K\mu_l}{c_3 r(x)^4} \right) \Gamma_c + \rho_l g \sin \beta,$$

$$c_3 = 4 \tan^2 \alpha \left( \frac{1}{\tan \alpha} + \alpha - \pi/2 \right)^3.$$

$\Gamma_c$ , is the mass flow rate through the cross-section of the groove, and the parameter ‘K’ is a function of the groove half angle,  $a$ , and the liquid contact angle. Equation is valid for both the evaporative and adiabatic regions

$$\Gamma_c = \int_0^{\Gamma_c} d\Gamma_c = \left( \frac{2\omega_b}{h_{fg}} \right) \int_x^{x_{max}} q''(x) dx.$$

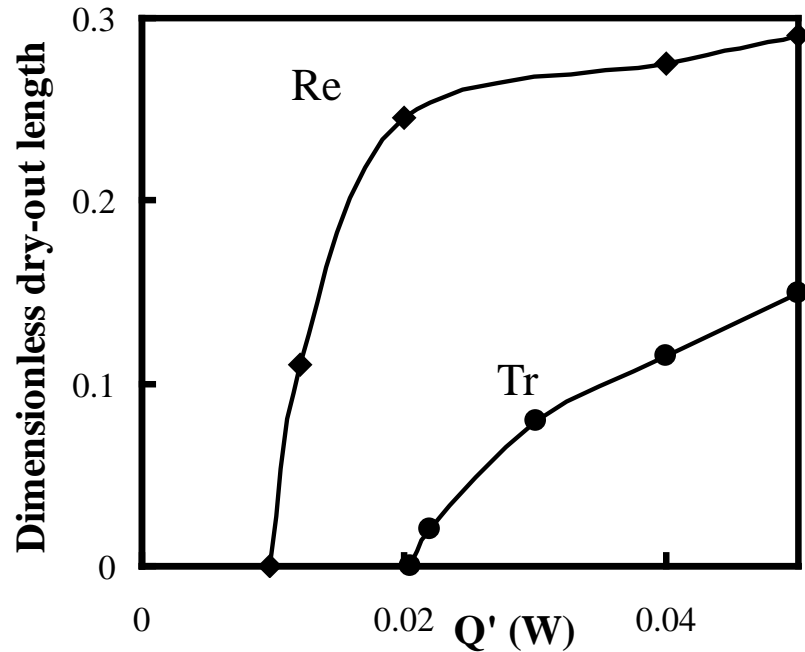
## Numerical Solution for two heat pipe geometries – triangular (400 $\mu\text{m}$ side) and rectangular (800 $\mu\text{m}$ x 400 $\mu\text{m}$ )



Profiles of the dimensionless radius of curvature along the length of the heat pipe for different values of heat input and heat pipe geometry

The behavior of the radius of curvature gives a qualitative idea of the capillary pumping capacity

For the same heat input, the liquid meniscus will be more depressed (higher curvature) at the hot end for the case of a rectangular heat pipe compared to a triangular heat pipe.



Variation of the dimensionless  
dry-out length.

Critical heat input: the flow resulting from the curvature change will not be able to meet the evaporation rate. The radius of curvature at the hot end reaches a value close to zero.

## Operating Limits of HP and MHP

### Capillary Limit

Working fluid circulation in a heat pipe is achieved through the capillary pressure head developed within the grooves

The capillary pressure head must be greater than the sum of pressure losses along the vapor-liquid path.

The approximate maximum heat transport for steady state (Cotter)

$$Q_{\max} = \frac{0.16\beta\sqrt{K_l K_v}}{8\pi H(1)} \frac{\sigma h_f}{v_l} \sqrt{\frac{v_l}{v_v}} \frac{A^2}{L}$$

Where  $K_l$  and  $K_v$  are flow shape factors and  $H(1)$  is an integral of the fraction of the total heat transport over the length of the pipe, and  $\beta$  is dimensionless geometric factor.

## Sonic Limit

The vapor mass flow rate increases with decrease in the condenser pressure.

As the velocity reaches the sonic velocity at the end of the evaporator, further reduction in condenser pressure will not lead to any increase in mass flow rate.

This velocity of vapor is called the sonic limit.

$$Q_{s,\max} = A_v \rho_v h_f \left( \frac{\gamma_v R T_v}{2(\gamma_v + 1)} \right)^{1/2}$$

Where  $\gamma$  is the ratio of specific heats and  $R$  is gas constant

## Entrainment Limit

Very high vapor velocity in opposite direction may cause waves and the interfacial shear forces may become greater than the liquid surface tension forces.



Entrainment of liquid droplets



Limits axial heat flux

Entrainment limit can be estimated

$$Q_{e,\max} = A_v h_R \left( \frac{\sigma \rho_v}{2r_h} \right)^{1/2}$$

where  $r_h$  is the hydraulic radius of the wick structure

## Viscous Limit

At low operating temperatures, the vapor pressure difference between the evaporative and the condenser region may be very small.

The viscous forces within the vapor region may actually be larger than the pressure gradients caused by the imposed temperature field.

The no-flow and low flow condition in the vapor portion of a heat pipe is referred to as the viscous limitation.

Most often observed in cryogenic heat pipes.

$$Q_{v,\max} = \frac{r_v^2 h_f g \rho_v P_v A_v}{16 \mu_v L_{\text{eff}}}$$

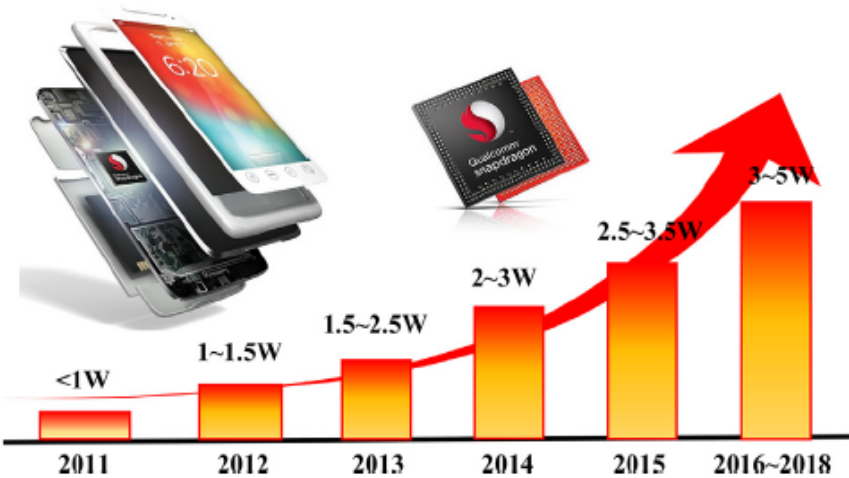
$r_v$  is the equivalent radius of vapor space,  $L_{\text{eff}}$  effective length of heat pipe.

## Major Conclusions

- Effects of body forces are small compared to surface force (true for smaller channels)
- The liquid will be equally distributed among all corners
- Increase in the apex angle reduces capillary suction capability
- The profile of the radius of curvature is used to predict the onset of the dry-out point.
- Dry-out length increases with increase in number of corners, heat input and inclination.

# Ultra-thin Micro Heat Pipes for Electronic Cooling

*To address the development requirements of mobile electronics,*



## Power consumption of CPU processors of mobile phones

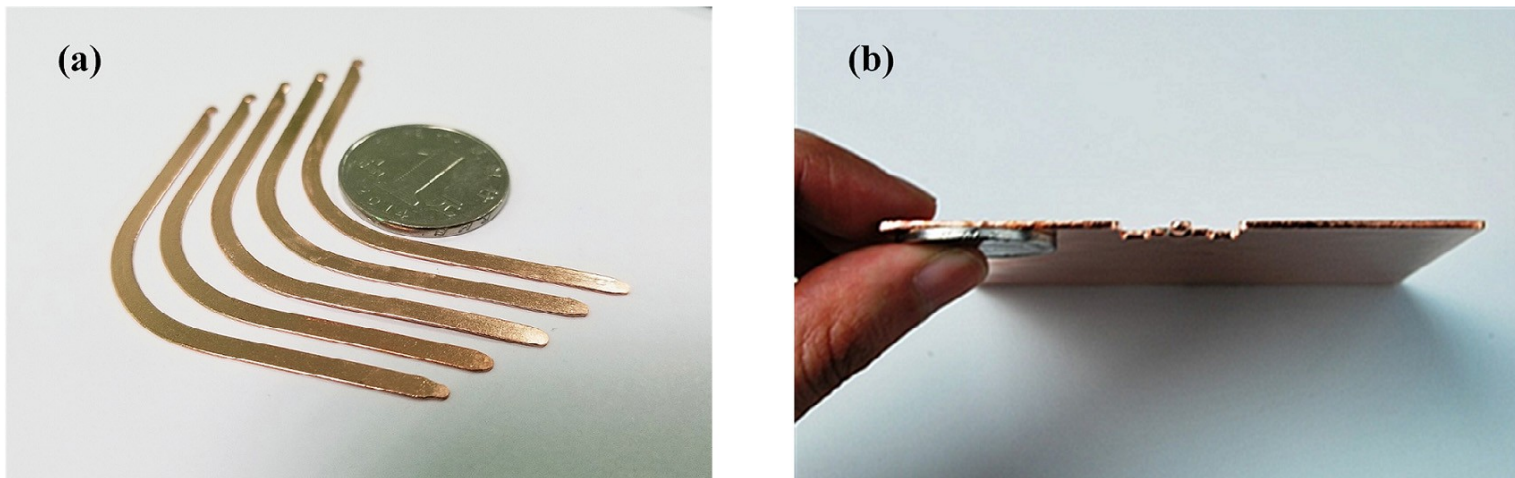
Research in the field of UTHPs has focused on the thickness range 1.0–1.5 mm. However, as the smartphone develops and becomes popularized rapidly, UTHPs with thicknesses below 0.6 mm have become the current research focus.

The rapid development of UTHPs has provided a highly efficient method to cool electronic devices with high power density and limited heat dissipation space.<sup>63</sup>



Applications of UTHPs in portable electronic devices.

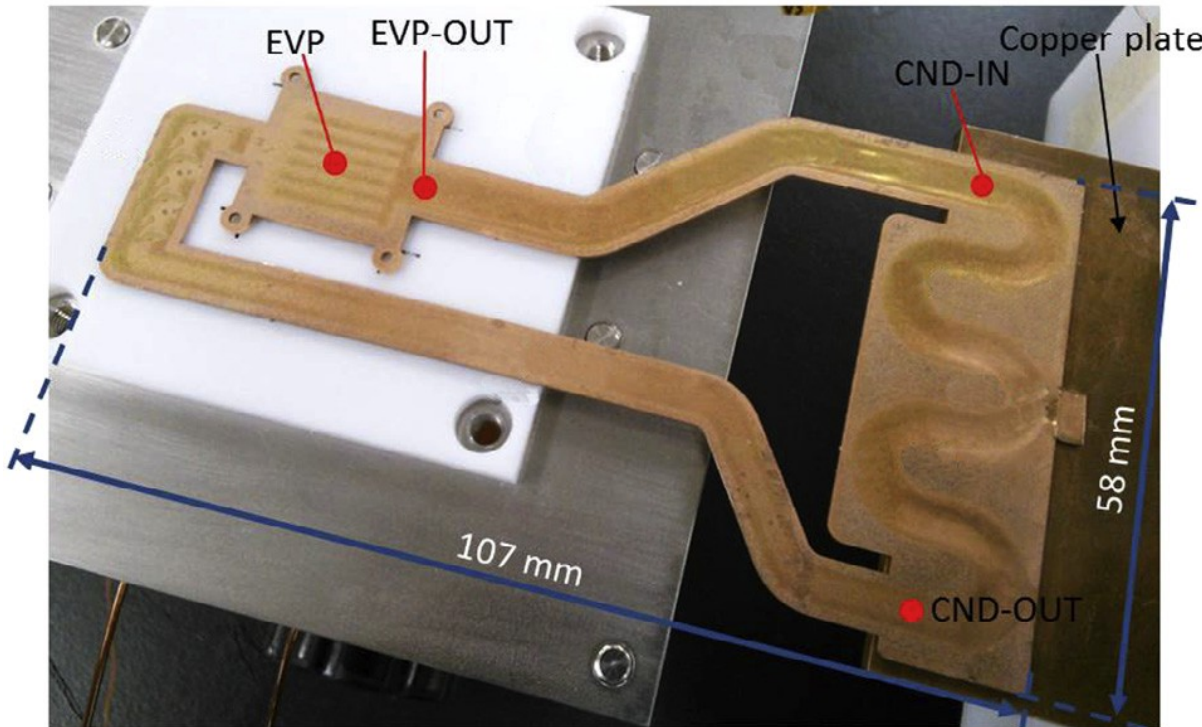
# Ultra-thin flat-plate heat pipes



Images of UFHPs: (a) flattened heat pipe and (b) vapor chamber

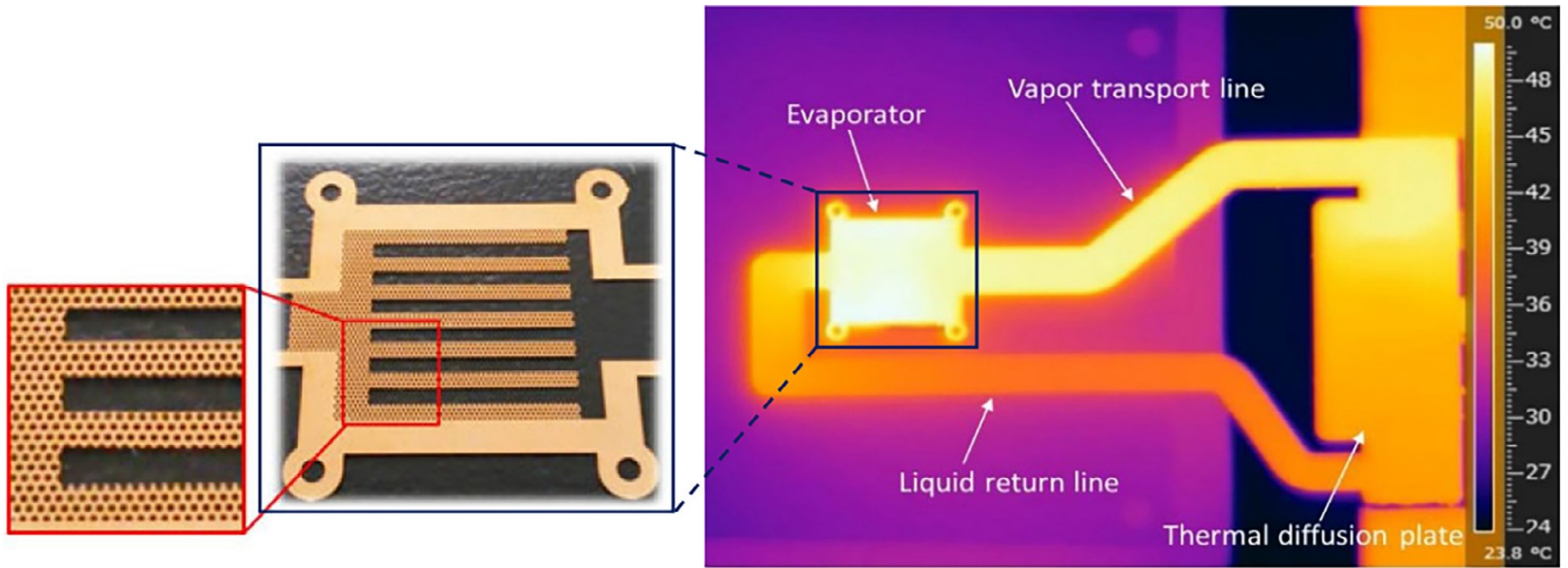
A flat-plate heat pipe is a chamber of low thickness filled with a two-phase working fluid. It can be divided into flattened heat pipes (FHPs) and vapor chambers (VCs) based on the packaging forms. The FHPs are fabricated by flattening conventional cylindrical heat pipes directly, and the composition and operational principles are similar to that of the micro heat pipes,

# Ultra-thin loop heat pipes



ULHP for the thermal management of a mobile phone

The loop heat pipe (LHP) is widely utilized for thermal control of electronic equipment in various fields from aerospace to terrestrial industries. LHPs possess certain unique features such as long heat transport distances, lower thermal resistance, reliable operation against gravity and design flexibility.<sup>66</sup>



Wick structure of evaporator section and infrared image of steady state operation of ULHP

# **Interfacial Phenomena in a Thin Film**

# MOTIVATION

---

- Interfacial phenomena involve the study of
    - Capillary forces
    - Marangoni stresses (flow due to surface tension gradient)
    - Liquid/Vapor Interfacial Phase-Change
    - Intermolecular forces (van der Waals interactions, etc.)
  - These concepts are important in explaining fundamental phenomena like spreading, coating, adsorption, stability, pattern formation, evaporation, condensation, etc.
-

# MOTIVATION : APPLICATIONS

---

## 1. Miniature Heat Pipes

Passive fluid flow and phase-change heat transfer  
(evaporation and condensation)

## 2. Surfactant adhesion/spreading

Spreading of surfactant containing drops

## 3. MEMS/Microfluidics

Fluid flow and phase-change in micro-channels, droplets

## 4. Micro-electronics

Stability of thin solid films on Si, adhesive properties of  
thin porous films for spin coating applications etc.

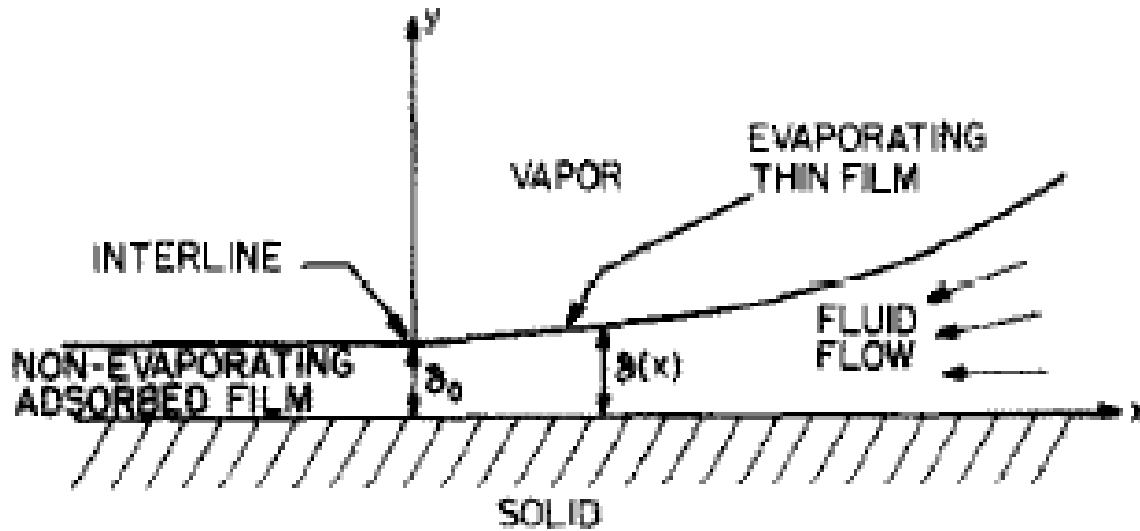
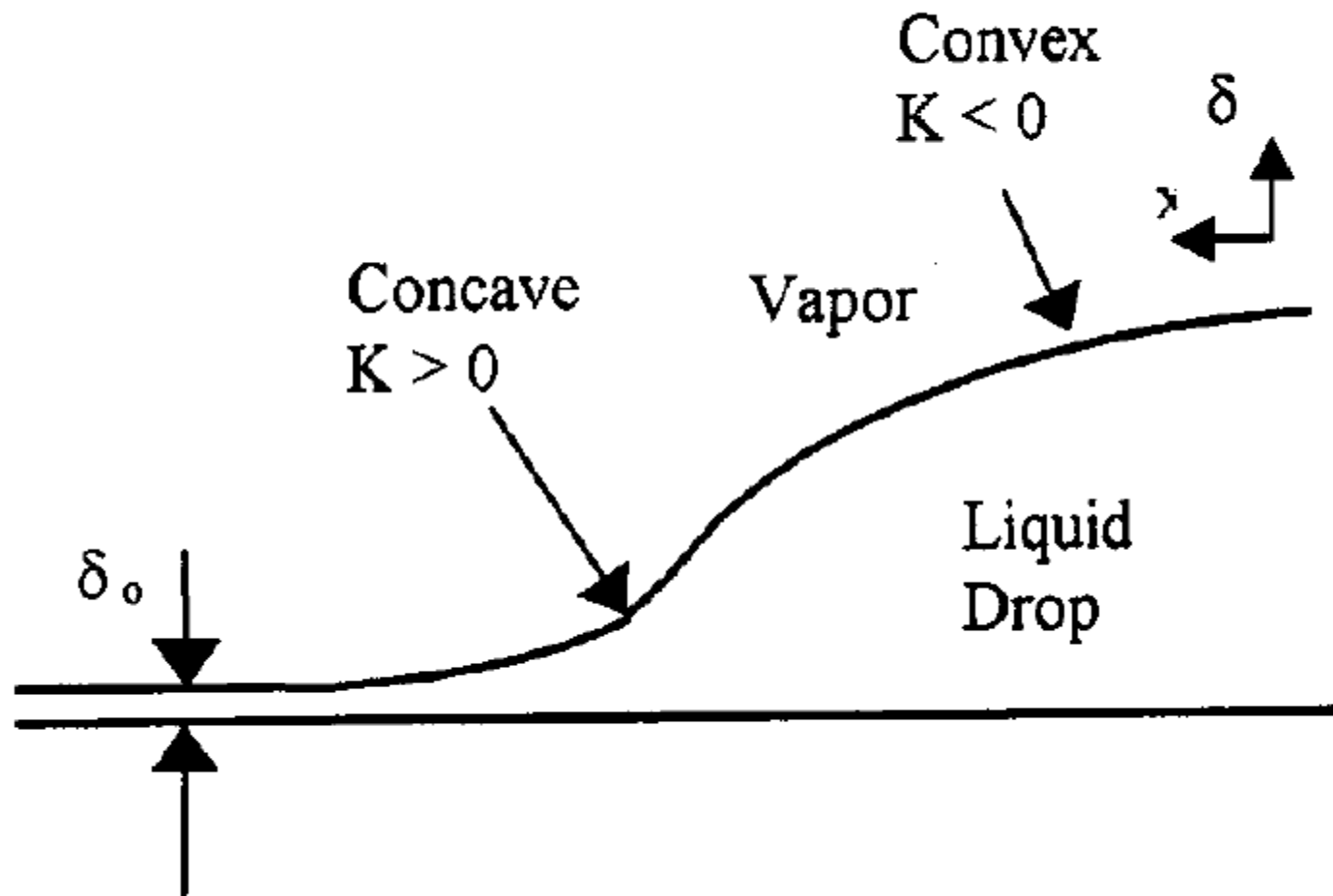


FIG. 1. Interline junction of vapor, adsorbed evaporating thin film and adsorbed non-evaporating thin film.

The heat transfer and other transport phenomena in the **contact line** (interline) region, where the liquid, vapor and the solid are in close proximity are important in many technologically important processes, e.g., rewetting of a hot spot.



Schematic drawing of the measured interfacial profile of a condensing drop

# INTRODUCTION

---

Capillary Pressure :  $\sigma_{1v} K$

K is the curvature,  
+ve for a concave surface,  
-ve for a convex surface

Disjoining pressure :

$$\Pi = \frac{-\bar{A}}{\delta^3} ; \quad \delta < 20nm$$

$\bar{A}$  is the modified Hamaker constant,  
B is the dispersion constant

$$= -\frac{B}{\delta^4} ; \quad \delta > 20nm$$

They are negative for a wetting system

**Capillary and disjoining pressures are functions of the thickness profile.**

## Augmented Young-Laplace equation

$$\Delta P = P_l - P_v = -\sigma K - \Pi$$

where  $P_v$  is the vapor pressure,  $P_l$  is the pressure inside the liquid,  $K$  is the curvature of the liquid–vapor interface,  $\sigma$  is the surface tension, and  $\delta$  is the film thickness of the liquid.

The second term on the right-hand side of the equation signifies the van der Waals interactions and is defined as<sup>49</sup>

$$\frac{\partial \Delta G^{vdw}}{\partial \delta} = \frac{A}{6\pi\delta^3} = -\Pi,$$

Where  $\Delta G^{\text{vdw}}$  is the excess interfacial free energy per unit area due to the van der Waals interactions. It includes the contributions from dipolar interactions (purely entropic) and dispersion energy. The symbol A is the Hamaker constant

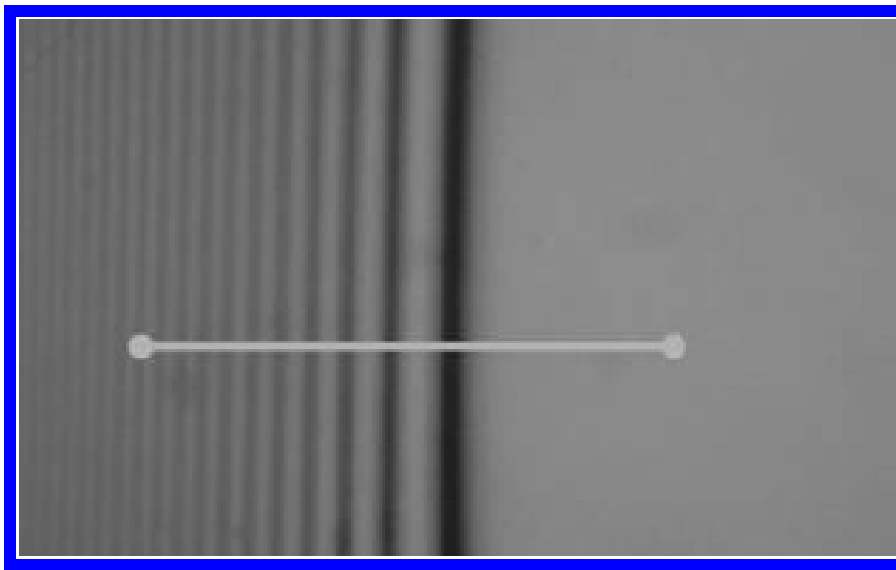
A negative value of the Hamaker constant (van der Waals interaction) signifies that a thin film in the microscopic region, with a thickness of that studied herein, will be stable and will reduce the free energy of the system.

We use the sign convention that a negative Hamaker constant and a positive disjoining pressure ( $\Pi$ ) represent a system showing a stable, adsorbed wetting film.

The Hamaker constant, A, for two phases, 1 and 2, interacting across a medium 3 can be expressed in terms of the refractive indices and the dielectric constants of the three phases.

$$A = \frac{3}{4} kT \left( \frac{\varepsilon_1 - \varepsilon_3}{\varepsilon_1 + \varepsilon_3} \right) \left( \frac{\varepsilon_2 - \varepsilon_3}{\varepsilon_2 + \varepsilon_3} \right) + \frac{3h\nu_e}{8\sqrt{2}} \frac{(n_1^2 - n_3^2)(n_2^2 - n_3^2)}{(n_1^2 + n_3^2)^{1/2}(n_2^2 + n_3^2)^{1/2}\{(n_1^2 + n_3^2)^{1/2} + (n_2^2 + n_3^2)^{1/2}\}},$$

where  $\varepsilon$  is the static dielectric constant,  $k$  is the Boltzmann's constant,  $h$  is the Planck's constant,  $\nu_e$  is the plasma frequency of the free electron gas and  $n$  is the refractive index.



Typical interference pattern observed for heptane on glass

# Force field characterization model

$$\Pi + \sigma K - \rho_l g H = 0 \quad \text{Force balance at equilibrium}$$

$$\Pi(\text{Disjoining Pressure}) = \frac{-B}{\delta^n} \quad \text{Disjoining pressure}$$

$$\Delta P = P_l - P_v = -\sigma K - \Pi \quad \text{Augmented Y-L equation}$$

$$\sigma K - \frac{B}{\delta^4} = \sigma K_\infty \quad Q = 0$$

Isothermal condition,  $K_\infty$  is the curvature of the capillary meniscus

$$\sigma \frac{d^2 \delta}{dx^2} - \frac{B}{\delta^4} = \sigma K_\infty \quad \text{Using simplified form of curvature}$$

## Non-dimensionalization

$$\eta = \frac{\delta}{\delta_0} \quad Z = x \left( \frac{K_\infty}{\delta_0} \right)^{1/2}$$

$$\frac{d^2\eta}{dZ^2} + \left( \frac{-B}{\sigma K_\infty \delta_0^4} \right) \frac{1}{\eta^4} = 1.$$

Parameter,  $\alpha$ ,  
defined as

$$\alpha^4 = \frac{-B}{\sigma K_\infty \delta_0^4}$$

$\alpha$  is a measure of the deviation of a specific meniscus from the equilibrium conditions,  $\alpha = 1$  at equilibrium

$$\left( \frac{d\eta}{dZ} \right)^2 = 2\eta + \frac{2}{3} \frac{\alpha^4}{\eta^3} + C_1 \rightarrow$$

BC

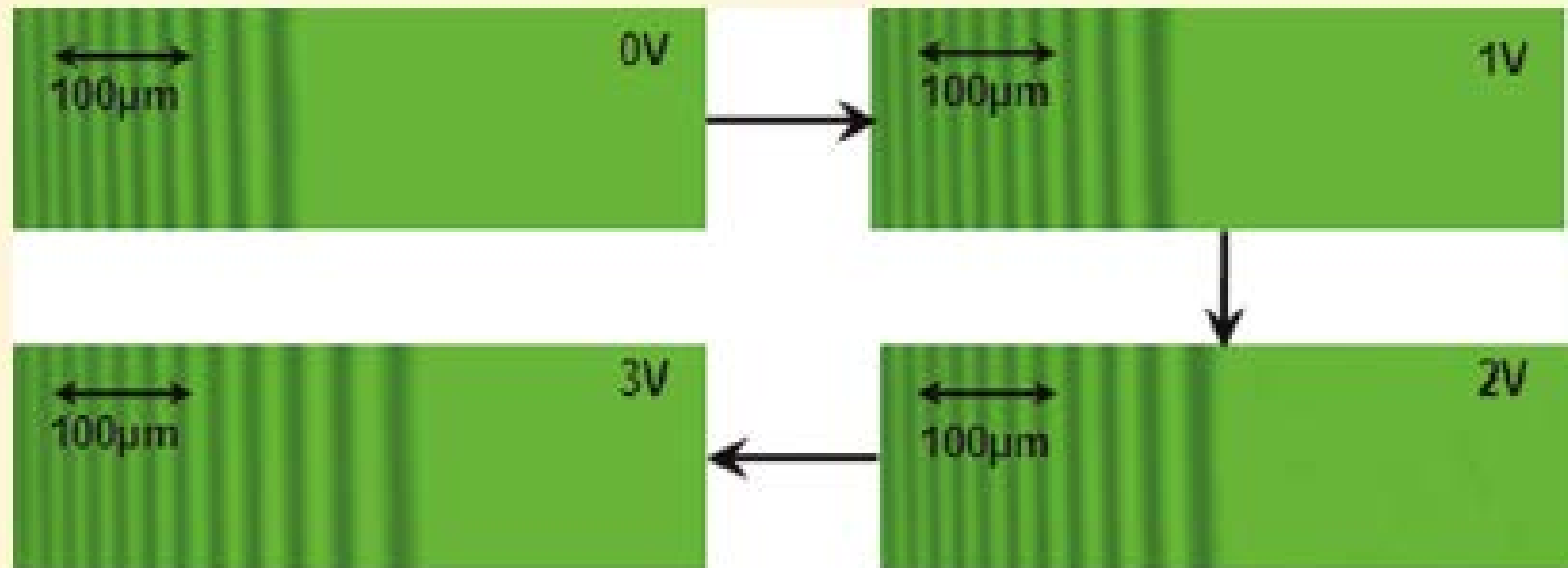
$$\eta = \alpha, \frac{d\eta}{dZ} = 0,$$



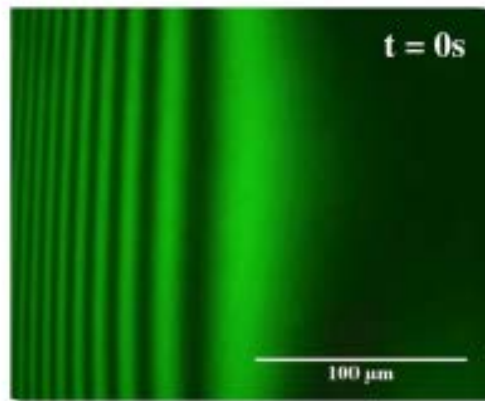
$$\frac{d\delta}{dx} = -(K_\infty \delta_0)^{1/2} \sqrt{2\eta + \frac{2}{3} \frac{\alpha^4}{\eta^3} - \frac{8}{3}\alpha}$$

Slope of a curved thin film can be obtained accurately using Y-L eqn.

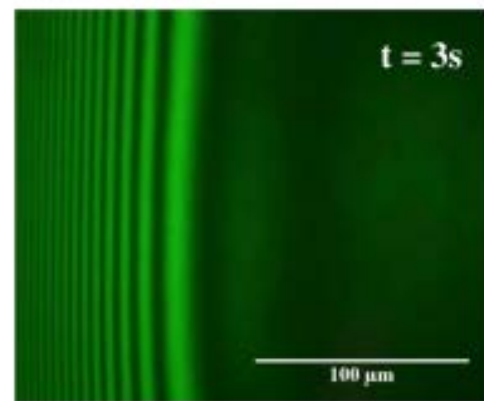
**IN-SITU evaluation of B**



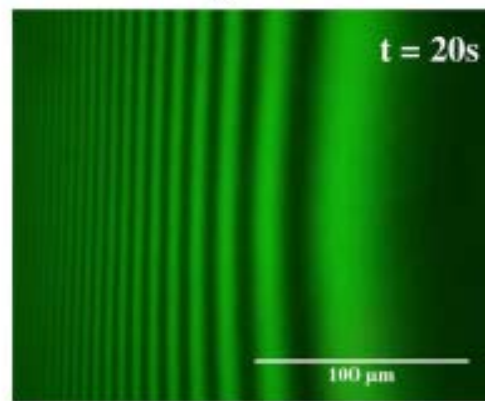
**Spreading of a surfactant ( 0.1 CMC SDS) laden thin water film on a  $\text{SiO}_2$  substrate on application of electric field ( 0-3V )**



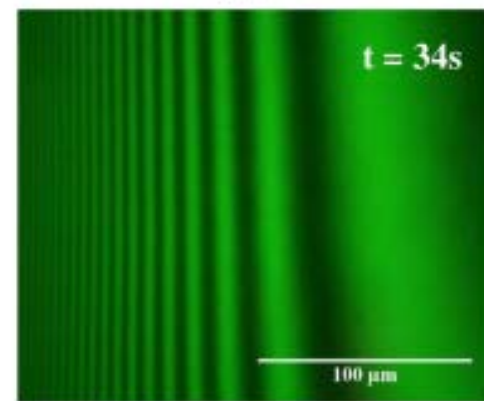
(a)



(b)



(c)



(d)

**Image sequence depicting the dynamics of the thin film when subjected to a magnetic field**

# Lecture 8

**Scaling dimensions and other issues**

## Scaling dimensions and issues

Consequences of size reduction for different processes - relevance of material properties and behavior, processes, and miniaturized devices

1 Material properties

2. Processes

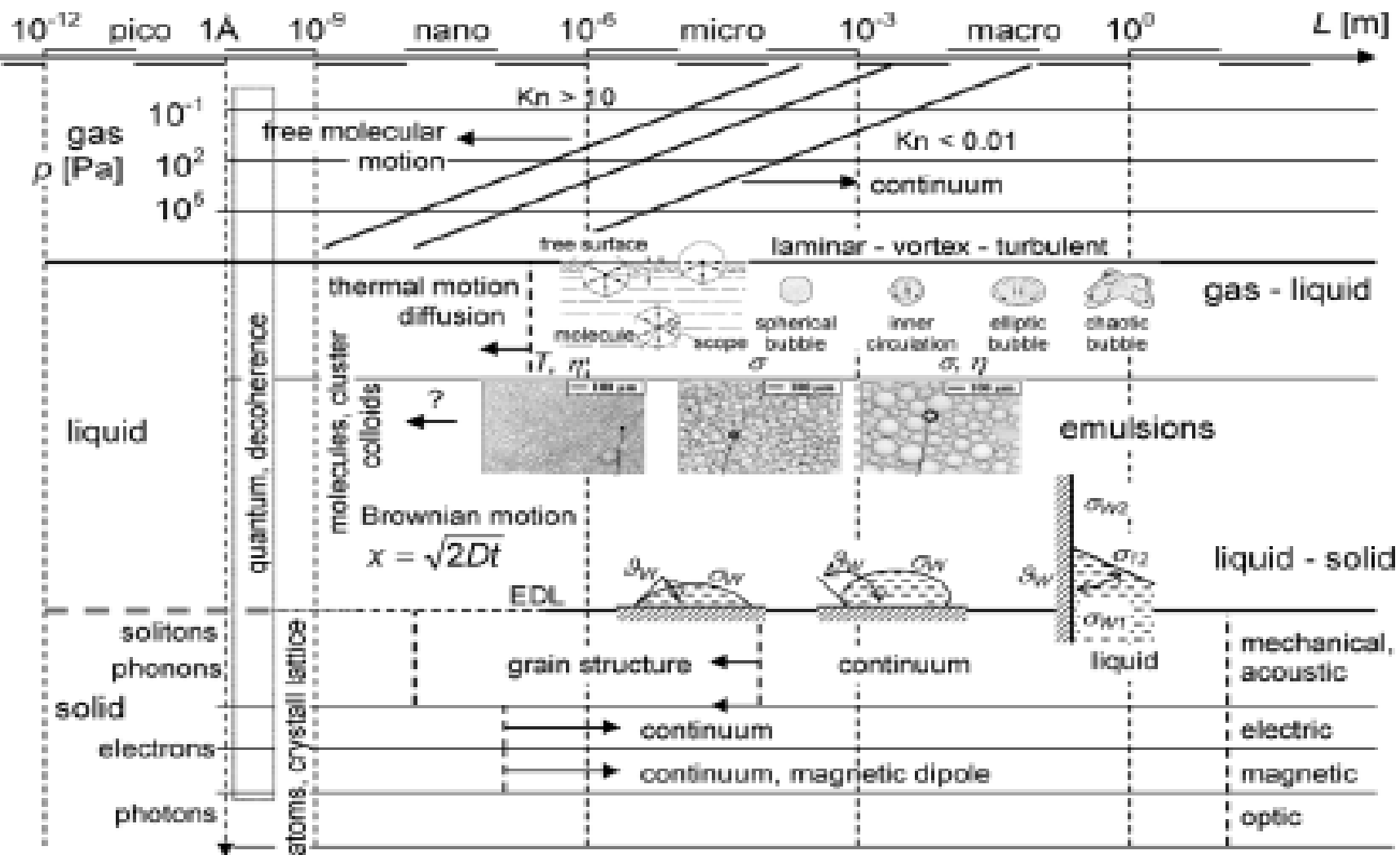
3. Devices

## 1. Material properties

With decreasing length, not only the material properties change, e.g., behavior of rarefied gases in pipes and channels, the operation and efficiency of unit operations are affected in various ways

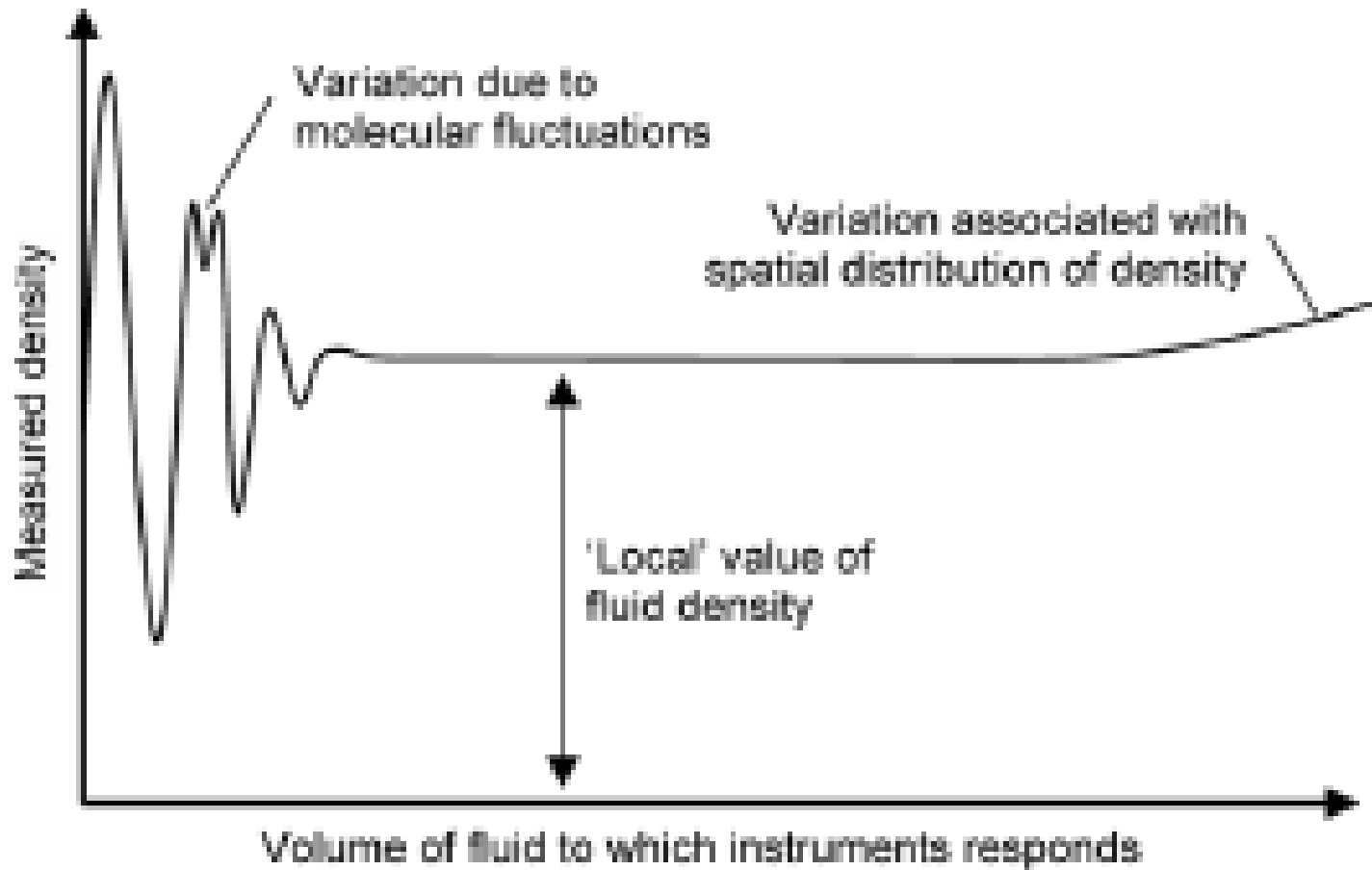
The miniaturization of chemical equipment mostly emphasizes the length reduction of the main dimensions.

Information also needed for the intensive state variables, e.g whether constant process conditions like pressure, temperature, or concentration remain unchanged when reducing the size of the system.



Typical length scales of material properties and behavior in gas, liquid, and solid phase as well as interfacial phenomena. For comparison, the electron sheath of atoms has a diameter of approx.  $10^{-10}$  m, the nucleus of an atom is approx.  $10^{-15}$  m, electrons are approx.  $10^{-18}$  m in diameter.

# What is continuum?



Effect of size of sensitive volume on the density measured by an instrument. Other macroscopic variables like velocity or temperature show a similar reaction with the observed behavior

## Continuum Hypothesis

- Neglect the fact that real substances are composed of discrete molecules
- Model matter from the start as a smoothed-out **continuum**
- Information about a continuum represents the microscopic information averaged over a volume.
- **Classical thermodynamics** is concerned only with continuum

## Thermodynamic Equilibrium

A system in thermodynamic equilibrium satisfies:

- mechanical equilibrium (no unbalanced forces)
- thermal equilibrium (no temperature differences)
- chemical equilibrium

## Continuum hypothesis

Decreasing the volume may influence the properties of the fluids and the measurement of process parameters like density, velocity, or temperature.

Physical quantities and fluid properties are usually treated as being spread uniformly over a control volume.

Very large control volumes, as in atmospheric systems, show local non-uniformities like depression systems in weather formation.

Variations and fluctuations also occur in small systems, where the behavior of single molecules become important.

With decreasing volume, molecular fluctuations disturb the smooth measurement. If only a few molecules are measured, the single molecule behavior becomes important and varies in an irregular way.

*The fluid can be regarded as a continuum, where the measured fluid property is constant for sensitive volumes, which are small on a macroscopic scale but large on a microscopic scale.*

A  $10 \mu\text{m}$  cube contains approx.  $3 \times 10^{10}$  molecules of air at normal temperature and pressure, which is large enough to take an average over the molecules.

A microstructured device with dimensions and process conditions in that range can be treated with continuum methods.

However, in some applications the limits of the continuum hypothesis are reached and a description of rarefied gases beyond the continuum hypothesis is needed.

## Continuum Assumption

The continuum assumption in fluid mechanics is only valid for sufficient molecules within a given volume to achieve a stable estimate of the macroscopic flow properties.

The ratio of the characteristic length scale  $L$  to the mean molecular spacing  $\delta$  should satisfy to achieve a **statistically stable estimate of the macroscopic properties**.

$$\frac{L}{\delta} > 100$$

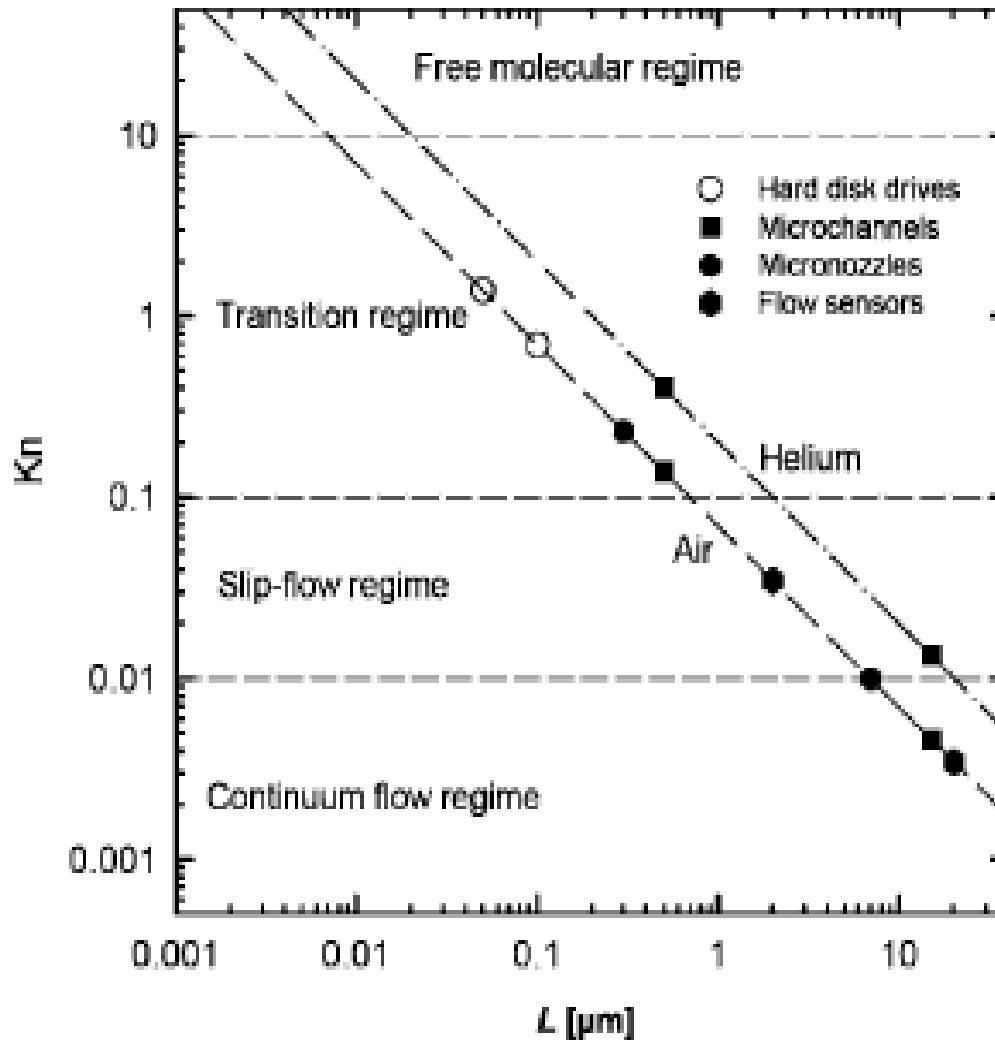
In other words, there should be at least 100 molecular spaces along each face of the sample volume, giving a total of 1 million molecules within the control volume.

The mean free path  $\lambda$  divided by the characteristic length  $L$  of the system gives the dimensionless **Knudsen number**  $Kn$

$$Kn = \frac{\lambda}{L}$$

*The flow regimes of gases concerning rarefaction effects can be classified according to the range of the Kn number.*

Generally, rarefied gas behavior is classified into four different regimes according to the range of the  $Kn$  number



Characteristic length scales of typical microfluidic components and the corresponding Knudsen number at standard atmospheric conditions

$$\underline{\mathbf{Kn} < 10^{-2}}$$

The continuum and thermodynamic equilibrium assumptions are appropriate and flow situations can be described by conventional no-slip boundary conditions.

$$10^{-2} < \mathbf{Kn} < 10^{-1}$$

**Slip Flow Regime**

Navier-Stokes equations remain valid provided tangential slip-velocity and temperature-jump boundary conditions are implemented at the walls of the flow domain

$$10^{-1} < \text{Kn} < 10$$

## Transition flow regime

Continuum and thermodynamic equilibrium assumptions of the Navier-Stokes equations begin to break down and alternative analysis methods e.g., particle-based DSMC (direct simulation Monte Carlo) approaches, or molecular dynamics (MD) simulations must be employed.

Stress-strain relationship for the fluid becomes non-linear within a distance of approximately one mean free path from the wall (the so-called Knudsen layer)

# **$\text{Kn} > 10$**

## **Free molecular flow**

The mean-free path of the molecules is far greater than the characteristic length scale and, consequently, molecules are reflected from a solid surface and travel, on average, many length scales, before colliding with other molecules.

**The above limits are empirical**

**Most microfluidic devices operate in the slip-flow regime or early transition flow regime.**

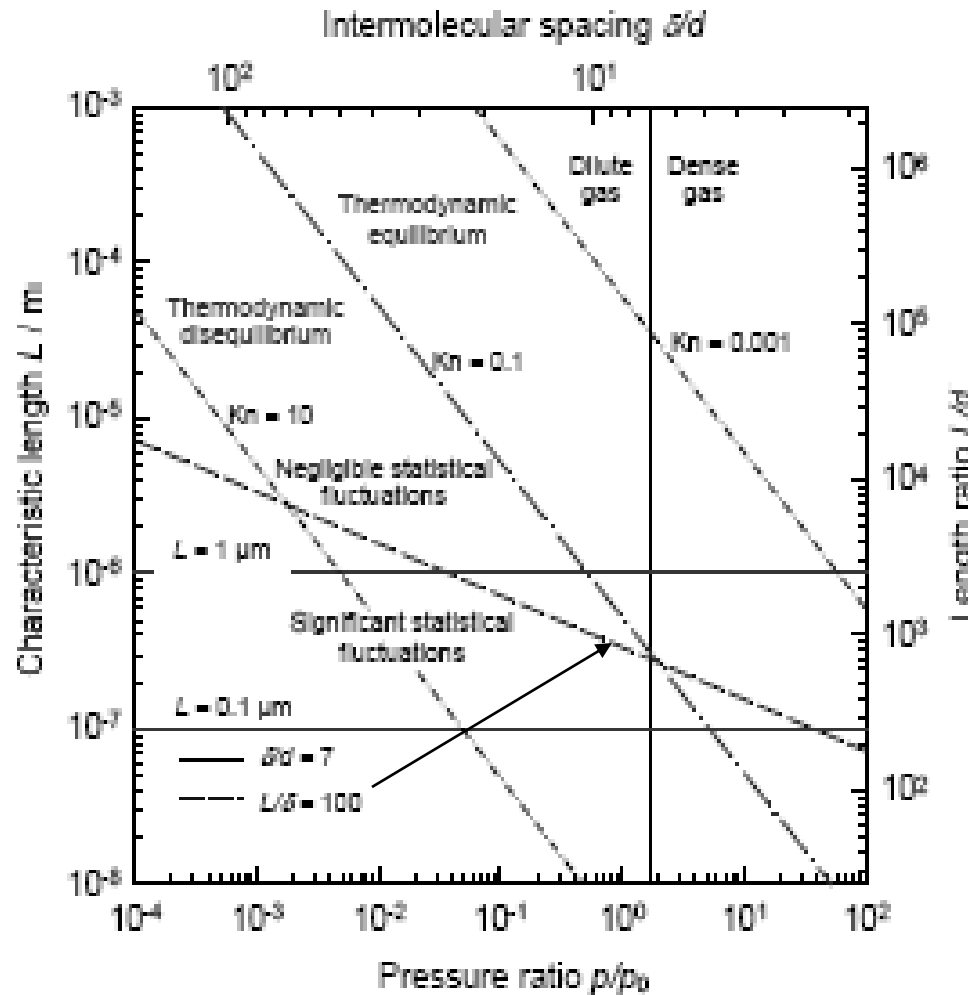
The characteristic length scale of the device or flow problems are difficult to define. Often the gradient of a macroscopic quantity is used for the definition, for example, of the density:

$$L = \frac{\rho}{|\nabla \rho|}$$

---

Alternative method to display the transition between continuum behavior and molecular behavior. The conditions of a hard sphere gas are illustrated with a molecular diameter  $d = 4 \times 10^{-10} \text{ m}$ , which is approximately the molecular diameter of air.

$d$  = mol. dia.  
 $\delta$  = average  
 distance  
 between the  
 molecules  
 $\lambda$  = mean free  
 path



$d$  = mol. dia.  
 $\delta$  = average  
 distance  
 between the  
 molecules  
 $\lambda$  = mean free  
 path

Limiting criteria for the application of the Navier-Stokes Eqns to air with  $d = 4 \times 10^{-10} \text{ m}$ , collision cross section  $\sigma = \pi d^2$

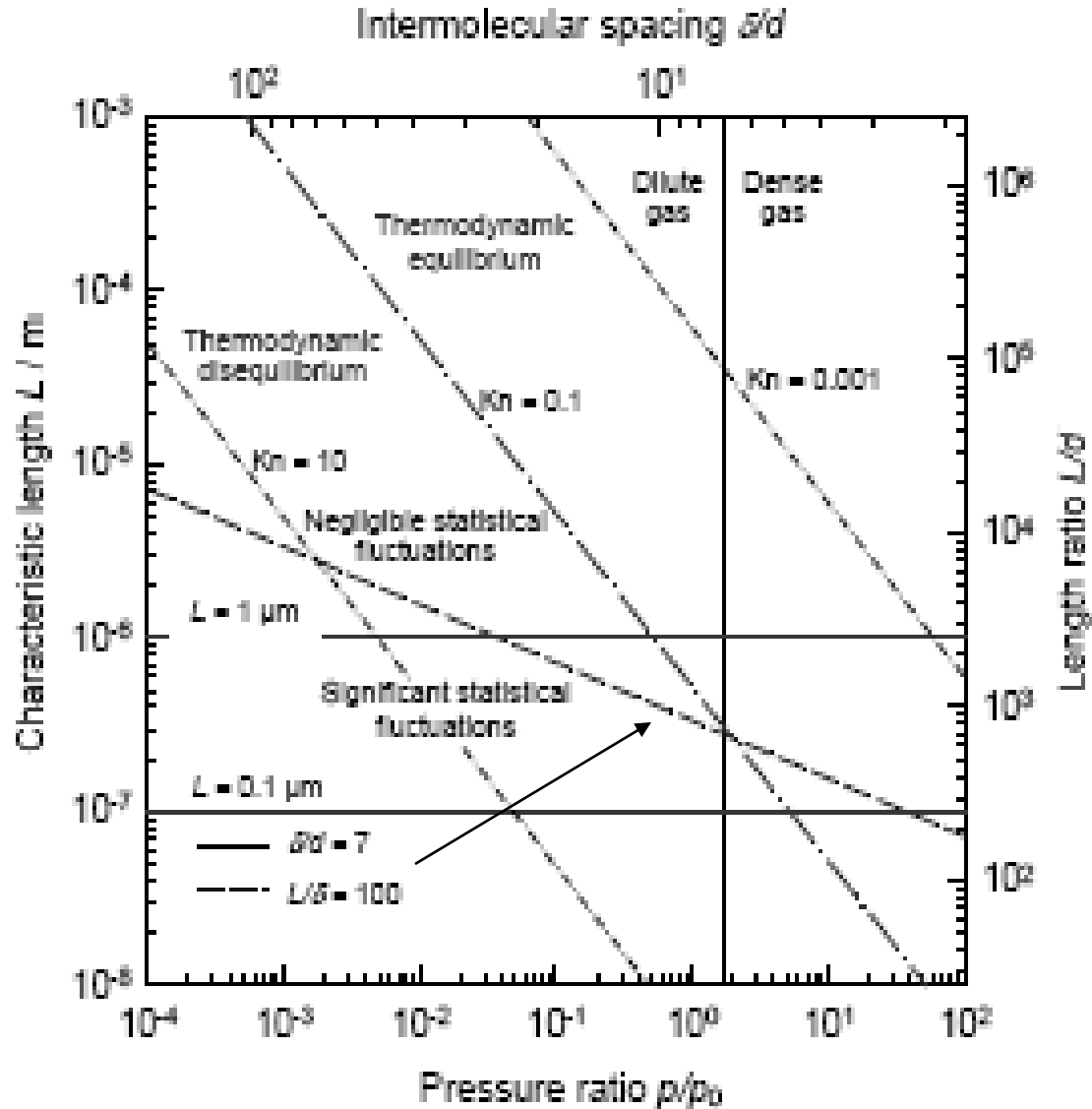
$$\underline{\delta / d = 7, L / \delta = 100, \text{Kn} = \lambda / L = 10^{-1}}$$

The left-hand ordinate represents the characteristic length scale  $L$ , while the right-hand ordinate shows the length scale normalized with the molecular diameter,  $L/d$ .

The bottom abscissa represents the density normalized with a reference pressure  $p/p_0$ , which is equivalent to the normalized number density  $n/n_0$  or density ratio  $p/p_0$ .

The top axis represents the average distance between the molecules normalized with the molecular diameter  $\delta/d$ .

$d$  = mol. dia.  
 $\delta$  = average  
 distance  
 between the  
 molecules  
 $\lambda$  = mean free  
 path



$\delta / d = 7, L / \delta = 100, Kn = \lambda / L = 10^{-1}$

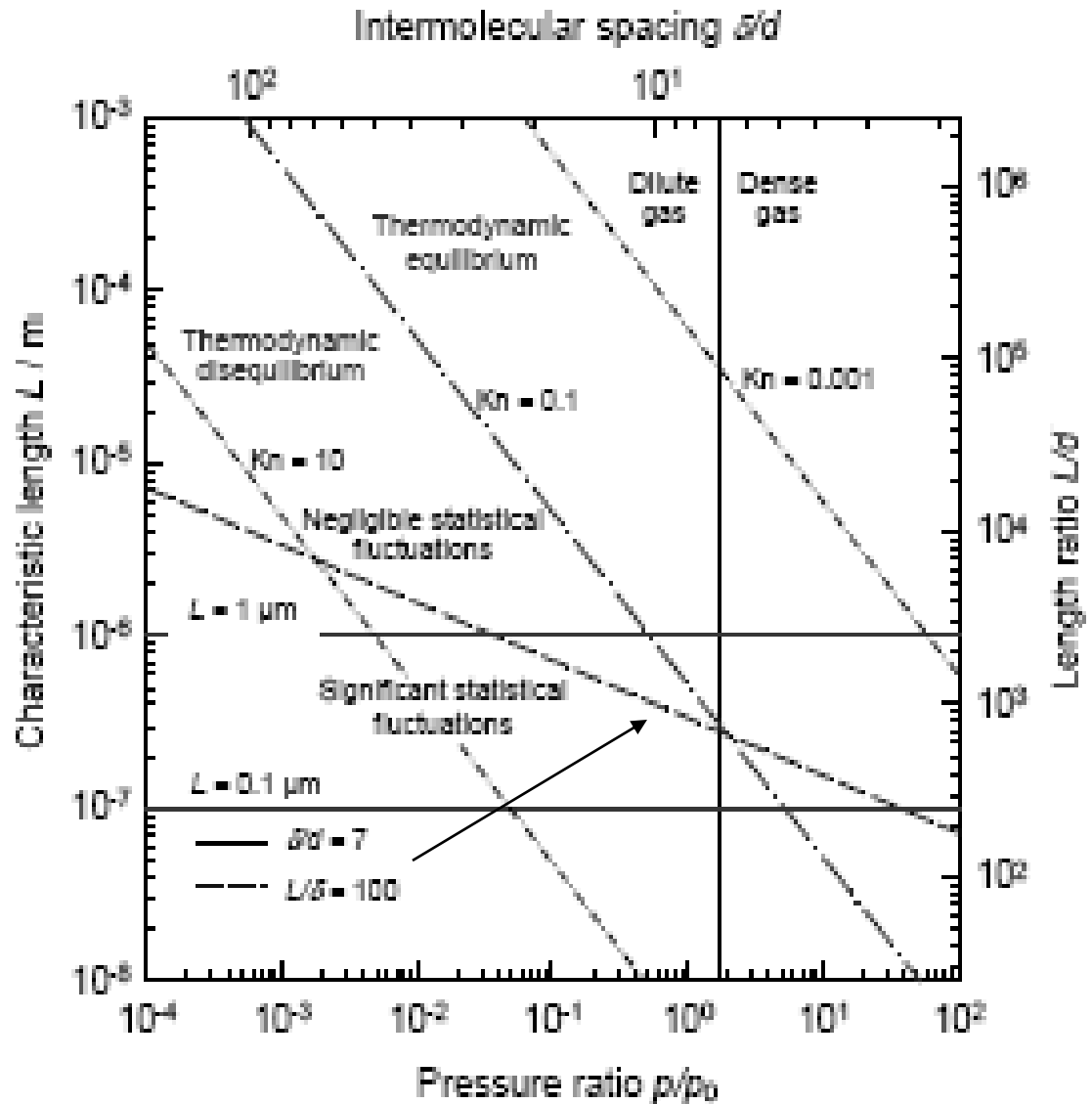
The figure shows the applicability limits of the Navier-Stokes equations given by  $\delta / d = 7$ ,  $L / \delta = 100$ , and  $\text{Kn} = \lambda / L = 10^{-1}$ .

Air at standard ambient conditions has a pressure of 101.315 kPa, a number density of  $2.68666 \times 10^{25} \text{ m}^{-3}$ , a density ratio of unity (by definition) and  $\delta / d = 8.5$ .

With these values, air can be assumed to be a dilute gas, but is close to the upper limit of the dilute gas assumption.

The  $L / \delta = 100$  line represents the limit of statistical fluctuations. The **continuum approximation** is only valid if there are sufficient molecules within a given volume to achieve a statistically stable estimate of the macroscopic flow properties.

$d$  = mol. dia.  
 $\delta$  = average  
distance  
between the  
molecules



$$\delta / d = 7, L / \delta = 100, Kn = \lambda / L = 10^{-1}$$

Thermodynamic equilibrium

$$Kn = \lambda/L = 10^{-1}$$

Continuum Approximation

$$L/\delta = 100$$

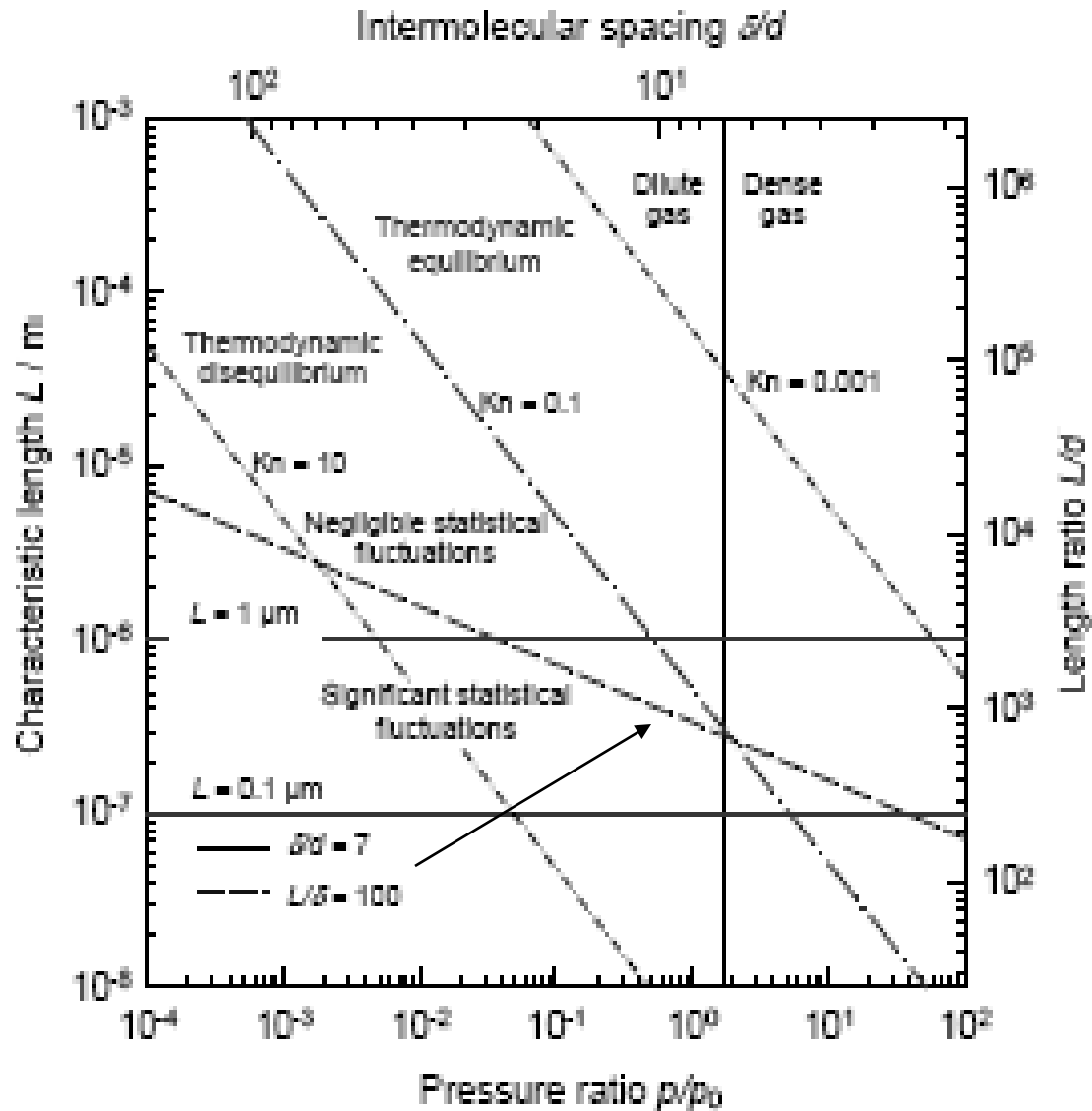
Dilute gas

$$\frac{\delta}{\sigma} > 7$$

The line with  $\text{Kn} = \lambda/L = 10^{-1}$  gives the validity limit of the thermodynamic equilibrium assumption.

According to Figure, the thermodynamic equilibrium assumption first fails if the flow dimensions are reduced in size, followed by a failure in the continuum assumption for a dilute gas.

$d$  = mol. dia.  
 $\delta$  = average  
 distance  
 between the  
 molecules  
 $\lambda$  = mean free  
 path



$$\delta / d = 7, L / \delta = 100, \text{Kn} = \lambda / L = 10^{-1}$$

For a dense gas, the continuum assumption first fails, followed by a failure in the thermodynamic equilibrium assumption.

Hence, special care should be taken for the limiting conditions of the Navier-Stokes equations.

The usual flow classification system based solely on the magnitude of the local Knudsen number, is only one parameter to completely describe the system.

---

## Statistical mechanics and mean free path

In a perfect gas, the molecules are regarded as hard spheres interacting only in very short encounters with other molecules or with the boundary (wall, surface, or other limiting elements).

At the molecular scale, the ratio of the mean molecular spacing  $\delta$  and the mean molecular diameter  $\sigma$  is an important parameter.

Gases with the condition 
$$\frac{\delta}{\sigma} > 7$$

are referred to as **dilute gases**. If the condition is not satisfied the gas is considered a **dense gas**.

Air at standard conditions is regarded as a dilute gas, but pressurized air with 0.6 MPa is considered as a dense gas.

It can be assumed that the probability of a molecule moving in a certain direction is equal for all three space coordinates.

This can be expressed by the constant ratio of the derivative of the **probability distribution function (PDF)**  $f(w)$  to the function itself and the velocity component  $w$ .

$$\frac{f'(w)}{wf(w)} = \frac{d \ln f(w)}{wdw} = -2\gamma$$

$$\ln f(w) = c_i - \gamma w^2$$

For convenience, the integration constant is set to  $-2\gamma$  and determined with the kinetic energy of the molecules

$$\gamma = \frac{M_m}{2kT} = \frac{M}{2RT}$$

with the mass of a single molecule  $M_m = M_k/R$ , the Boltzmann constant  $k = 1.38 \times 10^{-23} \text{ J/K}$ , and the universal gas constant  $R = 8.314 \text{ J/kmol K}$ .

The integration constant  $c_i$  is determined by normalizing the sum of the probability to unity.

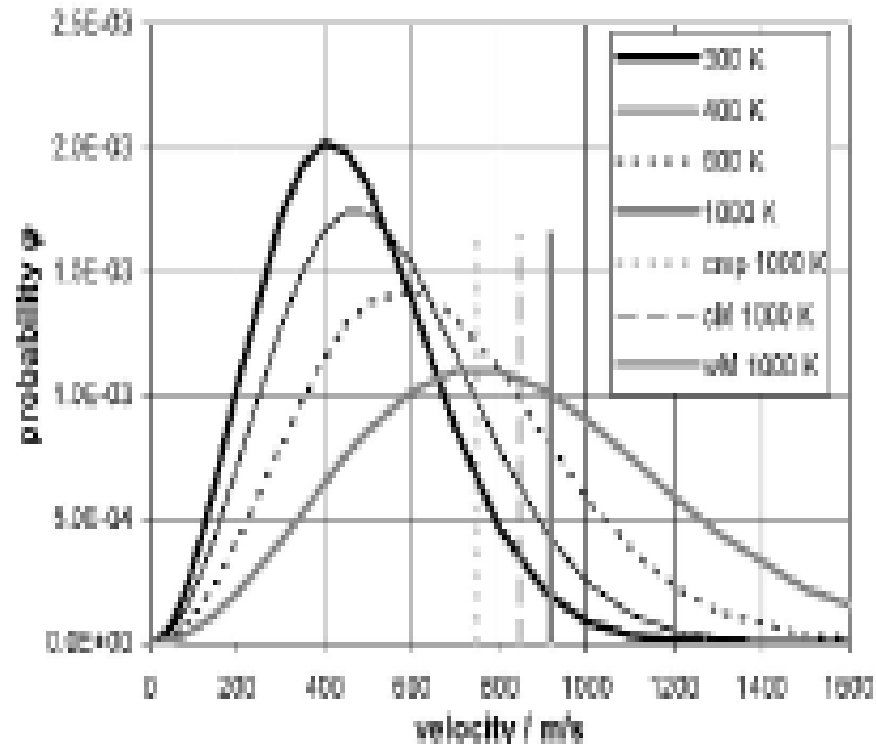
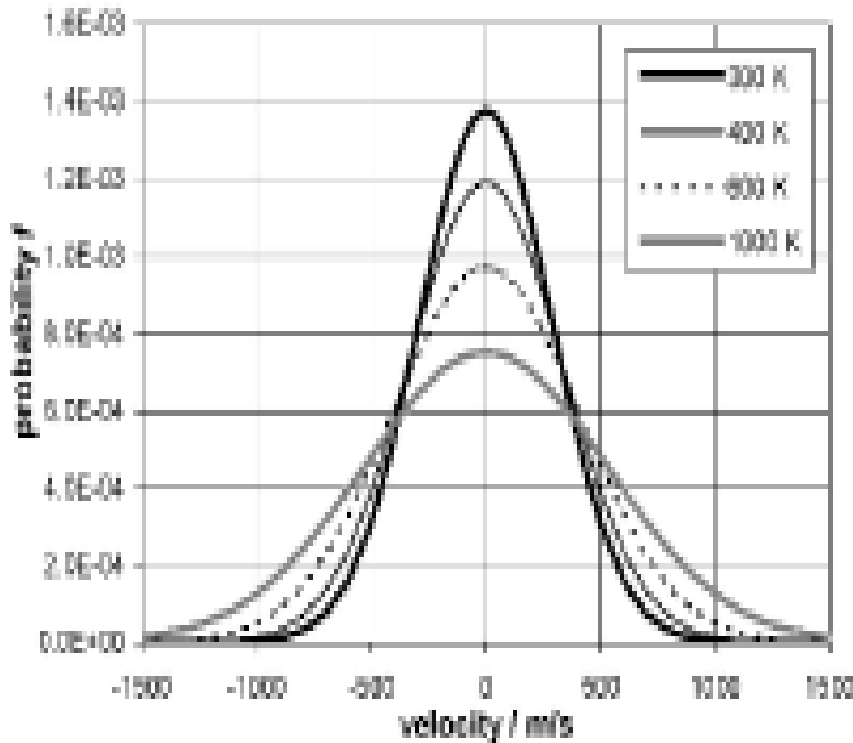
The integration gives the probability distribution for one velocity component  $w$ , which stands for the other components  $u$  and  $v$  as well.

$$f(w) = \left( \frac{M}{2\pi RT} \right)^{1/2} \exp\left( -\frac{M}{2R T} w^2 \right)$$

This is the Maxwell velocity distribution of a perfect gas in thermodynamic equilibrium.

The integration over a sphere in all three space coordinates gives the probability of the absolute velocity value  $c$ , independent from the direction

$$\begin{aligned} \varphi(c) dc &= 4\pi c^2 F(c) dc \\ \Rightarrow \varphi(c) &= 4\pi c^2 \left( \frac{M}{2\pi R T} \right)^{3/2} \exp\left( -\frac{c^2 M}{2R T} \right) \end{aligned}$$



Both probability distributions are displayed for air ( $R_m = 287\text{J/kg K}$ ) with four different temperatures. For higher temperatures, the gas molecules move faster, and the distribution becomes wider.

The most probable velocity of a molecule is determined to be

$$\bar{c}_{mp} = \sqrt{\frac{2RT}{M}}$$

where the probability density distribution has its maximum [ $d\phi(c)/dc = 0$ ] .  $\phi(c)$  is zero at  $c = 0$  and at  $c = 1$ . Thus a maximum is present in between. Value of  $c$  at this maximum is the most probable velocity.

The mean velocity ( $= \int_0^{\infty} w f(w) dw$ )

from the distribution is

$$\bar{c}_M = \sqrt{\frac{8RT}{\pi M}}$$

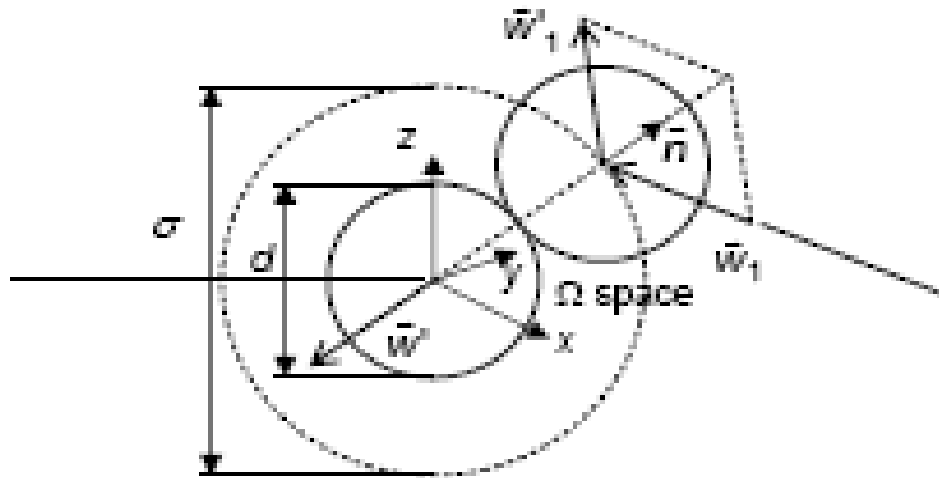
The mean velocity from the kinetic energy of a molecule is given by

$$\bar{w}_M = \sqrt{\frac{3RT}{M}}$$

The model provides

- frequency at which the molecules collide
- distance traveled between collisions
- transport properties of gases

## Geometrical situation of a binary encounter



The molecules are treated as hard spheres with a diameter of  $d$  and a collision cross section  $\sigma = \pi d^2$ .

With the number of molecules in a unit volume  $N_A$ , the number of encounters between the molecules and the mean time between these encounters can be determined.

Multiplied with the mean velocity, an estimation of **the mean free path of a molecule**, the average length between two collisions, can be derived:

$$\lambda = \frac{kT}{\sqrt{2} p \sigma}$$

The mean free path can also be expressed by

$$\lambda = \frac{1}{\sqrt{2} n \sigma}$$

the number of particles  $n$  in a control volume, which is also given by  $n = N/V = \delta^{-3}$

With the mean velocity of the particles between two collision  $c_m$ , the characteristic time between two collisions is calculated by

$$t_c = \frac{\lambda}{c_M} = \frac{k}{4 p \sigma} \sqrt{\frac{\pi T}{R}}$$

The collision time is proportional to the square root of the temperature and inverse proportional to the pressure.

## Flame distance and explosion limits

The typical dimension of microstructured equipment is just below the extinction length or “quench distance” of many fast reactions and oxidations, which is approx. 1 mm. The measurement of the extinction length or distance is standardized. It is combined with the maximum experimental safety gap MESG, where a flame is stopped to proceed further on.

Concept important in reactions with strong exo, or endothermic behavior and high-energy transfer, like explosive reactions, fuel cell applications etc.

These applications benefit from the high transfer rates in microchannels with precise temperature control.

# Fundamentals, Balances, and Transport Processes

*Beginning with simple atomic encounters from statistical mechanics, macroscopic balance equations and transport properties are derived*

Main mixing and separation unit operations grouped according to their driving force

Unit operation	molecular / thermal	mechanical/ext. force	electro-magnetic
Mixing and aggregation,	diffusion <sup>1)</sup> dissolving <sup>2)</sup>	spraying <sup>2)</sup> aeration <sup>2)</sup>	electro-phoretic mixing <sup>1)</sup>
Combination,	extracting <sup>2c)</sup>	stirring <sup>2)</sup>	mixing with magnetic beads <sup>2)</sup>
Control of segregation, desorption <sup>2c)</sup>		active mixing <sup>1, 2)</sup> dosing <sup>1, 2)</sup>	
Separation	thermodiffusion <sup>1)</sup> pressure diffusion <sup>1)</sup> counter-current diffusion <sup>1)</sup> condensation <sup>2a)</sup> evaporation <sup>2a)</sup> crystallization <sup>2a)</sup>	sedimentation <sup>2)</sup> cycloning <sup>2)</sup> centrifugation <sup>2)</sup> pressure diffusion <sup>1, 2)</sup> (ultracentrifuge) filtration osmosis	electro deposition <sup>2)</sup> magneto deposition <sup>2)</sup> electro filtration electro dialysis electro osmosis electrophoresis
superscripts for <i>employed phases:</i>	distillation/ rectification <sup>2a)</sup>	gas permeation classification	magneto-striction
1) single phase	drying <sup>2b)</sup>	sorting	
2) multiphase	absorption <sup>2c)</sup>		
a) with own co-phase	adsorption <sup>2c)</sup>		
b) own + additional co-phase	extraction <sup>2c)</sup>		
c) additional co-phase	ion exchange <sup>2c)</sup> membrane processes.		

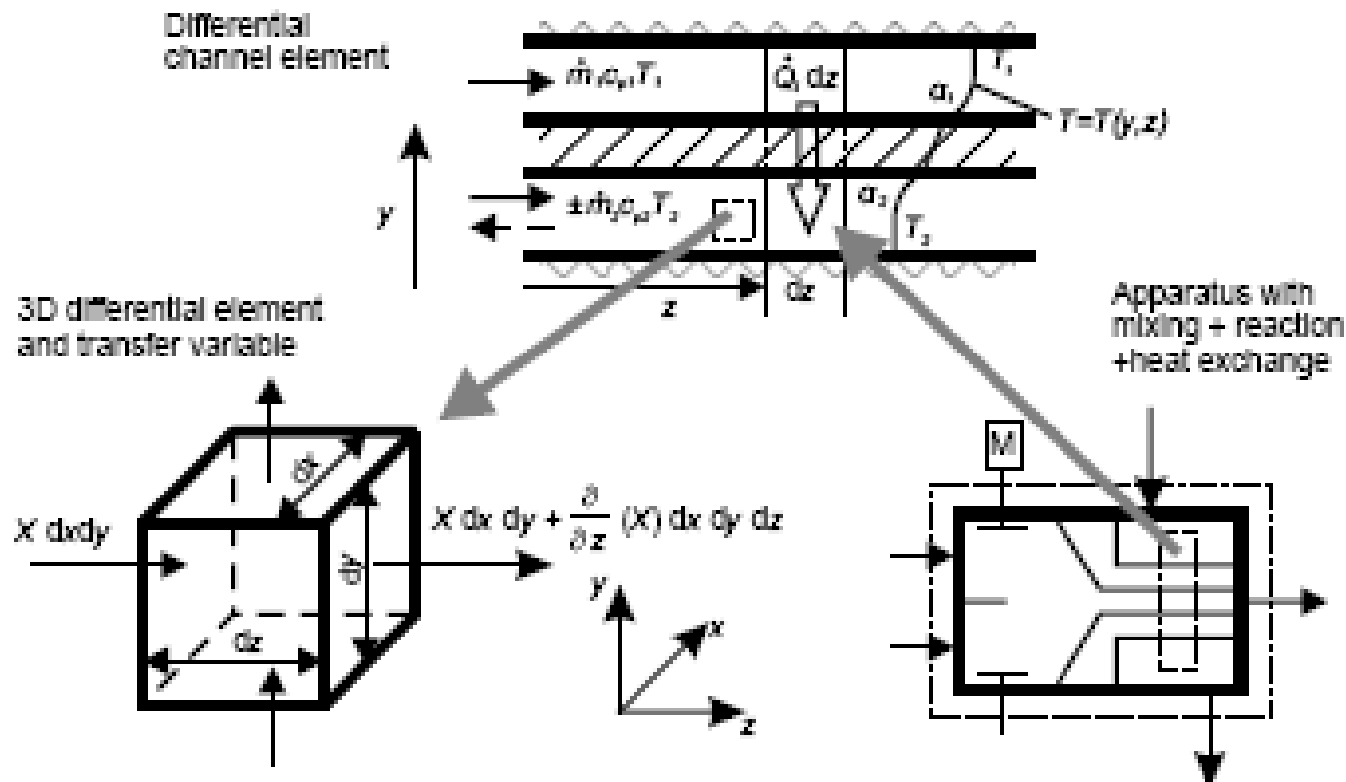
## Balances and Transport Equations

Conservation and balance equations of mass, species, momentum, energy, as well as the definition of the entropy and its application.

The conservation laws of mass (continuity equations) and energy (first law of thermodynamics) can be described as

$$\begin{bmatrix} \text{System change} \\ \text{with time} \end{bmatrix} = \begin{bmatrix} \text{Incoming} \\ \text{Flow} \end{bmatrix} - \begin{bmatrix} \text{Outgoing} \\ \text{Flow} \end{bmatrix} + \begin{bmatrix} \text{Source or} \\ \text{Sink} \end{bmatrix}$$

# Macroscopic balance equations



Overview of the various balancing volumes in process engineering : 3D differential element for general calculations, 1D differential element and complete equipment (active mixer ) for process balances.

X stands for mass, species, momentum or energy.

The general balance equation with temporal and spatial derivatives of a system and a differential element with the volume  $V$  is written as ( with  $X$  as the general balanced value):

$$V \cdot \frac{\partial X}{\partial t} = w \left[ X \, dy \, dx - \left( X \, dy \, dx + \frac{\partial X}{\partial z} dz \, dy \, dx \right) \right]$$

In a steady process, the temporal derivative vanishes,  $\partial/\partial t = 0$  .

In systems with high velocities, the convective transport is dominant compared to conductive and diffusive fluxes.

For systems with dominant chemical reactions, only a change of substance needs to be considered.

Within the systems since no mass is generated or destroyed, hence, no sink or source appears in the balance equation.

For time dependent mass flow rates,

$$\frac{\partial m}{\partial t} = m_{in} - m_{out}$$

The momentum of a moving fluid can be expressed as the product of the mass and the flow velocity.

The integral of the momentum over the volume results in a net force of the fluid on the volume boundary or on the equipment.

In general, the momentum balance of a device can be written as

$$\sum J_{in} = \sum J_{out} - \sum J_{loss}$$

The momentum loss can be interpreted as the viscous momentum loss, which is expressed as pressure loss along the channel or device flow.

For fluid flow through an arbitrary channel:

$$\frac{\partial(mw)}{\partial t} = \left( \dot{mw} \right)_{in} - \left( \dot{mw} \right)_{out} + (pA_i)_{in} - (pA_i)_{out} + mg + F_z$$

Starting point for Navier-Stokes equation.

Additional forces in microfluidic applications result from surface effects

Similar to the mass, the energy itself is conserved according to the first law of thermodynamics for open systems.

$$\sum \dot{E}_{in} = \sum \dot{E}_{out} + \sum \dot{E}_{diss}$$

The energy dissipation takes into account that energy conversion from one form into another is accompanied by natural losses.

These losses are characterized by the entropy generation during a process according to the second law of thermodynamics.

In case of a channel with constant cross section, without chemical reactions and work consumed or produced, the entire energy of the fluid can be expressed according to the first law of thermodynamics

$$m e = \rho A \left( u + \frac{1}{2} w^2 + g z \right)$$

The enthalpy form of the energy balance can be written as

$$\rho \frac{dh}{dt} = \frac{dp}{dt} + \varepsilon - \operatorname{div} \vec{q}$$

The caloric equation of state gives the correlation between the internal energy or enthalpy and the temperature

$$du = c_v dT \quad ; \quad dh = c_p dT$$

the energy equation can be rewritten as

$$\rho c_p \frac{dT}{dt} = \frac{dp}{dt} + \varepsilon - \operatorname{div} (k \operatorname{grad} T)$$

$k$  = thermal conductivity, (W/m K)

The solution of this equation gives the temperature distribution.

Isobaric process with no dissipation – usual form of energy equation

$$\rho c_p \frac{dT}{dt} = - \operatorname{div} (k \operatorname{grad} T)$$

A chemical reaction within the system influences not only the species equation, but the reaction enthalpy  $\Delta h_R$  must also be considered in the energy balance due to the apparent heat consumption or release.

$$\Delta h_R = h_p - h_r$$

enthalpy of the reactants  $h_r$  and the products  $h_p$

---

Dividing the transferred heat by the temperature, a new state variable, the entropy  $s$  (*state function*), is derived for further characterization of the states and processes.

$$ds \geq \frac{dq}{T} \quad \text{equal for rev. proc}$$

The dissipation function  $\varepsilon$  is the friction loss per volume and time unit.

Entropy always increases [ $ds > 0$ ] by dissipation and irreversible processes, such as pressure loss or concentration homogenization by mixing.

The entropy production is a major indication of the efficiency of a process.

The entropy production is a major indication of the efficiency of a process.

Various control strategies are used for energy savings and entropy minimization.

For continuous flow systems, high pressure losses and unnecessary throttling should be avoided.

In mixing, high solution concentrations as well as high dilutions lead to high separation effort.

Heat transfer devices with high temperature gradients induce high entropy production.

## Elementary transport processes and their description

## Elementary transport processes and their description

The entire change of a state variable is described by the transport processes of conduction in the immobile phase (solids or resting fluids), convection in the fluid phase (gases and liquids), and by the generation or depletion in the control volume.

$$\begin{bmatrix} \text{Total Flow} \\ \text{Density} \end{bmatrix} = \begin{bmatrix} \text{Conduction over} \\ \text{the boundary} \end{bmatrix} + \begin{bmatrix} \text{Convection over} \\ \text{the boundary} \end{bmatrix} + \begin{bmatrix} \text{Source} \\ \text{or} \\ \text{Sink} \end{bmatrix}$$

Conductive transport is driven by a parameter gradient; convective transport is always accompanied by a volume flow rate with a certain mean velocity.

Transfer coefficients:  $D$ ,  $v = \mu/\rho$ ,  $\alpha = k/\rho c_p$  ( $m^2/s$ )

The dynamic behavior of viscous fluids is governed by  $Re = wd\rho/\mu$

Species transfer in convective flow, both  $Re$  and  $Sc (= \mu/\rho D)$

$Sc$  indicates the ratio between the momentum and species transfer.

For  $Sc = O(1)$ , as with gases, momentum transfer and species transfer are in the same order-of-magnitude.

Concentration gradients behave similar to velocity gradients.

For high  $Sc$  such as for liquids, concentration gradients continue much longer than velocity gradients, important for mixing issues.

## Convective heat transfer – both Re and Pr

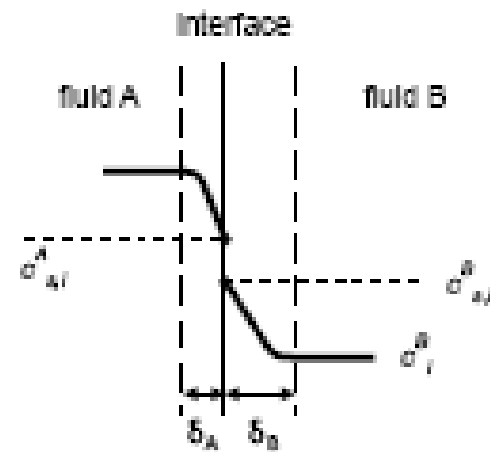
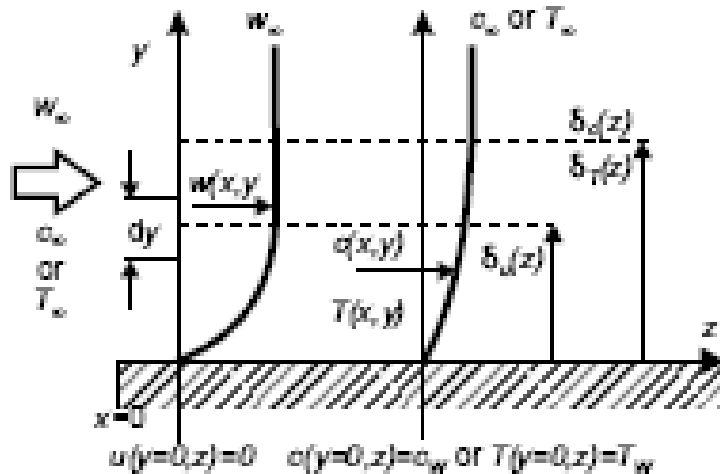
Low Pr numbers - oils or organic liquids.

The Pr numbers of air or water have the order of O(1), permitting a heat transfer as fast as momentum transfer.

Coupled heat and mass or species transfer, such as convective condensation of aerosol droplets, are described by thermal diffusivity and diffusion coefficient. Both coefficients are combined to Lewis number  $Le (=Sc/Pr) = \alpha/D$ , ( $\alpha=k/\rho c_p$ )

A high Le number allows droplet generation from vapor cooling, while for low Le numbers, vapor will directly condense at the wall.

# Two-film model for the fluid/fluid exchange of mass, species, energy



## Species transport equations

$$J_i^A = \beta_i^A A (c_{i,bulk}^A - c_{i,interface}^A); \quad J_i^B = \beta_i^B A (c_{i,interface}^B - c_{i,bulk}^B); \quad \beta_i = \frac{D_{Ai}}{\delta_i}$$

For the absorption of a gas into a liquid Henry's law  $p_{i,g} = H_i c_{ij}$

For the evaporation or condensation of a binary mixture (distillation, rectification), Raoult's law

$$p_i = p_t y_i = \pi_i x_i$$

Concentration difference at the interface of emulsions => Nernst distribution

# Molecular velocities and macroscopic fluid properties

Macroscopic gas properties from kinetic theory and molecular behavior

Bird, Stewart, Lightfoot

Viscosity from the kinetic theory of gases : Chapman and Cowling

$$\mu = 0.499 \rho \lambda \bar{c}_m \quad \lambda = \text{mean free path}; \bar{c}_m = \text{mean molecular velocity}$$

$$\mu = \frac{M_m}{\sqrt{6} \pi \sigma^2} \sqrt{RT} \quad \mu \neq f(p), \mu \uparrow \sqrt{T}, \text{ unlike liquids where } \mu \downarrow \text{ with } \uparrow T$$

$$k = \frac{k}{\pi^{3/2} \sigma^2} \sqrt{RT} \quad D_{AB} = \frac{1}{3} \lambda \bar{c}_m$$

# **Modeling, Calculation Methods, and Simulation**

1. Physical variables and dimensional analysis
2. Similarity and scaling laws
3. Order-of-magnitude analysis
4. Lumped element modeling
5. Numerical simulation and analytical modeling

# Momentum Transfer

In single-phase flow, the fluid motion in microchannels is determined by wall friction, viscous forces and inertial forces.

Continuity Equation

$$\frac{D\rho}{Dt} = \frac{\partial \rho}{\partial t} + \operatorname{div}(\rho \vec{w})$$

Equation of motion

$$\frac{\partial(mw)}{\partial t} = \left( \dot{mw} \right)_{in} - \left( \dot{mw} \right)_{out} + (pA_i)_{in} - (pA_i)_{out} + mg + F_z$$

For one-dimensional differential channel elements with viscous flow, the momentum balance can be written as

$$\frac{\partial(\rho Aw)}{\partial t} = -\frac{\partial(\rho w Aw)}{\partial z} - \frac{\partial(pA)}{\partial z} + p \frac{\partial A}{\partial z} - \tau L_c - \rho A g$$

$L_c$  is the perimeter of the differential channel element

With continuity equation, the above equation can be simplified for all space co-ordinates as ( $\vec{k}$  is the sum of external forces)

$$\rho \frac{\vec{Dw}}{Dt} = \rho \left( \frac{\partial}{\partial t} + \vec{w} \cdot \vec{div} \right) \vec{w} = - \vec{grad} p + \mu \nabla^2 \vec{w} + \vec{k}$$

The 2<sup>nd</sup> term on LHS is also called the inertial term and describes convection. It is the only nonlinear term in the Navier-Stokes eqn.

## The energy equation for fluid dynamics

The total energy conservation can be expressed as the sum of Mechanical and thermal parts.

Mechanical Energy

$$\frac{\rho}{2} \frac{\vec{D}\vec{w}}{Dt} = \vec{\rho w} \cdot \vec{g} + \frac{\partial \rho}{\partial t} - \frac{D p}{Dt} - \Phi$$

Thermal Energy

$$\rho \frac{D h}{Dt} = -\operatorname{div} \vec{q} + \frac{D p}{Dt} + \Phi$$

The dissipation  $\Phi$  of mechanical energy is accompanied by entropy production  
- inner product of the viscous stress tensor and the velocity gradient tensor.

## Relevant boundary conditions

- no wall slip, i.e. zero normal and parallel velocity at the wall (if no suction or blowing occurs, and for gases with  $\text{Kn} < 0.01$ ),
- no temperature jump at the wall, i.e. the temperature and/or temperature gradients can be described at the wall.

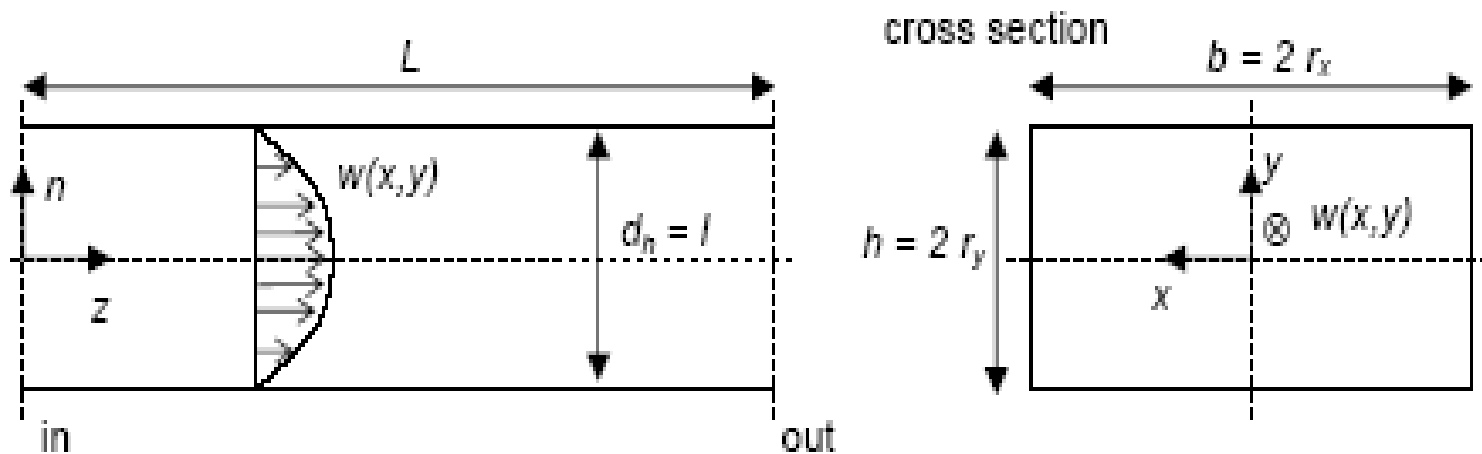
For constant density, non-viscous flow in all three directions, the momentum balance can be written as

$$\frac{\partial \vec{w}}{\partial t} = -(\vec{w} \cdot \vec{\nabla}) \vec{w} - \frac{\vec{\text{grad}} p}{\rho} + \vec{g} \quad \text{Euler equation}$$

Additional forces in microchannel flow may occur with surface effects in multiphase flow, such as bubbles and droplets.

# Momentum Transport of Single-Phase Flow

## Basic equations for long, small channels



Typical setup for a slender microchannel with rectangular cross section.

Length in flow directions is much larger than cross-sectional dimensions

dimensionless variables are introduced with reference values for slender channels with rectangular cross section (width b, depth h, length L, hydraulic diameter  $d_h = 1$ )

$$z^* = z^* = \frac{z}{l \text{Re}}; \quad y^* = \frac{y}{l}; \quad w^* = \frac{w}{w_r}; \quad v^* = \frac{v \text{Re}}{w_r}; \quad p^* = \frac{p - p_r}{\rho w_r^2};$$

$$T^* = \frac{T - T_r}{\Delta T}; \quad \eta^* = \frac{\eta}{\eta_r}; \quad \lambda^* = \frac{\lambda}{\lambda_r}; \quad \Phi^* = \frac{\Phi l^2 \text{Re}^2}{w_r^2}$$

The equations describing a steady and incompressible flow in long channels with variable viscosity and thermal conductivity are

the continuity equation

$$\frac{\partial v^*}{\partial y^*} + \frac{\partial w^*}{\partial z^*} = 0,$$

the z - momentum equation

$$v^* \frac{\partial w^*}{\partial y^*} + w^* \frac{\partial w^*}{\partial z^*} = - \frac{\partial p}{\partial z^*} + \frac{\partial}{\partial y^*} \left[ \eta^* \frac{\partial w^*}{\partial y^*} \right] + \frac{1}{Re^2} \frac{\partial}{\partial z^*} \left[ \eta^* \frac{\partial w^*}{\partial z^*} \right],$$

## The y – momentum equation

$$\frac{1}{\text{Re}^2} \left[ v^* \frac{\partial v^*}{\partial y^*} + w^* \frac{\partial v^*}{\partial z^*} \right] = - \frac{\partial p}{\partial y^*} + \\ + \frac{1}{\text{Re}^2} \left[ \frac{\partial}{\partial y^*} \left( \eta^* \frac{\partial v^*}{\partial y^*} \right) + \frac{\partial}{\partial z^*} \eta^* \frac{\partial v^*}{\partial z^*} \right]$$

## Thermal energy equation

$$v^* \frac{\partial T^*}{\partial y^*} + w^* \frac{\partial T^*}{\partial z^*} = \frac{1}{\text{Pr}} \frac{\partial}{\partial y^*} \left[ \lambda^* \frac{\partial T^*}{\partial y^*} \right] + \\ + \frac{1}{\text{PrRe}^2} \frac{\partial}{\partial z^*} \left[ \lambda^* \frac{\partial T^*}{\partial z^*} \right] + \frac{\text{Ec}}{\text{Re}^2} \Phi^*.$$

Reynold's number =  $\rho w_r l / \eta_r$  ; Prandtl number =  $\nu / \alpha$

Eckert number =  $w_r^2/c_p \Delta T$

In flow regimes with high Re numbers, the terms with  $1/\text{Re}^2$  are very small and can be ignored.

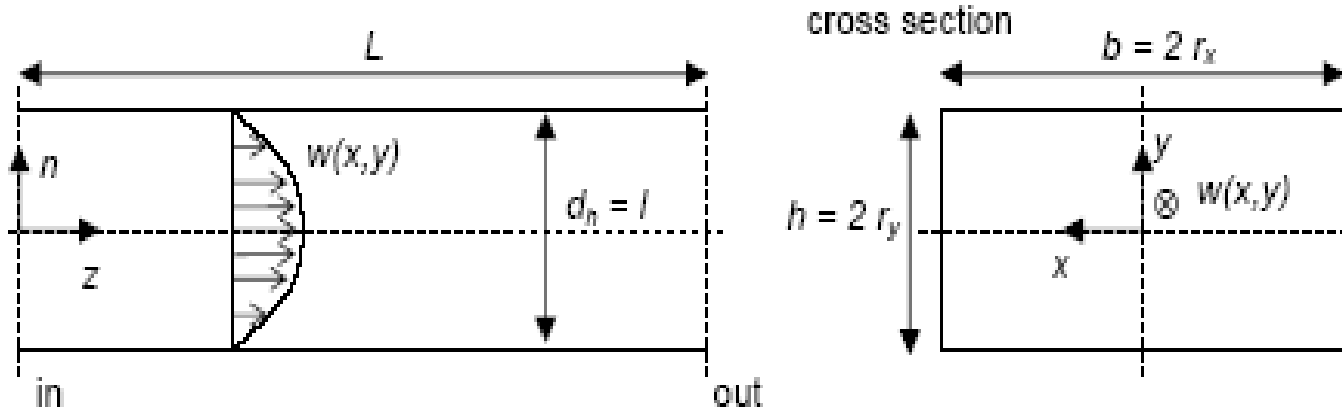
In microflows where the Re number is in the order of  $O(1)$ , the full Navier-Stokes equations must be considered and the influence of  $u$  and  $v$  velocities is not negligible.

When considering the energy equation, the viscous dissipation cannot be neglected in microchannels,

The ratio  $\text{Ec}/\text{Re}^2 = v^2/(c_p \Delta T d^2)$  ( $v$  = kinematic viscosity) does not incorporate velocity and is proportional to the inverse square of the hydraulic diameter.

# Lecture 10

## Basic equations for long, small channels



Typical setup for a slender microchannel with rectangular cross section.

$z$  - momentum equation

$$v^* \frac{\partial w^*}{\partial y^*} + w^* \frac{\partial w^*}{\partial z^*} = - \frac{\partial p}{\partial z^*} + \frac{\partial}{\partial y^*} \left[ \eta^* \frac{\partial w^*}{\partial y^*} \right] + \frac{1}{Re^2} \frac{\partial}{\partial z^*} \left[ \eta^* \frac{\partial w^*}{\partial z^*} \right],$$

The describing PDEs of the velocity  $w$  through a certain cross sectional area is comparable to the displacement of a thin membrane or the stress function in a bar under torsion. That means for the velocity

$$w(x, y) = \frac{\Delta P}{\eta L} \phi$$

with  $\Delta p/L$  as pressure loss per length and  $\phi$  as the torsion function.

A solution for the torsion function on a rectangular cross section can be found with a Fourier series:

$$\phi = \sum_{m,n=1}^{\infty} \frac{16(2r_x)^2(2r_y)^2}{mn\pi^4(n^2 4r_x^2 + m^2 4r_y^2)} \sin\left(\frac{m\pi x}{2r_x}\right) \sin\left(\frac{n\pi y}{2r_y}\right),$$

with  $2r_x$  and  $2r_y$  as the width and depth of the channel. The sum of the first 4 elements is sufficient for rectangular channels with an aspect ratio of approx.  $a = 1$ .

Higher order elements are negligible, but must be considered for flat channels.

The basic equations are valid for laminar flow with a typical Re number below the critical Re number at the transition from laminar to turbulent flow.

The critical Re numbers for internal flows are in the range of  $\text{Re}_c = \mathcal{O}(10^3)$ .

circular pipe flow:  $\text{Re}_c \approx 2300$  ( $/ = d$ , diameter)

rectangular channel flow:  $\text{Rec} \approx 2300$  ( $/ = d_h$ : hydraulic diameter  $d_h = 4A/l_p = 2bh/(b+h)$ )

plane channel flow:  $\text{Rec} \approx 2000$  ( $/ = h$ , distance of the walls)

plane Couette flow:  $\text{Rec} \approx 1800$  ( $/ = b$ , distance of the walls)

The governing equations can be simplified for long channel geometries with established mean values for the velocity and for constant fluid properties.

For different locations 1 (at the inlet) and 2 (at the outlet) of the channel, the basic equations can be written as:

continuity equation:

$$\rho w_2 A_2 = \rho w_1 A_1$$

momentum equation or mechanical energy equation, also called the Bernoulli equation

$$\frac{w_2^2}{2} + \frac{p_2}{\rho} + g y_2 = \frac{w_1^2}{2} + \frac{p_1}{\rho} + g y_1 + w_{t12} - \varphi_{12}$$

technical energy  $w_{t12}$  and the dissipation  $\varphi_{12}$

The Bernoulli equation, is complemented by the technical energy  $w_{t12}$  and the dissipation. It represents the momentum balance and the mechanical energy balance.

$W_{t12}$ : specific technical work, positive for added work (pump, actuator, etc.) and negative for produced work (turbine, opened valve, etc.) between location 1 and 2,

Thermal energy       $e_2 = e_1 + q_{12} + \varphi_{12}$

$q_{12}$ : specific heat, positive for added heat (heating, light or electromagnetic waves, etc.) and negative for cooled fluid (heat loss to ambient, etc.) between locations 1 and 2

$\varphi_{12}$ : specific viscous dissipation, simultaneously decreasing the mechanical energy and increasing the inner energy between location 1 and 2. The viscous dissipation is linked to the pressure loss  $\Delta p$ .

The pressure loss  $\Delta p_{12}$  in a slender channel is determined from the Bernoulli equation (neglecting technical work).

$$\Delta p_{12} = \rho \varphi_{12} = p_1 - p_2 + \frac{\rho}{2} (w_1^2 - w_2^2) + g (y_1 - y_2)$$

For a constant cross section and negligible gravitation forces, the viscous dissipation in a channel element correlates with the pressure loss:

$$\varphi_{12} = \frac{p_1 - p_2}{\rho}$$

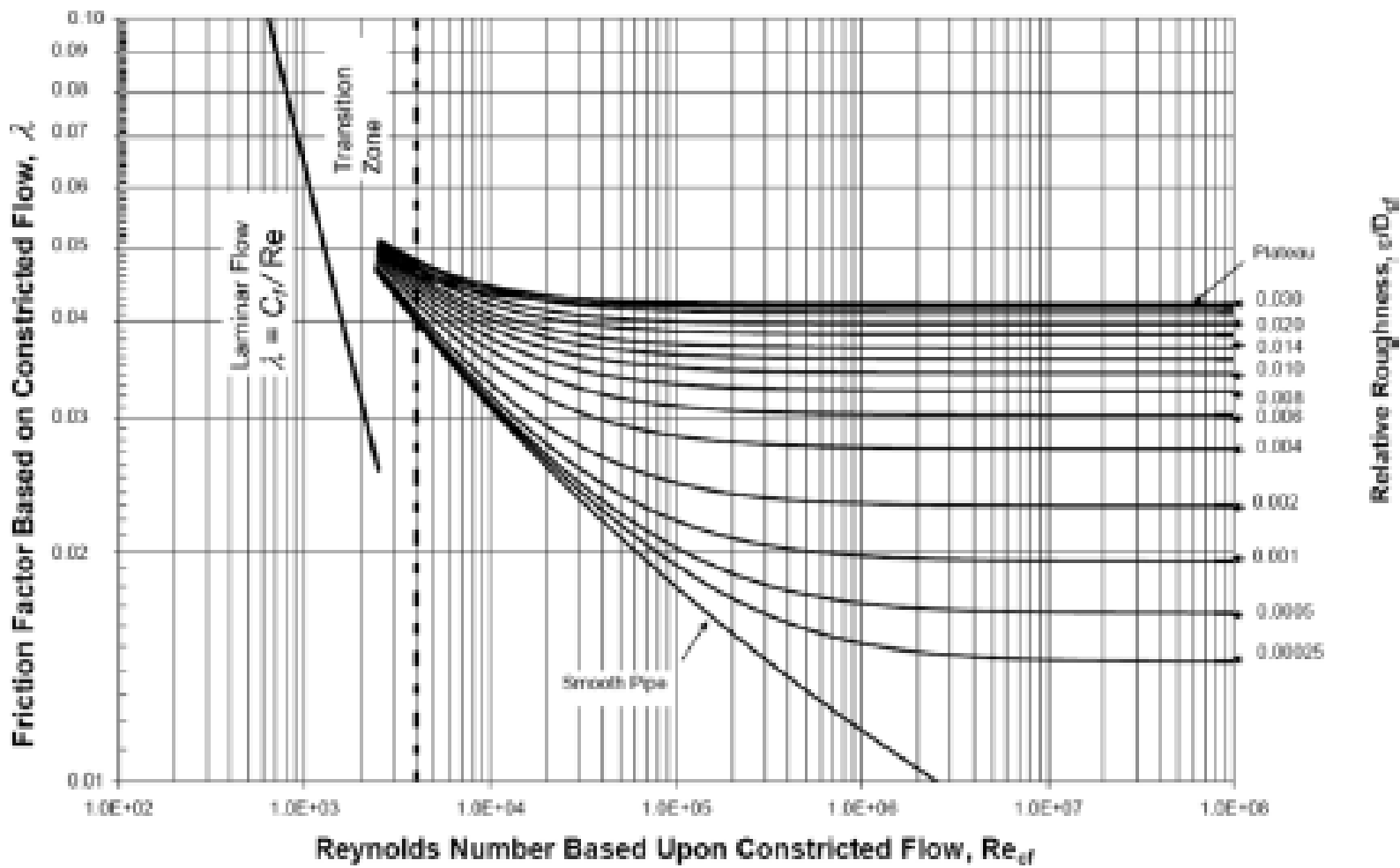
The pressure loss is approximated by the sum of individual losses consisting of fittings, bends, valves and straight pipes of length  $l_i$

$$\Delta p = \sum_i \left( \lambda_i \frac{l_i}{d_{h,i}} + \zeta_i \right) \cdot \frac{\rho}{2} w_{ref,i}^2$$

The reference velocity  $w_{ref,i}$  must be determined for each channel element  $i$ .

The channel friction factor  $\lambda$  of the straight pipe is determined by the flow regime and the cross section.

The pressure loss coefficient  $\zeta_i$  is affected by flow internals, such as curves, bends, fittings, and other channel joints.



Flow friction factors for straight channels with a rough surface according to Moody

# Channel friction factor coefficients $C_f$ in fully developed flow through straight microchannels with different cross-sections.

Cross section, char. length	$C_f = \lambda \cdot Re$	$w_{max}/\bar{w}$
circle, $D$	64	2.000
square, $h$	56.92	2.0962
rectangular, $h; b$ aspect ratio $\alpha_A = h/b$ see also Eq. 3.67	$96 [1 - 1.3553\alpha_A + 1.9467\alpha_A^2 - 1.7012\alpha_A^3 + 0.9564\alpha_A^4 - 0.2537\alpha_A^5]$	–
slab, $\alpha \rightarrow 0$	96	1.500
hexagon	60	–
60° trapezoid $h/b =$		
4.00	55.66	2.181
2.00	55.22	2.162
1.00	56.60	2.119
0.50	62.77	1.969
0.25	72.20	1.766
KOH trapezoid $h/b = 1.00$	56.15	2.137

## Convective Fluid Dynamics in Microchannels

The flow in microchannels is generally regarded as straight laminar flow. This is correct for straight channels with low flow velocity and, therefore, low Re numbers.

In straight channels, the flow remains laminar with straight streamlines below a Re number of 2300, although first flow disturbances with wavy streamlines may appear for even lower Re numbers.

Straight laminar flow changes when the fluid flows through curves, bends, or around obstacles.

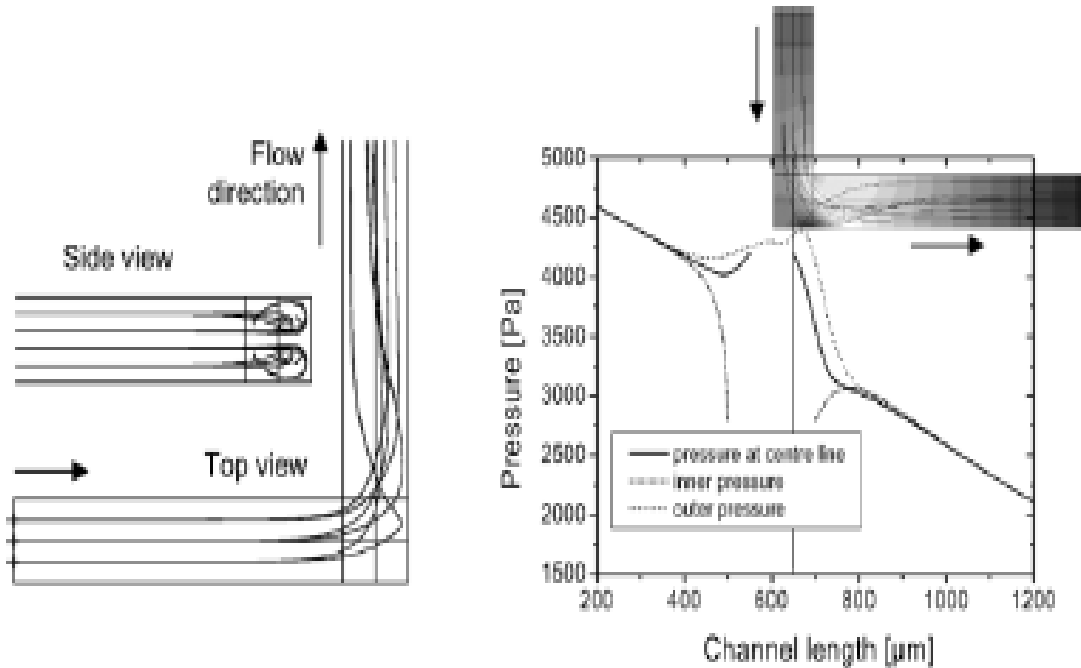
Centrifugal forces in bends push the fluid from the center of the channel, where the bulk fluid flows with high velocity, to the outward side.

At the wall, the fluid is forced either upwards or downwards, producing a symmetric, double vortex filling the entire channel.

This flow regime in curved channel elements is often called Dean flow.

$$\text{Dean Number} = \text{Re} \left( D / R_c \right)^{1/2}$$

The viscous wall friction acts against the centrifugal force and, therefore, dampens the vortex flow.



Left: Vortices in a  $90^\circ$  bend (L-mixer) with laminar vortex flow,  $\text{Re} = 99$ ,  $w^- = 0.85 \text{ m/s}$ ; Right: Pressure distribution in the  $90^\circ$  bend at the center plane of the channels,  $100 \times 100 \mu\text{m}^2$ ,  $\text{Re} = 99$ .

The investigated flow regimes are laminar with vortex formation. No onset of turbulence was observed in the bends.

In the inlet channel, a uniform pressure distribution in the cross section can be observed.

Due to the curvature of the bend the flow is altered into a new direction. At the outer side of the bend, the pressure is increased, comparable to the stagnation point of an impinging jet.

At the inner side of the bend, the pressure decreases directly at or shortly behind the sharp corner, which often results in recirculation, separation flow, or cavitation.

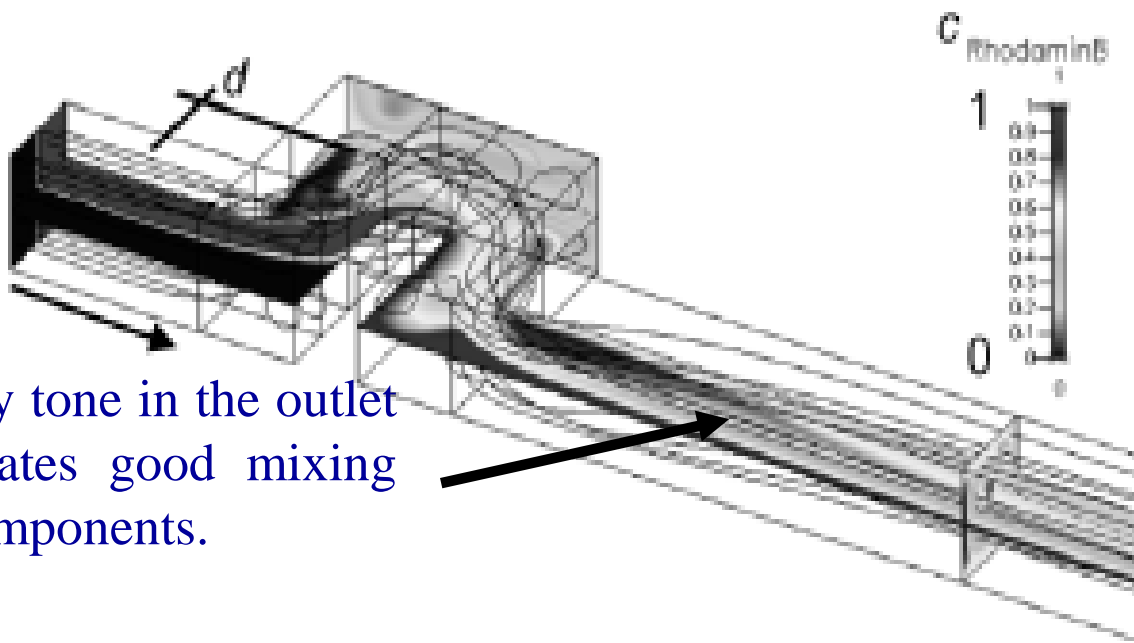
Approx.  $100 \mu m$  behind the bend, a uniform pressure establishes in the cross section.

At this point, the vortices are already damped and straight laminar flow is established again, as shown by the streamlines in left side

The pressure loss in the bend results in vortex formation and is the basis for further calculation in mixing theory.

# Mixing Elements

## U-shaped 90° bend mixing element



The light gray tone in the outlet section indicates good mixing of the two components.

Streamlines and concentration profiles ( $\text{Sc} = 3700$  for aqueous Rhodamin B solution) in a combined 90° bend mixer (U-mixer) with channel dimensions of  $300 \times 300 \mu\text{m}$ , offset  $d$ , mass flow rate of 250 g/h, ( $\text{Re} = 270.7$ )

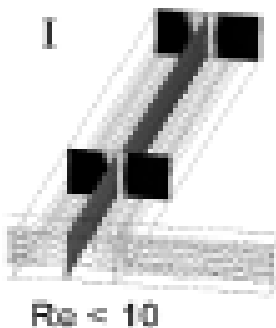
# **Fluid dynamics in T-junctions with symmetric inlet conditions**

Dynamics of the mixing process in T-junctions are treated with symmetrical inlet conditions and 1 : 1 mixing of the reactants.

CFD simulations and visualizations

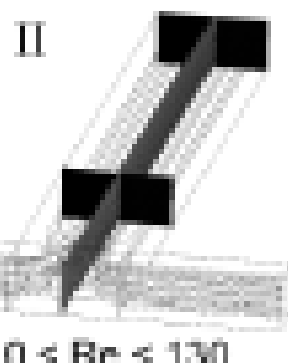
T-shaped micromixer ( $T600 \times 300 \times 300$  which represents a mixing T with rectangular cross sections, a mixing channel width of 600  $\mu\text{m}$ , two symmetric inlet channels with a width of 300  $\mu\text{m}$ , and 300  $\mu\text{m}$  overall depth)

## Classification of the investigated flow regimes in symmetrical T-shaped micromixers



$Re < 10$ ,  $Dn < 10$ , regime I straight laminar flow, steady velocity profile with straight streamlines, diffusion dominates the mass transfer;

$$Dn = Re \left( D / R_c \right)^{1/2}$$



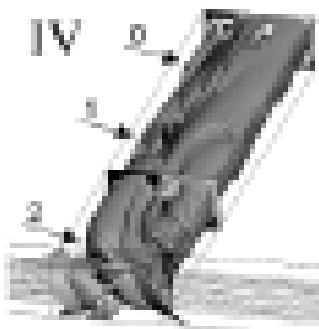
$10 < Re < 130$  (approx.),  $Dn > 10$ , regime II symmetric vortex flow, Dean flow with characteristic  $Dn$  number.

straight laminar flow is disturbed by the centrifugal forces created by an increasing  $Re$  number, and symmetric vortex flow establishes in the mixing channel



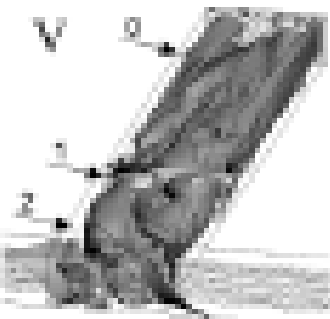
$130 < \text{Re} < 240$

$130 < \text{Re} < 240$  (approx.), regime III engulfment flow, breakup of the symmetry, fluid swaps to the opposite side. This leads to small lamellae, short diffusion lengths, and high mixing quality.



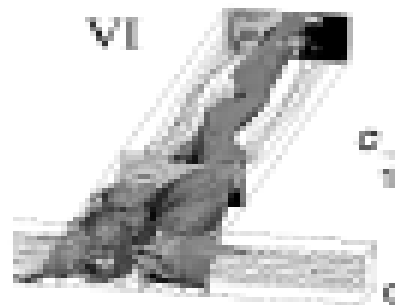
$240 < \text{Re} < 400$

$240 < \text{Re} < 400$  (approx.), regime IV regular, periodic pulsating flow, reproducible vortex break down



$400 < Re < 500$

$400 < Re < 500$  (approx.), regime V quasi-periodic pulsating flow, vortex breakdown, broad range of mixing quality;



$500 < Re$

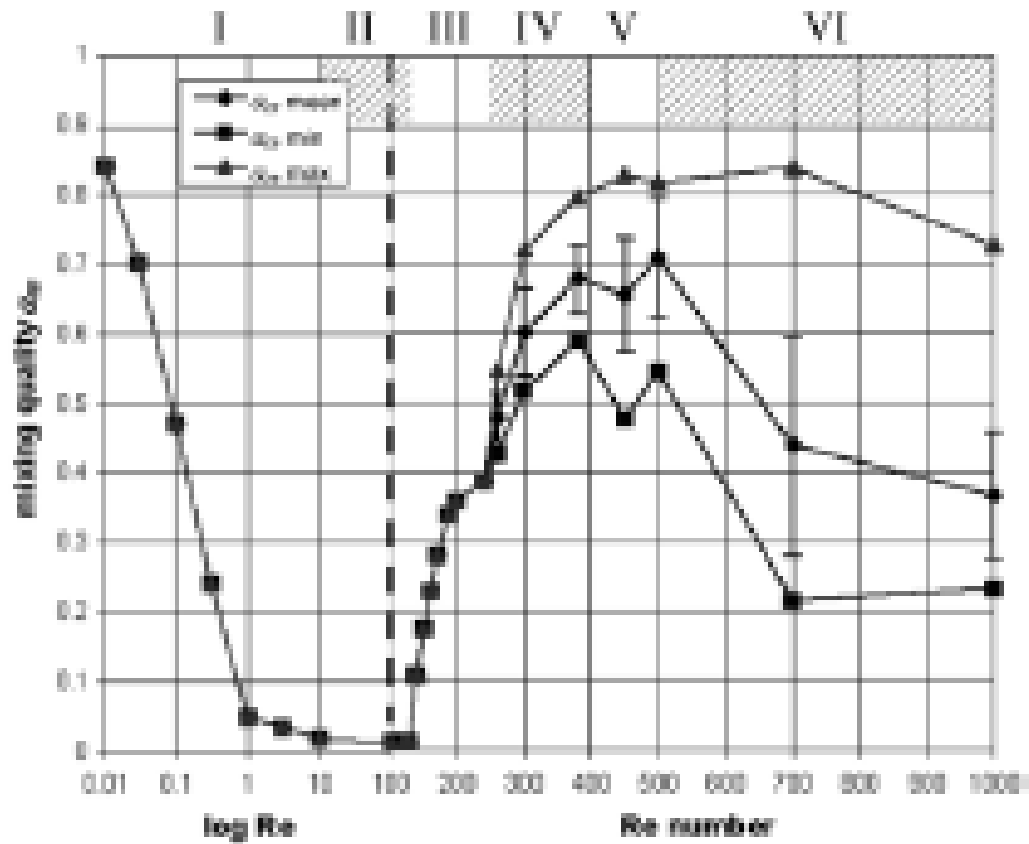
$500 < Re$  (approx.), regime VI chaotic pulsating flow, vortex breakdown, decreased mixing quality and single flushes of fluid swapping to the opposite side

Flow regimes with Re numbers higher than 1000 are avoided in T-shaped micromixers.

High Re numbers are unsuitable due to high flow velocities producing intolerably high pressure loss.

The mixing quality is the standardized concentration field variance  $\sigma_c$  and is often used to characterize the state of mixing

$$\alpha_m = 1 - \sqrt{\frac{\sigma_c^2}{\sigma_{c,\max}^2}}$$



Development of the mixing quality  $\alpha_m$ ; for  $0.01 < \text{Re} < 100$  on a logarithmic scale and for  $100 < \text{Re} < 1000$  on a linear scale

A T-shaped micromixer with typical channel dimensions from  $50 < d_h < 600$   $\mu\text{m}$  exhibits the most suitable mixing characteristics in the range of  $200 < \text{Re} < 700$  due to the moderate flow velocities, ranging from  $1 < w^- < 50$  m/s for gases and  $0.1 < w^- < 10$  m/s for liquids

# **Heat Transfer and Micro Heat Exchangers**

# Heat Transfer Fundamentals: The energy balance

For a control volume:

$$\sum \dot{E}_{in} - \sum \dot{E}_{out} \pm \sum \dot{E}_{loss} = 0$$

First law of thermodynamics with a dissipation term  $\Phi$  for closed systems

$$dE_{sys} = dU + dQ + dW + \Phi$$

For open systems, ( $P_t$  is the technical power).

$$d\dot{E}_{sys} = d\dot{H} + d\dot{Q} + d\dot{P}_t + \Phi$$

The dissipation  $\Phi$  takes into account that the energy conversion from one form into another is accompanied by natural losses.

For a process device with mass flow rate  $m$ , heat flux  $q$  over the boundary, technical work  $W_t$ , or mechanical power  $P$ , and chemical reaction, the energy equation is written as

$$\dot{Q} = \left( \dot{m}(u_2 - u_1) \right) + \left( \dot{m} \left( \frac{p_2}{\rho} - \frac{p_1}{\rho} \right) \right) + \left( \dot{m} g (z_2 - z_1) \right) + m \left( \frac{\alpha_2 \overline{V_2^2}}{2} - \frac{\alpha_1 \overline{V_1^2}}{2} \right) + \dot{E}_q + P$$

The temporal energy change in a system consists of

- energy flowing in and out/dissipation,
- pressure,
- gravity,
- KE,
- energy produced inside the system (chemical reactions).
- technical work or mechanical power  $P$ .

The energy of the fluid flowing in a straight channel, without chemical reactions and technical work consumed or produced.

$$e = \left( u + \frac{w^2}{2} + g y \right)$$

With Fourier law  $q = -\lambda \partial T / \partial x$  for conductive heat transfer perpendicular to the channel axis, the energy equation can be written as

$$\begin{aligned} \frac{\partial}{\partial t} \left( \rho \left( u + \frac{w^2}{2} \right) \right) &= - \frac{\partial}{\partial z} \left( \rho w \left( u + \frac{w^2}{2} \right) \right) + \rho g y - \\ &\quad - \frac{\partial}{\partial z} (p w) - \frac{\partial}{\partial z} \left( \lambda \frac{\partial T}{\partial x} \right) - \frac{\partial}{\partial z} (\tau w) + w_t, \end{aligned}$$

Bernoulli equation for the energy balance in channel flow and can be simplified to suit each process.

For open systems and flow processes, the inner energy is replaced by the enthalpy  $h = u + p/\rho$ .

For flow processes, the total enthalpy  $ht = u + p/p + w^2/2 + g y$  is applied together with the kinetic and potential energy part.

With the energy dissipation ( $\varepsilon$ ) from shear stress and velocity gradient, the enthalpy form of the energy equation can be written as

$$\rho \frac{dh}{dt} = \varepsilon - \nabla \cdot q$$

With the caloric equation of state, the correlation between the inner energy  $u$  or enthalpy  $h$ , and the temperature ( $d u = c_v d T$  and  $d h = c_p d T$ ) the energy equation can be rewritten as

$$\rho c_p \frac{dT}{dt} = \varepsilon + \operatorname{div}(\lambda \operatorname{grad} T)$$

Solving this equation gives the temperature distribution for the actual process.

# Heat conduction in small systems

Fourier's law of heat transfer describes the correlation between the steady heat flow and the driving temperature difference.

$$\dot{Q} = -\lambda A(r) \frac{dT}{dr}$$

The integration over the coordinate r leads, for constant heat conductivity  $\lambda$ , to

$$T_1 - T_2 = \dot{Q} \frac{1}{\lambda} \int_{r_1}^{r_2} \frac{1}{A(r)} dr$$

The integrated area divided by the thermal conductivity is often called the thermal resistance  $R_{th}$  in analogy to electrical resistance.

## Thermal resistance of the simple geometrical elements plate, cylinder, and sphere.

plate or slab	cylindrical element	spherical element
$A = \text{const.}$	$A = 2\pi r L$	$A = 4\pi r^2$
$R_{th} = \frac{1}{\lambda} \frac{r_2 - r_1}{A}$	$R_{th} = \frac{1}{\lambda} \frac{\ln(r_2/r_1)}{2\pi L}$	$R_{th} = \frac{1}{\lambda} \frac{(1/r_1 - 1/r_2)}{4\pi}$

The heat conductivity in microsystems is influenced by the [microstructure of the material](#). Grain boundaries and crystal lattices form additional resistances to heat transfer.

In regular crystals, the heat transfer coefficient is dependent on the crystal orientation, and the Fourier equation of heat transfer must be expanded to the tensor notation

$$\dot{q} = -\lambda \frac{dT}{dx} \rightarrow \vec{q} = -\Lambda \cdot \text{grad } T$$

with the heat conductivity tensor

$$\Lambda = \begin{pmatrix} \lambda_{11} & \lambda_{12} & \lambda_{13} \\ \lambda_{21} & \lambda_{22} & \lambda_{23} \\ \lambda_{31} & \lambda_{32} & \lambda_{33} \end{pmatrix}.$$

The solution of the three-dimensional heat conduction is often only possible with numerical methods.

The time dependent second Fourier law is derived from a differential element with the balance of the heat capacity and the heat conduction

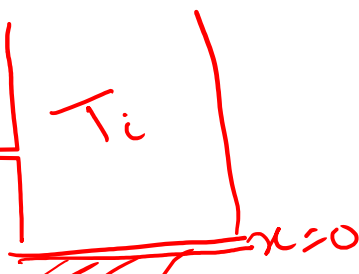
$$\rho A(r) c_p \frac{\partial T}{\partial t} = \frac{\partial}{\partial r} \left( \lambda A(r) \frac{\partial T}{\partial r} \right).$$

Constant material properties, such as heat capacity  $c_p$  and heat conductivity  $\lambda$ , and mathematical simplification for different geometrical bodies ( $n = 0$  for a plate,  $n = 1$  for a cylinder, and  $n = 2$  for a sphere) lead to,

$$\frac{\partial T}{\partial t} = a \left( \frac{\partial^2 T}{\partial x^2} + \frac{n}{r} \frac{\partial T}{\partial r} \right)$$

with the heat diffusivity  $\alpha = \lambda / \rho c_p$ .

The transient temperature development in a semi-infinite body, is given in one-dimensional form by



$$\frac{\partial T}{\partial t} = a \frac{\partial^2 T}{\partial x^2}; \quad t \geq 0, \quad x \geq 0.$$

$$T(x, t)$$

$$T(x, 0) = T_i$$

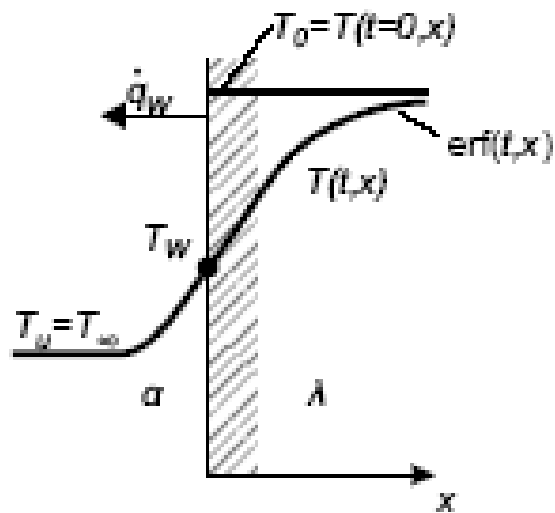
$$T(x=0, t>0) = T_S$$

$$T(x \rightarrow \infty, t>0) = T_i$$

The transient temperature development in a semi-infinite body, is given in one-dimensional form by

$$\frac{\partial T}{\partial t} = a \frac{\partial^2 T}{\partial x^2}; \quad t \geq 0, \quad x \geq 0.$$

The introduction of the dimensionless temperature  $\theta$  leads to



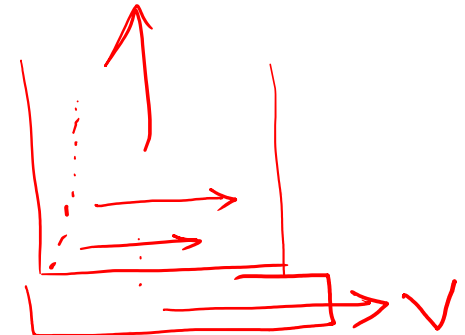
$$\frac{\partial \theta}{\partial t} = a \frac{\partial^2 \theta}{\partial x^2} \quad \text{with} \quad \theta = \frac{T - T_0}{T_w - T_0},$$

describing the temperature development in a solid body with defined wall temperature  $T_w$

Temperature distribution in a semi-infinite body during cooling

With constant wall temperature  $T_w = \text{const.}$ , the dimensionless temperature is determined by the error function

$$\frac{T - T_0}{T_w - T_0} = \operatorname{erf}(x^*) \quad \text{with} \quad x^* = \frac{x}{2\sqrt{at}}$$



The wall heat flux can be calculated from this equation.

For a constant  $\alpha$  at the wall, the solution is derived with the help of two dimensionless numbers, the Fourier number ( $a$  = thermal diffusivity) and the Biot number ( $\alpha$  = heat transfer coefficient)

$$Fo = \frac{a t}{x^2} \qquad Bi = \frac{\alpha x}{\lambda_s}$$

The temperature development during cooling of the body is given by

$$\theta_C = \frac{T - T_\infty}{T_0 - T_\infty} = \operatorname{erf}(x^*) - e^{FoBi^2 + Bi} \operatorname{erfc}\left(\sqrt{Fo} Bi + x^*\right)$$

and for heating

$$\theta_H = 1 - \theta_C.$$

$$t_c = a t \left( \frac{\alpha}{\lambda} \right)^2 = Fo \cdot Bi^2$$

The characteristic time for heating or cooling is drawn from the combination of the Fo and Bi numbers and does not depend on the length (semi-infinite body).

**Miniaturization will not influence the temperature development and the heat flux for a semi-infinite body.**

For small bodies (high Fo and low Bi number), the temperature distribution can be approximated by asymptotic solutions.

The temperature inside a small body is only a function of time

$$\theta = \frac{T - T_{\infty}}{T_0 - T_{\infty}} = \exp\left(-\frac{\alpha A t}{m c_p}\right) \quad \text{for } \text{Fo} > 0.3 \text{ and } \text{Bi} < 0.2,$$

More exact for the three basic geometries (plate  $n = 0$ , cylinder  $n = 1$ , sphere  $n = 2$ ):

$$\theta = \exp(-(n+1)\text{Bi Fo})$$

# Convective heat transfer in microchannels

The total heat transfer in microstructured devices consists of heat conduction through the walls and convective heat transfer from the wall into the fluid in microchannels.

For straight laminar flow, the dimensionless heat transfer coefficient, the Nu number, is constant.

For constant wall heat flux,  $\text{Nu}_q = 4.3$ , for constant wall temperature  $\text{Nu}_T = 3.66$ .

In a wide gap or narrow slit, the Nu number is 7.54 ( $q = \text{const.}$ ) and 8.24 ( $T = \text{const.}$ ) for double-sided heat transfer,

and 4.86 ( $q = \text{const.}$ ) and 5.39 ( $T = \text{const.}$ ) for single-sided heat transfer.

For smaller channels, the heat transfer coefficient increases due to the constant Nu number.

With decreasing channel dimensions, the transfer area and the mass flow through the channel are also decreased, hence, the transported heat is limited by these conditions.

To maintain a high heat transfer coefficient with a high transport rate, an optimum channel dimension must be found - fabrication process.

At the entrance of a channel or behind channel elements, such as channel junctions, expansions or contractions, the disturbed flow enhances the radial transport in the channel.

This results in increased pressure loss as well as increased heat or mass transfer.

Dimensionless channel length  $X^*$ , starting at the entrance,

$$X^* = \frac{L}{d_h} \text{Pe} = \frac{L}{d_h} \text{Re} \cdot \text{Pr}$$

Pe is the heat transfer Peclet number.

The mean Nu number in the entrance flow  $\text{Nu}_{\text{me}}$  is calculated with the mean Nu number in straight channel flow,  $\text{Nu}_m$  according to the following correlation

$$\text{Nu}_{\text{me}} = \frac{\text{Nu}_m}{\tanh(2.432 \text{Pr}^{1/6} X^*{}^{1/6})}.$$

This equation is valid for the entire channel length  $X^*$  and  $\text{Pr} > 0.1$

Beyond a certain length, the velocity and temperature profiles do not alter - fully-developed flow

In turbulent flow (for  $\text{Re} > \text{Re}_{\text{crit}} = 2300$  in channel flow) the pressure loss is proportional to the square mean velocity and the heat transfer can be calculated according to Gnielinski

$$\text{Nu} = \frac{\xi/8 (\text{Re} - 1000) \text{Pr}}{1 + 12.7\sqrt{\xi/8}(\text{Pr}^{2/3} - 1)} \left(1 + \left(\frac{d_h}{l}\right)^{2/3}\right) K_{\text{Pr}}$$

with  $\xi = (1.8 \log_{10}(\text{Re}) - 1.5)^{-2}$  and  $K_{\text{Pr}} = (\text{Pr}_{\text{fluid}}/\text{Pr}_{\text{wall}})^{0.11}$ .

This correlation is valid for  $0.5 < \text{Pr} < 2000$ ,  $2300 < \text{Re} < 5 \cdot 10^6$  and  $1 < L/d_h < \infty$ .

Turbulent flow does not often occur in microchannels, however, the manifolds or inlet and outlet headers may produce turbulent conditions.

Surface roughness effect on heat transfer is less significant than on momentum transfer

## Rarefied gases with slip boundary conditions

The previous equations are valid above the continuum limit (Knudsen number = mean free path/characteristic length).

$$\underline{\mathbf{Kn} < 10^{-2}}$$

The continuum and thermodynamic equilibrium assumptions are appropriate and flow situations can be described by conventional no-slip boundary conditions.

$$\begin{aligned} & \mathbf{10^{-2} < Kn < 10^{-1}} \\ & \mathbf{\text{Slip Flow Regime}} \end{aligned}$$

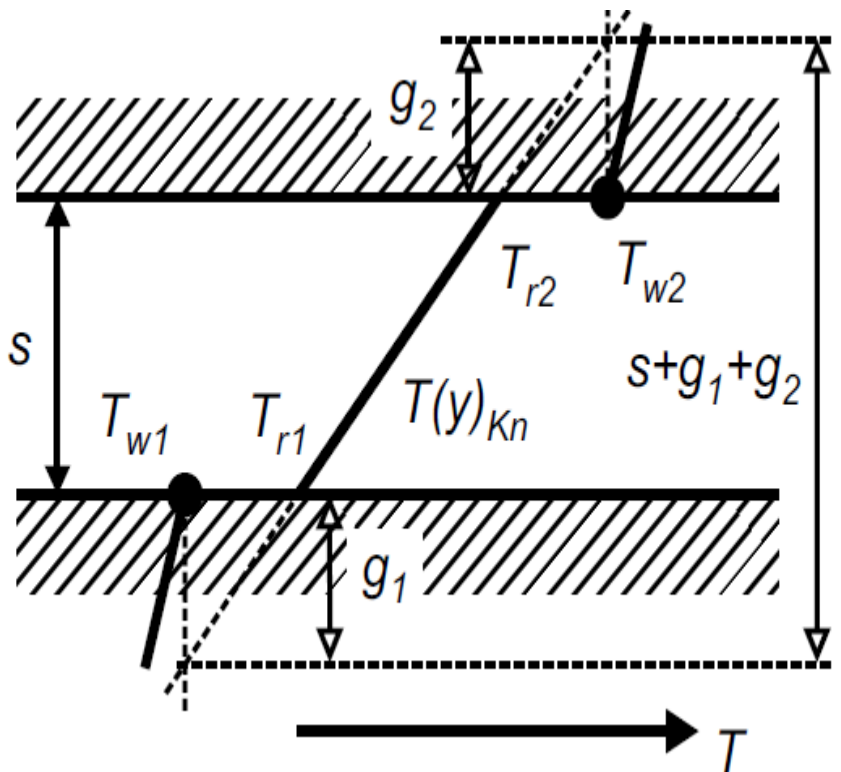
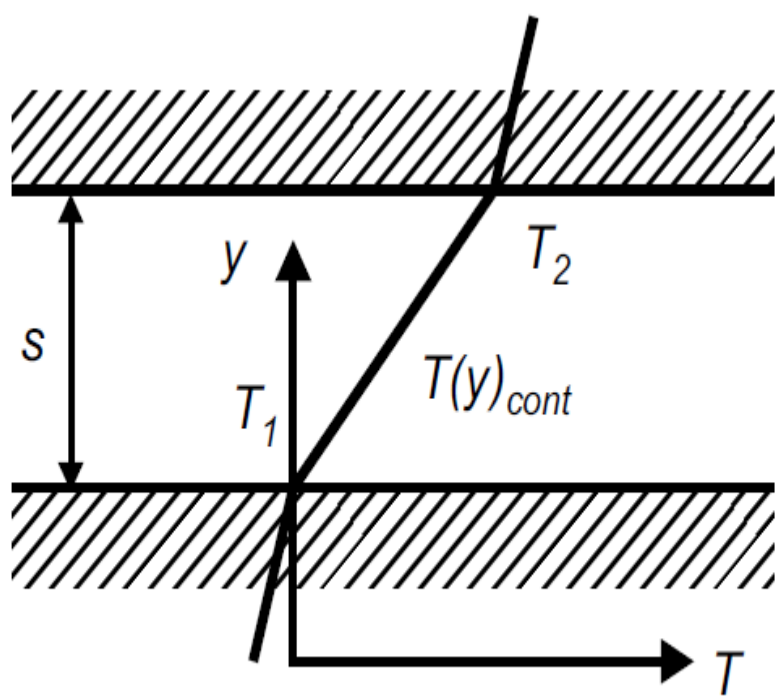
Navier-Stokes equations remain valid provided tangential slip-velocity and temperature-jump boundary conditions are implemented at the walls of the flow domain

For rarefied gases, the transfer processes at the wall differ due to the low number of gas particles.

The **reduced flow resistance** is produced by the slip velocity at the wall, which results from the molecular motion and insufficient momentum transfer between the wall and bulk fluid.

The molecular motion in the gas influences energy transfer into the fluid. A temperature jump occurs at the wall, which **increases the heat transfer resistance**.

## Temperature gradient in a gap



Left: linear development for dense gases ( $\text{Kn} < 0.01$ );

Right: temperature jump in rarefied gases ( $\text{Kn} > 0.01$ ).

## Accommodation Coefficient, $\beta$

When a particle impacts with a surface, energy is transferred in the form of heat and stress, which leads to two main types of accommodation coefficients - thermal and transverse momentum.

**The thermal accommodation coefficient** is the fraction of heat transferred between the surface and the molecule. “The ratio of the average energy actually transferred between a surface and impinging gas molecules scattered by the surface, to the average energy which would theoretically be transferred if the impinging molecules reached complete thermal equilibrium with the surface.

### **Transverse Momentum Accommodation Coefficients (TMAC)**

The TMAC is the fraction of the momentum normal to the wall that is transferred to the wall in terms of stress. This stress is commonly known as pressure. By creating a pressure on the wall some of the vertical momentum is lost.

For rarefied gas flow ( $0.01 < \text{Kn} < 0.1$ ), the boundary condition of the gas velocity at the wall is described by, (slip length  $\zeta$ )

$$w(x = 0) = \zeta \left( \frac{\partial w}{\partial x} \right)_{y=0}$$

The slip length  $\zeta$ , can be calculated with the accommodation coefficient  $\beta$  and the mean free path  $\Lambda$  of the molecules.  $\beta$  describes the efficiency of the momentum and energy transfer from molecules to the wall and vice versa.

$$\zeta \approx \frac{2 - \beta}{\beta} \Lambda \quad \beta = 2, \text{ from Kinetic theory for continuum regime}$$

Experimental data for  $\beta$  can be found in the literature.

The temperature jump at the wall is described in a similar way with the temperature jump coefficient  $g$

$$T(x = 0) = T_r = T_W + g \left( \frac{\partial T}{\partial x} \right)_{x=0}$$

The temperature jump coefficient  $g$  can be determined via kinetic theory from the thermal accommodation coefficient  $\gamma$ , a material parameter  $f$ , and the mean free path  $\Lambda$

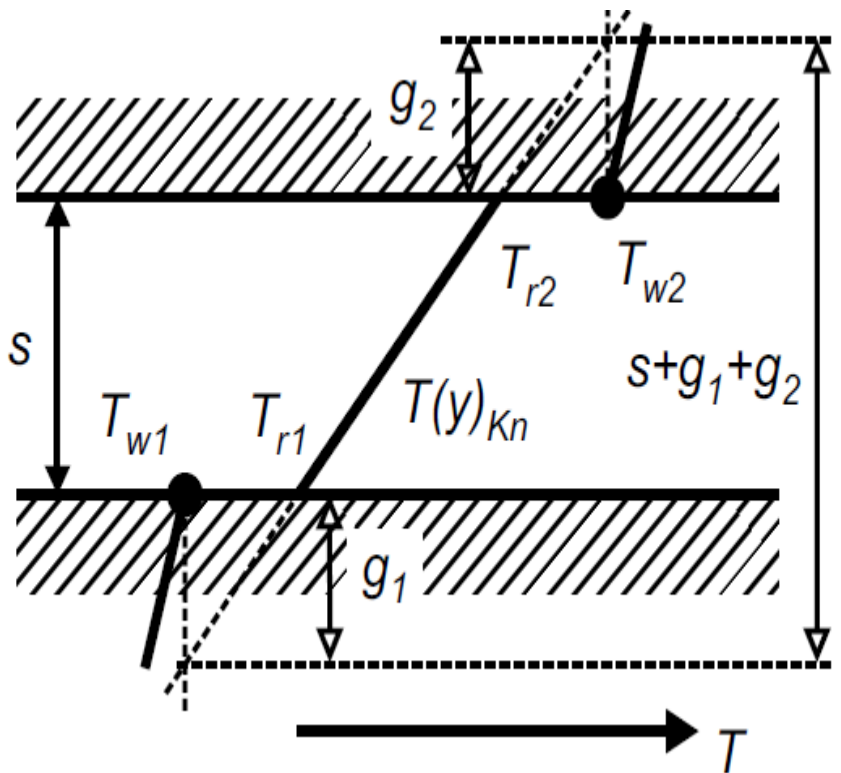
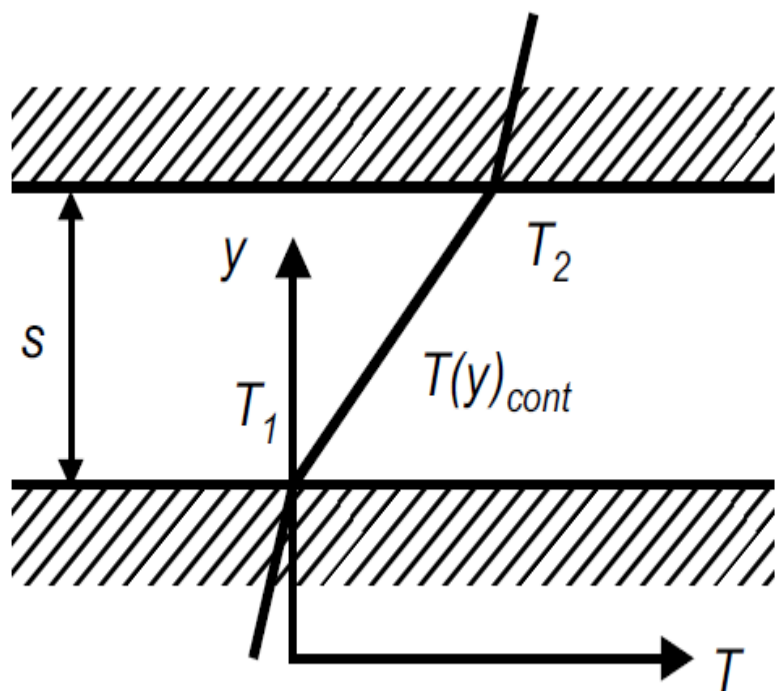
$$g = \frac{2 - \gamma}{\gamma} \frac{15}{8} f \Lambda$$

The material parameter  $f$  is calculated from the linearized Boltzmann transport equation and is given by

$$f = \frac{16}{15} \frac{\lambda}{\eta c_v} \frac{1}{\kappa + 1} = \frac{16}{15} \text{Pr} \frac{\kappa}{\kappa + 1}$$

$\lambda$  = thermal conductivity,  $\eta$  = viscosity,  $\kappa$  = isentropic exponent =  $c_p/c_v$

## Temperature gradient in a gap



left: linear development for dense gases ( $\text{Kn} < 0.01$ ); right: temperature jump in rarefied gases ( $\text{Kn} > 0.01$ ).

For flow processes, the ratio of the temperature jump coefficient and the characteristic length is important and can be derived from  $g = \frac{2-\gamma}{\gamma} \frac{15}{8} f \Lambda$  as

$$\frac{g}{l_{char}} = \frac{2-\gamma}{\gamma} \frac{15}{8} f \text{Kn} \quad \Lambda - \text{mean free path}$$

For monatomic gases with  $\kappa = 5/3$ ,  $\text{Pr} = 2/3$  ( $\rightarrow f = 1$ ), and complete accommodation  $\gamma=1$ , the length ratio reduces to

$$\frac{g}{l_{char}} = \frac{15}{8} \text{Kn}$$

The linear temperature distribution in a gap (of size  $s$ ) is determined with the jump coefficient  $g$  and the starting equation  $T(x=0) = T_r = T_W + g \left( \frac{\partial T}{\partial x} \right)_{x=0}$  as

$$\frac{T(y) - T_2}{T_1 - T_2} = \left( 1 - \frac{y + g_1}{s + g_1 + g_2} \right)$$

The temperature jump coefficient  $g$  can be regarded as an additional distance of the gap.

For  $0.1 < \text{Kn} < 10$ , monatomic gases, and complete accommodation, the temperature gradient is only a function of the Kn number.

$$\frac{T(y/s) - T_2}{T_1 - T_2} = \left( 1 - \frac{y/s + (15/8) \text{ Kn}}{1 + (15/4) \text{ Kn}} \right)$$

The derivation of the temperature profile and comparison of the coefficients yields the heat flux for  $0.1 < \text{Kn} < 10$ , which can be expressed as the ratio to the continuum heat flux.

$$\frac{\dot{q}}{\dot{q}_{cont}} = \frac{1}{1 + (15/4) \text{ Kn}}$$

For  $\text{Kn} > 10$  (free molecular flow), the ratio of the heat fluxes in a gap are also dependent on the Kn number.

$$\frac{\dot{q}_{FM}}{\dot{q}_{cont}} = \frac{4}{15 \text{ Kn}}$$

The distance between the plates plays no role in this regime; the molecules only hit the walls and not each other. The unsteady heat transfer of rarefied gases can be treated in the same manner.

Assuming a round capillary with the outer radius  $r_A$  and constant wall heat flux  $q$ , the heat transfer of rarefied gas flow (for  $\text{Kn} < 0.1$ ) is expressed with the dimensionless heat transfer coefficient, the Nu number

$$\text{Nu}_q = \frac{\dot{q}}{(T_W - \bar{T})} \frac{r_A}{\lambda} = \frac{\alpha r_A}{\lambda} = 24 \left( 11 - 6 \Delta \bar{w} + (\Delta \bar{w})^2 + 24 \frac{g}{r_A} \right)$$

The dimensionless slip velocity  $\Delta w$  is determined with the slip length from the Eq. for slip length

$$\zeta \approx \frac{2 - \beta}{\beta} \Lambda$$

$$\Delta w = \frac{w(r_A)}{\bar{w}} = \left( 1 + \frac{r_A}{4 \zeta} \right)^{-1}.$$

For non-circular cross sections, the half of the hydraulic diameter  $d_h$  can be taken for  $r_A$ .

The Nu number for constant wall temperature is approx. 5 % higher than for constant wall heat flux.

A numerical study with the Monte-Carlo method indicated that the slip flow model correctly represents convective heat transfer between continuum and molecular flow.

The influence of the axial heat conduction must be considered, however, the viscous heat dissipation, expansion cooling can be neglected.

## Microfluidic Networks for Heat Exchange

Transport processes in micro process engineering are governed by two different mechanisms: the **conductive** and the **convective** transfer of a species or energy.

The fluid flow in microchannels is often regarded to be laminar with dominant conductive transport.

On structured surfaces and in bent and curved flow, secondary transversal flow components are introduced into the straight laminar flow, which enhance the transport processes.

Thus, two strategies enhance the overall transport in pressure-driven flow in passive devices: the implementation of small diameter channels with a short diffusion length and the creation of secondary flow structures perpendicular to the main flow direction.

The typically low flow rates in single microstructured elements can be enlarged by internal and external numbering-up or equal-up of the desired effects.

The internal numbering-up is limited by the available space and the uniform distribution of the fluids. A relative maldistribution of the liquids of approx. 5 % will lead to a corresponding decrease in the heat transfer efficiency.

## Status-quo of microfluidic networks for device cooling

Goal: to provide high thermal performance with low pressure loss.

Cooling of electronic equipment is often accomplished in long, straight channels, which produces relatively low heat transfer coefficients.

With a cost effective manufacturing and proper system integration, a heat dissipation rate of up to  $10 \text{ MW/m}^2$  ( $1 \text{ kW/cm}^2$ ) appears possible for single phase liquid flow.

The setup of different branching levels to spread fluid over an area and collect it again can be managed with the Constructal Theory of Bejan

## Constructal theory of Bejan

The **constructal design** approach begins with the smallest elements on zero level and connects these with those on the next higher level.

This approach is inverse to the **fractal description of branched systems**, where an element is repeatedly miniaturized till almost infinitely small structures.

In nature, systems have a finite smallest size, and therefore, follow the constructal approach.

Optimum size of channel elements and the corresponding area covered

## Murray's law

### The Physiological Principle of Minimum Work: The Vascular System and the Cost of Blood Volume, 1926, PNAS

In every segment of vessel, flow is achieved with the least possible biological work.

Two energy terms contribute to the cost of maintaining blood flow: (a) the energy required to overcome viscous drag in a fluid obeying Poiseuille's law, and (b) the energy metabolically required to maintain the volume of blood and vessel tissue involved in the flow.

The larger the radius, the smaller is the power,  $P_f$ , required for flow, but the larger is the power,  $P_m$ , required for metabolic maintenance of the blood and vessel wall tissue.

The vessel can be neither too large nor too small if the total power,  $P_t = P_f + P_m$ , is to be minimized.

## Murray's law

The optimum flow distribution and cross sections of the channels on different branching levels are influenced by - Murray's law, applicable, for example, in the branching of blood vessels or plant capillaries.

*If the sum of the inner radii to the power of three on each branching level is constant, the channel network will need minimal power consumption or exhibit minimal pressure loss for a given flow rate.*

For channels with circular cross section, the diameter of the highest and largest level element  $d_n$  to the power of 3 is equal to the sum of the diameters  $d_z$  of the next level elements to the power of 3.

$$d_n^3 = \sum_i d_{z,i}^3$$

The level with the largest elements has the notation “n” due to n branching levels of the system. The zero level of the system is the smallest level following the notation of the constructal design method.

For a symmetrical bifurcation, the above equation gives the following correlation for the diameters on various branching levels z

$$d_n^3 = 2^z d_z^3 \quad or \quad d_z/d_n = 2^{-z/3}$$

This correlation serves for an equal wall shear stress in the channels on each branching level z

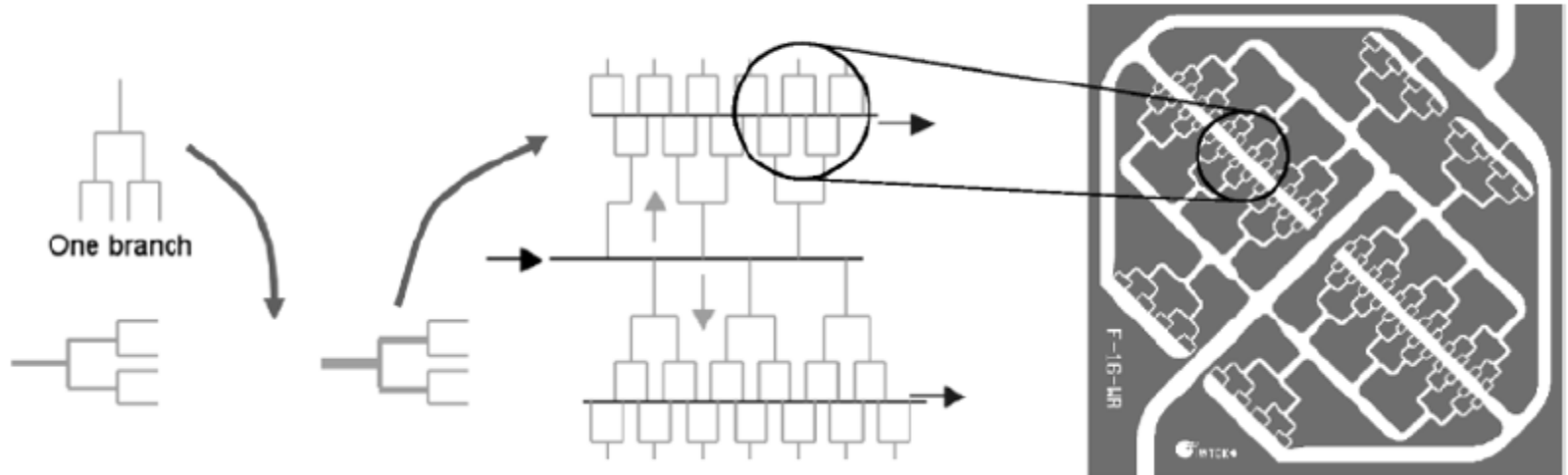
Since the original derivation of Murray's law, it has been noted that the application of other optimization principles (not just that of minimum work) result in the final expression: minimizing the total mass of the network, minimizing volume for a constant pressure drop and flow rate, keeping the shear stress constant in all channels, or minimizing flow resistance for a constant volume.

## Combined channel elements

Low pressure loss and a low mean driving temperature difference  $\Delta T$  are essential for an optimum operation and suitable heat exchanger performance.

Both effects lead to appropriate geometrical optimization of dendritic channel networks with minimal entropy generation, presented under the concept of “Bejan’s“constructal theory”

## Heat exchanger channel network



Setup of a two level heat exchanger network from branched channels (left to right)

Figure shows the combination of the branched elements from zero level to the desired covered area. The channel dimensions and the covered area are determined by the actual situation

The channel cross sections are designed according to Murray's law - the relation between the channel cross sections in different branched and connected levels.

The optimization of a channel network to a minimal pressure loss shows that the cube of the diameters of a parent channel should equal the sum of the cubes of the daughter channel diameters

This law can be derived from laminar flow in a branched circular tube system, but is also present in biological systems, such as plants and mammals.

To maintain a homogeneous fluid flow and temperature distribution, the emphasis must be focused on proper fluid distribution.

## **Micro Heat Exchanger Devices**

The balance equations for cooling and heating, as well as the transfer correlation, are valid independently from the length scale.

Two approaches: LMTD and  $\varepsilon$  – NTU method

Typical overall heat transfer coefficients of microstructured heat exchangers range from  $2.6 \text{ kW/m}^2 \text{ K}$  for gas/liquid flow to  $26 \text{ kW/m}^2 \text{ K}$  for liquid/liquid flow.

Conventional plate heat exchangers exhibit very good heat transfer characteristics, ranging from  $0.2$  to  $2.5 \text{ kW/m}^2 \text{ K}$ , under optimum conditions up to  $5 \text{ kW/m}^2 \text{ K}$  for gas/liquid and liquid/liquid flow, respectively.

## **Design issues for exchange equipment**

While microstructured heat exchangers deliver high transfer rates, they also have drawbacks, application limits, and factors to be considered during design and operation.

- Axial heat conduction in the relatively thick walls
- Equal distribution on a large number of channels
- Fouling or blocking of single passages or complete parts

## **SUMMARY**

Microstructured equipment and related transport processes promise successful application in various fields, where high transfer rates, intelligent incorporation of microstructures in macro devices, and new process routes are needed.

High gradients and high specific surface in devices with various construction materials lead to fast equilibrium state.

The characteristic dimensions of microstructured internals are in the range of boundary layers, where high gradients enforce the transfer processes.

Cascading of effects and integration of various elements enhance and guide the entire process. Opportunities in the area of process intensification/new technologies.

# Microfluidic network for flow, heat and mass transfer

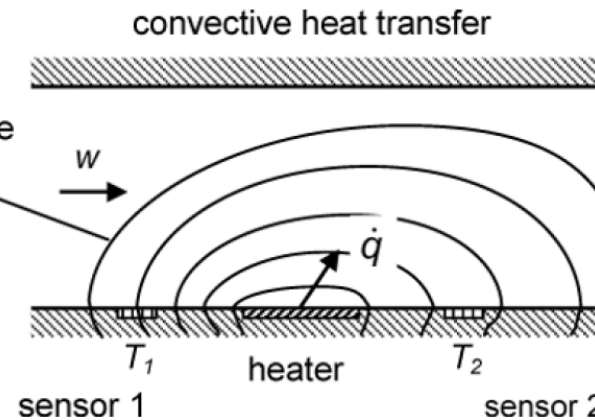
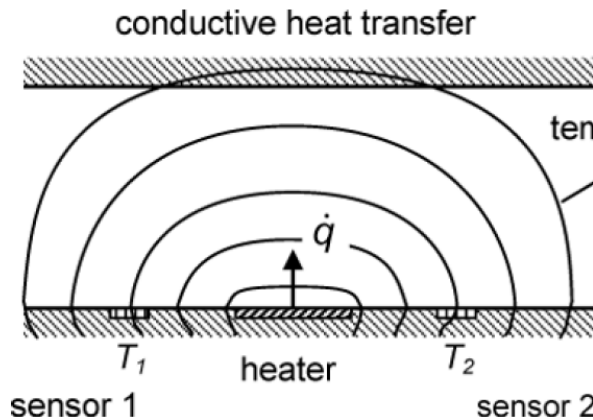
Example



# Convective cooling for flow measurement

An interesting application of convective heat transfer is **flow velocity sensing** within a microchannel or on a surface.

A thermal flow sensor consists mainly of the heating element and temperature sensors, which measure the temperature of the heater and the fluid before and after the heater



Method A – heating of the fluid

Method B – Cooling of the heater

Setup of a thermoelectric flow sensor, in a channel consisting of a heater and two temperature sensors up- and downstream of the heater

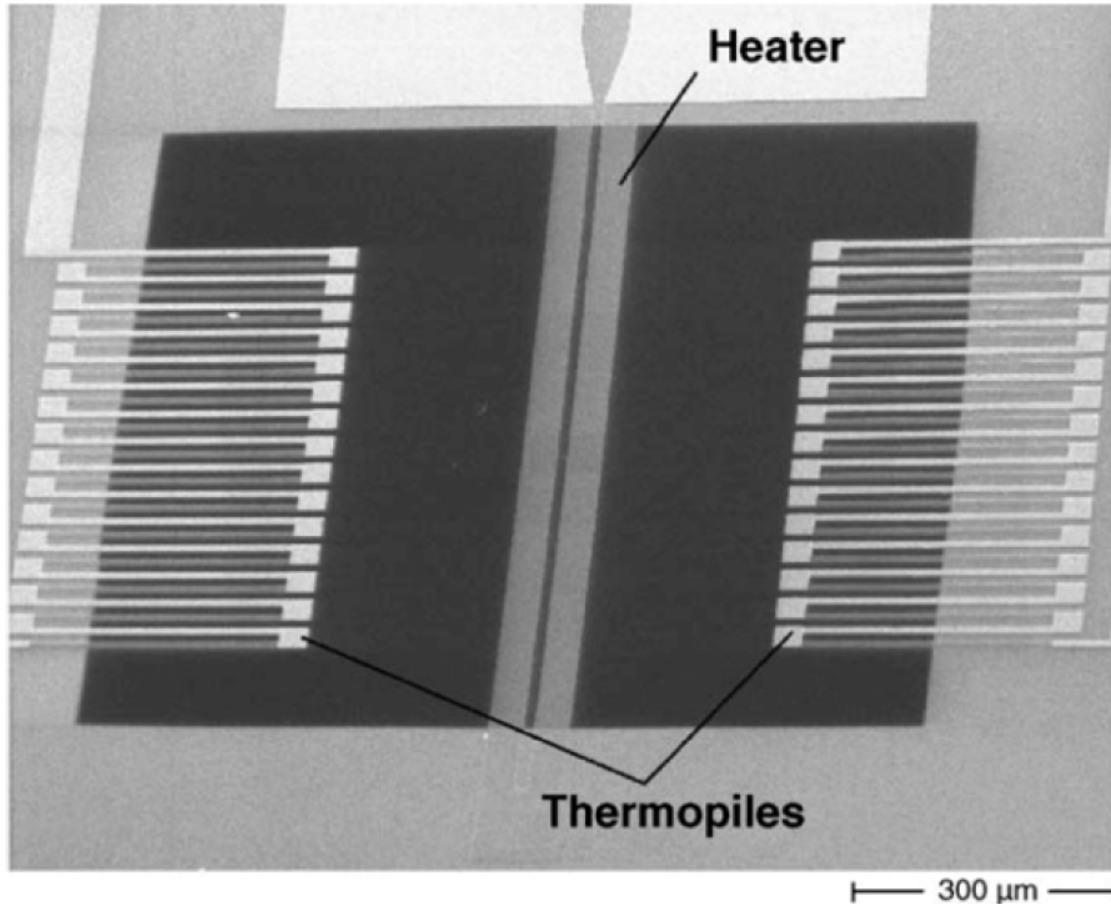
The complete sensor arrangement involves three complex domains: fluid flow, heat transfer, and thermoelectric energy and signal conversion.

The flow-induced heat transfer (convection) and the parallel heat conduction in the sensor wall/substrate determine the thermal signal domain, which is measured as temperature.

The basic sensor setup can be classified into two different techniques or methods. In method A, heating of the fluid imposes a temperature profile in the channel or near the wall, which is measured at certain positions by thermocouples.

In second method (B), fluid flow cools the heater, where temperature or electrical power is measured.

## Local temperatures of a heated area- direction-sensitive velocimetry



Thermoelectric flow sensor consisting of an electrical heater on a thin membrane with parallel meandering thermoelectric sensors, two thermopiles with 15 thermo-elements

The dissipated electrical power in the heater spreads into the flowing fluid and the wall or substrate.

At steady-state, the energy balance of the heater/sensor expresses the electrical heating power  $P$  on one side and the dissipated heat into the substrate  $Q_S$  and into the fluid  $Q_f$  on the other side

$$P = \dot{Q}_S + \dot{Q}_f = G_S (T_H - T_S) + G_f (T_H - T_f)$$

where  $T_H$ ,  $T_S$ , and  $T_f$  are the temperature of the heater, the substrate, and the bulk fluid, respectively,  $G_S$  is related to the solid thermal conductivity and  $G_f$  is the convective heat transfer coefficient..

**The flow measurement relies on the variation of  $G_f$  with the flow and can be measured, from the temperature difference resulting from the applied electrical power of the heater.**

If the sensor measures the mean temperature of the fluid, the energy dissipation into fluid is determined by

$$\dot{Q}_f = \dot{m}c_p (T_S - T_f)$$

If the heat dissipation into the substrate is  $\dot{Q}_S$

$$P = \dot{Q}_S + \rho_f c_p A_C (T_S - T_f) \bar{w}$$

The fabricated sensor must be calibrated

Convective cooling of an electrical heater and measuring its temperature according to 2<sup>nd</sup> method avoids errors, such as measuring the heated fluid temperature or the unknown heat dissipation into the substrate. For this reason, many sensors are located on a thin membrane or fabricated on polymers or other thermal insulators, which minimizes parasitic heat losses and increases the sensor accuracy.

Convective heat transfer into the fluid

$$\dot{q}_f = \frac{\dot{Q}_f}{A_H} = \alpha_w (T_H - T_f)$$

The heat transfer from cooling the heater is similar to cooling a plate on one side by surface flow

$$Nu = \frac{\alpha z}{\lambda_f} = 0.332 Pr^{1/3} Re^{1/2}$$

For the entire length of the heater – (equations are valid for laminar flow)

$$Nu_L = \frac{\alpha l_H}{\lambda_f} = 0.664 Pr^{1/3} Re^{1/2}$$

Both equations are valid for laminar flow.

Correlation between dissipated power, flow velocity and measured temperature difference is thus

$$\frac{\dot{Q}_f}{A_H} = \frac{\text{Nu} \lambda_f}{l_H} (T_H - T_f) = 0.664 \lambda_f \text{Pr}^{1/3} \left( \frac{\bar{w}}{l_H v} \right)^{1/2} (T_H - T_f)$$

Arranging the above equations to correlate the electrical heating power with the flow velocity gives the following equation.

$$P = G_S (T_H - T_S) + 0.664 \lambda_f A_H \text{Pr}^{1/3} \left( \frac{\bar{w}}{l_H v} \right)^{1/2} (T_H - T_f)$$

A detailed analysis of the correlation requires many parameters, such as heat conductivity of the substrate, fluid properties, correct geometry of the sensor.

For practical applications, the correlation between electrical power, measured temperature difference, and flow velocity can be reduced to (laminar flow)

$$P = \left( C_1 + C_2 w^{1/2} \right) (T_H - T_f)$$

Both coefficients can be determined by calibration measurements

The application of heat transfer measurements is a widespread and generally accepted method for determining the flow rate in channels.

## Single channel element calculation

- design rules and correlations for high performance heat exchangers and microchannel networks

Heat transfer in laminar, channel flow, fully developed and constant heat flux

$$Nu = \frac{hD}{\lambda} = 4.3$$

At the entrance or after a bend, the straight laminar flow is disturbed, an additional pressure loss occurs, and transverse flow components enhance the transport process in the channel. The enhancement is given by

$$Nu_{me} = \frac{Nu_m}{\tanh(2.432 \Pr^{1/6} X^{* 1/6})}.$$

With the dimensionless entrance length  $X^*$  given by

$$X^* = \frac{L}{d_h} \text{Pe} = \frac{L}{d_h} \text{Re} \cdot \Pr$$

To determine the optimum channel length  $x$ , the above equation is used to get

$$\frac{x}{d_h} = \text{Re} \cdot \left( 0.411 \cdot \operatorname{arctanh} \left( \frac{\text{Nu}_{\text{m}}}{\text{Nu}_{\text{me}}} \right) \right)^6$$

To yield a heat transfer enhancement of 30 % ( $\text{Nu}_{\text{me}}/\text{Nu}_{\text{m}} = 1.3$ ), the entrance length divided by the hydraulic diameter should be less than  $0.005\text{Re}$ ,

for a heat transfer enhancement of 10 %, the length should not exceed  $0.06\text{Re}$ .

For longer channels, the pressure loss increases without additional benefit to the heat transfer.

# Drops on Homogeneous and Non-homogeneous Surfaces

Corrections needed to Young's Law

## The Shape of Micro-drops



Comparison of the shape between micro-drops and macro-drops

$$\frac{\Delta P_{\text{Laplace}}}{\Delta P_{\text{hydrostatic}}} \approx \frac{\gamma}{\rho g \ell}$$

The two pressures are of the same order when

$$\ell \approx \sqrt{\frac{\gamma}{\rho g}}$$

$\ell$  is called the **capillary length**. A drop of dimension smaller than the capillary length has a shape resembling that of a spherical cap. A drop larger than the capillary length is flattened by gravity.

## Bond Number

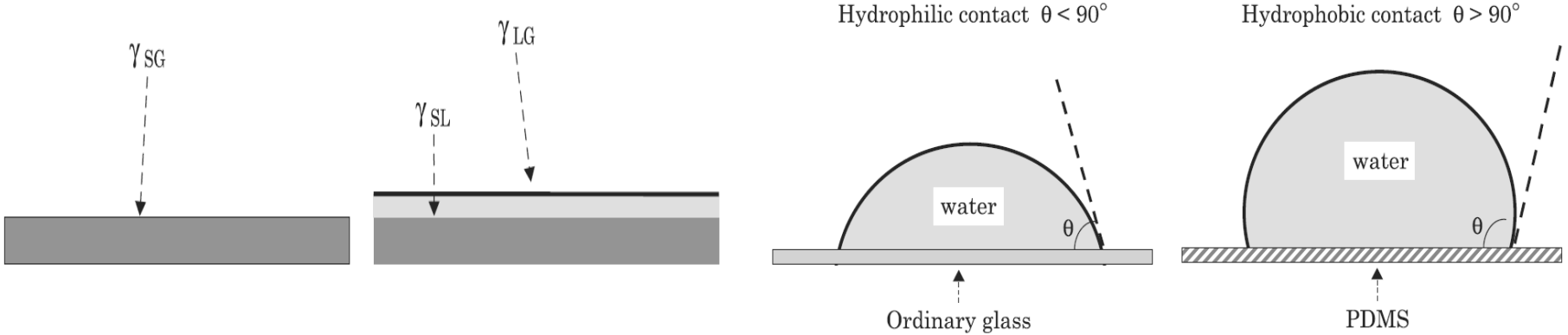
$$Bo = \frac{\rho g R^2}{\gamma}$$

*R is of the order of the drop radius. If  $Bo < 1$ , the drop is spherical (microscopic drops), or else the gravitational force flattens the drop on the solid surface (large drops).*

The capillary length is of the order of 2 mm for most liquids, even for mercury.

These equations are valid for a **perfectly flat surface**.

## Wetting: Partial or Total Wetting



A liquid spreads on a substrate in a film **if the energy of the system is lowered by the presence of the liquid film .**

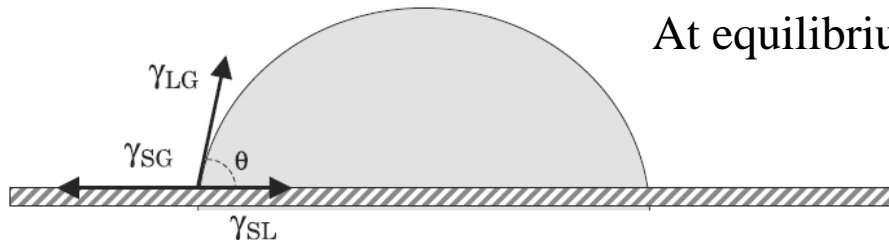
The surface energy per unit surface of the dry solid surface is  $\gamma_{SG}$ ; the surface energy of the wetted solid is  $\gamma_{SL} + \gamma_{LG}$ .

The spreading parameter  $S$  determines the type of spreading (total or partial)

$$S = \gamma_{SG} - (\gamma_{SL} + \gamma_{LG})$$

If  $S > 0$ , the liquid spreads on the solid surface; if  $S < 0$  the liquid forms a droplet.

## Contact Angle—Young's Law

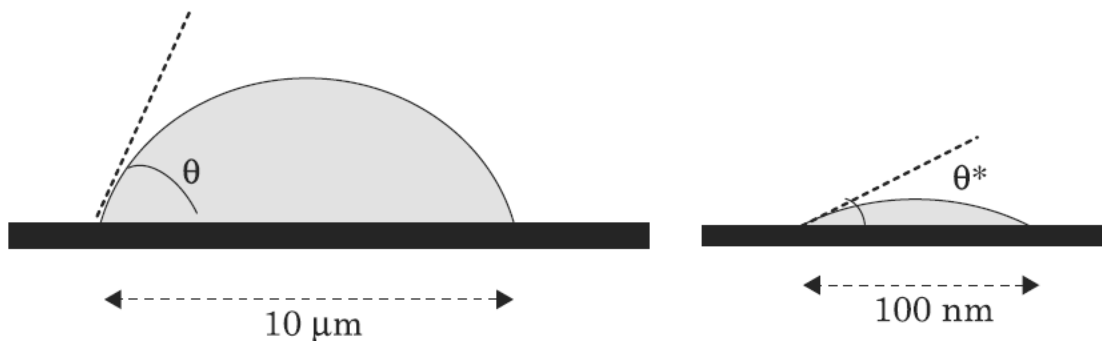


At equilibrium, the resultant of the forces must be zero.

$$\gamma_{LG} \cos \theta = \gamma_{SG} - \gamma_{SL}$$

Schematic of forces at the contact line

## Nano-bubbles and droplets

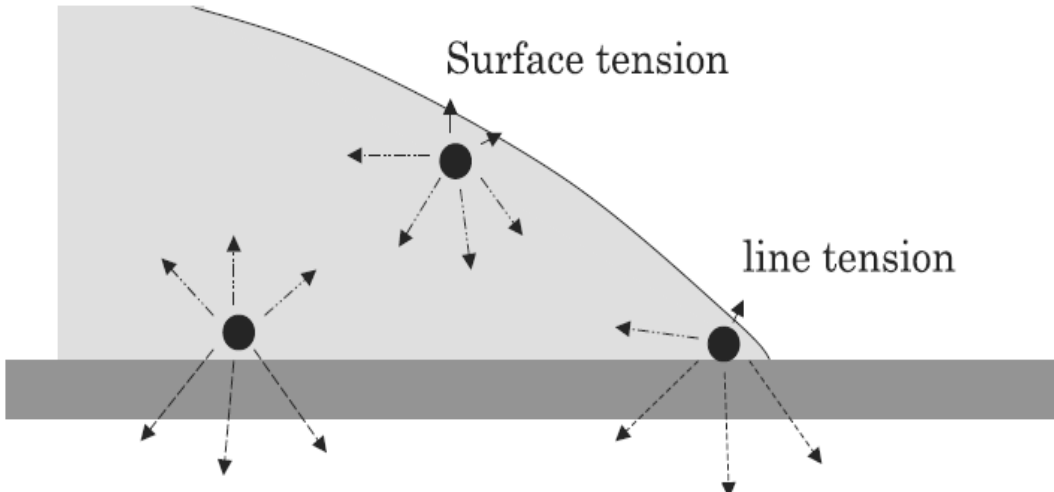


$\theta^*$  is the real contact angle,  $r$  is the contact radius

Recent measurements have shown that nano-bubbles have very flat profiles—the base radius is 5–20 times larger than the height —because the contact angle of the bubble is much smaller than the macroscopic contact angle of the bubble on the same substrate

$$\gamma_{LG} \cos \theta = \gamma_{SG} - \gamma_{SL}$$

## Modified Young's Law at Nanoscale



The molecules close to the triple line experience a different set of interactions than at the interface. To take into account this effect, a line tension term has been introduced in Young's law

$$\gamma_{SG} = \gamma_{SL} + \gamma_{LG} \cos \theta^* + \frac{\gamma_{SLG}}{r} \quad \cos \theta^* = \cos \theta - \frac{\gamma_{SLG}}{r \gamma_{LG}}$$

Where  $r$  is the contact radius,  $\gamma_{SLG}$  the line tension (unit N), and  $\theta^*$  the real contact angle.

For droplet contact radius larger than 10  $\mu\text{m}$ , the effect of the line tension is negligible; the value of the second term is *of the order of  $10^{-4}$* . But it is not the case for nano-drops and nano-bubbles.

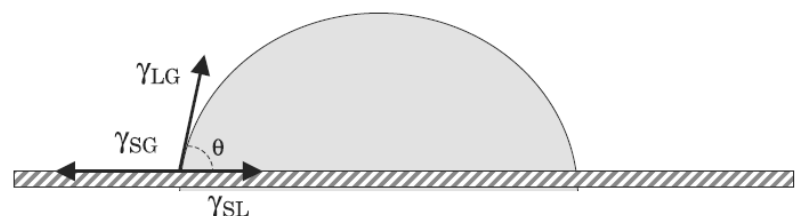
Young's law can be more rigorously derived from free energy minimization.

Consider a sessile droplet large enough for the effect of the triple line to be neglected. The change of free energy due to a change in droplet size can be written as

$$\begin{aligned} dF &= \gamma_{SL} dA_{SL} + \gamma_{SG} dA_{SG} + \gamma_{LG} dA_{LG} \\ &= (\gamma_{SL} - \gamma_{SG} + \gamma_{LG} \cos \theta) dA_{SL} \end{aligned}$$

where  $\theta$  is the contact angle.

At mechanical equilibrium  $dF = 0$  and

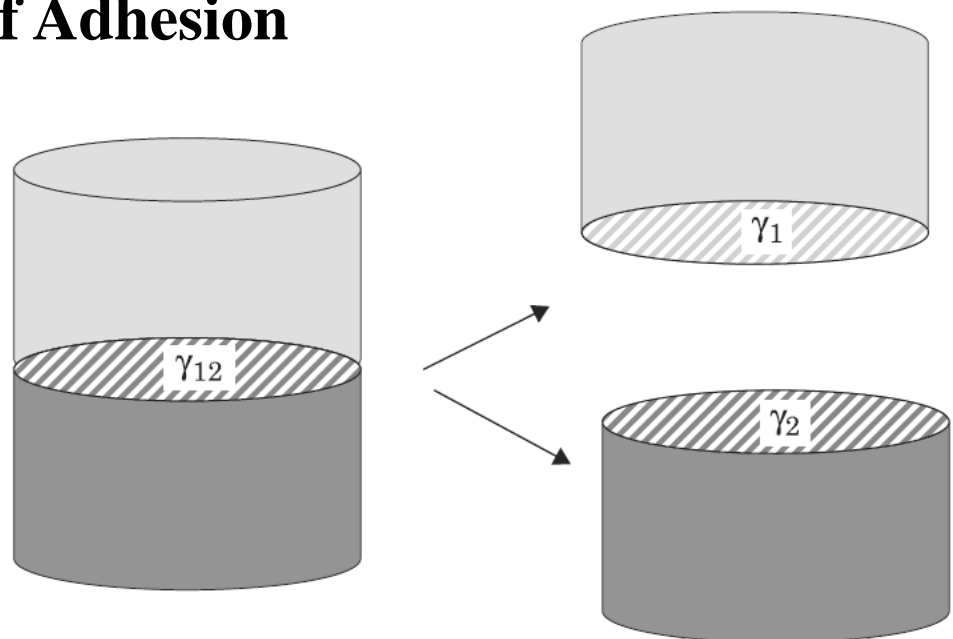


$$\gamma_{SL} - \gamma_{SG} + \gamma_{LG} \cos \theta = 0.$$

# Work of Adhesion

Imagine a body contacting another body on a surface  $S$ . *The* surface energy of  $S$  when there is contact is

$$E_{12} = \gamma_{12} S$$



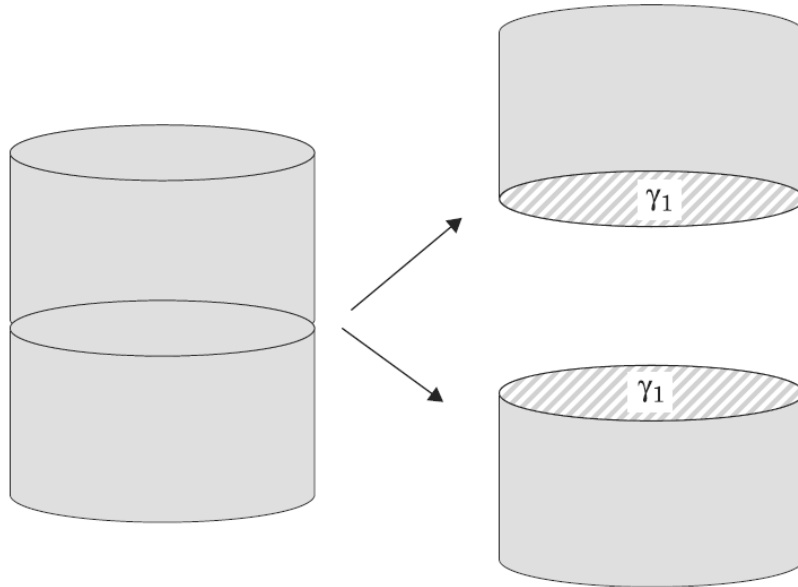
The work of adhesion is the work required to separate the two bodies.  
After separation, the surface energies are

$$E = E_1 + E_2 = (\gamma_1 + \gamma_2) S$$

The work of adhesion (per unit area) is then

$$W_a = \gamma_1 + \gamma_2 - \gamma_{12}$$

# Work of Cohesion

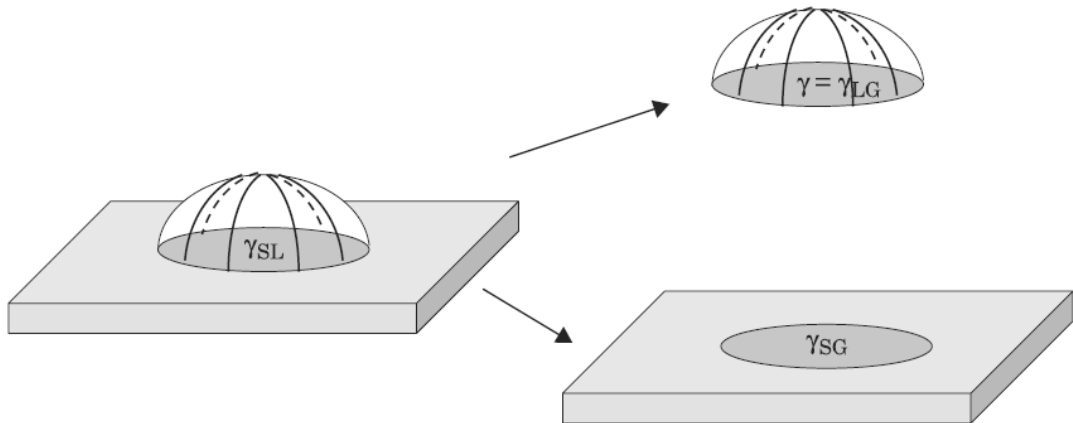


The work of cohesion is obtained similarly, but this time the body being split is homogeneous. The same reasoning yields

$$W_c = 2\gamma_1$$

In other words, the surface energy is half the work of cohesion

# Work of Adhesion - Young–Dupr e Equation



Work of adhesion for a liquid and a solid

Using the work of adhesion  $W_a = \gamma_1 + \gamma_2 - \gamma_{12}$

with the surface tensions  $\gamma_1 = \gamma_{LG} = \gamma$ ,  $\gamma_2 = \gamma_{SG}$ , and  $\gamma_{12} = \gamma_{SL}$ , we obtain

$$W_a = \gamma + \gamma_{SG} - \gamma_{SL}$$

$$W_a = \gamma + \gamma_{SG} - \gamma_{SL} \quad \gamma_{LG} \cos \theta = \gamma_{SG} - \gamma_{SL}$$

## Work of Adhesion - Young–Dupr e Equation

Upon substitution of Young's law [ $\gamma_{LG} \cos \theta = \gamma_{SG} - \gamma_{SL}$ ], one can obtain the Young–Dupr e equation for the work of adhesion as

$$W_a = \gamma (1 + \cos \theta)$$

For a super-hydrophobic contact,  $\theta = \pi$ ;  $W_a = 0$ : *no work is required to separate a super-hydrophobic liquid from a solid.*

Thus a droplet of water rolls freely over a super-hydrophobic surface.

The more hydrophobic is the contact between a liquid and a solid, the smaller is the work of adhesion.

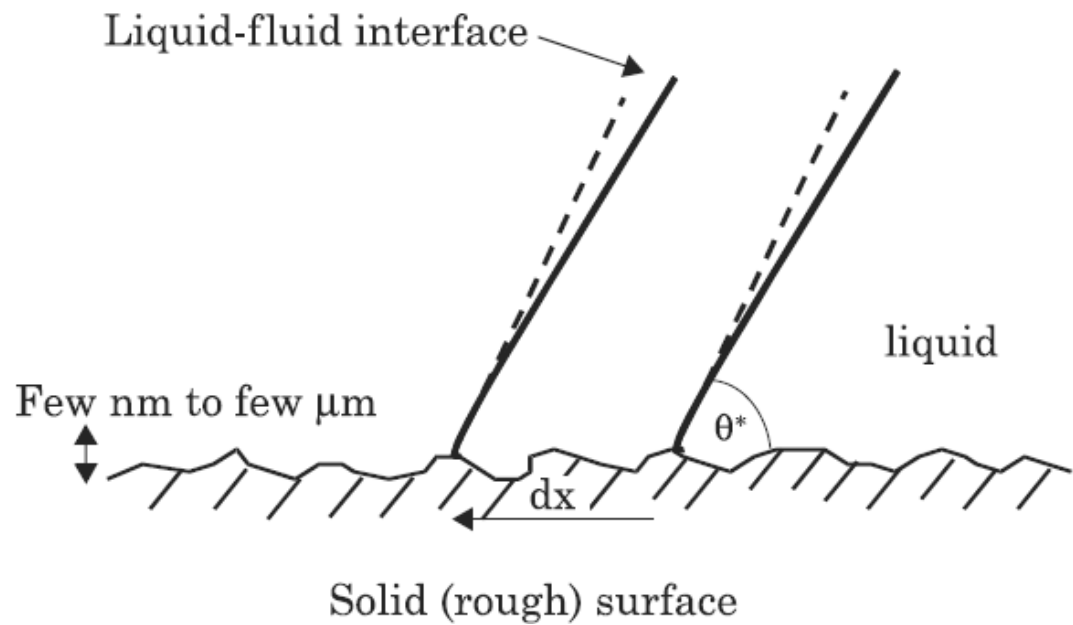
# Drops on Inhomogeneous Surfaces

Young's law should be corrected to take into account the imperfections of the surface.

Roughness amplifies the hydrophilic or hydrophobic character of the contact.

$\theta^*$  is the angle with the surface with roughness and  $\theta$  the angle with the smooth surface.

The size of the roughness is very small, so that the molecules of the liquid are macroscopically interacting with a plane surface but microscopically with a rough surface.



$$[\gamma_{LG} \cos \theta = \gamma_{SG} - \gamma_{SL}]$$

$$W_a = \gamma + \gamma_{SG} - \gamma_{SL}$$

$$S = \gamma_{SG} - (\gamma_{SL} + \gamma_{LG})$$

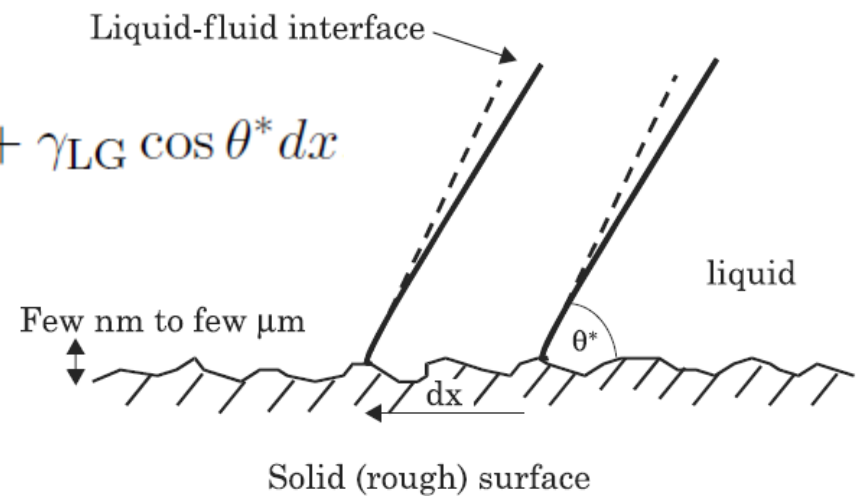
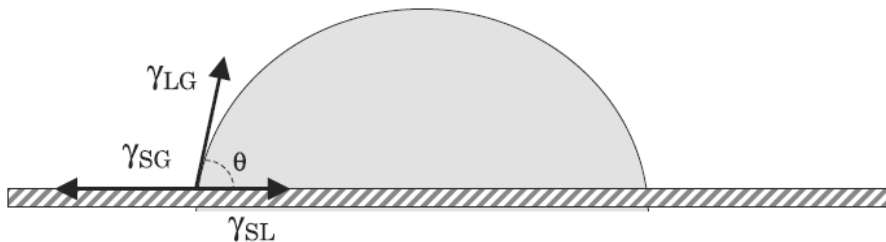
For a very small displacement of the contact line, the work of the different forces acting on the contact line is given by

$$dW = \sum \vec{F} \cdot d\vec{l} = \sum F_x dx = (\gamma_{SL} - \gamma_{SG}) rdx + \gamma_{LG} \cos \theta^* dx$$

where  $r$  is the roughness ( $rdx$  is the real distance on the solid surface when the contact line is displaced by  $dx$ ). Therefore, by definition,  $r > 1$ .

Thus the change in energy is

$$dE = dW = (\gamma_{SL} - \gamma_{SG}) rdx + \gamma_{LG} \cos \theta^* dx$$

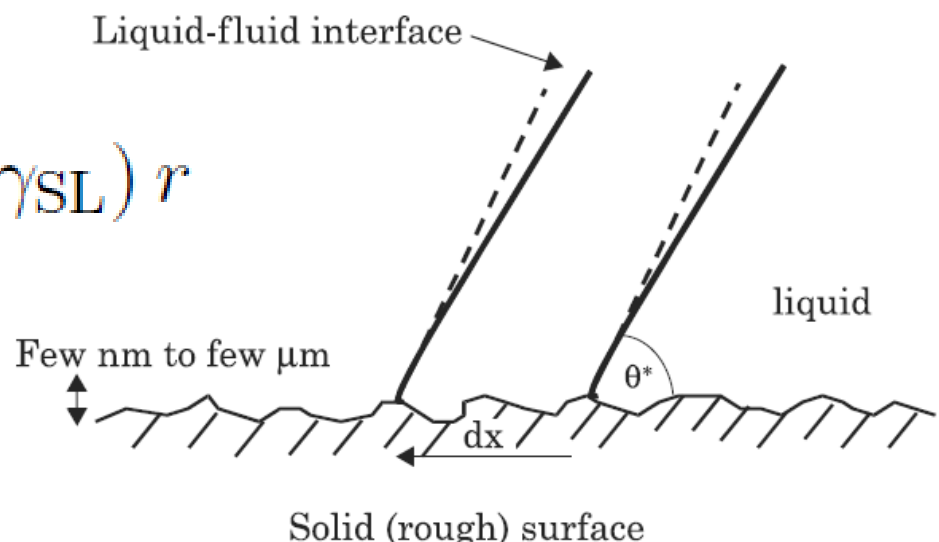


The drop finds its equilibrium state after the small perturbation  $dx$ , it finally stops at a position where its energy is minimum, so

$$\frac{dE}{dx} = 0$$

Therefore,

$$\gamma_{LG} \cos \theta^* = (\gamma_{SG} - \gamma_{SL}) r$$

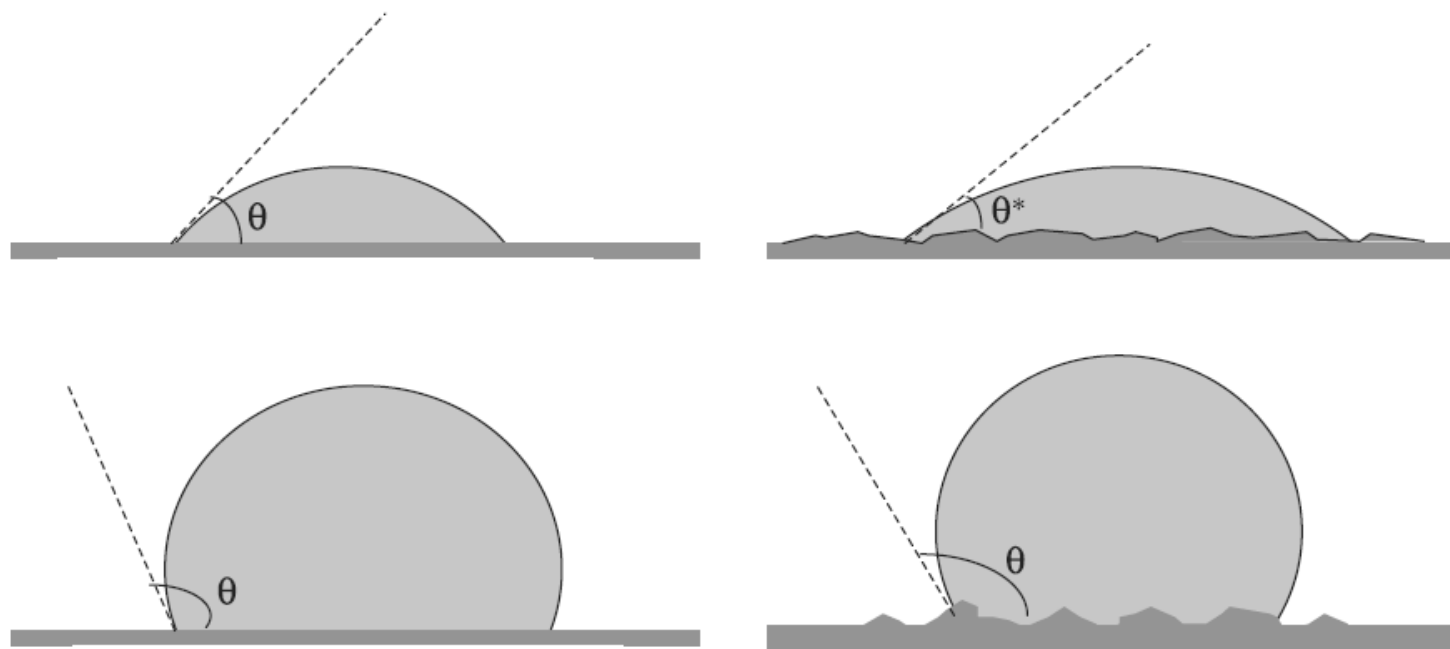


$$\gamma_{LG} \cos \theta^* = (\gamma_{SG} - \gamma_{SL}) r$$

Young's law for a smooth surface     $\gamma_{LG} \cos \theta = \gamma_{SG} - \gamma_{SL}$

Substitution gives Wenzel's Law                   $\cos \theta^* = r \cos \theta$

As  $r > 1$ , this relation implies that                   $|\cos \theta^*| > |\cos \theta|$



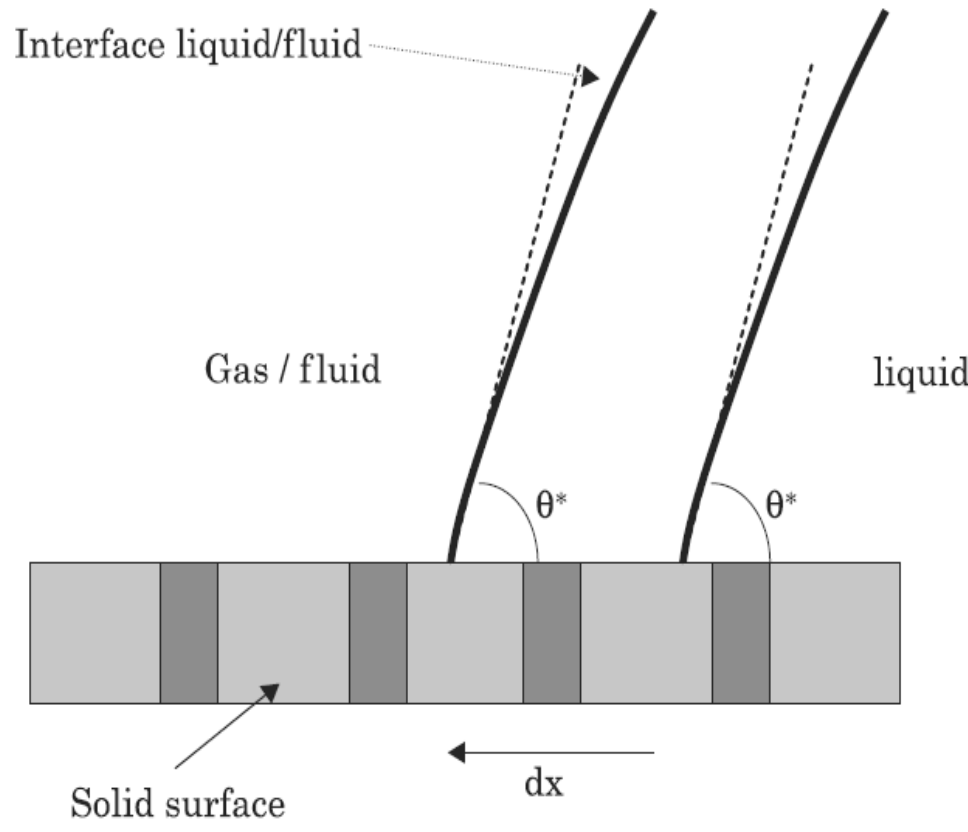
$$|\cos \theta^*| > |\cos \theta|$$

If  $\theta$  is larger than  $90^\circ$  (hydrophobic contact), then  $\theta^* > \theta$  and the contact is still more hydrophobic due to the roughness.

If  $\theta$  is smaller than  $90^\circ$  (hydrophilic contact), then  $\theta^* < \theta$  and the contact is still more hydrophilic.

**Surface roughness increases the wetting character.**

# Cassie–Baxter Law



Chemically inhomogeneous solid surfaces.

Small size heterogeneities compared to interaction size between the liquid and the solid wall.

A solid wall constituted by microscopic inclusions of two different materials.

$\theta_1$  and  $\theta_2$  are the contact angles for each material at a macroscopic size, and  $f_1$  and  $f_2$  are the surface fractions of the two materials.

$$\gamma_{LG} \cos \theta = \gamma_{SG} - \gamma_{SL}$$

The energy to move the interface by  $dx$  is

$$dE = dW = (\gamma_{SL} - \gamma_{SG})_1 f_1 dx + (\gamma_{SL} - \gamma_{SG})_2 f_2 dx + \gamma_{LG} \cos \theta^* dx$$

Minimizing  $dE$

$$\gamma_{LG} \cos \theta^* = (\gamma_{SG} - \gamma_{SL})_1 f_1 + (\gamma_{SG} - \gamma_{SL})_2 f_2$$

Using Young's Law

$$\gamma_{LG} \cos \theta = \gamma_{SG} - \gamma_{SL}$$

**Casey-Baxter Relation**  $\cos \theta^* = f_1 \cos \theta_1 + f_2 \cos \theta_2$

$$\cos \theta^* = f_1 \cos \theta_1 + f_2 \cos \theta_2 \quad f_1 + f_2 = 1 \quad \text{or} \quad \sum_i f_i = 1$$

The Cassie–Baxter law explains some unexpected experimental results.

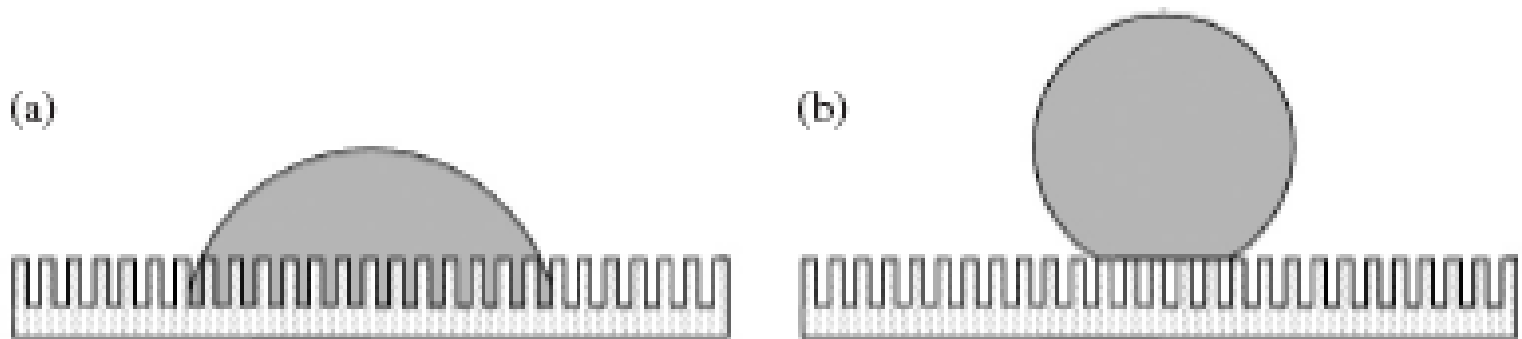
Sometimes during micro-fabrication—a microfabricated surface may present chemical inhomogeneity and the wetting properties are not those that were intended.

For example, if a uniform layer of Teflon is deposited on a rough substrate, the surface should become hydrophobic.

However, if the layer is too thin, the Teflon layer may be porous and the coating inhomogeneous; the wetting properties are then modified according to the Cassie–Baxter law and the gain in hydrophobicity may not be as large as expected.

The scale of change of the different chemical materials of the solid surface is *very small compared to that of the drop*

## Topographically patterned surfaces



Droplets wetting rough surfaces

(a) **Wenzel state** with enhanced solid–liquid interfacial area

(b) **Cassie–Baxter state** with entrapped air underneath the droplet.

In Fig. (a), roughness increases the actual solid–liquid interfacial area  $A_{sl}$  *with respect to the apparent, projected one*  $A_{sl,p}$ .

Lessons from nature

## Microfabricated Substrate - Case of Hydrophobic Contact

Contact angle of a sessile drop sitting on microfabricated pillars



If the drop penetrates between the pillars, one can write the Wenzel angle as

$$\cos \theta_W = r \cos \theta$$

If the drop stays on top of the pillars, one can write the Cassie law

$$\cos \theta_C = f \cos \theta + (1 - f) \cos \theta_0$$

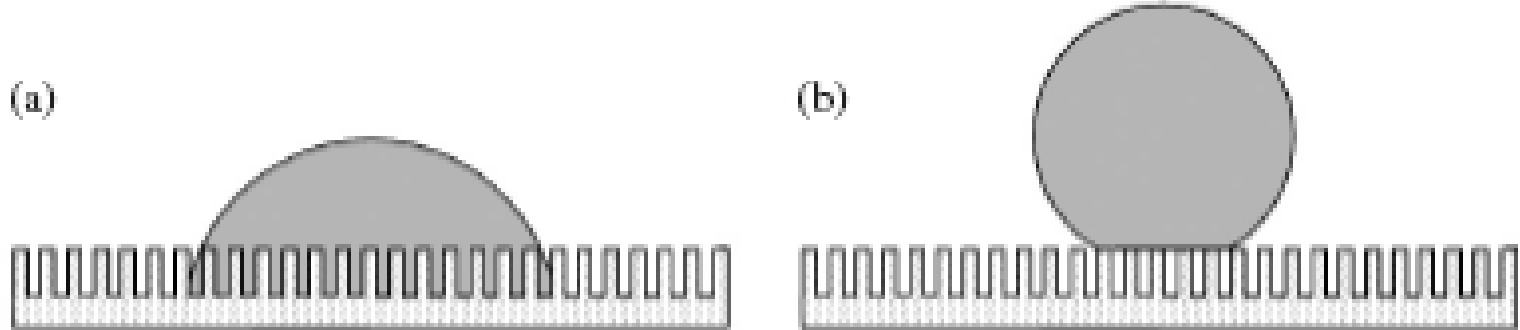
$\theta_C$  is the “Cassie” contact angle,  $\theta_0$  the contact angle with the layer of air, and  $f$  the ratio of the contact surface (top of the pillars) to the total horizontal surface.

## Wenzel's law

$$\cos \theta = r \cdot \cos \theta_Y \text{ with } r = A_{sl}/A_{sl,p}$$

Quantitatively, the validity of the picture turns out to be limited to a range of  $\theta_C < \theta_Y < 90^\circ$ , with  $\theta_C$  depending on the surface roughness .

As a result, the contact angle on a rough surface will be **increased** or **(decreased)** as compared to the contact angle on a smooth surface of the same material, depending on whether  $\theta_Y > 90^\circ$  or ( $\theta_Y < 90^\circ$ ), respectively.



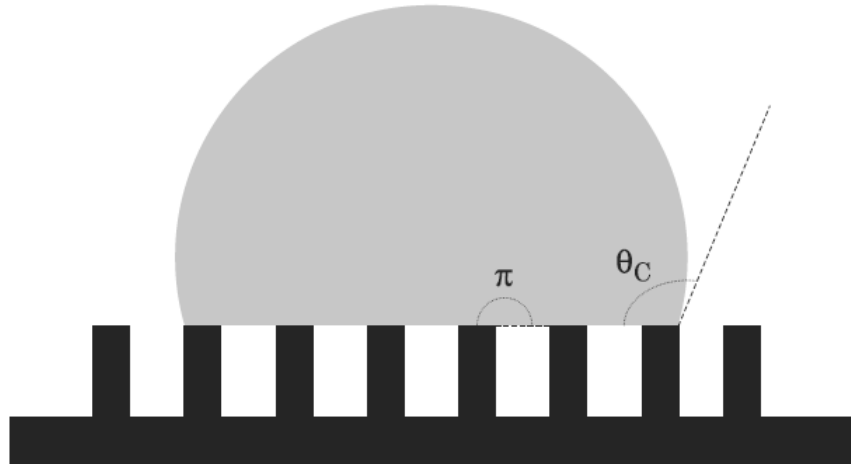
*For  $\theta_Y > 90^\circ$ , a completely different liquid morphology is possible (Fig. b).*

$A_{sl}$  is dramatically reduced and much of the apparent solid–liquid interface is in fact a liquid–vapor interface.

This reduction in  $A_{sl}$  gives rise to a very high mobility with extremely small contact angle hysteresis.

In this state, the contact angle is given by the **Cassie–Baxter equation**,  
 $\cos \theta = -1 + f \cdot (1 + \cos \theta_Y)$ , where  $f$  is the fractional surface area of the pillar tops and  $\theta_2$  (on air) =  $180^\circ$

The range of stability for both morphologies depends on the aspect ratio, the spacing between the pillars, and the contact angle



*Sketch of a Cassie drop (fakir effect). The interface between the pillars is roughly horizontal.*

If the pillars are not too far from each other, the value of  $\theta_0$  is roughly  $\theta_0 = \pi$

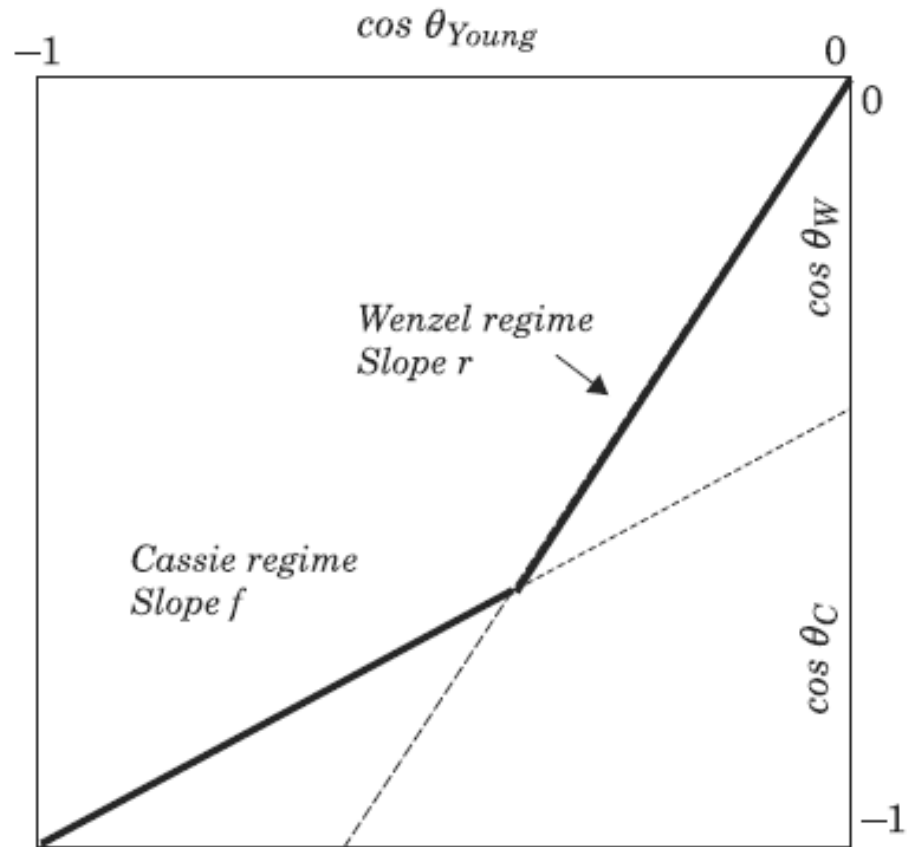
$$\cos \theta_C = -1 + f(1 + \cos \theta)$$

Plot the Wenzel and Cassie Laws

$$\cos \theta_W = r \cos \theta$$

$$\cos \theta_C = -1 + f(1 + \cos \theta)$$

$$r = \frac{S_{\text{total}}}{S_{\text{horizontal}}} > f = \frac{S_{\text{top}}}{S_{\text{horizontal}}}$$



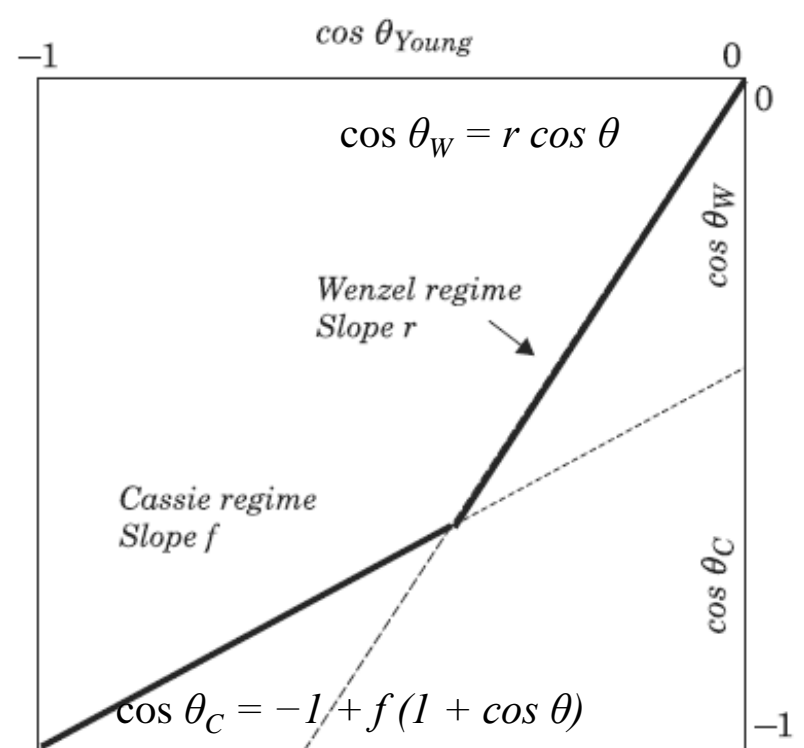
Plot of the Wenzel and Cassie laws for a sessile droplet sitting on a surface textured with micro-pillars.

The two lines intersect at a Young contact angle  $\theta_i$  defined by  $\theta_C = \theta_W$ , so that

$$\cos \theta_i = \frac{f - 1}{r - f}$$

In the diagram, for a given Young angle, there are two contact angles

From energy considerations—for example using Laplace's law—it can be deduced that the real contact angle is the smaller one.



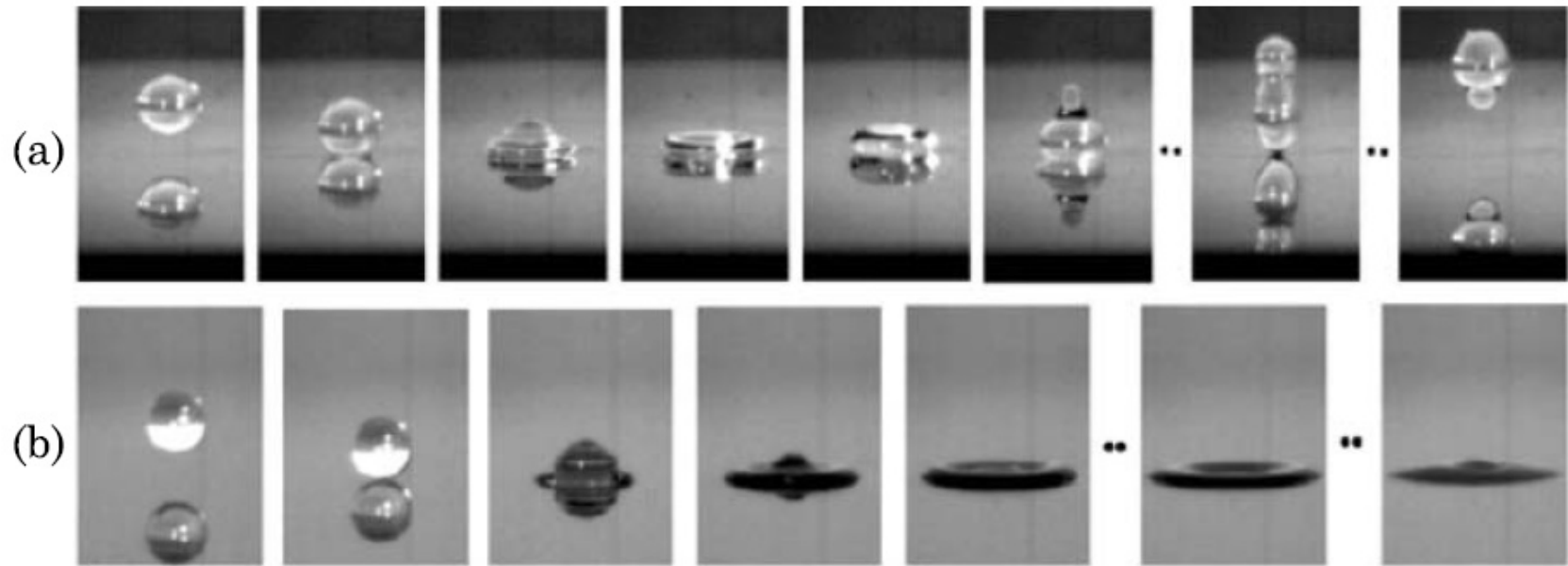
So when the Young contact angle is not very hydrophobic ( $\theta < \theta_i$ ), the contact corresponds to a Wenzel regime and the drop wets the whole surface.

When the Young contact angle is more hydrophobic ( $\theta > \theta_i$ ), the drop is in a Cassie regime and sits on top of the pillars.

General rule, exceptions are common, droplets are sometimes at metastable regimes.

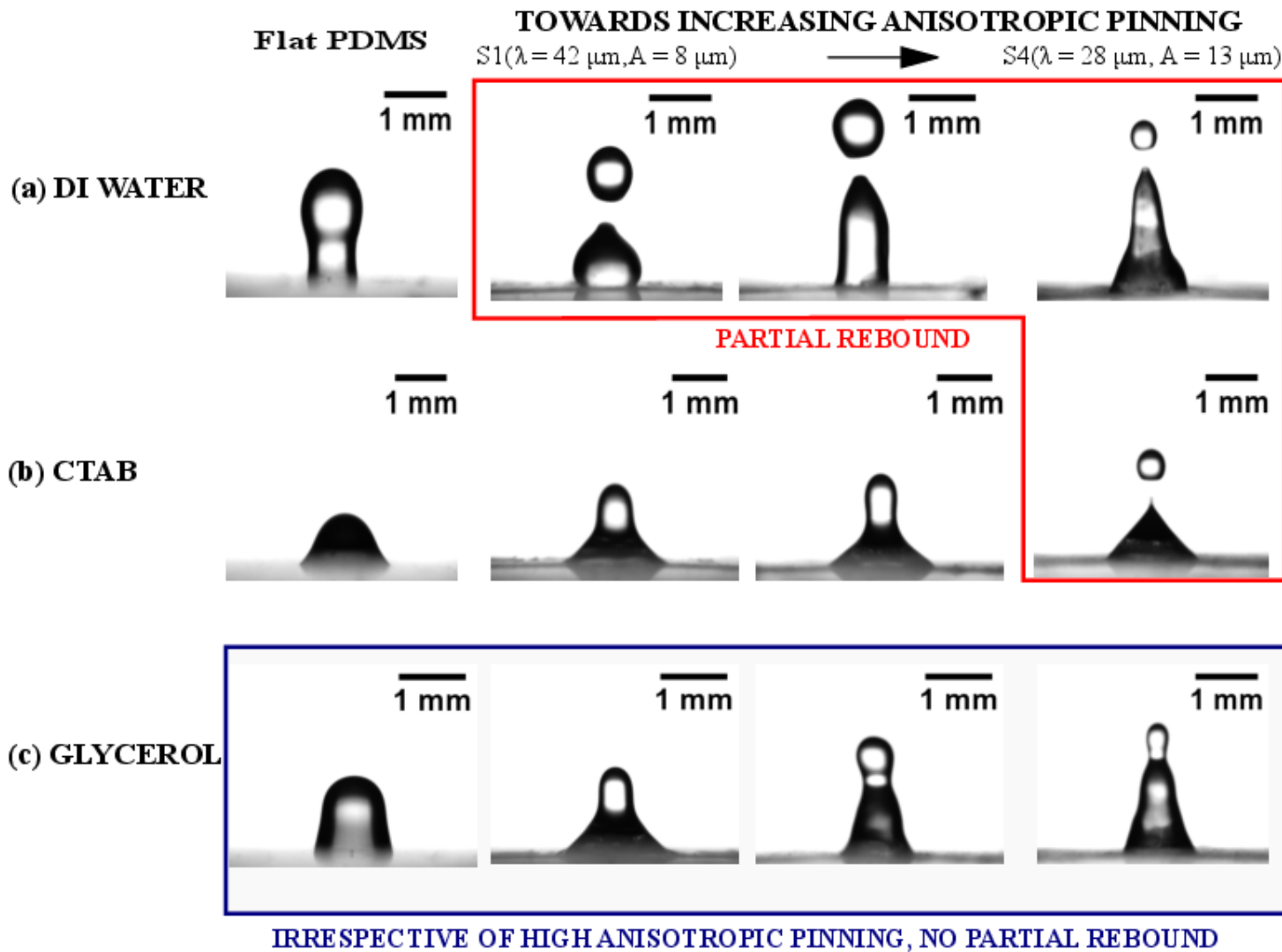
## Fabricated Surfaces: The Transition Between the Wenzel and Cassie Laws

PDMS, Teflon, SU8, glass, silicon, gold. Plastics are generally hydrophobic whereas glass and metals are hydrophilic and silicon neutral.



Chemical deposition of a hydrophobic/hydrophilic coating on top of the substrate. A flat gold plate with  $\text{CF}_4\text{--H}_2\text{--He}$  plasma deposition becomes very hydrophobic.

(a) A water droplet bounces back from the surface treated with  $\text{CF}_4\text{--H}_2\text{--He}$  plasma deposition, (b) whereas it spreads on the original gold surface



Partial rebound over flat as well as wrinkled PDMS surfaces with varying topography. Partial rebound is observed for DI water even for moderately wrinkled surfaces (S1), whereas for CTAB it is experienced for narrow wrinkles (S4) only. No partial rebound is seen for Glycerol for even highly wrinkled surfaces.



Water drops stay on ordinary lenses

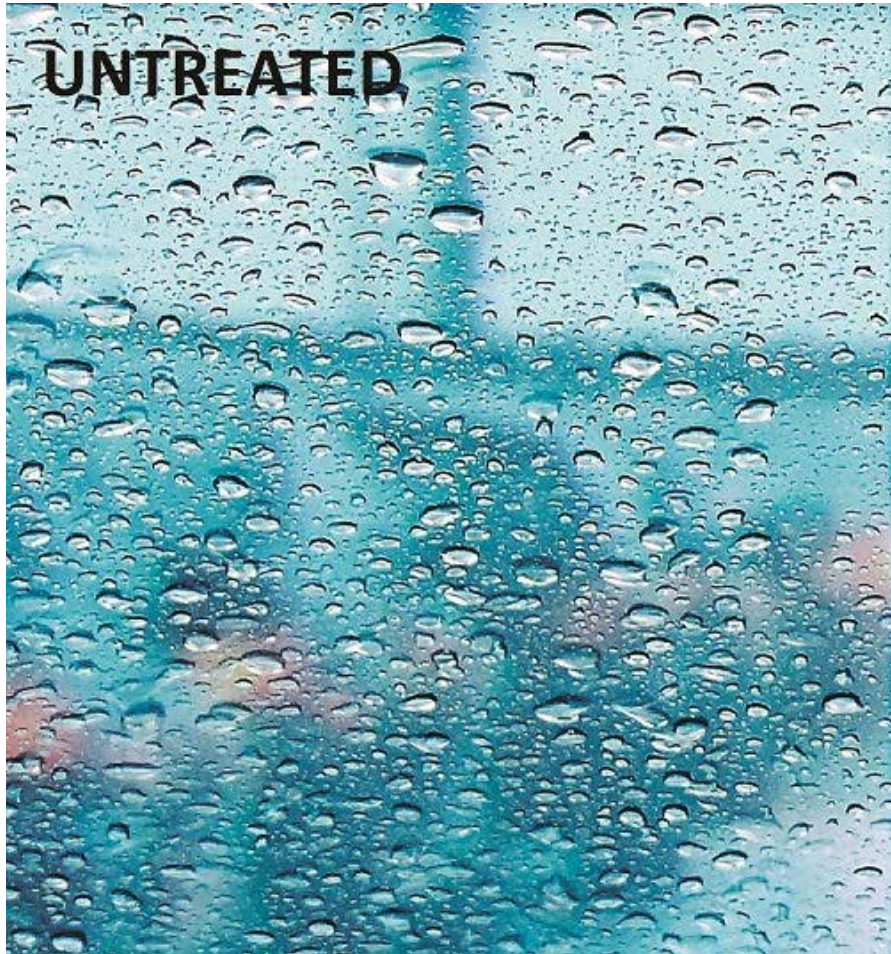


Water drops roll off Titan Advantage

**Super Hydrophobic**  
Water droplets roll off.

**Dust Repellant**  
Does not attract dust due  
to anti-static property.

**Smudge Resistant**  
Easy to clean fingerprints  
and dirt.

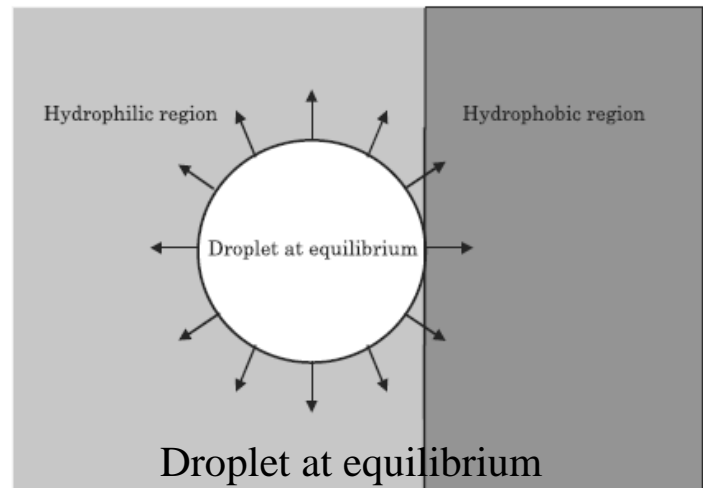
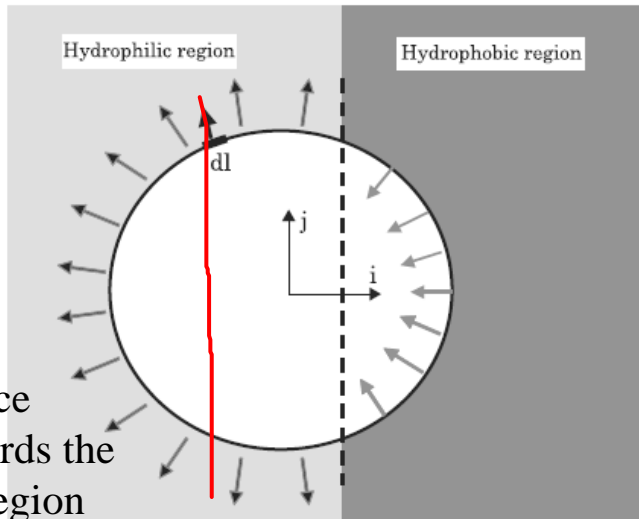


Water repellent treatment to make the viewing surface hydrophobic

# Drops Moving by Capillarity

At the microscopic scale there are other forces to move fluids that are not efficient at the macroscopic scale. These forces are electro-osmosis and capillarity. In particular capillarity is widely used for actuating droplets.

## 1. Drop Moving Over a Transition of Wettability



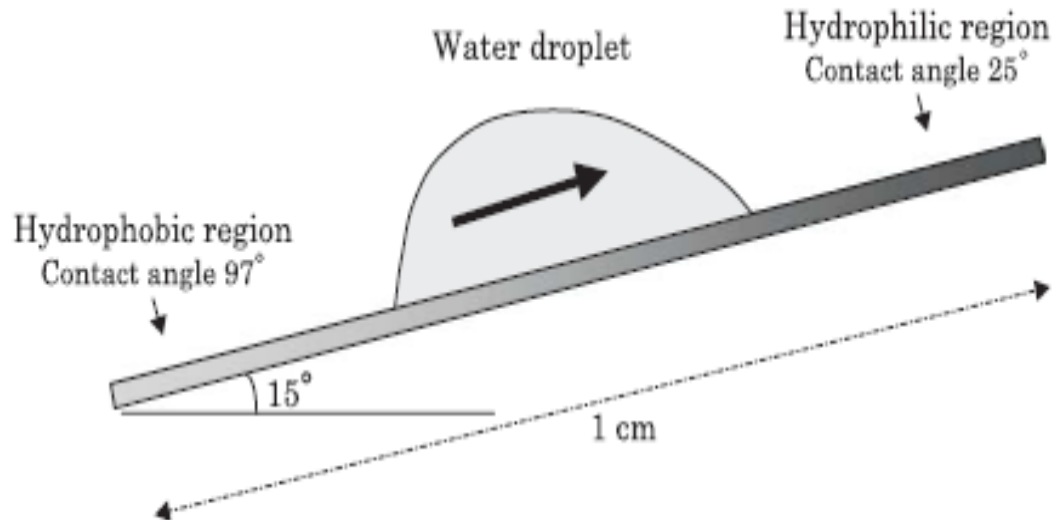
If  $L_1$  and  $L_2$  are the contact lines in the hydrophilic and hydrophobic planes, and  $\theta_1$  and  $\theta_2$  the contact angles, the force acting on the drop is

$$\begin{aligned} F_x &= \int_{L_1} (\gamma_{SG} - \gamma_{SL})_1 (\vec{i} \cdot d\vec{l}) - \int_{L_1} (\gamma_{SG} - \gamma_{SL})_2 (\vec{i} \cdot d\vec{l}) \\ &= \int_{L_1} \gamma_{LG} \cos \theta_1 (\vec{i} \cdot d\vec{l}) - \int_{L_2} \gamma_{LG} \cos \theta_2 (\vec{i} \cdot d\vec{l}) < 0. \end{aligned}$$

## 2. Drop Moving Uphill

Capillary forces may be sufficient to make micro-drops move upwards on an inclined plane.

M.K. Chaudhury and G.M. Whitesides, "How to make water run uphill," *Science*, Vol. 256, pp. 1539–1541, 1992.



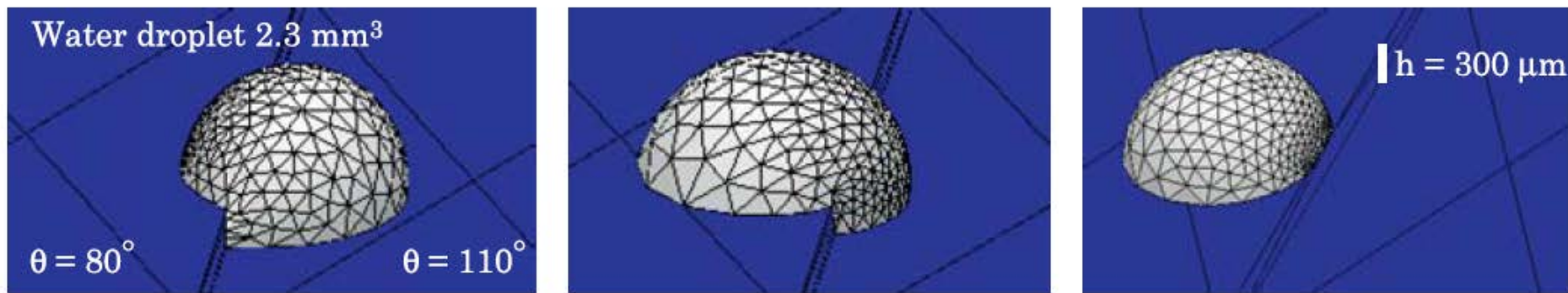
The required gradient in surface free energy was generated on a polished silicon wafer by exposing it to the diffusing front of a vapor of decyltrichlorosilane,

The average velocity is approximately 1 to 2 mm/s

A drop moves uphill towards the more hydrophilic region.

### 3. Drop Moving up a Step

A micro-drop of water is initially located on a step at the boundary of a hydrophilic region (on top of the step) and a hydrophobic region (at the base of the step). The drop progressively moves towards the hydrophilic region, even if this region is located at a higher level (simulation result)

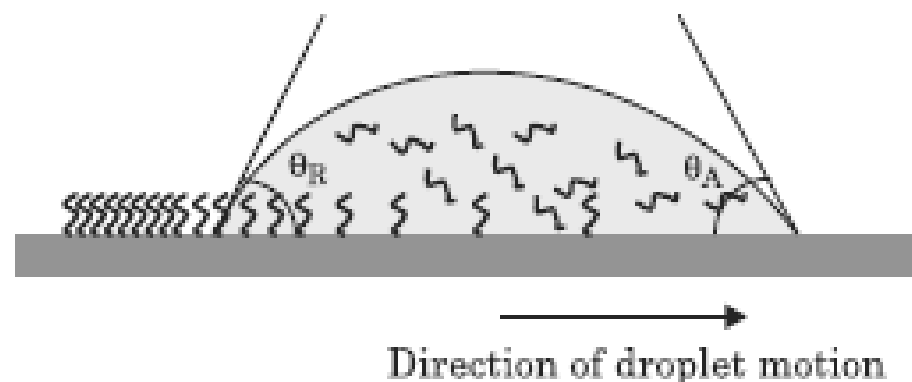
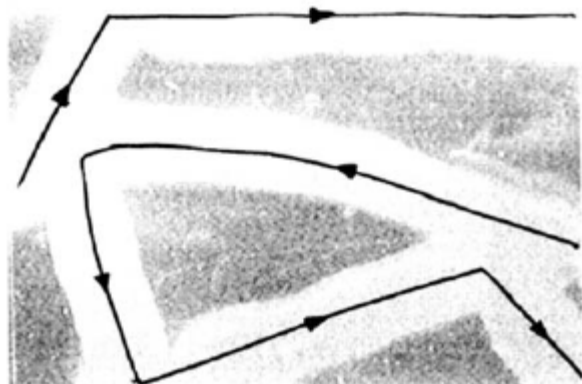


Motion of a drop up a step towards the hydrophilic plane  
(simulation)

## 4. Drop Moving Over a Gradient of Surface Concentration of Surfactant

Chemical reactions between the liquid of the droplet and the substrate can create droplet motion. A droplet of n-alkanes containing silane molecules is placed on a hydrophilic surface. Silane molecules form dense grafted monolayers on silicon or glass, rendering the surface hydrophobic.

If such a droplet is deposited on a glass surface and pushed with a pipette, then the droplet continues to move on the substrate. It moves in nearly linear segments and changes its direction each time it encounters a hydrophobic barrier. The droplet cannot cross its own tracks.



The advancing contact line has a hydrophilic Young contact angle. Molecules of silane concentrate at the vicinity of the receding contact line and form a hydrophobic layer.

**Electrowetting  
and  
Digital Microfluidics**

Different driving forces become pertinent in microscale systems in contrast to their macroscale counterparts to drive fluids.

## **Surface tension force**

Important in microscale domain owing to the fact that the **surface to volume ratio** increases significantly in microscale.

The control of surfaces and surface energies is one of the most important challenges both in microtechnology in general as well as in microfluidics. For liquid droplets of sub-millimetre dimensions, **capillary forces dominate.**

The control of interfacial energies (both liquid–vapour and solid–liquid interfaces) has therefore become an important strategy for manipulating droplets at surfaces.

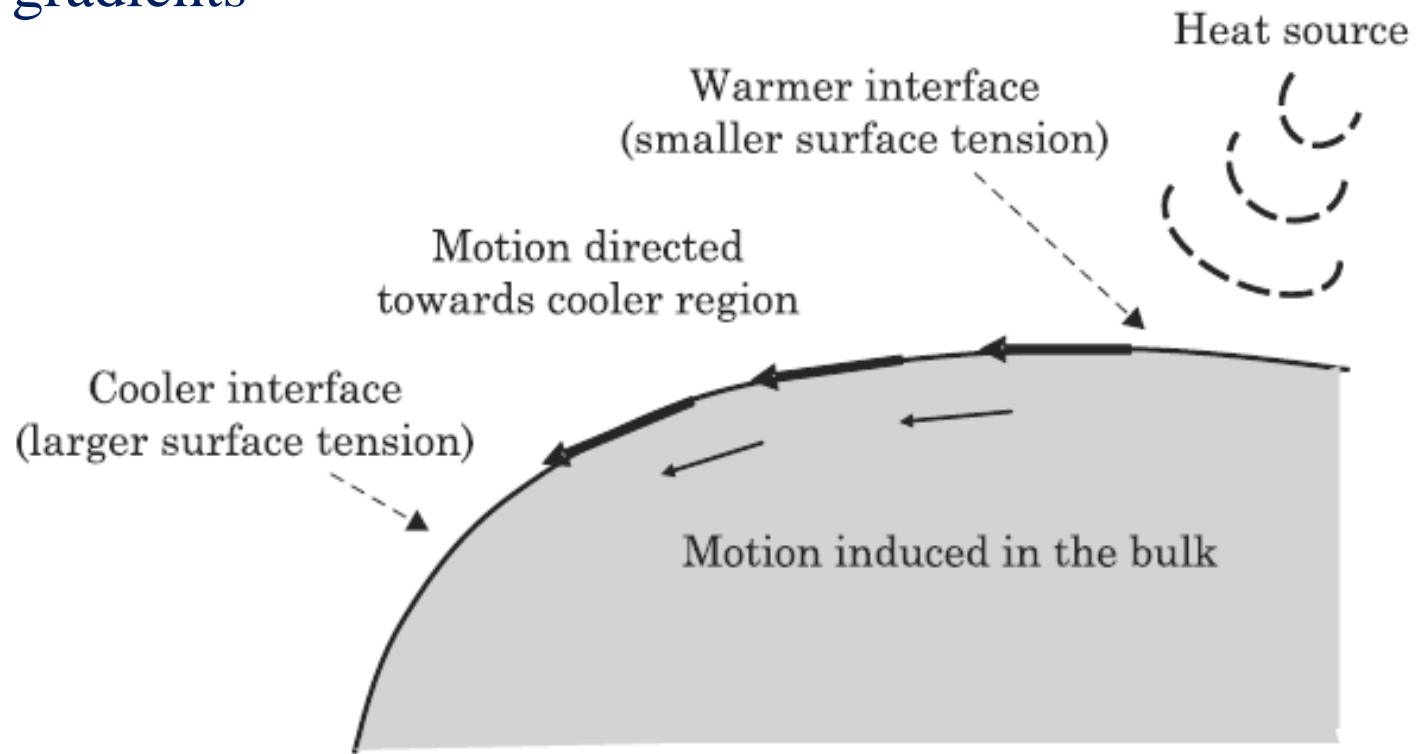
Precise manipulation of droplets in the micrometer scale.

Four fundamental fluidic operations (creating, transporting, cutting, and merging) with droplets are utilized to digitize droplet- based fluidic system which has evolved into a new microfluidics paradigm

## Digital Microfluidics

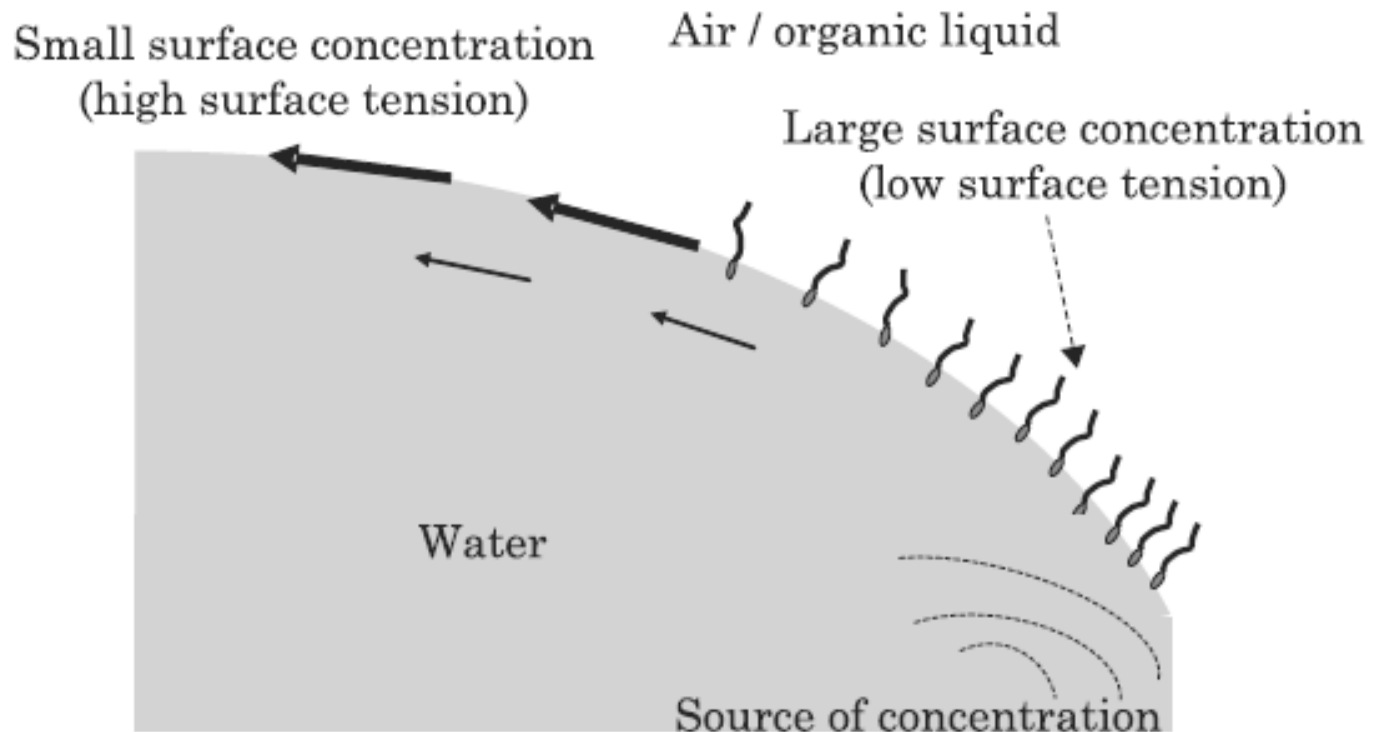
## Ways to influence the interfaces

### Temperature gradients



Interface motion induced by a thermal gradient between two regions of the surface. The interface motion propagates into the bulk due to viscous forces.

# Gradients in the concentration of surfactants across droplets



Gives rise to gradients in interfacial energies, mainly at the liquid–vapour interface, and thus produce forces that can propel droplets making use of the thermocapillary and Marangoni effects.

**Marangoni convection** occurs if the variation of the surface tension force dominates the viscosity forces.

A dimensionless number—the Marangoni number (thermal)—determines the strength of the convective motion

$$Ma = \frac{\Delta\gamma R}{\rho v \alpha}$$

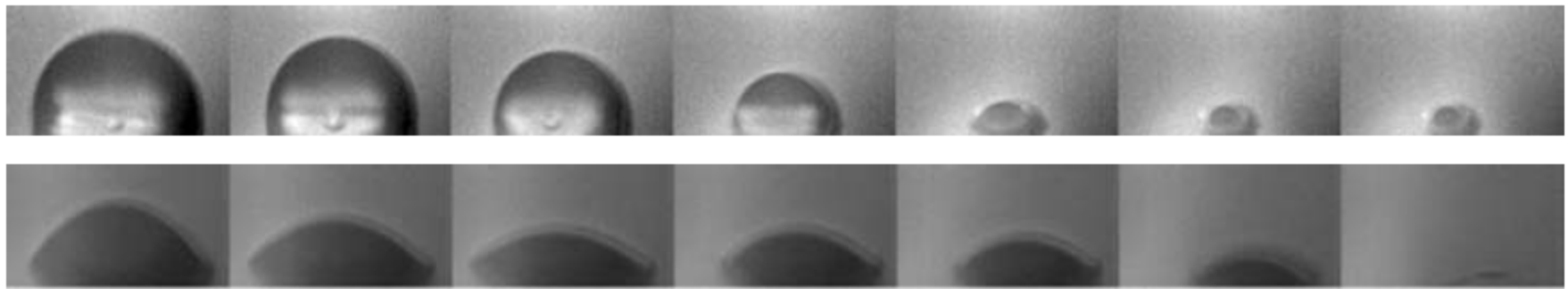
where  $R$  is the radius of the spherical cap,  $\rho$  the density of the liquid,  $v$  the kinematic viscosity,  $\alpha$  the thermal diffusivity, and  $\Delta\gamma$  the variation of surface tension on the interface.

The Marangoni number represents the ratio between the tangential stress and the viscosity.

## Examples of the role of the interface/contact line

### Evaporation of sessile droplets

It has been observed experimentally that wetting and non-wetting droplets do not evaporate in the same way.

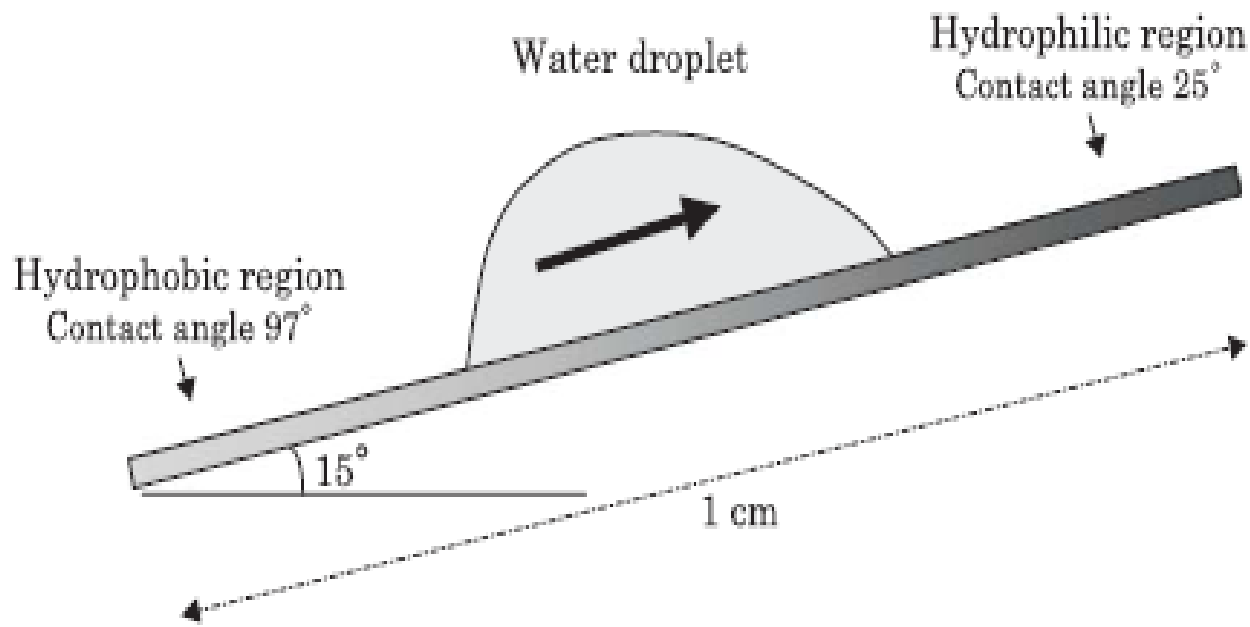


Water Droplet on hydrophobic (top) and hydrophilic (bottom) surfaces

In the case of a non-wetting droplet, it is the **contact angle that remains constant (CCA)**, the contact radius decreases gradually.

In the case of a wetting droplet the **contact radius remains constant (CCR)** during the evaporation process, the contact angle decreases gradually. It is as if the contact line was pinned on the initial contact line.

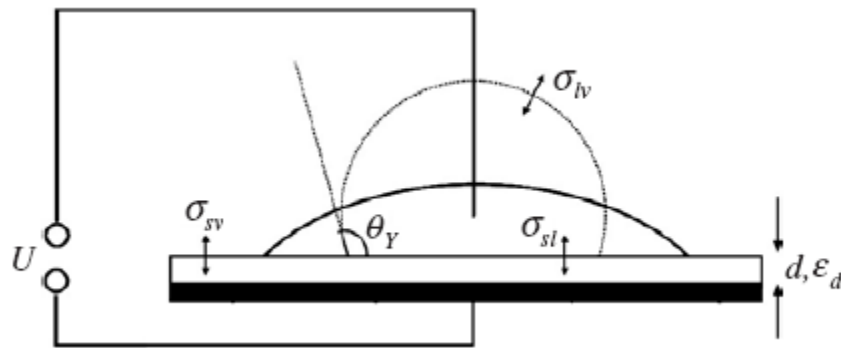
## Chemical and topographical structuring of surfaces - local wettability



The main disadvantage of chemical and topographical patterns is their **static nature**, which prevents active control of the liquids.

**Electrocapillarity**, the basis of modern electrowetting, was first described in detail in 1875 by Gabriel Lippmann.

*the capillary depression of mercury in contact with electrolyte solutions could be varied by applying a voltage between the mercury and electrolyte*



Generic electrowetting set-up. Partially wetting liquid droplet at zero voltage (dashed) and at high voltage (solid).

**Electrowetting (EW)** has proven to be very successful:

Contact angle variations of several tens of degrees are routinely achieved.

**Switching speeds** are limited (typically to several milliseconds) by the hydrodynamic response of the droplet rather than the actual switching of the equilibrium value of the contact angle.

Excellent stability without noticeable degradation

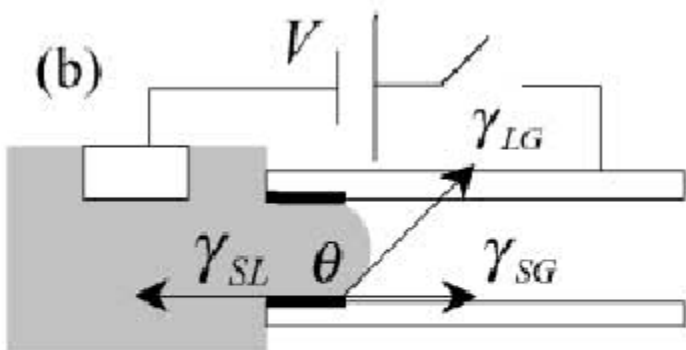
Nowadays, droplets can be moved along freely programmable paths on surfaces; they can be split, merged, and mixed with a high degree of flexibility.

**However, electrolysis start within a few milli-volts to make EW difficult to use for practical applications.**

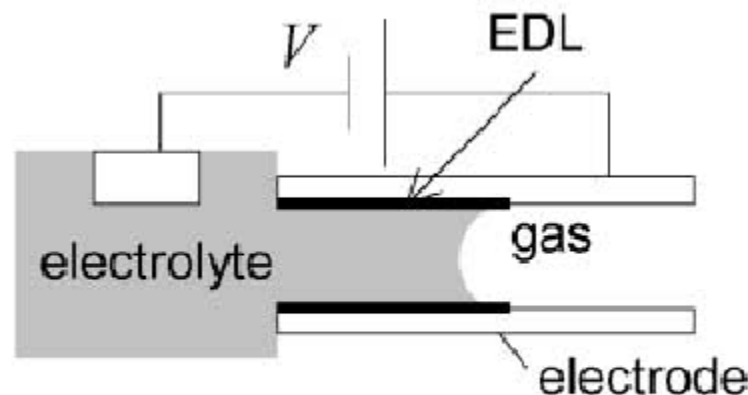
## Electrowetting (EW)

In EW an electrical double layer (EDL) is formed between the electrode and aqueous solution that is between 1 nm and 10 nm thick.

Applying a voltage difference may cause a hydrophobic surface to behave like a hydrophilic one. The electric energy counterbalances the free surface energy and lowers the surface tension  $\gamma_{\text{sl}}$ .



hydrophobic: retracting

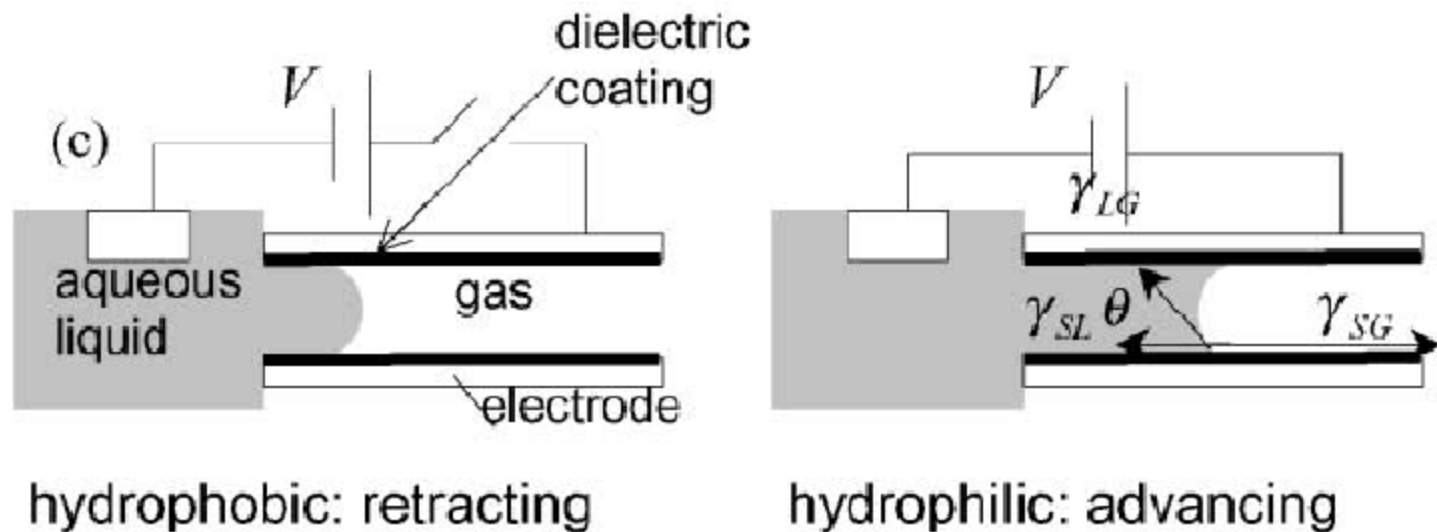


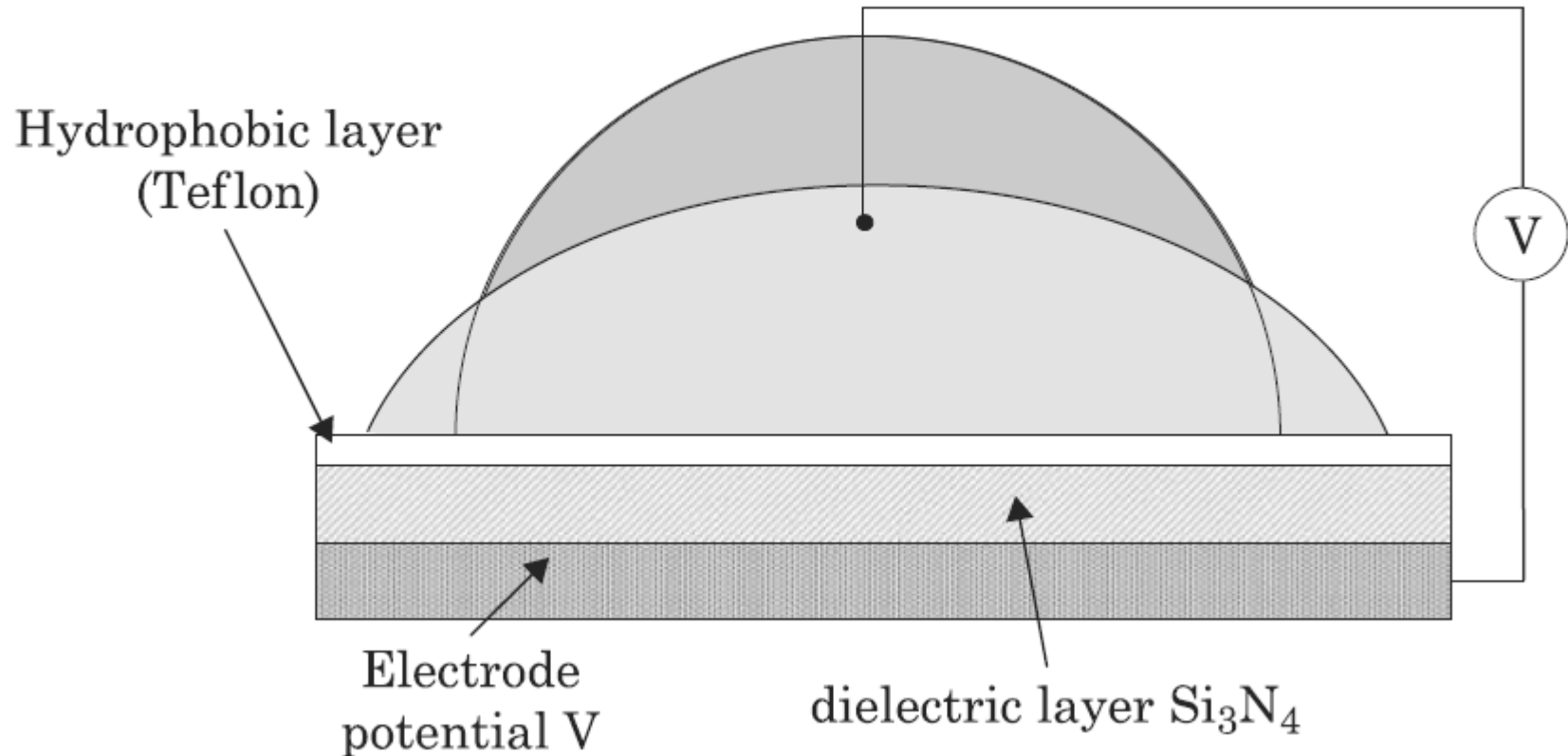
hydrophilic: advancing

## Electrowetting-on-dielectric (EWOD)

Berge in the early 1990 introduced the idea of using a thin insulating layer to separate the conductive liquid from the metallic electrode in order to eliminate the problem of electrolysis - **Electrowetting on dielectric (EWOD).**

In EWOD there is no electric double layer, but the change in the energy balance takes place in the hydrophobic dielectric layer; A Teflon layer,  $0.8\ \mu\text{m}$  thick was used as the dielectric. Lee, J., Moon, H., Fowler, J., Schoellhammer, T., and Kim, C.-J. (2002). Electrowetting and electrowetting-on-dielectric for microscale liquid handling. *Sens. Actuators, A*, 95:259–268.





EWOD

# Electrowetting: basics to applications

Electrowetting has become one of the most widely used tools for manipulating tiny amounts of liquids on surfaces.

Applications range from ‘lab-on-a-chip’ devices to adjustable lenses and new kinds of electronic displays.

## Issues

Fundamental and applied aspects.

Basic electrowetting equation,

Origin of the electrostatic forces that induce both contact angle reduction and the motion of entire droplets.

## *Issues – contd.*

Limitations of the electrowetting equation

Failure of the electrowetting equation, namely the saturation of the contact angle at high voltage,

The dynamics of electrowetting

Overview of commercial applications

# Theoretical background

## Basic aspects of wetting

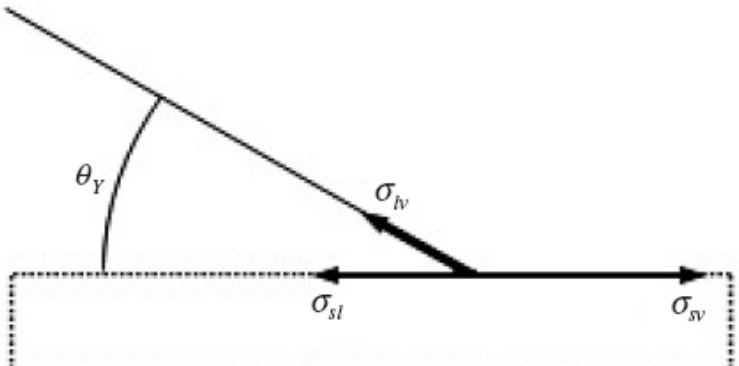
In electrowetting, one is generically dealing with droplets (typical size of the order of 1 mm or less) of partially wetting liquids (aqueous salt solutions) on planar solid substrates.

Bond number  $Bo = \sqrt{g \Delta \rho R^2 / \sigma_{lv}}$  measures the strength of gravity with respect to surface tension.



**If  $Bo < 1$** , the strength of gravity is neglected and the behavior of the droplets is determined by surface tension alone.

The free energy F of a droplet is a function of the droplet shape.



Force balance at the contact line

The free energy  $F$  of a droplet is the sum of the areas  $A_i$  of the interfaces between the three phases, weighted by the respective interfacial energies, i.e.  $\sigma_{sv}$ ,  $\sigma_{sl}$ , and  $\sigma_{lv}$ :

$$F = F_{if} = \sum_i A_i \sigma_i - \lambda V \quad (1)$$

$\lambda$  is equal to the pressure drop across the liquid–vapour interface.

Minimization of Eq. (1) leads to the following condition that any equilibrium liquid morphology has to fulfill -

**Laplace Equation**

$$\Delta P = \sigma_{lv} \left( \frac{1}{r_1} + \frac{1}{r_2} \right) = \sigma_{lv} K \quad (2)$$

**Young Equation**  $\cos \theta_Y = \frac{\sigma_{sv} - \sigma_{sl}}{\sigma_{lv}}$  (3)

relates Young's equilibrium contact angle to the interfacial energies

**Both equations are approximations intended for mesoscopic scales.**

## Electrowetting theory for homogeneous substrates

The thermodynamic and electrochemical approach - Lippmann's derivation  
- direct metal – electrolyte interfaces

Upon applying a voltage  $dU$ , an electric double layer builds up spontaneously at the solid–liquid interface consisting of charges on the metal surface on one hand and of a cloud of oppositely charged counter-ions on the liquid side of the interface.

Since the accumulation is a spontaneous process, it leads to a reduction of the (effective) interfacial tension,  $\sigma_{eff}$

$$d\sigma_{sl}^{eff} = -\rho_{sl} dU \quad (4)$$

$\rho_{sl} = \rho_{sl}(U)$  is the surface charge density of the counter-ions,  $U$  = applied voltage

The voltage dependence of  $\sigma_{sl}^{eff}$  is calculated by integrating this equation

Simplifying assumption - the counter-ions are all located at a fixed distance  $d_H$  (*of the order of a few nanometres*) from the surface (**Helmholtz model**).

In this case, the double layer has a fixed capacitance per unit area,

$$C_H = \frac{\epsilon_0 \epsilon_1}{d_H} \quad C_H = \rho / U$$

Where  $\epsilon_1$  is the dielectric constant of the liquid.

$$\sigma_{sl}^{eff}(U) = \sigma_{sl} - \int_{U_{pzc}}^U C_H U dU = \sigma_{sl} - \frac{\epsilon_0 \epsilon_1}{2d_H} (U)^2 \quad (5)$$

$U_{pzc}$  is the potential (difference) of zero charge and approximated to zero.

Mercury surfaces—like those of most other materials—acquire a spontaneous charge when immersed into electrolyte solutions at zero voltage. The voltage required to compensate for this spontaneous charging is  $U_{pzc}$

$\gamma_{LG} \cos \theta = \gamma_{SG} - \gamma_{SL}$

This equation for  $\sigma_{sl}^{eff}$  is inserted into Young's equation.

For an electrolyte droplet placed directly on an electrode surface one can find ( $U_{pzc}$  approximated to zero)

$$\cos \theta = \cos \theta_Y + \frac{\epsilon_0 \epsilon_1}{2d_H \sigma_{lv}} (U)^2 \quad (6)$$

$\theta_Y$  - equilibrium contact angle at zero applied voltage,  $\epsilon_0$  - permittivity of free space,  $\epsilon_1$  - dielectric constant of the insulating layer,  $\sigma_{lv}$  -surface tension between the liquid and the vapor, and  $U$  - voltage

For typical values of  $d_H$  (2 nm),  $\epsilon_1$  (81), and  $\sigma_{lv}$  (0.072 mJ m<sup>-2</sup>) the ratio on the rhs of equation is on the order of 1 V<sup>-2</sup>.

**The contact angle thus decreases rapidly upon the application of a voltage.**

This equation is only applicable within a voltage range below the onset of electrolytic processes, i.e. typically up to a few hundred millivolts.

Modern applications of electrowetting usually circumvent this problem by introducing a thin dielectric film, which insulates the droplet from the electrode.

In EWOD, the electric double layer builds up at the insulator–droplet interface.

Since the insulator thickness  $d$  is usually much larger than  $d_H$ , the total capacitance of the system is reduced tremendously.

The system may be described as two capacitors in series, namely the solid–insulator interface (capacitance  $c_H$ ) and the dielectric layer with

$$c_d = \frac{\epsilon_0 \epsilon_d}{d}$$

$\epsilon_d$  is the dielectric constant of the insulator.

Since  $c_d \ll c_H$  , the total capacitance per unit area  $c \approx c_d$ .

With this approximation, the finite penetration of the electric field into the liquid, is neglected (liquid treated as a perfect conductor) and the voltage drop occurs within the dielectric layer.

Equation (5) is replaced by

$$\sigma_{sl}^{eff}(U) = \sigma_{sl} - \frac{\epsilon_0 \epsilon_d}{2d} U^2 \quad (7)$$

It is assumed that the surface of the insulating layer does not give rise to spontaneous adsorption of charge in the absence of an applied voltage, i.e.  $U_{pzc} = 0$ .

In this equation the entire dielectric layer is considered part of one effective solid–liquid interface with a thickness of the order of  $d$ , typically  $O(1 \mu\text{m})$ .

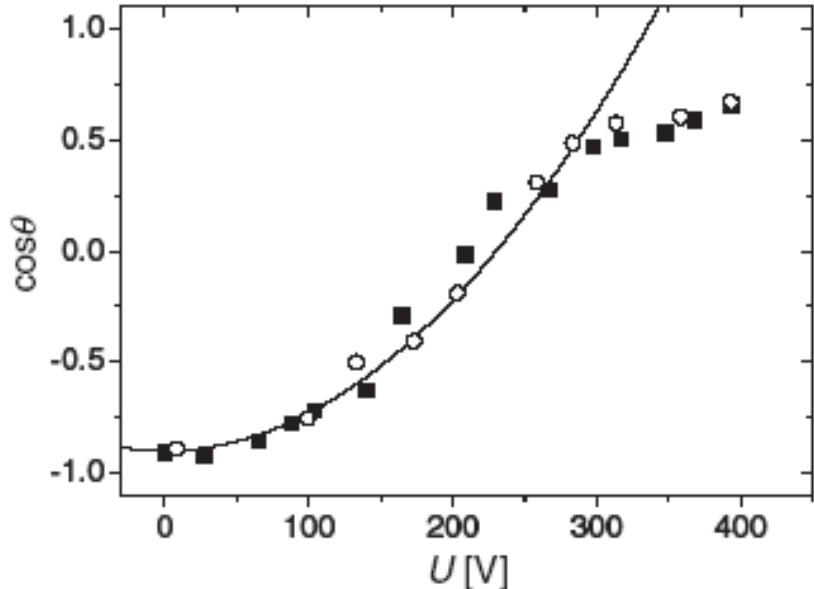
Combining Eq. (7) with Eq. (3), the basic equation for EWOD is obtained

$$\cos \theta = \cos \theta_Y + \frac{\epsilon_0 \epsilon_d}{2 d \sigma_{lv}} U^2 = \cos \theta_Y + \eta \quad (8)$$

$\eta = \frac{\epsilon_0 \epsilon_d}{2 d \sigma_{lv}} U^2$  is the **dimensionless electrowetting number** which measures the strength of the electrostatic energy compared to surface tension.

The ratio in the middle of Eq. (8) is typically four to six orders of magnitude smaller than that in Eq. (6),  $\frac{\epsilon_0 \epsilon_1}{2 d_H \sigma_{lv}}$  depending on the properties of the insulating layer.

Consequently, the voltage required to achieve a substantial contact angle decrease in EWOD is much higher.



Contact angle versus applied voltage for a glycerol–salt (NaCl) water droplet.

*Filled* (open) symbols: increasing (decreasing) voltage.

Solid line: parabolic fit according to Eq. (8)

Equation (8) is found to hold as long as the voltage is not too high.

Beyond a certain system dependent threshold voltage, however, the contact angle has always been found to become independent of the applied voltage -

- **Contact angle saturation phenomenon**

At high voltage, the contact angle has always been found to saturate.

In particular, no voltage-induced transition from partial to complete wetting has ever been observed. (On the basis of equation (8), such a transition would be expected to occur at

$$U_{spread} = (2\sigma_{lv}d(1 - \cos \theta_Y)/(\varepsilon_0\varepsilon_d))^{(1/2)}.$$

*Instead,  $\theta$  adopts a saturation value  $\theta_{sat}$  varying between  $30^\circ$  and  $80^\circ$ , depending on the system*

Contact angle saturation is still not well understood.

**Digital microfluidics** refers to describe two different technologies —

- **an open system** - droplet position is controlled by actuating electrodes arranged in a two-dimensional array
- **confined system** - droplets are manipulated inside microchannels.

These systems enable the miniaturization of reactions by compartmentalizing reactions in droplets of nanoliter to microliter volumes.

Compartmentalization in droplets provides rapid mixing of reagents, control of the timing of reactions, control of interfacial properties, and the ability to synthesize and transport solid reagents and products.

Droplet-based microfluidics can help to enhance and accelerate chemical and biochemical screening, protein crystallization, enzymatic kinetics, assays.

# Complex surfaces and droplet morphologies

- *Morphological transitions on structured surfaces*

- e.g. hydrophobic surface (e.g.  $\theta = 180^\circ$ ) with a stripe of variable wettability.

For moderate wettability contrasts, there is only one stable morphology, which is a droplet slightly stretched along the stripe.

- *Patterned electrodes*

- multilayer substrates with various patterned electrodes separated by dielectric layers

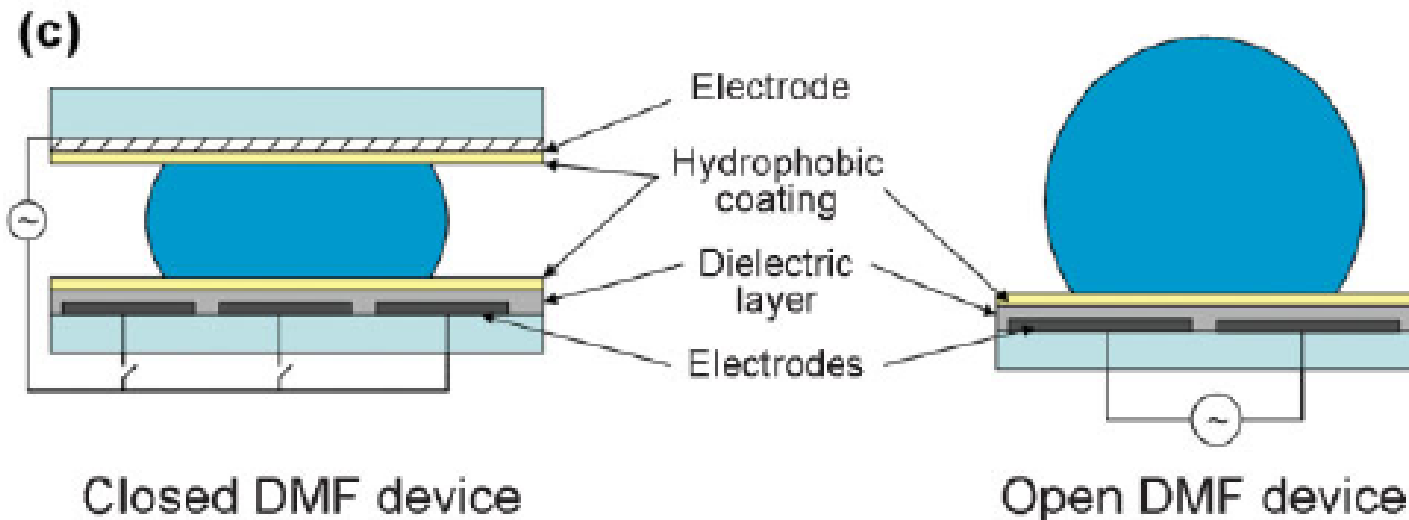
- *Topographically patterned surfaces*

- Superhydrophobicity and hydrophilicity are amongst the most spectacular consequences of surface roughness

DMF is typically implemented in one of two different configurations –

The **closed format** (also known as the two-plate format), in which droplets are sandwiched between two substrates patterned with electrodes (the substrates house driving and ground electrodes, respectively).

The **open format** (also known as the single-plate format), in which droplets are placed on top of a single substrate, housing both actuation and ground electrodes.



In both configurations, **an insulating layer of a dielectric material** is deposited on top of the actuation electrodes, to limit current and prevent electrolysis.

Typically, the insulating layer is covered by an **additional hydrophobic coating**, which reduces droplet-sticking to the surface.

**Closed DMF devices** are best suited for a **wide range of droplet operations** – dispensing, moving, splitting, and merging are all feasible.

**Open DMF devices** are typically not efficient for splitting and dispensing; however, the open format facilitates **fast sample and reagent mixing**, the capacity to move large droplets, and better access to samples for external detectors.

Additionally, **evaporation rates are higher in open-format devices**, which may be advantageous or inconvenient, depending on the application.

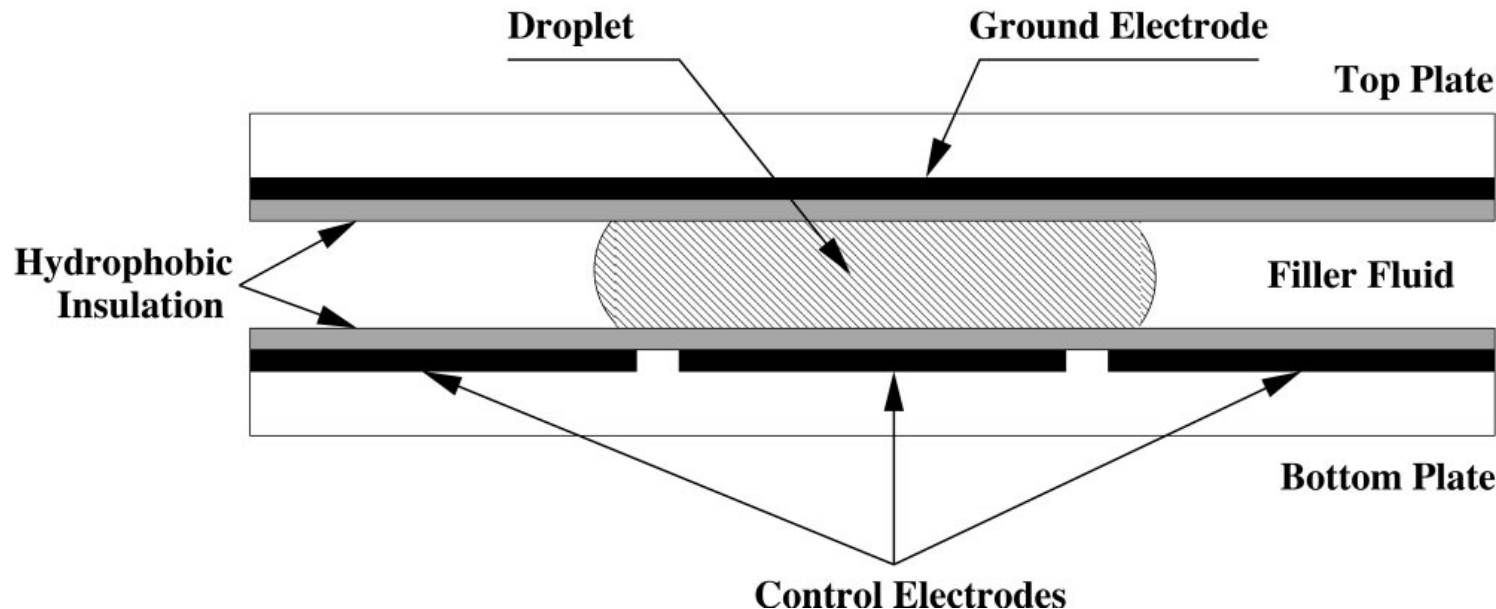
Liquid motion could only be achieved above some **threshold voltage**.

This observation is attributed to contact angle hysteresis: droplet motion can only set in when the contact angle on the leading edge of the droplet exceeds the local advancing contact angle.

Reynolds numbers of electrowetting-induced flows are rather low.

With typical velocities of the order of  $v \approx 10^{-2} - 10^{-1} \text{ m s}^{-1}$  and droplet sizes of  $R \approx 10^{-3} \text{ m}$  or less, one obtains  $Re = \rho v R / \mu \approx 100$  for water and even smaller values for more viscous liquids. Hence, the flow is usually laminar.

Within the range of validity of the electrowetting equation EW-induced motion is analogous to the motion of droplets on chemically heterogeneous substrates,



A droplet of polarizable and conductive liquid is sandwiched between two sets of planar electrodes. The upper plate consists of a single continuous ground electrode, while the bottom plate consists of an array of independently addressable control electrodes. Both electrode surfaces are covered by a thin layer of hydrophobic insulation.

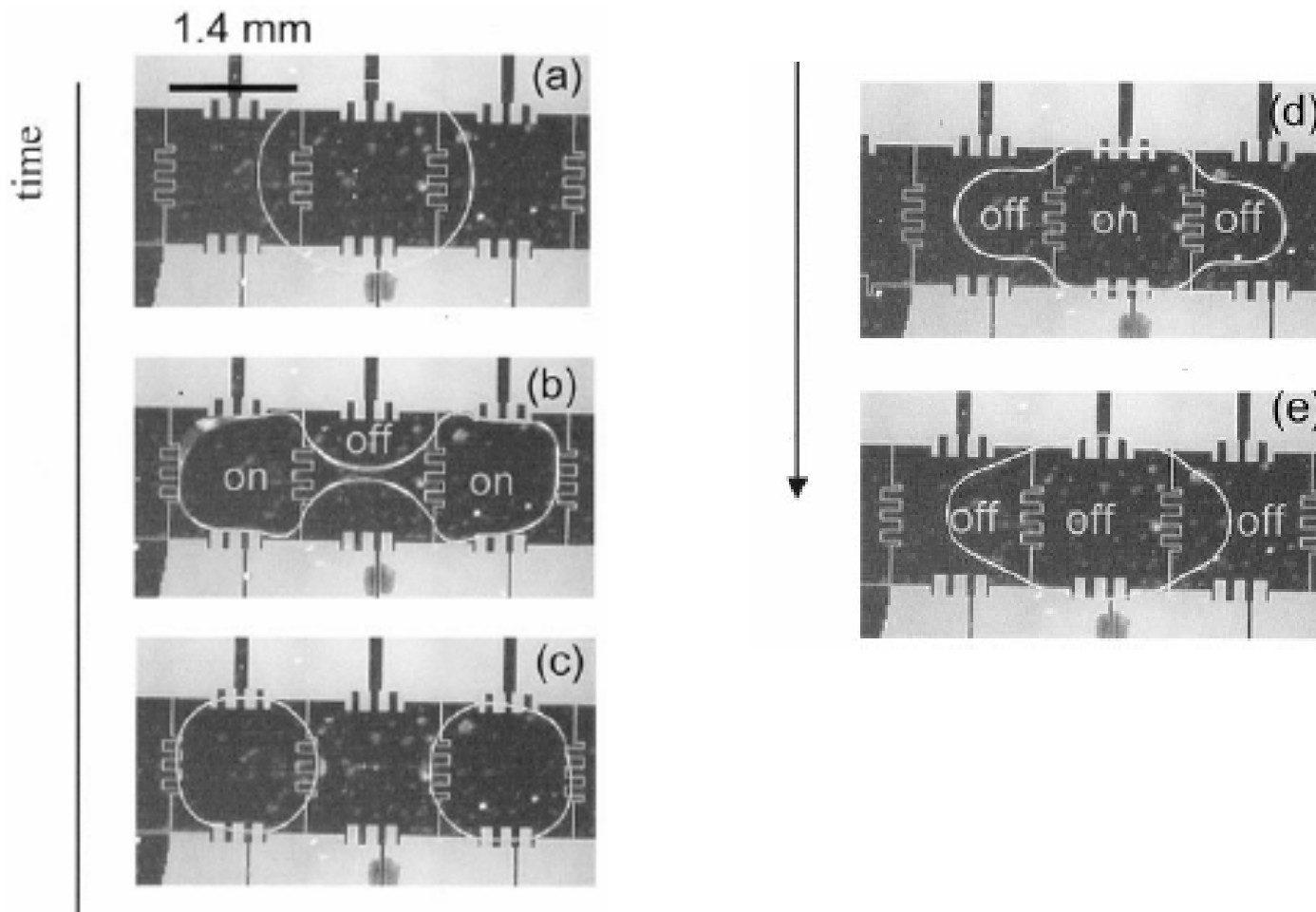
The system geometry and droplet volume are controlled such that the footprint of the droplet overlaps at least two adjacent control electrodes while also making contact to the upper ground electrode.

Initially all electrodes are grounded and the contact angle everywhere is the equilibrium contact angle of the droplet.

When an electrical potential is applied to a control electrode underneath the droplet, a layer of charge builds up at the interface between the droplet and the energized electrode resulting in a local reduction of the interfacial energy.

Since the solid insulator controls the capacitance between the droplet and the electrode the effect does not depend on the electrolyte's specific space-charge effects as did uninsulated electrode implementations.

If a portion of the droplet also overlaps a grounded electrode, the droplet meniscus is **deformed asymmetrically** and a pressure gradient is established between the ends of the droplet which results in bulk flow towards the energized electrode.



Sequential images of successful cutting and merging of droplets at 25 V  
(gap size  $d = 70 \mu\text{m}$ , electrode is 1.4 mm x 1.4 mm, volume is 0.2  $\mu\text{l}$ ).

One of the substrates contains the patterned electrodes for liquid actuation.

The other substrate consists of a homogeneous electrode that provides electrical contact to the droplet(s) independently of its (their) position.

- transparent ITO layer on a glass substrate, covered with a thin hydrophobic layer that gives rise to a large contact angle and weak contact angle hysteresis but does not prevent electrical contact.

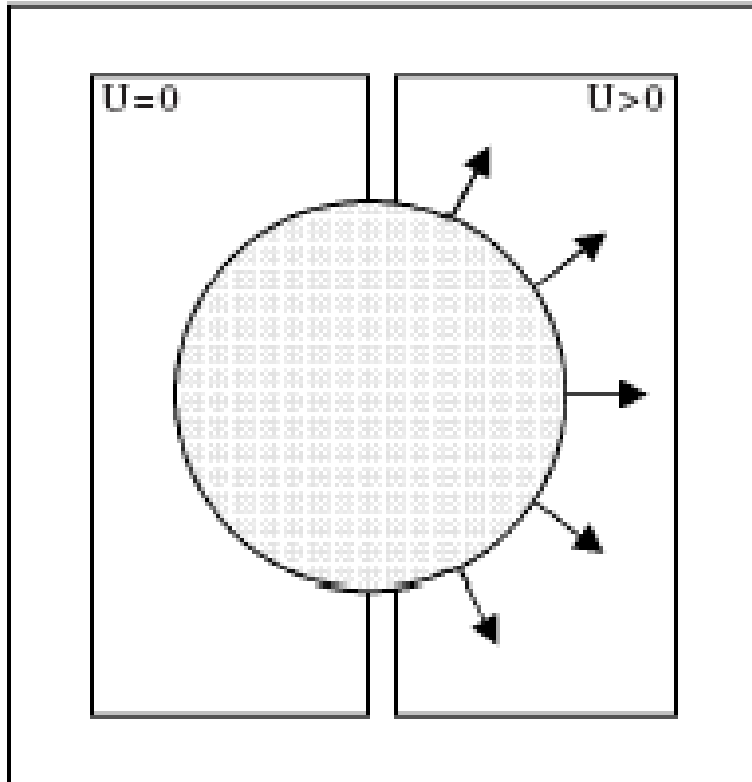
Droplet actuation- droplet edges must overlap with at least two adjacent electrodes.

With substrate separations of 100–500 $\mu\text{m}$  and electrode sizes of the order of 1 mm, this means **typical droplet volumes of 0.1–1  $\mu\text{l}$** .

Routine tasks e.g., moving, merging, mixing, and splitting of droplets

## Dynamic aspects of electrowetting

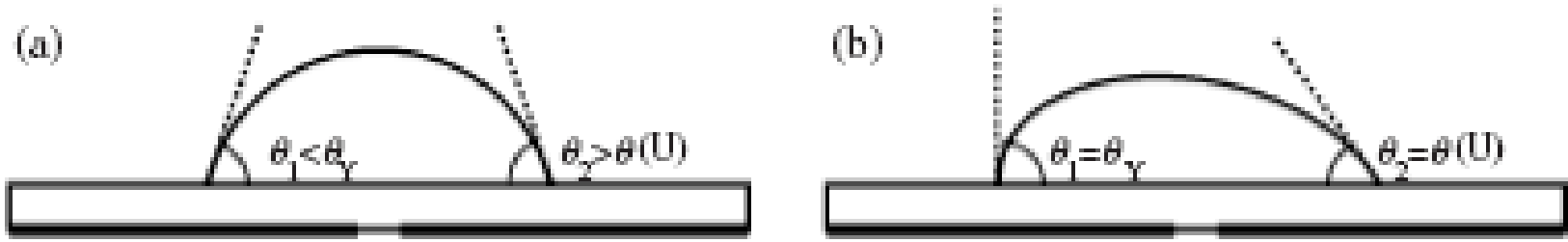
For many practical applications, the dynamic response of the liquid is of interest



Top view of a droplet partially overlapping with an **activated (right)** and a **deactivated (left)** electrode. Arrows indicate the force acting on the contact line.

The contact angle assumes a time and speed dependent value which is determined by local dissipative processes and flow fields at the vicinity of the TCL.

On the other hand, the entire droplet also responds on a global scale, e.g. by a translation of its centre of mass,



Side view of imbalanced droplets partially overlapping with a **deactivated (left) and with an activated (right) electrode**. (a) Droplet dominated by contact line friction; (b) droplet dominated by bulk viscous dissipation.

There are several contributions to the net force which oppose the motion.

If the dissipation is dominated by **contact line friction**, the pressure within the droplet equilibrates quickly and the droplet retains its spherical cap shape but with a time dependent dynamic contact angle  $\theta_d$

*If bulk viscous effects dominate, the contact angle assumes its local equilibrium angle everywhere along the contact line. As a result, the drop shape is non-spherical and a hydrodynamic pressure gradient arises and drives fluid flow within the droplet.*

In most practical situations, an intermediate behaviour is expected.

By considering the static mechanical equilibrium, the bubble driving force produced by electrowetting actuation may be approximated as follows:

$$F_{Driving} = 2\gamma w \sin\left(\frac{\theta_R + \theta_L}{2}\right) (\cos\theta_R - \cos\theta_L)$$

where  $\gamma$  is the interfacial tension between the liquid and the bubble, and  $w$  is the width of the bubble base that linearly scales with the radius  $R$  of the bubble.

Here, the contact angle  $\theta_R$  of the bubble is modulated by electrowetting actuation and decreases from the equilibrium contact angle  $\theta_e$  with a large span (generally  $\sim 40^\circ$ ).

$$F_{Driving} = 2\gamma w \sin\left(\frac{\theta_R + \theta_L}{2}\right) (\cos\theta_R - \cos\theta_L)$$

Therefore, the sine term can be roughly approximated to the sine of the equilibrium contact angle  $\theta_e$ , whereas the difference in the cosines increases as the contact angle  $\theta_R$  for the bubble is decreased by electrowetting modulation.

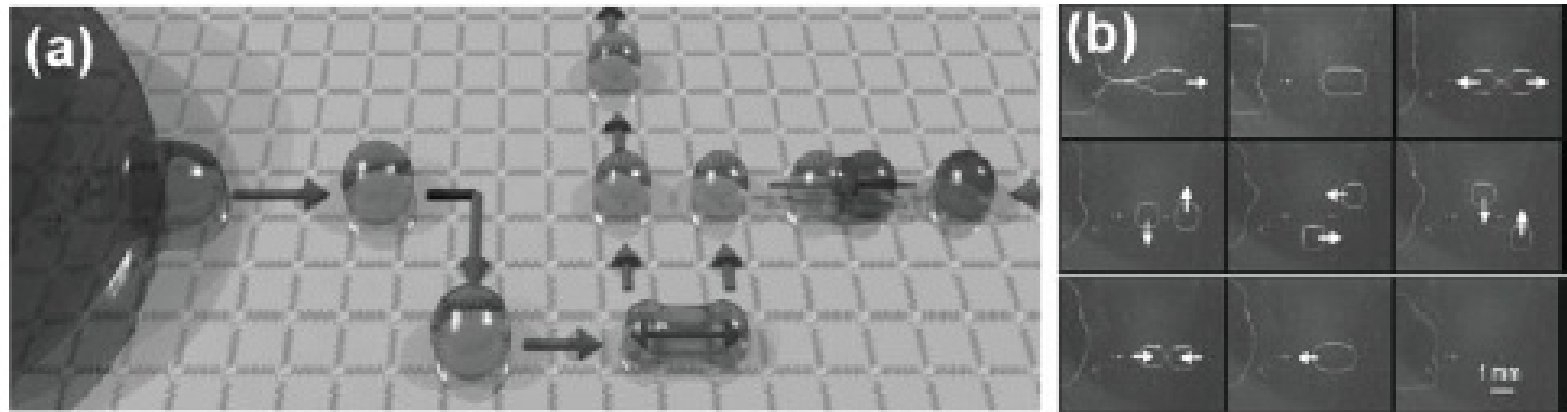
Based on these relationships, it can be concluded that the maximum driving force can be achieved when the equilibrium contact angle is close to 90° and the contact angle modulation is maximized by electrowetting actuation.

This force can be in the micro Newton range.

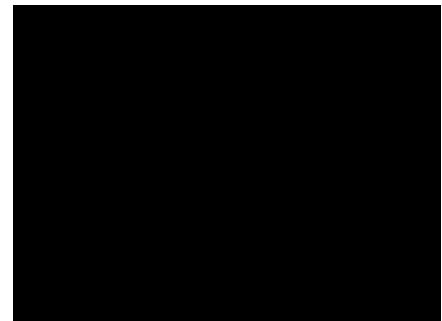
## Digital Revolution In Microfluidics

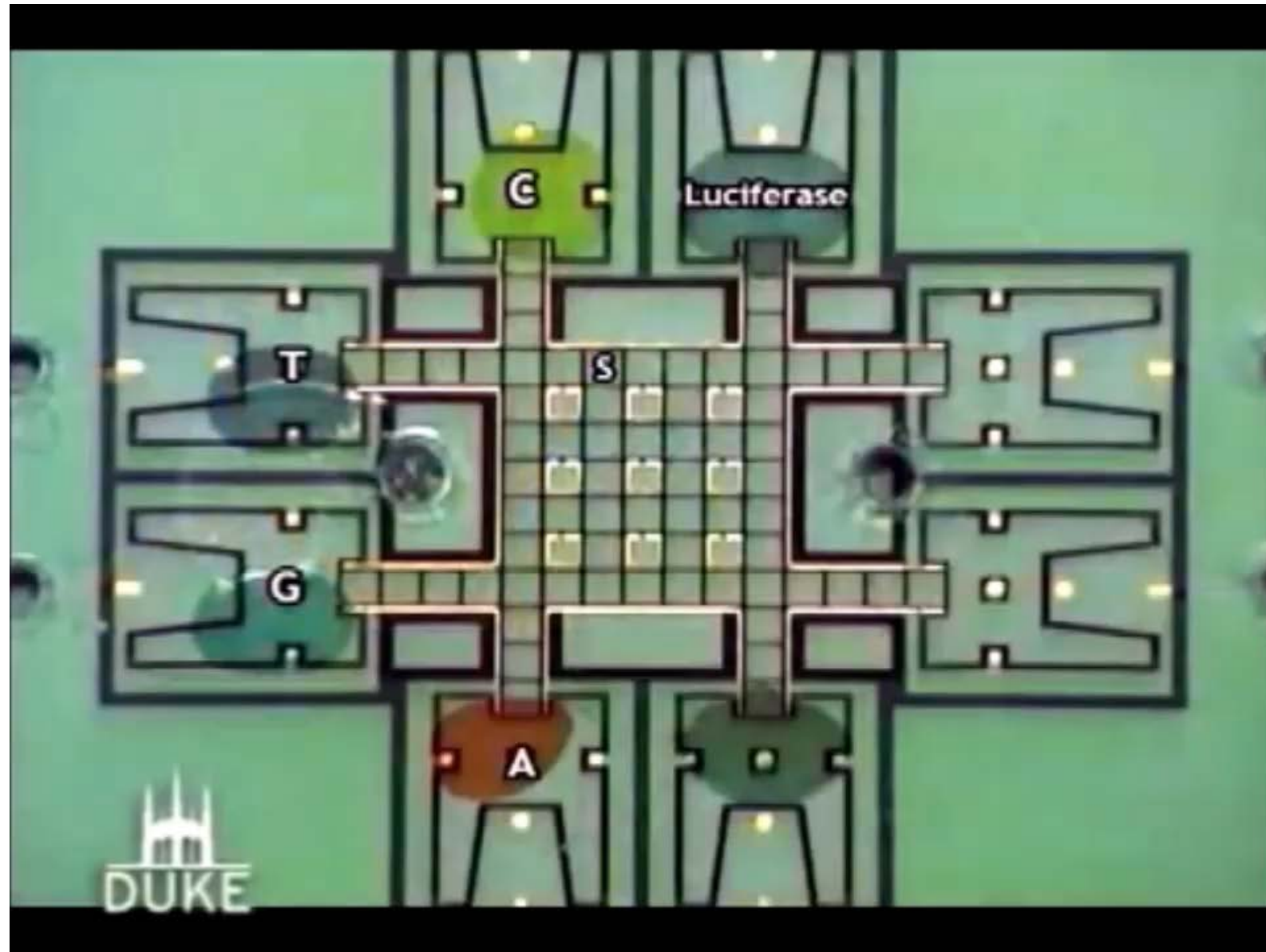
In digital microfluidics (DMF), discrete droplets are manipulated by applying electrical fields to an array of electrodes.

In contrast to microchannels, in DMF each sample and reagent is individually addressable, which facilitates exquisite control over chemical reactions.



The DMF paradigm. a) Schematic and b) pictures from a movie depicting the four principle DMF processes: dispensing, moving, splitting, and merging.

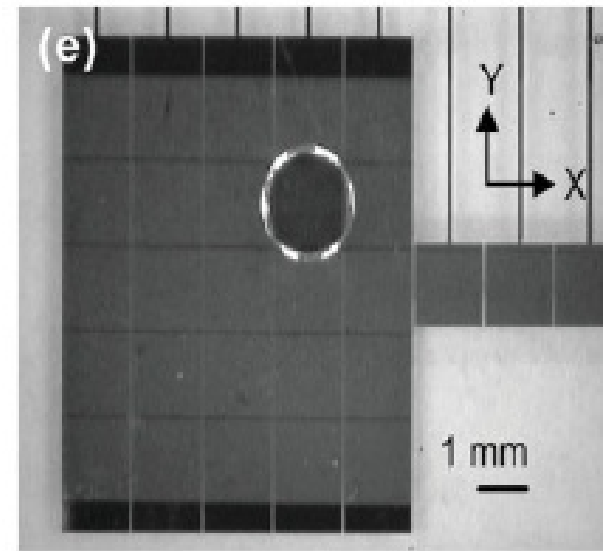
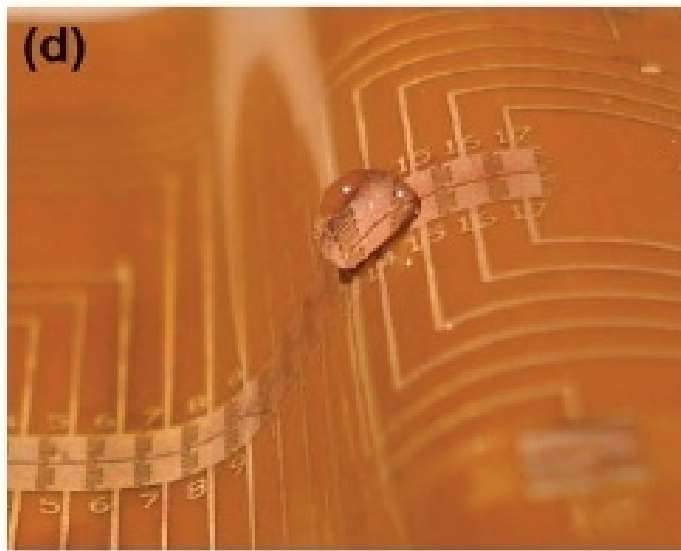




Secondly, droplets serve as discrete microvessels, in which reactions can be carried out without cross-talk between samples or reagents.

DMF is inherently an array-based technique, good match for array-based biochemical applications.

DMF devices are straightforward to use, and are reconfigurable for any desired combination of droplet operations.



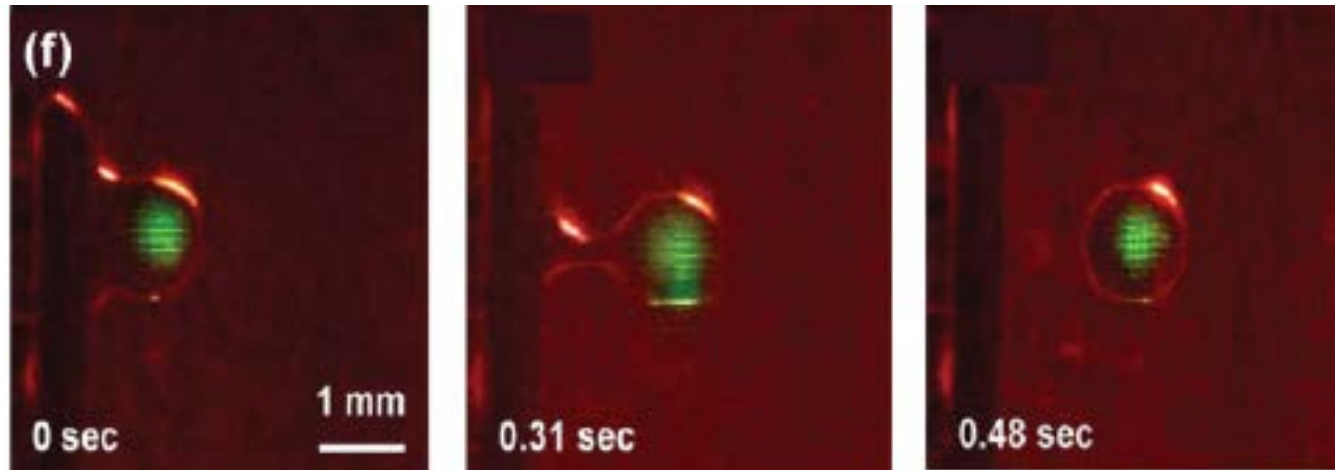
d) Picture of an ATDA (all-terrain droplet actuation) device, capable of manipulating droplets on flexible substrates. e) Picture of a DMF device powered by a cross reference electrode array.

**DMF devices** are typically fabricated in a clean-room facility using conventional techniques, such as photolithography and etching.

**Electrodes** are formed from substrates common to such facilities (e.g., chromium, gold, indium-tin oxide (ITO), and doped polysilicon).

The **insulating dielectric layer** - vapor deposition (parylene, amorphous fluoropolymers, and silicon nitride), thermal growth (silicon oxide), or spin-coating (PDMS or SU-8).

The **hydrophobic coating** - spin-coating a thin layer of Teflon-AF.



*Series of pictures from a video (left-to-right) depicting droplet dispensing on an **optically driven** DMF device.*

While many DMF devices are used to actuate droplets in air, another common technique uses **droplets suspended in oil**, which prevents evaporation and reduces the voltages required for droplet actuation.

Fouling by a variety of bio-fluids containing high concentrations of potential surface-fouling molecules, including blood, serum, plasma, urine, saliva, sweat, and tear **could be minimized** by suspending droplets in an immiscible oil.

Oil-immersed systems have **drawbacks**,

- requirement of gaskets or other structures to contain the oil bath,
- liquid–liquid extraction of analytes into the surrounding oil,
- the incompatibility with oil-miscible liquids (e.g, organic solvents),
- the incompatibility with assays requiring drying droplets onto the device surface.

## Biological Applications of Digital Microfluidics

DNA Extraction, Repair, and Amplification- Handling, purifying, detecting, and characterizing samples of DNA - genome research

Proteomics and Enzyme Assays - drug development, prepare peptide and protein samples for matrix assisted laser desorption/ionization mass spectrometry

Cell Assays Cell-based assays have been a popular target for miniaturization, as the reagents and other materials are often prohibitively expensive.

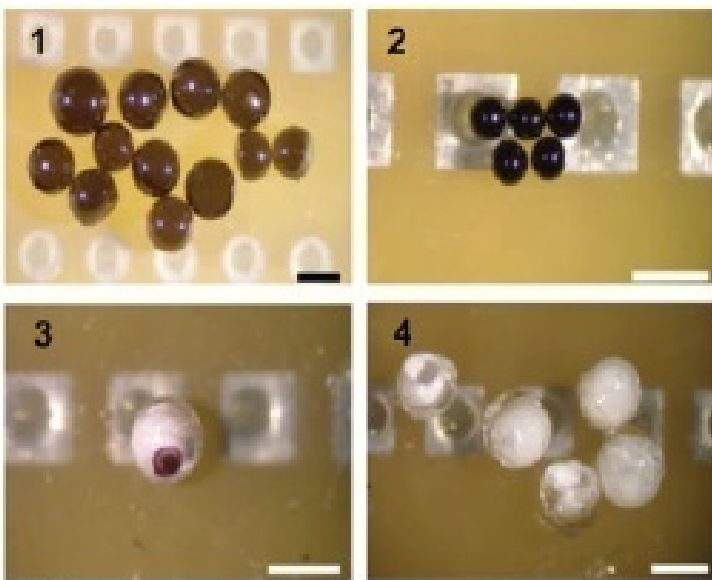
Immunoassays to detect analytes in biological samples with high selectivity.

## Optical applications

**Microlenses** - Liquid lenses are flexible. Their curvature and hence their focal length can be tuned by adjusting their shape. This can be achieved by changing the contact angle of sessile droplets via electrowetting. This allows for the design of optical systems with variable focal length that can be addressed purely electrically,

Fibre optics **Display technology** - electrowetting-based reflective display

## **Particle Synthesis**



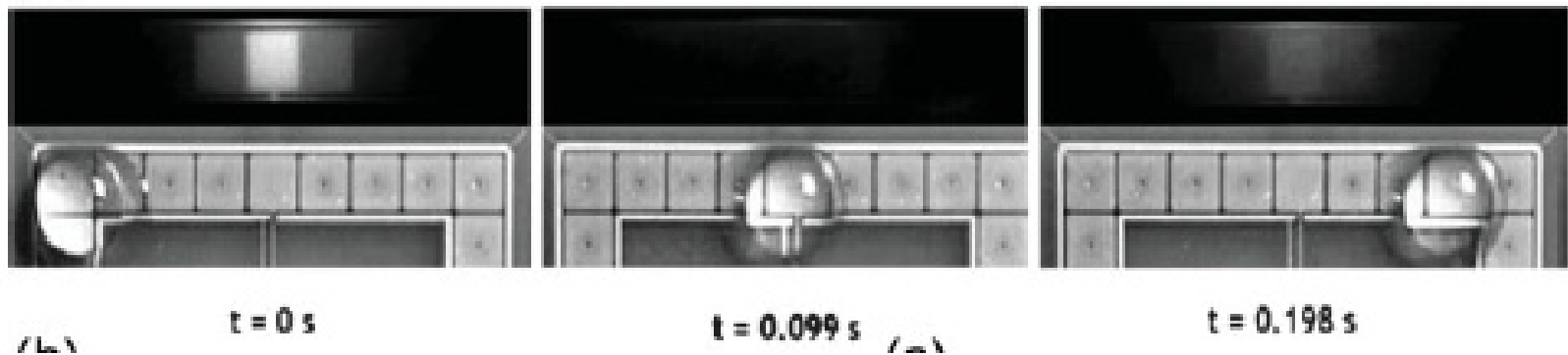
Particles being synthesized using DMF.

Conductive gold/SU-8 particles (1), semiconducting polypyrrole particles (2), “eyeball” microbeads (3), and “cups”, formed by drying water droplets that were originally encapsulated in latex (4). Scale bars: 1 mm.

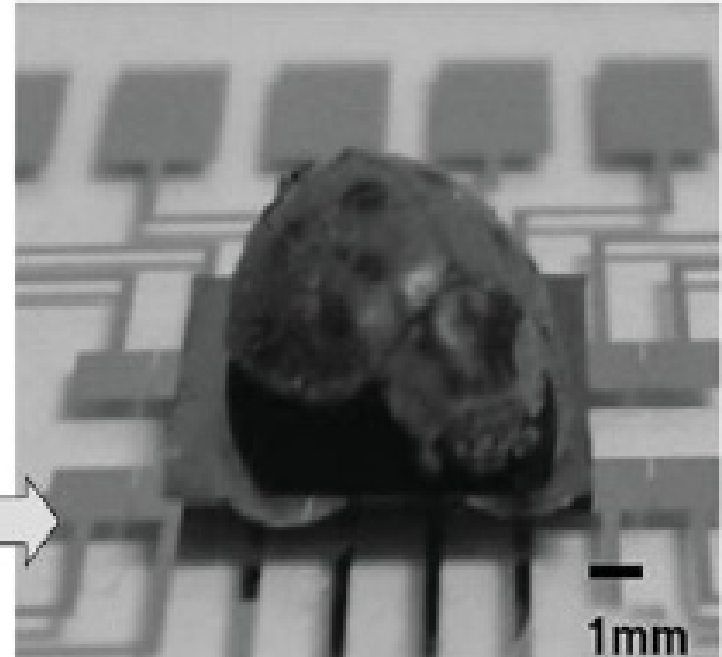
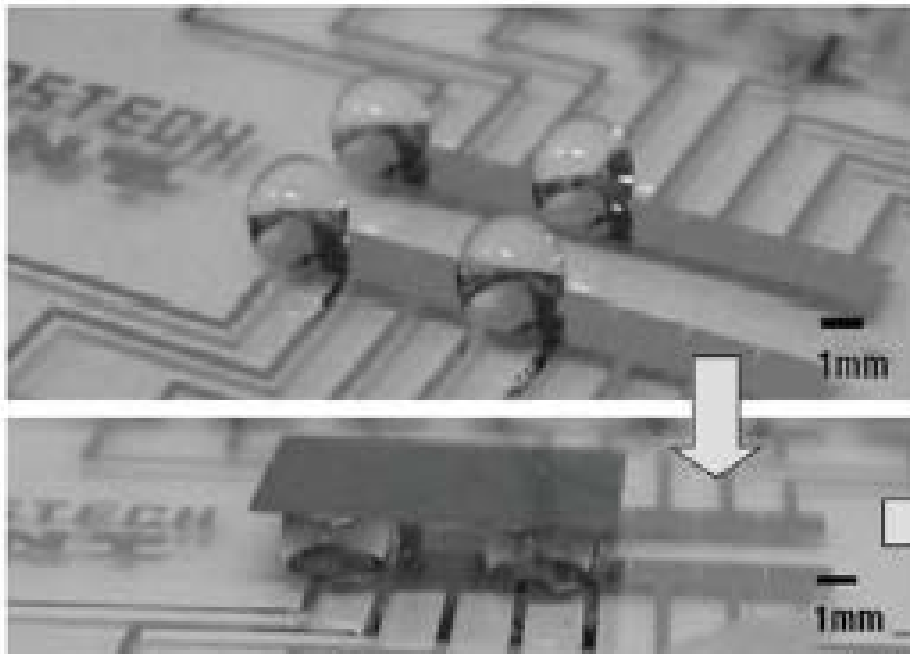
## Electronics Cooling

Microchannels have been applied to electronics cooling, and have been shown to be capable of achieving cooling rates as high as  $100\text{W/cm}^2$  may not be sufficient to cool local hot spots on integrated circuits ( $300\text{W/cm}^2$ ).

DMF seems well suited for this application, as droplets can be moved directly to hot spots, by-passing the regions not requiring cooling.



Pictures depicting the use of DMF to cool an artificial hot spot (an imbedded microheater). The top half of each frame shows an infrared image of the hot spot (white - hot); the temperature drops significantly during and after the droplet passes over it.



Pictures of a microbelt conveyer system based on DMF;

**A lady bug carried on a silicon wafer supported by four droplets.**

Sens. Actuators A 2006, 130–131, 537.



Small is the next  
big thing